

**STUDIES ON SURFACE MODIFICATIONS OF ACTIVATED
CARBON FOR REMOVAL OF ORGANIC AND BIOLOGICAL
POLLUTANTS FROM WATER**

by

AOLA SUPONG



Submitted to

NAGALAND UNIVERSITY

In Partial Fulfillment of the Requirements for Award of the Degree

of

DOCTOR OF PHILOSOPHY IN CHEMISTRY

**DEPARTMENT OF CHEMISTRY
NAGALAND UNIVERSITY
LUMAMI-798627
NAGALAND, INDIA**

2021

DEDICATED

To

My Parents

(Oja & Oba)

NAGALAND



UNIVERSITY

(A Central University Estd. By the Act of Parliament No. 35 of 1989)

DEPARTMENT OF CHEMISTRY

Headquarters: LUMAMI, ZUNHEBOTO DISTRICT-798627 NAGALAND, INDIA

DECLARATION

I, Miss. Aola Supong, bearing registration No. 720/2016 hereby declare that the content of the thesis entitled **“STUDIES ON SURFACE MODIFICATIONS OF ACTIVATED CARBON FOR REMOVAL OF ORGANIC AND BIOLOGICAL POLLUTANTS FROM WATER”** is the result of my own research on the subject. I also declare that the contents of this thesis did not form basis of the award of any previous degree to me or to the best of my knowledge to anybody else, and that the thesis has not been submitted by me for any research degree in any other university/institute.

This is being submitted to Nagaland University for the degree of Doctor of Philosophy in Chemistry.

Aola Supong
Aola Supong 8/4/21

[Signature]
Head 9/04/21
Department of Chemistry
Nagaland University

[Signature]
8/4/21
Supervisor

[Signature]
8/4/21
Co-Supervisor

NAGALAND



UNIVERSITY

(A Central University Estd. By the Act of Parliament No. 35 of 1989)

DEPARTMENT OF CHEMISTRY

Headquarters: LUMAMI, ZUNHEBOTO DISTRICT-798627 NAGALAND, INDIA

CERTIFICATE

This is to certify that **Miss. Aola Supong** registered as a Research Scholar for Ph.D. (Science) degree in Chemistry in Nagaland University and has been working under our guidance and supervision. Her thesis entitled **“STUDIES ON SURFACE MODIFICATIONS OF ACTIVATED CARBON FOR REMOVAL OF ORGANIC AND BIOLOGICAL POLLUTANTS FROM WATER”** is being forwarded for submission for the Ph.D. (Science) degree of this University. It is certified that she has fulfilled all the requirements according to the rules of this University regarding investigations embodied in her thesis and the work described in this thesis is original and has not been submitted for any other degree or diploma in this or any other University.

(Dipak Sinha)
Supervisor

(Upasana Bora Sinha)
Co-supervisor

NAGALAND UNIVERSITY



HEAD QUARTERS : LUMAMU

Ph. D COURSE WORK EXAMINATION

This is to certify that **Mr/Ms..... AOLA SUPONG.....**
of Nagaland University bearing Roll No. **Ph.D/02/2015** is qualified in the Ph.D Course Work Examination
in the Department of **CHEMISTRY** Nagaland University held in the Year **2016**

D.B.S.L

Head of Department

Heena

Department of Chemistry

Nagaland University

[Signature]
Dean
School of Sciences
Nagaland University
Lumamu

ACKNOWLEDGEMENTS

I express my deep sense of gratitude to **Prof. Dipak Sinha**, my supervisor, for giving me the opportunity to conduct my research work under his supervision in the first place. He has always been supportive and approachable. He helped me discover my potentials and encouraged me to develop my research skills. His profound knowledge, constant encouragement, guidance and valuable inputs helped me succeed in all stages of my research and achieved greater heights in my life.

I express my profound gratitude to **Prof. Upasana Bora Sinha**, my co-supervisor, for her immense love, guidance, availability and support throughout the research investigation and preparation of the thesis.

I extend my sincere gratitude to all the teaching faculties of Chemistry Department, Nagaland University; **Prof. M. Indira Devi (Head of Department)**, **Dr. I. Tavishe Phucho**, **Dr. M. Prabhakar**, **Dr. Nurul Alam Choudhury**, and **Dr. Seram Dushila Devi**, for their extended help and encouragement throughout my research period.

My sincere gratitude to **Nagaland University**, for providing the basic facilities to conduct my research. I am also grateful to the University grant commission (NFHE 2015-2017) and Department of science and Technology (DST-INSPIRE 2019-till date) for providing financial assistance.

I owe my sincere thanks to **Prof. Talijungla**, Department of Botany, Nagaland University for extending facilities for performing microbiological works.

I extend my appreciation to **Dr. Pranjal Bharali**, Department of Environmental Sciences and **Miss. Temsurenla**, Research Scholar, Department of Botany, Nagaland University for extending their help in biological related works.

My sincere appreciation to **Dr. R.L Goswamee**, CSIR-NEIST for allowing me to use their instruments during preparation of my samples.

I extend my sincere gratitude to **Prof. Nikhil Guchhait**, Department of Chemistry, Calcutta University for extending computational facility.

My gratitude and thanks to the non-teaching staff of the Department of Chemistry, Nagaland University for the help extended in different occasions.

I owe my deepest gratitude to my Lab mates, **Dr. Parimal Chandra Bhomick, Dr. Chubaakum Pongener, Ms. Mridushmita Baruah, Mrs. Champa Gogoi, Mr. Supongtoshi Jamir, Mr. Suraj Kumar, Mr. Soremo L Ezung and Mr. Shishak** for their love and support.

Special thanks to my research scholars from other laboratories and department for their wonderful friendship and encouragement.

On my personal note, I would like to acknowledge my family members for their unconditional love, support and continuous prayers throughout my research work.

Last but not the least; I humbly give all praises and honour to my Saviour for showering me with His unfailing love, blessings and abundant grace.



Aola Supong

CONTENTS

<i>List of Figures</i>	<i>x</i>
<i>List of Tables</i>	<i>xiv</i>
CHAPTER 1: Introduction	1-36
1.1 Introduction	1
1.2 Crystalline structure of activated carbon	2
1.3 Porous structure of activated carbon	2
1.4 Chemical structure of activated carbon	3
1.5 Raw material for the synthesis of activated carbon	5
1.6 Preparation of activated carbon	6
1.7 Surface modification of activated carbon	7
1.7.1 Chemical modification of activated carbon	8
1.7.2 Physical modification	10
1.7.3 Biological modification	12
1.8 Applications of activated carbon	13
1.9 Adsorption process	15
1.10 Present study	16
1.11 Aims and objectives of the work	17
References	19
	37-57
CHAPTER 2: Materials and methods	
2.1 Raw precursor for the preparation of activated carbon	37
2.1.1 <i>Tithonia diversifolia</i>	37
2.1.2 <i>Saccharum ravennae</i>	38
2.2 Preparation and modification of activated carbon	38
2.3 Characterisation of activated carbon	39
2.4 Analytical instruments used for characterisation	41
2.5 Application of the prepared activated carbon	42
2.6 Description of pollutants considered for the present study	44
2.7 Adsorption models	47
2.7.1 Adsorption isotherms	47
2.7.2 Adsorption kinetics	49
2.7.3 Validation of the adsorption models	51
2.8 Thermodynamic studies	51
2.9 Density Functional theory (DFT) studies	52
References	54
CHAPTER 3: Removal of phenols using activated carbon synthesized from <i>Tithonia diversifolia</i>	58-118
3.1 Introduction	58
3.2 Materials and methods	60
3.2.1 Taguchi design of experiment	61
3.2.2 Preparation of activated carbon	62

3.2.3 Characterization of carbon sample	62
3.2.4 Theoretical study	63
3.3 Results and discussions	63
3.3.1 Taguchi design of experiments	63
3.3.2 Characterization of activated samples	65
3.3.3 Cost analysis	70
SECTION A: Removal of Bisphenol A using <i>Tithonia diversifolia</i> activated carbon	72
3.3.4 Adsorption studies of Bisphenol A	72
3.3.5 Adsorption Isotherm studies	75
3.3.6 Adsorption kinetics studies	77
3.3.7 Thermodynamic study	80
3.3.8 Computational studies	80
3.3.9 Comparison of <i>Tithonia diversifolia</i> activated carbon with other adsorbent material	84
SECTION B: Removal of phenol and 2,4-dinitrophenol using <i>Tithonia diversifolia</i> activated carbon	86
3.4 Adsorption studies of phenol and 2,4-dinitrophenol	86
3.4.1 Adsorption Isotherm studies	90
3.4.2 Adsorption kinetics studies	91
3.4.3 Thermodynamic study	94
3.5 Effect of co-existing ions	94
3.6 Regeneration studies	95
3.7 Adsorption mechanism	96
3.8 Theoretical calculations	97
3.9 Comparative study of adsorption capacity of various adsorbents	106
3.10 Application to real water samples	107
3.11 Conclusion	108
References	110
	119-142
CHAPTER 4 : Removal of Coliform and <i>Escherichia coli</i> using activated carbon synthesized from <i>Tithonia diversifolia</i>	
4.1 Introduction	119
4.2 Materials and method	121
4.2.1 Collection and preparation of supporting media for biofilter column	121
4.2.2 Construction of biofilter column	121
4.2.3 Preparation of bacteria column	122
4.2.4 Removal experiment of <i>E.coli</i> by biofilter columns	123
4.2.5 Real water sample analysis	123
4.2.5.1 Determination of total heterotrophic bacteria	124
4.2.5.2 Determination of total coliform and <i>E.coli</i> bacteria	125
4.2.5.3 Biochemical identification of coliform and <i>E.coli</i> bacteria	126
4.2.5.4 Removal of total coliform and <i>E.coli</i> from real water sample	129

4.3 Results and discussions	130
4.3.1 Removal of synthetic <i>E.coli</i> solution by biofilter column with different supporting media	130
4.3.2 Real water analysis	133
4.3.3 Biochemical identification <i>E.coli</i> bacteria	135
4.4 Conclusions	138
References	140
CHAPTER 5: Removal of 4-nitrophenol using activated carbon synthesized from Ravenna grass	143-167
5.1 Introduction	143
5.2 Materials and method	144
5.2.1 Ravenna grass activated biocarbon preparation	144
5.2.2 Characterization of Ravenna grass activated biocarbon	144
5.2.3 Batch adsorption study of 4-Nitrophenol	145
5.2.4 Theoretical study of 4-Nitrophenol adsorption onto activated carbon	145
5.3 Results and discussion	147
5.3.1 Characterisation of activated carbon	147
5.3.2 Batch adsorption studies	151
5.3.2.1 Effect of adsorbent dose	151
5.3.2.2 Effect of contact time	151
5.3.2.3 Effect of initial concentration	152
5.3.2.4 Effect of pH	152
5.3.2.5 Effect of temperature	153
5.3.3 Adsorption isotherm studies	153
5.3.4 Adsorption kinetic studies	155
5.3.5 Thermodynamic study	155
5.3.6 Theoretical calculations	156
5.3.7 Comparative study of Ravenna grass activated carbon with other adsorbents	160
5.3.8 Cost analysis	162
5.4 Conclusion	163
References	164
CHAPTER 6: Removal of <i>Escherichia coli</i> using Ravenna grass activated carbon Ravenna grass activated carbon modified by CTMATB	168-196
6.1 Introduction	168
6.2 Materials and Method	169
6.2.1 Preparation of activated carbon	169
6.2.2 Preparation of brominated activated carbon	170
6.2.3 Characterization of Br-AC	170
6.2.4 Density functional theory calculations	170
6.2.5 Determination of antibacterial activity	170
6.2.6 Molecular docking studies	171
	174

6.3 Results and discussions	175
6.3.1 Characterization of Br-AC	175
6.3.2 Possible bromination mechanism	180
6.3.3 Antibacterial activity of Br-AC	185
6.3.3.1 Well-diffusion assay	185
6.3.3.2 Concentration and pH-dependent antibacterial activity	186
6.3.3.3 Removal of <i>Escherichia coli</i>	187
6.3.3.4 SEM image of ruptured bacterial cell	187
References	191
CHAPTER 7: Summary and Conclusions	197-200

List of Figures

Figure 1.1	Comparison of the three-dimensional crystal lattice of (a) graphite and (b) turbostratic structure	2
Figure 1.2	Schematic of activated carbon with different types of pores	3
Figure 1.3	Carbon-oxygen surface groups on activated carbon surface	4
Figure 1.4	Hydrophilic character of activated carbon in presence of oxygen surface groups	4
Figure 1.5	Schematic representation of the acidic and basic behaviour of the oxygen-containing surface groups and delocalized π -electrons of the activated carbon surface	5
Figure 1.6	Categories of activated carbon modification techniques	8
Figure 1.7	Schematic diagram of the chemical modification of activated carbon	8
Figure 1.8	Cation exchange mechanism with the carboxylic acid functional group of activated carbon	9
Figure 1.9	Scheme of the present study	17
Figure 1.10	Outline of the thesis	18
Figure 2.1	Picture showing <i>Tithonia diversifolia</i> plant	37
Figure 2.2	Picture showing <i>Saccharum Ravenna</i> plant	38
Figure 2.3	Chemical structure of phenol	44
Figure 2.4	Chemical structure of 4-nitrophenol	45
Figure 2.5	Chemical structure of 2,4-dinitrophenol	45
Figure 2.6	Chemical structure of Bisphenol A	46
Figure 3.1	Graphical representation of the effect of control factors on the S/N ratio of BET surface area	64
Figure 3.2	SEM micrograph of: (a)TUC (b) 2TAK600 (c) 2TAK700 (d) 2TAK800 (e) 1TAK700 (f) 3TAK700	67
Figure 3.3	XRD patterns of <i>Tithonia diversifolia</i> carbons obtained at activation temperature of 500°C, 600 °C, and 700 °C at an impregnation ratio of 2:1	68
Figure 3.4	TGA/DTG profile of activated carbon samples (a) 2TAK500 (b) 0.5TAK600 (c) 0.5TAK700 (d) 0.5TAK500 (e) 3TAK500 (f) 1TAK500	69
Figure 3.5	FTIR spectra of a) 2TAK500 b) 2TAK600 c) 2TAK800 (impregnation ratio 2:1)	70
Figure 3.6	Effect of (a) adsorbent dose (b) contact time (c) initial BPA concentration and (d) pH on BPA adsorption	75
Figure 3.7	Linear fitting of (a) Langmuir (b) Freundlich (c) Temkin and (d) Dubinin–Radushkevich model	77
Figure 3.8	The plots of (a) Pseudo-first-order kinetics model (b) Pseudo-second-order kinetics model (c) Intraparticle diffusion model and (d) Elovich model.	79

Figure 3.9	Optimized structures of (a) AC-P (b) AC-OH (c) AC-COOH (d) AC-CHO	81
Figure 3.10	Optimized adsorption structure of BPA onto activated carbon(a) (C ₁₅ H ₁₅ O)-OH.....C(AC) (b) (C ₁₅ H ₁₅ O)-OH.....OH-(AC) (c) (C ₁₅ H ₁₅ O)-HO.....HO-(AC) (d) (C ₁₅ H ₁₅ O)-OH.....OCH-(AC) (e) (C ₁₅ H ₁₅ O)-HO.....HOOC -(AC) (f) (C ₁₅ H ₁₅ O)-OH.....OHOC-(AC)	83
Figure 3.11	Relative energy diagram of adsorption of Bisphenol A onto activated carbon	84
Figure 3.12	Effect of activated carbon dose on removal efficiency (Temperature- 298K; Contact time- 60 mins phenol, 80 mins DNP; pH 8 phenol, pH 6 DNP; Initial concentration- 300 mg L ⁻¹ phenol, 200 mg L ⁻¹ DNP)	85
Figure 3.13	Effect of contact time on removal efficiency (Temperature- 298K; pH 8 phenol, pH 6 DNP; Activated carbon dose- 0.3g; Initial concentration- 300 mg L ⁻¹ phenol, 200 mg L ⁻¹ DNP)	88
Figure 3.14	Effect of initial concentration on removal efficiency (Temperature- 298K; Activated carbon dose- 0.3g; Contact time- 60 mins phenol, 80 mins DNP; pH 8 phenol, pH 6 DNP)	88
Figure 3.15	Figure 3.15 Effect of temperature on removal efficiency (Activated carbon dose- 0.3g; pH 8 phenol, pH 6 DNP; Initial concentration- 300 mg L ⁻¹ phenol, 200 mg L ⁻¹ DNP; Contact time- 60 mins phenol, 80 mins DNP)	89
Figure 3.16	Effect of pH on removal efficiency (Contact time- 60 mins phenol, 80 mins DNP; Temperature- 298K; Activated carbon dose- 0.3g; Initial concentration- 300 mg L ⁻¹ phenol, 200 mg L ⁻¹ DNP)	90
Figure 3.17	(a) pseudo-first-order and (b) pseudo-second-order (c) Elovich and (d) Intraparticle diffusion adsorption kinetics plot for phenol and DNP.	93
Figure 3.18	Effect of co-existing ions on phenol and DNP adsorption onto activated carbon (Conditions: ionic concentration - 0.1 mol/L; activated carbon dose- 0.3g; Initial concentration- 300 mg L ⁻¹ phenol, 200 mg L ⁻¹ DNP; pH 8 phenol, pH 6 DNP; Contact time- 60 mins phenol, 80 mins DNP; Temperature-298K)	95
Figure 3.19	Regeneration of activated carbon over five cycles (regenerated carbon dose-0.3g; contact time- 60 minutes (Phenol), 80 minutes (DNP). adsorbate concentration- 300 mg L ⁻¹ (Phenol), 200 mg L ⁻¹ (DNP); 298K temperature.	96
Figure 3.20	Schematic representation of the different mechanism for phenol and DNP adsorption on activated carbon	98
Figure 3.21	Optimised molecular structure of (a) Phenol and (b) 2,4-dinitrophenol (c) AC (d) OH-AC (e) CHO-AC (f) COOH-AC (g) COOH+OH+CHO-AC	99
Figure 3.22	Optimised structure representing (a) P-HO-----C-AC (b) DNP-HO-----C-AC (c) P-HO-----HO-AC (d) DNP-HO-----HO-AC (e) P-OH-----OHC-AC (f) DNP-OH-----OHC-AC (g) P-HO-----HOOC-AC and (h) DNP-HO-----HOOC-AC interactions	103
Figure 3.23	Energy profile diagram of (a) Phenol and (b) 2,4-dinitrophenol	105

Figure 3.24	(a) Optimised structure of COOH+OH+CHO-AC (b) Interaction between COOH+OH+CHO-AC and phenol (c) Interaction between COOH+OH+CHO-AC and DNP	106
Figure 3.25	Removal efficiency of phenol and DNP in the real water environment	108
Figure 3.26	Wastewater collection site	108
Figure 4.1	Experimental set up of (a) PS (b) PB (c) PP (d) PAP (e) BAB and (f) SAS column for removal of bacterial pathogens	122
Figure 4.2	Wastewater collection site	124
Figure 4.3	Log reduction of <i>E.coli</i> (CFU/mL) by different biofilter column (PS-pristine sand, SAS-sand/activated carbon/sand, PB-pristine brick, BAB-brick/activated carbon/brick, PP-pristine pebbles, PAP-pebbles/activated carbon/pebbles). Error bars represent the standard deviation of average results of triplicate experiments	130
Figure 4.4	SEM image of (a) Brick (b) Sand and (c) Pebbles	131
Figure 4.5	EDX of (a) Brick (b) Sand and (c) Pebbles	132
Figure 4.6	Breakthrough curve of <i>E.coli</i> using different biofilter column	133
Figure 4.7	Multiple tube fermentation test for (a) total coliform bacteria in lactose broth (b) <i>E.coli</i> in brilliant green bile lactose broth	134
Figure 4.8	(a) Mixed culture of bacteria in the water sample and Pure culture of (b) Isolate 1 (c) Isolate 6 (d) Isolate 9	135
Figure 4.9	Result interpretation of biochemical tests (a) Gram character (b) catalase test (c) Motility (d) Triple sugar iron (e) Indole (f) Methyl red (g) Voges Proskauer and (h) Citrate utilization test	138
Figure 5.1	The optimized model of (a) AC (b) (AC)OH (c) (AC)COOH (d) (AC)CHO	146
Figure 5.2	SEM micrograph of (a) 1M RAC (b) 2M RAC and (b) 3M RAC	148
Figure 5.3	FTIR spectra of (a) 1M RAC (b) 2M RAC and (c) 3M RAC	149
Figure 5.4	XRD patterns of 1M RAC, 2M RAC and 3M RAC	150
Figure 5.5	TGA profile of 1M RAC, 2M RAC and 3M RAC	151
Figure 5.6	(a) Effect of adsorbent dose (b) Effect of contact time (c) Effect of initial 4-Nitrophenol concentration and (d) Effect of pH and (e) Effect of temperature on 4-Nitrophenol adsorption	154
Figure 5.7	Linear plot of (a) Pseudo-first-order and (b) Pseudo-second-order model for the adsorption of 4-Nitrophenol.	156
Figure 5.8	Optimized structures of 4-Nitrophenol adsorption onto activated biocarbon (a) (AC)C---OH(NP) (b) (AC)HO---HO(NP) (c) (AC)OH---OH(NP) (d) (AC)CHO---HO(NP) (e) (AC)COOH---OH(NP)	159
Figure 5.9	Relative energy diagram of 4-Nitrophenol adsorption onto functionalized activated biocarbon	160

Figure 5.10	Comparative cost of Ravenna grass activated biocarbon with some commercially available activated carbon.	162
Figure 6.1	Optimized structures of (a) AC-U (b) AC-OH (c) AC-COOH (d) AC-CHO	172
Figure 6.2	(a) MurA enzyme (b) Brominated AC-OH (c) Brominated AC-COOH and (d) Brominated AC-CHO	175
Figure 6.3	SEM and EDX images of (a) AC and (b) CTMATB-AC.	176
Figure 6.4	FTIR spectra of AC and Br-AC	177
Figure 6.5	XRD image of AC and Br-AC	178
Figure 6.6	(a) XPS wide scan spectrum of Br-AC (b) High-resolution C 1s spectrum and (c) High-resolution Br 3d spectrum	180
Figure 6.7	Optimized structure of (a) CTMATB (b) CTMATB---AC-U (c) CTMATB---AC-OH (d) CTMATB---AC-COOH (e) CTMATB---AC-CHO (f) dissociated Br ₂ (g) Br ₂ ---AC-U (h) Br ₂ ---AC-OH (i) Br ₂ ---AC-COOH and (j) Br ₂ ---AC-CHO	184
Figure 6.8	(a) Hydrophobic interaction between CTMATB and AC-OH (b) Hydrophobic interaction between CTMATB and AC-OH and (C) Physical interaction between CTMATB and AC-U via ammonium moiety	185
Figure 6.9	Inhibitory effect of (a)AC and (b) Br-AC against <i>E.coli</i>	186
Figure 6.10	Antibacterial activity against <i>E.coli</i> at (a) pH 5 (b) pH 6 (c) pH 7 (d) pH 8 (e) pH 9	186
Figure 6.11	Time kill curve for <i>E.coli</i> with Br-AC at MIC concentration.	187
Figure 6.12	SEM image of (a) Untreated <i>E.coli</i> cells and (b) Cells exposed to Br-AC	188
Figure 6.13	(a) Br ₂ ---AC-OH (b) Br ₂ ---AC-OH and (c) Br ₂ ---AC-OH at the active site of MurA showing the mode of interactions	189

List of Tables

Table 3.1	Control variables and their respective levels	61
Table 3.2	L ₁₆ orthogonal array of Taguchi method and the results of the conducted experiments	63
Table 3.3	Results of ANOVA	65
Table 3.4	Cost estimates for production of 250g <i>Tithonia diversifolia</i> activated carbon	71
Table 3.5	Adsorption isotherm parameters and correlation coefficients	76
Table 3.6	Kinetics parameters for the adsorption of BPA	79
Table 3.7	Thermodynamic parameters for the adsorption of BPA onto activated carbon	80
Table 3.8	Comparison of prepared activated carbon in this study with some other adsorbents reported in the literature for BPA removal	85
Table 3.9	Langmuir, Freundlich and Temkin isotherm parameters	91
Table 3.10	Kinetic parameters for the adsorption of phenol and DNP	93
Table 3.11	Thermodynamic parameters for phenol and DNP adsorption onto activated carbon	94
Table 3.12	Adsorption energy and bond distance of phenol-AC and DNP-AC system	102
Table 3.13	Comparative study of adsorption capacity of various adsorbents	107
Table 4.1	Biochemical tests and their uses	126
Table 4.2	AER value of biofilter columns	133
Table 4.3	Heterotrophic plate count for treated and untreated water	135
Table 4.4	Total coliform and <i>E.coli</i> bacteria count for treated and untreated water	135
Table 4.5	Test result of biochemical tests	136
Table 5.1	Adsorption isotherm parameters for 4-Nitrophenol adsorption onto activated carbon	155
Table 5.2	Plot parameters of pseudo-first-order and second-order-model	156
Table 5.3	Thermodynamic parameters for 4-Nitrophenol adsorption onto activated carbon	156
Table 5.4	Adsorption energies and bond distance between 4-Nitrophenol and activated biocarbon systems.	159
Table 5.5	Comparison of RAC with some other adsorbent materials for 4-Nitrophenol removal	161

Table 5.6	Cost estimates for production of 250g activated carbon	162
Table 6.1	Bond distance and Interaction energy obtained for various type of bromination interactions.	184
Table 6.2	The molecular interaction analysis of brominated carbons at the active site of MurA	189

CHAPTER 1

INTRODUCTION

This chapter presents a brief introduction of activated carbon, its structure and properties. The chapter also discusses the raw precursors used for activated carbon preparation, different types of activation procedures and modification techniques. The applications of the activated carbon and the phenomenon of adsorption are also discussed.

1.1 Introduction

Activated carbon in its broadest sense is a term that includes a wide range of carbonized materials with high surface area, well-developed pore structure, abundant functional groups, strong mechanical strength, high physicochemical stability, high adsorption capacity, and highly reactive surface[1,2]. By virtue of these attractive characteristics, activated carbon is considered a unique and versatile carbon material with a wide array of practical applications in supercapacitors, batteries, gas separation, wastewater treatment, energy storage, air purification, medicine and catalytic process etc.

The earliest documented use of activated carbon in the form of wood charcoal dates back to 3750 B.C. when it was first used by the Egyptians and Sumerians for smelting ores to create bronze[3]. By 1550 B.C., the Egyptians use of charcoal progressed to medicinal applications; it was used for adsorbing unpleasant odour from putrefying wounds and intestinal tracts[4]. Around 450 B.C., the ancient Hindus and Phoenicians discovered the antiseptic properties of charcoal and began using it to purify water. By 50 A.D., charcoals were used for the treatment of a wide range of ailments such as epilepsy, chlorosis, anthrax and vertigo[5]. In the 15th century, sailors blackened the inside of wooden water containers with fire to preserve the freshness of water for a longer period. Later, in the 18th century, wood charcoal found its way into sugar refinery and was used in large-scale for decolourising raw sugar syrup[6]. The first industrial-scale production of activated carbon took place in the 19th century mainly for use in sugar refineries[3]. These activated carbons were produced by various chemical and thermal activation processes, such as using metal chlorides or steam and CO₂ as the activating agent [1]. During the First World War, the release of poisonous gas accelerated the developments in the production of activated carbon and gas masks with better quality activated carbon were used for the adsorption of the hazardous gases. Later, considerable developments were made in the production of activated carbon using new raw precursors and activating agents and were used for water treatment, air purification and solvent recovery[4].

Today, activated carbon is used in a wide variety of applications. They are efficiently used to mitigate diverse environmental problems such as removal of organic, inorganic and biological pollutants from water, removal of toxic gases from air, carbon sequestration and remediation of contaminated soil[7,8,17,18,9–16]. Another broad area of application for activated carbon is the treatment, purification and decolourization of liquids in the food, pharmaceuticals, beverage and other industries[19–22]. Activated carbon is also well known for its application in metal recovery, medicine, catalytic process, cosmetics, solvent recovery, decaffeination of

coffee, soil improvement, among others[23–29]. The ever-continuous development and optimisation of the activated carbon production process and the use of new raw materials have led to the development of better-quality carbon in use today.

1.2 Crystalline structure of activated carbon

Activated carbons have a microcrystalline structure that consists of fused hexagonal rings of carbon atoms[30]. The microcrystalline structure of activated carbon is different from that of graphite with regard to the interlayer spacing. The interlayer spacing for graphite is 0.335 nm while for activated carbon, it ranges between 0.34 and 0.35 nm. The microcrystallite layers are also less ordered in activated carbons. This disorder in microcrystallite layers is caused by the presence of heteroatoms, and vacant lattice sites in activated carbons [31]. Biscoe and Warren proposed the term turbostratic for such a disordered form of the graphitic structure of activated structure activated carbon[32]. The comparison of the three-dimensional structure of graphite and the turbostratic structure of activated carbon is given in Figure 1.1.

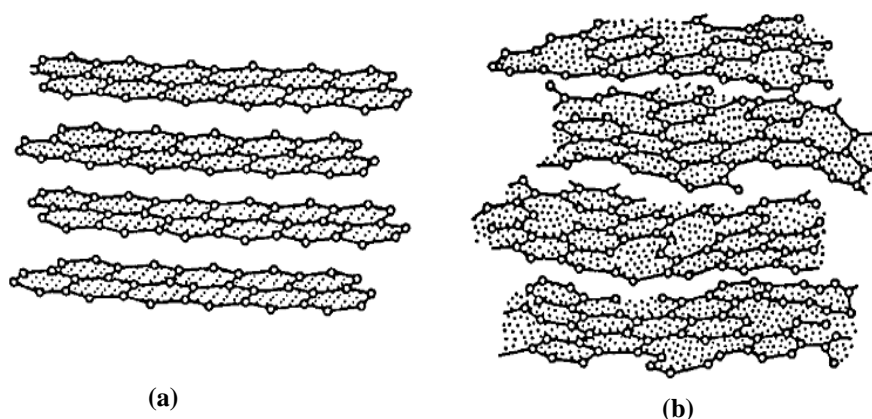


Figure 1.1 Comparison of the three-dimensional crystal lattice of (a) graphite and (b) turbostratic structure

1.3 Porous structure of activated carbon

Activated carbon has a highly developed internal surface which is characterized by a polydisperse porous structure consisting of pores of different shapes and sizes[1]. The most widely used activated carbon has a surface area typically ranging from 500 to 1500 m²g⁻¹ and pore volume on the order of 0.7 to 1.8 cm³ g⁻¹. However, both the pore volume and surface area can also be as high as 3000 m²g⁻¹ and 1 cm³ g⁻¹ respectively [1,15,33]. Based on the pore sizes, the International Union for Pure and Applied Chemistry (IUPAC) classified the pores into three types; micropores with an average diameter less than 2 nm, mesopores with a diameter between 2-50 nm and macropores having an average diameter more than 50 nm [34].

As illustrated in Figure 1.2, the pattern of the porous structure constitutes macropores opening up directly to the external surface, the mesopores branching off from the macropores and the micropores then branch off from the mesopores. The total surface area of activated carbon mainly corresponds to surface area within the micropores and therefore most of the adsorption takes place in the micropores. On the other hand, the mesopores and macropores serve as transport channels for the adsorbate to reach the micropores[35]. All pores have walls and therefore, they will comprise two types of surfaces, internal or microporous surface and external surface. The internal or microporous surface represent the walls of the micropores, while the external surface constitutes the walls of the mesopores and macropores as well as the edges and the outer facing aromatic sheets[36].

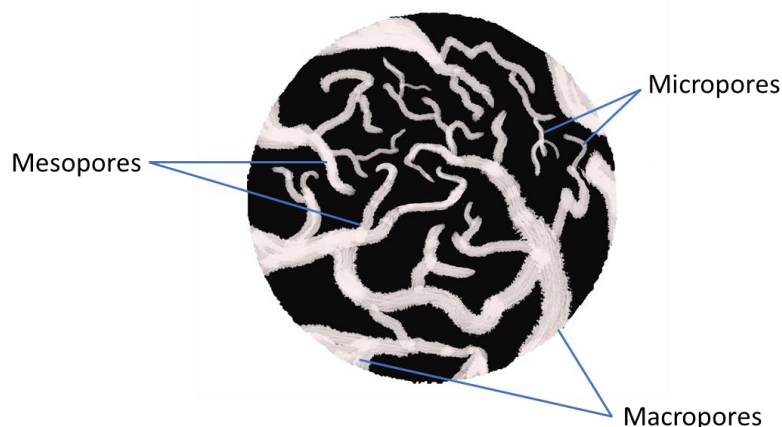


Figure 1.2 Schematic of activated carbon with different types of pores

1.4 Chemical structure of activated carbon

In addition to the microcrystalline and porous structure, the activated carbon has a chemical structure as well. The chemical characteristics of activated carbons are largely determined by the presence of heteroatoms such as oxygen, nitrogen, hydrogen, sulphur and phosphorus[37]. These heteroatoms are either derived from the raw material during carbonization or introduced during the activation process. The heteroatoms become associated with the edge carbon atoms or defect carbon rings and give rise to surface groups such as carbon-hydrogen, carbon-oxygen, carbon-sulphur, carbon-halogen and carbon-nitrogen, surface groups. Among these groups, carbon-oxygen surface groups are by far the most common and abundant along with hydrogen [36,38–40]. These carbon-oxygen surface groups are formed either by reaction of the carbon material with oxygen or oxidation of the carbon surface by gases and aqueous oxidants[41,42]. The amount and nature of carbon-oxygen surface groups depend on the nature of the carbon surface, its surface area and the oxidation conditions[41]. According to

the chemical properties, the carbon-oxygen surface groups are classified into three types: acidic, basic and neutral [43–46]. Acidic groups include carboxylic acids and anhydrides, lactones or lactols, and phenols, while carbonyl and ether oxygen is neutral or may form basic structures, such as quinone, chromene, ketone and pyrone groups[43,47–51]. Figure 1.3 represents the different types of oxygen functional groups on the activated carbon surface.

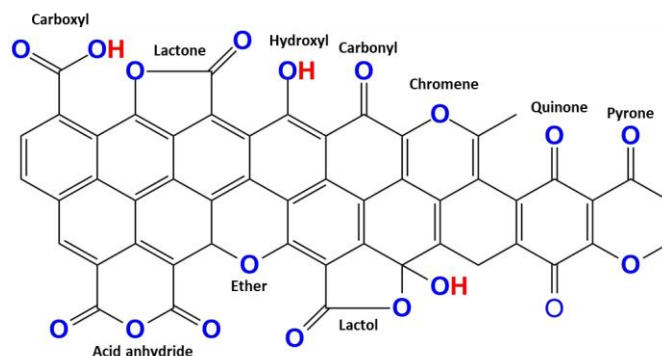


Figure 1.3 Carbon-oxygen surface groups on activated carbon surface[52]

The carbon-oxygen groups play a major role in activated carbon properties such as surface behaviour and reaction, surface charge, hydrophobicity, the electron density of graphene layers as well as catalytic properties and may be used for further surface modification[1,49,53]. The two principal effects of carbon-oxygen surface groups are; first, the influence on the hydrophobic/hydrophilic character of activated carbon. Activated carbons are hydrophobic in nature. However, the presence of carbon-oxygen surface groups renders hydrophilicity to the activated carbon surface by forming hydrogen bonds between the surface oxygen atoms and water molecules. The bonded water molecules may in turn form new hydrogen bonds with new water molecules. The schematic representation of the hydrophilic character of activated carbon is given in Figure 1.4.

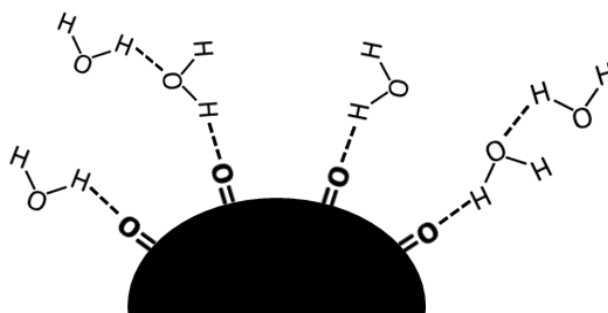


Figure 1.4 Hydrophilic character of activated carbon in presence of oxygen surface groups[54].

The second important effect is the influence of the oxygen-containing surface groups on the acidic or basic character of the activated carbon. Activated carbon surfaces are amphoteric by

nature *i.e.*, both acidic and basic sites co-exist on the surface. The acidic behaviour is associated with carboxyls, hydroxyls, lactones and phenols. On the other hand, pyrones, chromenes, ethers and carbonyls are responsible for the basic properties of the activated carbon surfaces. Depending on the aqueous medium, the activated carbon surface can have either a positive or negative charge. For example, the carboxyl, hydroxyl and lactone groups will behave as acidic groups if the pH of the medium is higher than the pK_a of these groups (basic medium)[54]. Another factor to be considered is the pH of the medium in relation to the pH of the zero-point charge (pH_{zpc}) of the activated carbon. If the pH of the aqueous medium is higher than the pH_{zpc} of the activated carbon, the acidic group dissociates and release protons into the medium, and the activated carbon acquires a positive charge. Whereas, at pH of the medium lower than the pH_{zpc}, the basic sites combine with protons present in the medium, leaving a positively charged surface[42]. The behaviour of the oxygen surface groups in an acidic-basic medium is schematically represented in Figure 1.5.

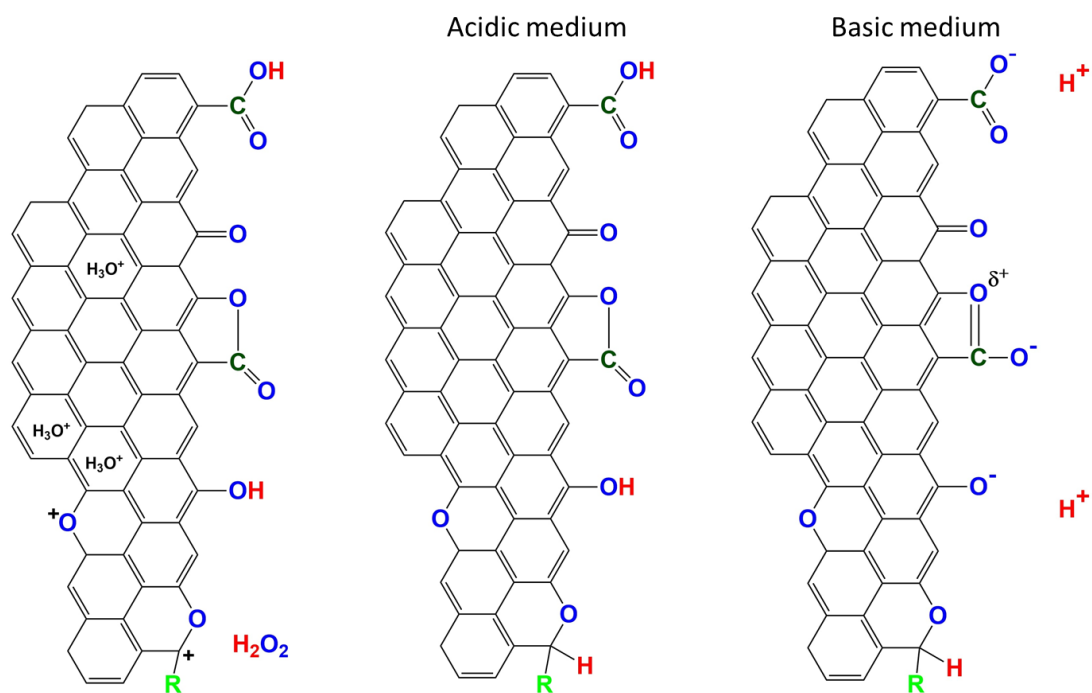


Figure 1.5 Schematic representation of the acidic and basic behaviour of the oxygen-containing surface groups and delocalized π -electrons of the activated carbon surface [55].

1.5 Raw material for the synthesis of activated carbon

Activated carbon can be synthesized from a variety of raw materials with high carbon content and low organic matter [56]. The raw materials chosen for the preparation of activated carbon should be abundant, inexpensive, renewable and safe [57,58]. Most of the commercial activated carbon are prepared from fossil-based precursors such as coal, peat, lignite and

wood, which are non-renewable as well as expensive and thereby, limiting their usage. Therefore, in recent years, extensive studies have been made on the preparation of activated carbon from agricultural waste and lignocelluloses biomass materials which are renewable and cost-effective [59–67]. Examples of biomass materials include African palm shell [68], pistachio-nut shells [69], fox nut[63], grape stalk[62], coffee husk [64], pecan shells [70], rice straws [71], *Arundo donax* cane [72], *Manihot esculenta* [73], *Citrullus lanatus* rind [74], *Mucuna pruriens* [75], waste tea leaves [76] neem husk [77], banana peel [64], almond shells [78], sugarcane bagasse[79], tamarind wood [80], jackfruit peel[81], Jatropha husk[82] [101], coconut husk [83], groundnut shell[84], rice husk[85], bamboo[86], kenaf fiber[87], sawdust[88], hazelnut shell[89], olive stone[15], palm shells[90], waste tea [91], sour cherry stones [92], plant waste [93], snail shell [94], wood chips [95], mushroom roots [96], woods [97,98], rice husk [85], bagasse [99], coconut shell [100] and many others.

In addition to the availability, cost-effectiveness and renewability of these biomass materials, another significant advantage is the presence of a high content of volatile matter, which is ideal to produce a highly porous structure of activated carbon[58]. From a commercial point of view, most of the biomass materials are just discarded as waste without proper utilization. Therefore, the conversion of agro-waste or biomass materials into value-added products such as activated carbon can eventually decrease the costs of waste disposal and the negative impact on the environment [14].

1.6 Preparation of activated carbon

Activated carbon can be prepared either through direct activation of dried raw precursor or through a two-step activation process which includes carbonization of the raw precursor followed by activation[2]. Depending on the nature of the activation process, activated carbon can be prepared in two ways: physical activation and chemical activation.

Physical activation

Physical activation typically follows a two-step activation process which involves carbonisation of the raw materials in an inert atmosphere to remove non-carbon species, followed by activation of the carbonized sample using oxidising gases such as steam, nitrogen, carbon dioxide or their mixtures at temperatures ranging from 600–1200°C [101–106]. This method can produce activated carbon with good porous structure as well as physical strength and is considered an inexpensive green approach since it is chemical free [58,107,108]. However, the limitations of physical activation lie in its long activation time high energy consumption and low adsorption capacity of the produced activated carbon[109].

Chemical activation

Chemical activation can be a single-step or two-step process. In the single-step process, the dried raw material is directly impregnated with oxidising and highly dehydrated chemicals and activated at high temperatures for a given time[37]. On the other hand, in the two-step process, the dried raw material is first carbonized at temperatures ranging from 400–600°C to obtain the char and secondly, the obtained char is impregnated with chemical agents and heated at high temperatures[109]. Eventually, activated carbon is obtained by repeated washing of the activated sample. In this step, the activated carbon is washed with acid or alkali, depending on the chemical reagents used in the preparation, and followed by washing with water. This washing of the sample creates pores by removing the chemical components from the carbon matrix[110].

The main chemicals used as potential activating agents are alkaline groups such as KOH, NaOH, K_2CO_3 and Na_2CO_3 [111–117], acidic groups such as H_3PO_4 , HCl, H_2SO_4 , HNO_3 [118–122] and metal salts such as $MgCl_2$, $FeCl_3$ and $ZnCl_2$ [123–127]. These chemical agents react with the carbon-matrices of the precursor and liberate gas products to form a porous structure[128]. Besides, they act as dehydrating or oxidizing agents that promote pyrolytic decomposition and increase the activated carbon yield by inhibiting tar and ash formation [58,128,129]. The activating agents play decisive roles in the formation of pores or surface chemical groups during the activation. Among the numerous chemical activating agents, potassium hydroxide is one of the most effective activating agents for preparing AC with an extremely high specific surface area[130].

As compared to physical activation, chemical activation is a more preferable choice since it produces activated carbon with higher surface area and pore volume[131]. Moreover, another advantage lies in its lower activation temperature and shorter activation time, making the process economically viable[132].

1.7 Surface modification of activated carbon

The most interesting and important property of activated carbon is that its surface can be suitably modified to improve the adsorption characteristics and enhance the affinity of the activated carbon towards a specific pollutant. To this end efforts to substantially improve the potential of carbon surface by using different chemicals or suitable treatment methods [133–137]. Based on the nature of the modification, the modification technique can be classified into three broad groups: (i) chemical modification, (ii) physical modification and (iii) biological modification (Figure 1.6)

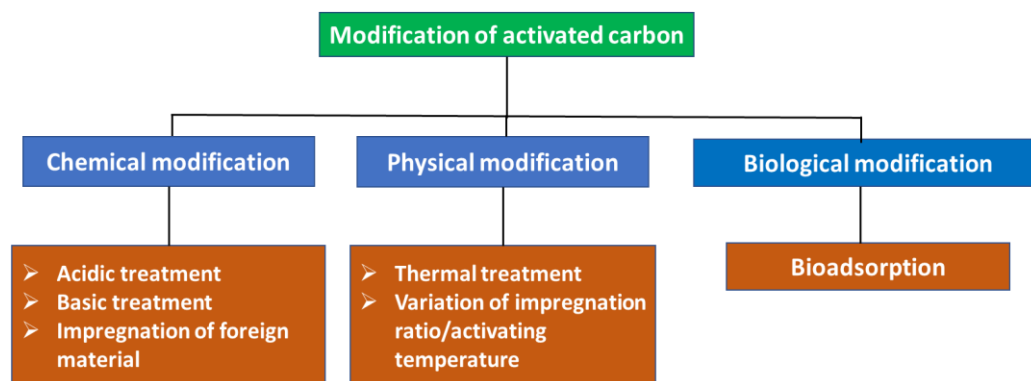


Figure 1.6 Categories of activated carbon modification techniques

1.7.1 Chemical modification of activated carbon

Chemical modification of activated carbon is achieved by modifying the inherent surface functional groups of activated carbon. In this method, the nature and concentration of the acidic and basic surface groups of the activated carbon are tailored to enhance its affinities towards a specific pollutant particularly inorganics and metals. The chemical modification of activated carbon is achieved by acidic treatment, basic treatment and impregnation of the activated carbon. The schematic representation of the chemical modification of activated carbon is given in Figure 1.7.

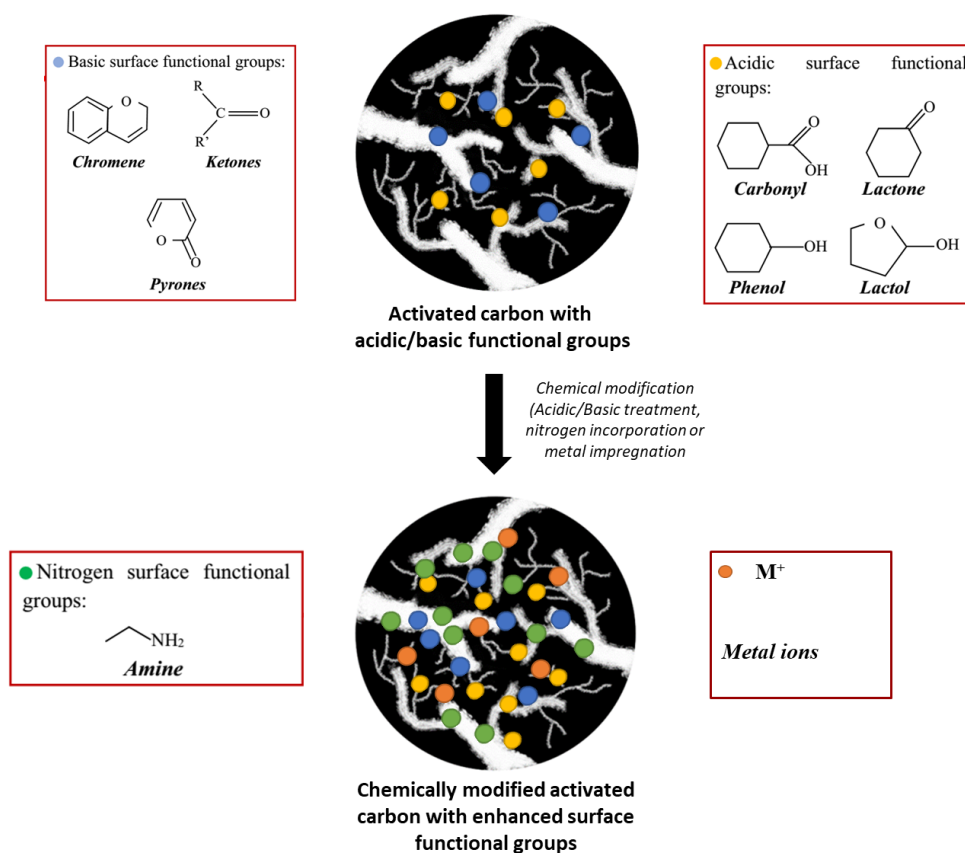


Figure 1.7 Schematic diagram of the chemical modification of activated carbon[138]

Acidic treatment

Acidic treatment of activated carbon is directed towards modifying carbon surfaces to increase the acidic surface functional groups such as carboxyl, hydroxyl, lactone and acid anhydride groups[139]. The most commonly used chemicals for acidic treatment of activated carbon are strong acid oxidizers such as nitric acid and sulphuric acid, however, other oxidizing agents such as hydrogen peroxide, oxygen and acetic acid are also used to increase the acidic group[140,141]. The acidic treatment of activated is found to be more favourable for enhancing the uptakes of metal ions and this enhanced removal of metal ions has been attributed to the formation of metal complexes due to cation exchange mechanism where the metal cation exchanges site with the hydrogen ion of the acidic functional group as illustrated in Figure 1.8. Although acidic treatment displays beneficial effects on the uptake of metal ions, it is found to have a detrimental effect on the textural properties of activated carbon such as BET surface area and pore volume [142–144].

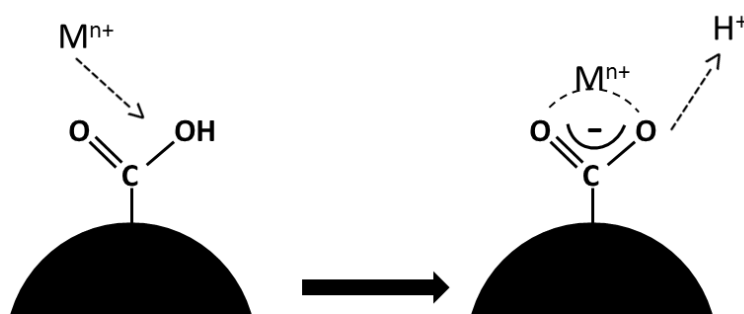


Figure 1.8 Cation exchange mechanism with the carboxylic acid functional group of activated carbon[142]

Basic treatment

Basic or alkaline treatment of activated carbon is aimed towards modifying the activated carbon surface through the introduction of positive charges which makes it favourable for enhancing the adsorption of negatively charged species[145]. The basic treatment of activated carbon is generally done using chemicals such as ammonia, urea and NaOH [43,146–150]. The treatment of activated carbon with such chemicals leads to the increase of increases the basic groups such as amides, aromatic amines, protonated amides and pyridine-type structures etc. Besides, under a basic environment, it is expected that OH^- ions react with the surface functional groups of AC. Studies on the basic treatment of activated carbon have indicated that the activated carbon with increased basicity is more effective in enhancing the removal of organic-based substances. For instance, the adsorption capacity of phenol was enhanced by as much as 29% using activated carbon modified with gaseous ammonia at 700°C. A four-fold

increase in perchlorate removal was observed using ammonia modified activated carbon. Also, urea treated activated carbon with increased basic properties were found to enhance the uptake capacity of phenol.

Impregnation

The term impregnation can be defined as the fine distribution of chemicals and/or metal particles in the pores of AC [145]. The impregnation of activated carbon with suitable chemicals helps in increasing the existing adsorptive capacity of activated carbon and in optimizing the catalytic properties of activated carbon by promoting its built-in catalytic oxidation capability and promoting synergism between activated carbon and the impregnating agent[151]. Several impregnation studies have proved to be useful for providing strategies for significantly increasing the adsorption potential and/or reactivity of the activated carbon towards various molecules. For instance, the adsorption of copper (II), zinc (II), chromium (VI) and cyanide (CN^-) ions onto the surface of activated carbon impregnated with tetrabutylammonium and sodium diethyldithiocarbamate (SDDC) showed an effective removal capacity of approximately two to five times greater than that of pristine activated carbon [152–154]. It was reported that the overall enhanced removal of the ions was a combination of the adsorption capacity of the pristine AC and the extent of ion exchange between the impregnated molecules and the ions. The impregnation of activated carbon with metals such as silver, copper, aluminium, nickel and iron also showed a significant increase in the adsorption capacity for molecules the host activated carbon cannot otherwise attract without the impregnant[153,155–158]. Another important utility of impregnation is rendering antibacterial properties to the pristine activated carbon. Several studies are being carried out to introduce antibacterial agents such as silver, copper, quaternary ammonium moieties, and zinc oxide etc on the activated carbon[159–163]. The impregnation of these antibacterial agents on the activated carbon offers a synergism effect of both antibacterial properties and adsorption and also prevents leaching of the chemicals. These antibacterial impregnated carbons have proven to be effective in the removal of various waterborne pathogens from water [164,165].

1.7.2 Physical modification

Physical modification of activated carbon involves the enhancement of the physical characteristics of the activated carbon such as pore volume and BET surface area. The enhancement of physical characteristics of activated carbon is carried out to significantly increase the contaminant removal efficiency, especially in the case of organic adsorptions.

The physical structure of activated carbon can be enhanced by various methods such as thermal treatment and by varying activating conditions i.e., activating agent, impregnation ratio and activating temperature[166]. The most common method for physical modification of activated carbon is the thermal treatment, where activated carbon is treated thermally in an inert atmosphere. However, a significant limitation of thermal treatment is that the surface oxygen functional groups (which are thermally unstable) can be decomposed at high temperatures, which may sometimes result in lesser adsorption capacity. It is in this context that promising modification techniques such as variation of activating conditions are being done to enhance the physical characteristics of the activated carbon. Activating conditions such as activating agent, impregnation ratio and activation temperature play a significant role in obtaining activated carbon with enhanced textural properties such as pore volume and surface area[112,167–169]. Several studies are reported in the literature about the effects of activation parameters on the textural properties of activated carbon.

Effect of activating agents

The enhancement of the pore volume surface area and activated carbon can be done by using different chemical activating agents. Among the various chemical activating agents, H_3PO_4 , ZnCl_2 , and KOH are the most widely used agents for increasing the textural properties of activated carbon [58,101]. The use of H_3PO_4 leads to the production of higher pore volumes containing both micropores and mesopores and also increases the carbon yield [58,170–173]. Zinc Chloride causes an increase in the inter-and intra-voids, resulting in the formation of activated carbon with high surface area and large porosity[63,174,175]. KOH on the other hand, produces well-developed micropores in activated carbon, leading to the development of high surface area [101,167,176–178].

Effect of chemical impregnation

The chemical impregnation ratio is defined as the ratio of the weight of the chemical activating agent to the weight of the carbon precursor, and it is one of the most important parameters that have a considerable impact on the surface area and pores development. Studies conducted by Giraldo and Moreno-Pirajan, 2012 [179] reported that the variation of impregnation ratio from 2:1 to 3:1 using ZnCl_2 and KOH as activating agents resulted in an increase in surface area and total pore volumes. Singh *et al.*, 2017 studied the chemical impregnation using potassium hydroxide [167] and reported that activation using an impregnation ratio of 1:2 at 600°C produced activated carbon with the highest degree of porosity and surface area [167]. Another study conducted by Sagili *et al.*, 2015 [180] on grape

industrial processing waste using zinc chloride as an activating agent, reported that a higher impregnation ratio results in mesopore formation while a lower impregnation ratio results in micropore formation. This is because a higher impregnation ratio results in greater swelling and stronger release of volatile matter contents leading to widening of pores[181]. Meanwhile, a lower impregnation ratio promotes the release of volatile matter contents but inhibits the deposition of tars resulting in more micropores formation[180]. Likewise, various studies have reported the strong impact of impregnation ratio on the surface area and pore volume of activated carbon [63,182,183].

Effect of activation temperature

Activation temperature is a crucial parameter that affects the textural properties of the activated carbon. The optimal temperature range depends on the type of precursor, activating agent, heating source, mixing method and so on. An excessively high activation temperature may decrease the specific surface area and carbon yield. This may be due to the excessive transformation of cross-linked substances in the solid phase to volatile matters in the gas phase [184,185]. Besides, a low activation temperature may result in a poor porous structure, because the activation energy is too low to initiate pyrolysis, resulting in an incomplete reaction[168]. Therefore, an optimal temperature range needs to be determined for each activation process to produce activated carbon with a relatively high surface area and pore volume. Generally, the favourable activation temperature using acidic activating agents is in the range of 400–500°C, whereas the favourable activation temperature when using alkaline and self-activating agents, is generally in the range of 750–850 °C [186,187].

1.7.3 Biological modification

The biological modification of activated carbon involves those processes in which microorganisms get adsorbed on the activated carbon, and the adsorbed microorganisms are further used for the enhanced removal of contaminants from water. The adsorption of microorganisms, intentionally or unintentionally, onto activated carbon has been the subject of interest for researchers for the past several decades. Most studies on biological modification of activated carbon are aimed at the removal of readily biodegradable compounds, having low molecular weight such as phenol from aqueous solutions. The beneficial effect of the biological modification is that the carbon-bed life can be prolonged by converting a portion of recalcitrant organics to biodegradable organics by preozonation[145]. The attached microorganisms then convert the biodegradable portion to biomass, carbon dioxide and waste products before this material can occupy adsorption sites on the activated

carbon[188]. Biological modified activated carbon has been used for the removal of a wide variety of pollutants such as phenols, 2,4-dichlorophenol, pesticides, natural organic matter and organic micropollutants, bromate etc.[189–191]. However, one distinct disadvantage of biological modification is the continuous formation of biofilm that may have an encapsulating effect on activated carbon. The continuous thickening of biofilm prevents the adsorbate species from diffusing through the biofilm and thus eventually reduces the adsorption rate[192].

1.8 Applications of activated carbon

Activated carbon is an excellent and versatile adsorbent with innumerable applications in various fields such as removal of odour, colour, undesirable organic and inorganic chemicals from water, solvent recovery, biomedical applications, separation and purification technologies, catalytic processes, pollution control, energy storage, spill clean-up, gas-phase adsorptions, supercapacitors, batteries, solar cells etc. [61,94,193–195]. The outstanding adsorbent properties of activated carbon are essentially attributed to their high surface area, well-developed porosity and high surface reactivity. Besides, the flexibility of activated carbon in the modification of its physical and chemical characteristics has paved the way for its application in a wide variety of fields[61]. Among the wide-ranging applications, the most extensive usage of activated carbon is in wastewater treatment for the removal of various organic, inorganic and biological pollutants. Many studies have reported the use of biomass-derived activated carbon for the removal of such pollutants from water, some of which are discussed below.

Removal of organic pollutants

Activated carbon has been used for the removal of various organic pollutants such as dyes, phenolic compounds, pharmaceuticals, pesticides etc. from water. Wang *et al.*, 2018 reported the removal of methylene blue from aqueous solution using distillers' grains derived activated carbon with an adsorption capacity of 934.579 mg/g[196]. Activated carbon from *Acacia mangium* and *Acacia nilotica* have proven their capability in the removal of 90.5% toxic textile Methyl orange dye [197] and 250mg/g Methylene Blue respectively[198]. Zbair *et al.*, 2018 [199] studied the removal of bisphenol A using argan nutshell-derived activated carbon and they reported a maximum adsorption capacity of 1250 mg/g at 293 K. Basic-treated activated carbon was efficient in the removal of phenolic compounds up to 322.5 mg/g whereas acidic-treated activated carbon was found to remove only 142.9 mg/ g phenolic compounds from aqueous[200]. Various biomass-derived activated carbons have also been

successfully used for the removal of pesticides such as 2,4-dichloro-phenoxy acetic acid (175.4 mg/g, bentazon (86.26 mg/g) and carbofuran (137.04 mg/g)[201,202]. Date stones activated carbon was also found to remove drin pesticides such as aldrin, dieldrin and endrin with a high adsorption capacity of 373.228 mg/g, 295.305 mg/g and 228.047 mg/g respectively[203].

Removal of inorganic pollutants

Various studies have reported the use of activated carbon for the low-cost and easy removal of inorganic pollutants including heavy metals and anionic pollutants from water[204,205]. For instance, bamboo-based activated carbon was used for the effective removal of Cd (II) with a maximum adsorption capacity of 12.08 mg g⁻¹ [206]. *Acacia nilotica* bark activated carbon showed a high removal efficiency of 93.1% for chromium[207]. Zhang *et al.*, 2010 studied the removal of Pb (II) using *Polygonum orientale* derived activated carbon and reported that interaction of lead with the activated carbon active site could be attributed to electrostatic attraction, hydrogen bonding, or hydrophobic attraction [208]. Alagumuthu and Rajan, 2010 [209] studied the efficiency of zirconium impregnated cashew nutshell activated carbon and cashew nut shell activated carbon for fluoride removal. They reported that Zirconium impregnated Cashew nutshell activated carbon showed a higher removal efficiency of 80.33% than the cashew nutshell activated carbon (72.67%), proving the potential of a modified activated carbon for removal of fluoride ions. The anionic pollutants in water like thiocyanate, phosphate, and molybdate have also been removed using agriculture waste coir pith activated carbon[210–212].

Removal of gaseous pollutants

The removal of gaseous compounds such as SO₂, NO₂, CO₂ etc. has also been achieved using various biomass-derived activated carbon. Activated carbon prepared using wood and almond shell was efficiently used for the removal of SO₂[213]. The adsorption of carbon monoxide and hydrocarbon were also studied using MgO modified durian peel activated carbon. The maximum carbon monoxide adsorption was found to be 99.14% and hydrocarbon adsorption was 87.73%[214]. Activated carbon prepared from the olive stone was used for remediating the emission of NO₂ gas [215] and the adsorption capacity was found to be around 131 mg/g. Various biomass-derived activated carbons were also found to be effective in the adsorption of volatile organic compounds (VOCs), trimethylamine and hydrogen sulphide [216–218].

Removal of biological pollutants

Activated carbon has shown great potential in the removal of biological pollutants, particularly waterborne pathogens from water. The efficient removal of two waterborne pathogenic bacteria, *Raoultellaterrigena* (ATCC 33257) and *Escherichia coli* (ATCC 25922) was achieved using negatively and positively charged types of activated carbon particles[219]. Li *et al.*, 2014 reported the use of Cu^{2+} and $\text{Cu}(\text{OH})_2$ modified activated carbon for the effective removal of *Escherichia coli* from urban stormwater. Their study yielded an estimated 2-log reduction of *E. coli* within 40 minutes[220]. The removal of 10^4 CFU/ml of *Escherichia coli* cells was achieved using a column containing silver nanoparticle impregnated activated carbon[221]. Pongener *et al.*, also reported the 99 and 98.7% coliform bacteria removal percentage using *Mucuna pruriens* and *Manihot esculenta* activated carbon columns respectively[75].

1.9 Adsorption process

Adsorption is a surface phenomenon that leads to the transfer of molecules from a gas or liquid phase to a solid surface. The molecules or atoms on the solid surface have residual surface energy due to unbalanced forces and when some substances collide with the solid surface, they are attracted by these unbalanced forces and stay on the solid surface. Depending on the nature of adsorption forces, the adsorption process may be categorised as physisorption or chemisorption. In the case of physisorption, the adsorbate molecules are bound to the adsorbent surface by weak van der Waals forces. Physical adsorption is generally carried out at a low temperature, and fast adsorption rate, low adsorption heat, and is nonselective. On the other hand, chemisorption refers to the sharing or exchange of electrons between the adsorbent surface and the adsorbed molecule. As a result of the reaction, a chemical bond is formed between the adsorbate and the adsorbent surface. Physical adsorption and chemical adsorption are not isolated and often occur together.

The adsorption process is generally described at the equilibrium by using adsorption isotherms models. These models describe the interaction between adsorbent and adsorbate and quantify the amount of substance attached to the surface. The most commonly used adsorption isotherms are the Langmuir, Freundlich and Temkin isotherms. These details of these models are discussed in Chapter 2. Another important aspect of the adsorption process is the study of adsorption kinetics, which describes the uptake rate of adsorbate, the nature of the adsorption mechanism and determines the rate-controlling step[222–224]. Several kinetic models, namely pseudo-first-order, pseudo-second-order, Weber and Morris intraparticle

diffusion model, and Elovich model are used to describe the kinetics of adsorption. Furthermore, thermodynamic studies help in understanding the effect of temperature on various thermodynamic parameters such as the Gibbs free energy, enthalpy and entropy, etc. Details regarding thermodynamic studies are discussed in Chapter 2.

1.10 Present study

Activated carbon is regarded as an excellent and versatile adsorbent for a diverse field of applications. Another interesting property of activated carbon is that its surface can be tailored to a specific chemical and physical attribute to enhance its affinities toward metal, inorganic and/or organic species present in aqueous solutions. However, its practical applicability is often limited by the high-cost and non-renewable nature of the precursor. In this context, the use of biomass precursor for activated carbon preparation yields an added advantage owing to their cost-effectiveness, wide availability, and eco-friendly nature.

Thus, keeping this in mind, the present study focussed on the usage of biomass materials as raw materials for the preparation of activated carbon. The activated carbon was prepared by chemical activation method using KOH as the activating agent. Further, the modification of the textural properties of activated carbon such as pore volume and BET surface area were studied by varying chemical impregnation ratios and activation temperatures. Surface area and pore volume play an important role in the removal of organic pollutants, particularly phenolic compounds. Therefore, the modification of the textural properties was done with the objective of increasing the activated carbons' affinity towards the removal of phenolic compounds. The modification of the activated carbon surface was also done using cetyltrimethylammonium tribromide (CTMATB) with an aim to render antibacterial properties to the activated carbon surface. The preparation of such antibacterial activated carbon would aid in the removal/killing of biological pollutants such as bacterial pathogens from water. The physicochemical characterisation of the produced activated carbon was done using different analytical techniques. The prepared activated carbons were then applied for the removal of phenol, 4-nitrophenol, 2,4-dinitrophenol, bisphenol A, coliform bacteria and *Escherichia coli* from water. Besides, theoretical studies were also conducted to understand the mechanism involved in the adsorption process. The outline of the work undertaken in this thesis is shown in Figure 1.9.

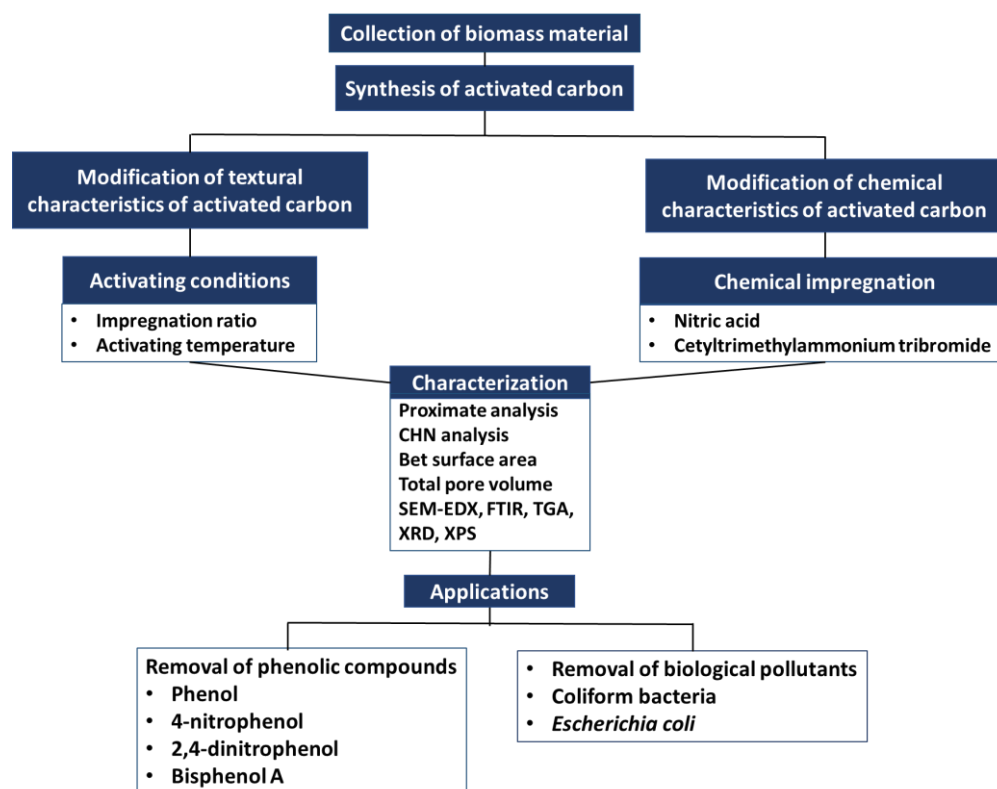


Figure 1.9 Scheme of the present study

1.11 Aims and objectives of the work

The objectives of the present work are as follows:

- To synthesise activated carbon from biomass-based material by chemical activation.
- To modify the physical and chemical characteristics of activated carbon
- Application of the activated carbon for removal of phenolic compounds such as phenol, 4-nitrophenol, 2,4-dinitrophenol and bisphenol A from aqueous medium.
- Removal of biological pollutants such as coliform bacteria and *E.coli* from aqueous medium by the produced activated carbon.
- To evaluate the adsorption process and mechanism using adsorption isotherms, adsorption kinetic models, and thermodynamic studies respectively.
- Theoretical studies to understand the interaction mechanism between the adsorbent and adsorbate.

The outline of the thesis is presented in Figure 1.10.

Chapter 1	Introduction
Chapter 2	Materials and Methods
Chapter 3	Removal of Phenols using activated carbon synthesized from <i>Tithonia diversifolia</i>
Chapter 4	Removal of Coliform bacteria and <i>Escherichia coli</i> using activated carbon synthesized from <i>Tithonia diversifolia</i>
Chapter 5	Removal of 4-nitrophenol using activated carbon synthesized from Ravenna grass
Chapter 6	Removal of <i>Escherichia coli</i> using Ravenna grass activated carbon modified by CTMATB
Chapter 7	Summary and Conclusions

Figure 1.10 Outline of the thesis

References

- [1] R.C. Bansal, M. Goyal, Activated carbon adsorption, 2005. doi:10.1680/bwtse.63341.147.
- [2] Z. Heidarinejad, M.H. Dehghani, M. Heidari, G. Javedan, I. Ali, M. Sillanpää, Methods for preparation and activation of activated carbon: a review, *Environ. Chem. Lett.* 18 (2020) 393–415. doi:10.1007/s10311-019-00955-0.
- [3] J.W. Patrick, Porosity in Carbons: Characterization and Applications, *Porosity in Carbons*. (1995) 253.
- [4] F. Çeçen, Ö. Aktaş, Activated Carbon for Water and Wastewater Treatment: Integration of Adsorption and Biological Treatment, 2011. doi:10.1002/9783527639441.
- [5] Active Carbon. By John W. Hassler. Chemical Publishing Co., Inc., Brooklyn, 1951. vi + 384pp. 14.5 × 23.5cm. Price \$7, J. Am. Pharm. Assoc. (Scientific Ed.). (1951). doi:10.1002/jps.3030400825.
- [6] F. Çeçen, Ö. Aktaş, Water and Wastewater Treatment: Historical Perspective of Activated Carbon Adsorption and its Integration with Biological Processes, in: *Act. Carbon Water Wastewater Treat.*, 2011. doi:10.1002/9783527639441.ch1.
- [7] P.S. Pamidimukkala, H. Soni, Efficient removal of organic pollutants with activated carbon derived from palm shell: Spectroscopic characterisation and experimental optimisation, *J. Environ. Chem. Eng.* (2018). doi:10.1016/j.jece.2018.04.013.
- [8] J. Liu, Y. Liu, J. Peng, Z. Liu, Y. Jiang, M. Meng, W. Zhang, L. Ni, Preparation of High Surface Area Oxidized Activated Carbon from Peanut Shell and Application for the Removal of Organic Pollutants and Heavy Metal Ions, *Water. Air. Soil Pollut.* (2018). doi:10.1007/s11270-018-4021-9.
- [9] A.R. Satayeva, C.A. Howell, A. V. Korobeinyk, J. Jandosov, V.J. Inglezakis, Z.A. Mansurov, S. V. Mikhlovsky, Investigation of rice husk derived activated carbon for removal of nitrate contamination from water, *Sci. Total Environ.* (2018). doi:10.1016/j.scitotenv.2018.02.329.
- [10] J. Li, X. Xing, J. Li, M. Shi, A. Lin, C. Xu, J. Zheng, R. Li, Preparation of thiol-functionalized activated carbon from sewage sludge with coal blending for heavy metal removal from contaminated water, *Environ. Pollut.* 234 (2018) 677–683. doi:10.1016/j.envpol.2017.11.102.
- [11] T.B. Nuria Fiol, Adsorption on Activated Carbon from Olive Stones: Kinetics and Equilibrium of Phenol Removal from Aqueous Solution, *J. Chem. Eng. Process Technol.* 04 (2013). doi:10.4172/2157-7048.1000165.
- [12] M. Hassan, R. Abou-Zeid, E. Hassan, L. Berglund, Y. Aitomäki, K. Oksman, Membranes based on cellulose nanofibers and activated carbon for removal of *Escherichia coli* bacteria from water, *Polymers (Basel)*. (2017). doi:10.3390/polym9080335.

- [13] J. Kazmierczak-Razna, P. Nowicki, R. Pietrzak, Toxic gases removal onto activated carbons obtained from hay with the use of microwave radiation, *Chem. Eng. Res. Des.* (2016). doi:10.1016/j.cherd.2016.02.018.
- [14] R. Yan, T. Chin, Y.L. Ng, H. Duan, D.T. Liang, J.H. Tay, Influence of Surface Properties on the Mechanism of H₂S Removal by Alkaline Activated Carbons, *Environ. Sci. Technol.* (2004). doi:10.1021/es0303992.
- [15] J. Saleem, U. Bin Shahid, M. Hijab, H. Mackey, G. McKay, Production and applications of activated carbons as adsorbents from olive stones, *Biomass Convers. Biorefinery.* (2019). doi:10.1007/s13399-019-00473-7.
- [16] A.E. Ogungbenro, D. V. Quang, K. Al-Ali, M.R.M. Abu-Zahra, Activated Carbon from Date Seeds for CO₂ Capture Applications, in: *Energy Procedia*, 2017. doi:10.1016/j.egypro.2017.03.1370.
- [17] X. Liu, G. Yu, Combined effect of microwave and activated carbon on the remediation of polychlorinated biphenyl-contaminated soil, *Chemosphere.* (2006). doi:10.1016/j.chemosphere.2005.08.030.
- [18] S.E. Hale, M. Elmquist, R. Brändli, T. Hartnik, L. Jakob, T. Henriksen, D. Werner, G. Cornelissen, Activated carbon amendment to sequester PAHs in contaminated soil: A lysimeter field trial, *Chemosphere.* (2012). doi:10.1016/j.chemosphere.2011.12.015.
- [19] G.M. Roy, Activated Carbon Applications in the Food and Pharmaceutical Industries, in: *Act. Carbon Appl. Food Pharm. Ind.*, 1994: pp. 193–200. <https://books.google.com/books?id=nmmpK0oDE20C&pgis=1>.
- [20] F. Mansour, M. Al-Hindi, R. Yahfoufi, G.M. Ayoub, M.N. Ahmad, The use of activated carbon for the removal of pharmaceuticals from aqueous solutions: a review, *Rev. Environ. Sci. Biotechnol.* (2018). doi:10.1007/s11157-017-9456-8.
- [21] Z.G. Wang, J.C. Jiang, X.L. Deng, Y. Xu, Study on the technology of manufacturing granular activated carbon from sawdust for decolorization of liquid, *Linchan Huaxue Yu Gongye/Chemistry Ind. For. Prod.* (2005).
- [22] K. Qureshi, I. Bhatti, R. Kazi, A.K. Ansari, Physical and Chemical Analysis of Activated Carbon Prepared from Sugarcane Bagasse and Use for Sugar Decolorisation, *Int. J. Chem. Biol. Eng.* (2008).
- [23] S. Bashkova, F.S. Baker, X. Wu, T.R. Armstrong, V. Schwartz, Activated carbon catalyst for selective oxidation of hydrogen sulphide: On the influence of pore structure, surface characteristics, and catalytically-active nitrogen, *Carbon N. Y.* 45 (2007) 1354–1363. doi:10.1016/j.carbon.2007.01.005.
- [24] K.K. Lee, G.Y. Han, K.J. Yoon, B.K. Lee, Thermocatalytic hydrogen production from the methane in a fluidized bed with activated carbon catalyst, in: *Catal. Today*, 2004. doi:10.1016/j.cattod.2004.06.080.
- [25] P.W. Albers, J. Pietsch, J. Krauter, S.F. Parker, Investigations of activated carbon catalyst supports from different natural sources, *Phys. Chem. Chem. Phys.* (2003). doi:10.1039/b212210n.

- [26] S.H. Chermahini, F.A.A. Majid, M.R. Sarmidi, Antioxidant properties of cashew leaves' extracts before and after treatment with activated carbon used in cosmetics, *J. Med. Plants Res.* (2011).
- [27] H. Hammani, F. Laghrib, A. Farahi, S. Lahrich, T. El Ouafy, A. Aboulkas, K. El Harfi, M.A. El Mhammedi, Preparation of activated carbon from date stones as a catalyst to the reactivity of hydroquinone: Application in skin whitening cosmetics samples, *J. Sci. Adv. Mater. Devices.* 4 (2019) 451–458. doi:10.1016/j.jsamd.2019.07.003.
- [28] S. Aktas, M.H. Morcali, Platinum recovery from dilute platinum solutions using activated carbon, *Trans. Nonferrous Met. Soc. China* (English Ed. (2011). doi:10.1016/S1003-6326(11)61091-1.
- [29] C.A. Snyders, C.N. Mpinga, S.M. Bradshaw, G. Akdogan, J.J. Eksteen, The application of activated carbon for the adsorption and elution of platinum group metals from dilute cyanide leach solutions, *J. South. African Inst. Min. Metall.* (2013).
- [30] Z. -G Zhao, Adsorption of phenylalanine from aqueous solution onto active carbon and silica gel, *Chinese J. Chem.* 10 (1992) 325–330. doi:10.1002/cjoc.19920100406.
- [31] Sadashiv Bubanale, M Shivashankar, History, Method of Production, Structure and Applications of Activated Carbon, *Int. J. Eng. Res.* (2017). doi:10.17577/ijertv6is060277.
- [32] J. Biscoe, B.E. Warren, An x-ray study of carbon black, *J. Appl. Phys.* 13 (1942) 364–371. doi:10.1063/1.1714879.
- [33] F. Çeçen, Ö. Aktaş, Activated Carbon for Water and Wastewater Treatment, 2011. doi:10.1002/9783527639441.
- [34] R.C. Bansal, M. Goyal, Activated carbon adsorption, CRC Press, Boca Raton, Florida, 2005.
- [35] H. Marsh, F. Rodríguez-Reinoso, Activated Carbon, 2006. doi:10.1016/B978-0-08-044463-5.X5013-4.
- [36] H. Marsh, F. Rodríguez-Reinoso, Activated Carbon, 2006. doi:10.1016/B978-008044463-5/50018-2.
- [37] M.A. Yahya, M.H. Mansor, W.A.A.W. Zolkarnaini, N.S. Rusli, A. Aminuddin, K. Mohamad, F.A.M. Sabhan, A.A.A. Atik, L.N. Ozair, A brief review on activated carbon derived from agriculture by-product, in: *AIP Conf. Proc.*, 2018. doi:10.1063/1.5041244.
- [38] M.L. Mart, M.M. Torres, C.A. Guzm, D.M. Maestri, Preparation and characteristics of activated carbon from olive stones and walnut shells, *Ind. Crops Prod.* 23 (2006) 23–28. doi:10.1016/j.indcrop.2005.03.001.
- [39] H.P.S. Abdul Khalil, M. Jawaaid, P. Firoozian, U. Rashid, A. Islam, H.M. Akil, Activated carbon from various agricultural wastes by chemical activation with KOH: Preparation and characterization, *J. Biobased Mater. Bioenergy.* 7 (2013) 708–714. doi:10.1166/jbmb.2013.1379.

- [40] K.C. Bedin, A.C. Martins, A.L. Cazetta, O. Pezoti, V.C. Almeida, KOH-activated carbon prepared from sucrose spherical carbon: Adsorption equilibrium, kinetic and thermodynamic studies for Methylene Blue removal, *Chem. Eng. J.* 286 (2016) 476–484. doi:10.1016/j.cej.2015.10.099.
- [41] L.R. Radovic, *Chemistry and physics of carbon*, 2007. doi:10.1201/9781420042993.
- [42] J.F. Kwiatkowski, *Activated carbon: Classifications, properties and applications*, 2011.
- [43] S.J. Park, Y.S. Jang, Pore structure and surface properties of chemically modified activated carbons for adsorption mechanism and rate of Cr(VI), *J. Colloid Interface Sci.* (2002). doi:10.1006/jcis.2002.8269.
- [44] Y. El-Sayed, T.J. Bandoz, Adsorption of valeric acid from aqueous solution onto activated carbons: Role of surface basic sites, *J. Colloid Interface Sci.* (2004). doi:10.1016/j.jcis.2003.10.006.
- [45] M. Domingo-García, F.J. López-Garzón, M. Pérez-Mendoza, Effect of some oxidation treatments on the textural characteristics and surface chemical nature of an activated carbon, *J. Colloid Interface Sci.* (2000). doi:10.1006/jcis.1999.6619.
- [46] H.F. Gorgulho, J.P. Mesquita, F. Gonçalves, M.F.R. Pereira, J.L. Figueiredo, Characterization of the surface chemistry of carbon materials by potentiometric titrations and temperature-programmed desorption, *Carbon N. Y.* (2008). doi:10.1016/j.carbon.2008.06.045.
- [47] A. Contescu, M. Vass, C. Contescu, K. Putyera, J.A. Schwarz, Acid buffering capacity of basic carbons revealed by their continuous pK distribution, *Carbon N. Y.* (1998). doi:10.1016/S0008-6223(97)00168-1.
- [48] H.P. Boehm, Surface oxides on carbon and their analysis: A critical assessment, *Carbon N. Y.* (2002). doi:10.1016/S0008-6223(01)00165-8.
- [49] V. Strelko, D.J. Malik, M. Streat, Characterisation of the surface of oxidised carbon adsorbents, *Carbon N. Y.* (2002). doi:10.1016/S0008-6223(01)00082-3.
- [50] R. Hurt, *Chemistry and Physics of Carbon. Volume 27* Edited by Ljubisa R. Radovic (Pennsylvania State University). Marcel Dekker: New York, Basel. 2001. xviii + 416 pp. \$225.00. ISBN 0-8247-0246-8., *J. Am. Chem. Soc.* (2001). doi:10.1021/ja015236x.
- [51] V.A. Garten, D.E. Weiss, A new interpretation of the acidic and basic structures in carbons ii the chromene-carbonium ion couple in carbon, *Aust. J. Chem.* 10 (1957) 309–328. doi:10.1071/CH9570309.
- [52] M.A. Montes-Morán, D. Suárez, J.A. Menéndez, E. Fuente, On the nature of basic sites on carbon surfaces: An overview, in: *Carbon N. Y.*, 2004. doi:10.1016/j.carbon.2004.01.023.
- [53] C. Moreno-Castilla, Adsorption of organic molecules from aqueous solutions on carbon materials, *Carbon N. Y.* (2004). doi:10.1016/j.carbon.2003.09.022.
- [54] J.A. Menéndez-Díaz, I. Martín-Gullón, Chapter 1 Types of carbon adsorbents and their

- production, Interface Sci. Technol. (2006). doi:10.1016/S1573-4285(06)80010-4.
- [55] T.J. Bandoz, Activated Carbon Surfaces in Environmental Remediation, Academic Press, New York, 2006.
- [56] O. Ioannidou, A. Zabaniotou, Agricultural residues as precursors for activated carbon production-A review, Renew. Sustain. Energy Rev. (2007). doi:10.1016/j.rser.2006.03.013.
- [57] G. Jolly, L. Dupont, M. Aplincourt, J. Lambert, Improved Cu and Zn sorption on oxidized wheat lignocellulose, Environ. Chem. Lett. 4 (2006) 219–223. doi:10.1007/s10311-006-0051-4.
- [58] M.A. Yahya, Z. Al-Qodah, C.W.Z. Ngah, Agricultural bio-waste materials as potential sustainable precursors used for activated carbon production: A review, Renew. Sustain. Energy Rev. 46 (2015) 218–235. doi:10.1016/j.rser.2015.02.051.
- [59] P.C. Bhomick, A. Supong, D. Sinha, Organic pollutants in water and its remediation using biowaste activated carbon as greener adsorbent, Int. J. Hydrol. 1 (2017) 31–33. doi:10.15406/ijh.2017.01.00017.
- [60] X.J. Jin, M.Y. Zhang, Y. Wu, J. Zhang, J. Mu, Nitrogen-enriched waste medium density fiberboard-based activated carbons as materials for supercapacitors, Ind. Crops Prod. 43 (2013) 617–622. doi:10.1016/j.indcrop.2012.08.006.
- [61] H. Treviño-Cordero, L.G. Juárez-Aguilar, D.I. Mendoza-Castillo, V. Hernández-Montoya, A. Bonilla-Petriciolet, M.A. Montes-Morán, Synthesis and adsorption properties of activated carbons from biomass of *Prunus domestica* and *Jacaranda mimosifolia* for the removal of heavy metals and dyes from water, Ind. Crops Prod. 42 (2013) 315–323. doi:10.1016/j.indcrop.2012.05.029.
- [62] I. Ozdemir, M. Şahin, R. Orhan, M. Erdem, Preparation and characterization of activated carbon from grape stalk by zinc chloride activation, Fuel Process. Technol. 125 (2014) 200–206. doi:10.1016/j.fuproc.2014.04.002.
- [63] A. Kumar, H.M. Jena, High surface area microporous activated carbons prepared from Fox nut (*Euryale ferox*) shell by zinc chloride activation, Appl. Surf. Sci. 356 (2015) 753–761. doi:10.1016/j.apsusc.2015.08.074.
- [64] T. Getachew, A. Hussien, V.M. Rao, Defluoridation of water by activated carbon prepared from banana (*Musa paradisiaca*) peel and coffee (*Coffea arabica*) husk, Int. J. Environ. Sci. Technol. 12 (2015) 1857–1866. doi:10.1007/s13762-014-0545-8.
- [65] M. Suneetha, B.S. Sundar, K. Ravindhranath, Removal of fluoride from polluted waters using active carbon derived from barks of *Vitex negundo* plant, J. Anal. Sci. Technol. 6 (2015) 15. doi:10.1186/s40543-014-0042-1.
- [66] S. Kumar, A. Gupta, J.P. Yadav, Removal of Fluoride by Thermally Activated Carbon Prepared From Neem and Kikar leaves, J. Environ. Biol. 29 (2008) 227–232.
- [67] R. Mariappan, R. Vairamuthu, A. Ganapathy, Use of chemically activated cotton nut shell carbon for the removal of fluoride contaminated drinking water: Kinetics

- evaluation, Chinese J. Chem. Eng. 23 (2015) 710–721. doi:10.1016/j.cjche.2014.05.019.
- [68] A.S. Ello, L.K.C. De Souza, A. Trokourey, M. Jaroniec, Development of microporous carbons for CO₂ capture by KOH activation of African palm shells, J. CO₂ Util. 2 (2013) 35–38. doi:10.1016/j.jcou.2013.07.003.
- [69] T. Yang, A.C. Lua, Characteristics of activated carbons prepared from pistachio-nut shells by physical activation, J. Colloid Interface Sci. 267 (2003) 408–417. doi:10.1016/S0021-9797(03)00689-1.
- [70] R.A. Shawabkeh, D.A. Rockstraw, R.K. Bhada, Copper and strontium adsorption by a novel carbon material manufactured from pecan shells, Carbon N. Y. 40 (2002) 781–786. doi:10.1016/S0008-6223(01)00198-1.
- [71] V. Fierro, G. Muñoz, A.H. Basta, H. El-Saied, A. Celzard, Rice straw as precursor of activated carbons: Activation with ortho-phosphoric acid, J. Hazard. Mater. 181 (2010) 27–34. doi:10.1016/j.jhazmat.2010.04.062.
- [72] T. Vernersson, P.R. Bonelli, E.G. Cerrella, A.L. Cukierman, Arundo donax cane as a precursor for activated carbons preparation by phosphoric acid activation, Bioresour. Technol. 83 (2002) 95–104. doi:10.1016/S0960-8524(01)00205-X.
- [73] C. Pongener, D. Kibami, K.S. Rao, D. Sinha, Synthesis and Characterization of Activated Carbon from the Biowaste of the Plant Manihot Esculenta, Chem. Sci. Trans. 4 (2015) 59–68. doi:10.7598/cst2015.958.
- [74] O. Üner, Ü. Geçgel, Y. Bayrak, Adsorption of Methylene Blue by an Efficient Activated Carbon Prepared from Citrullus lanatus Rind: Kinetic, Isotherm, Thermodynamic, and Mechanism Analysis, Water. Air. Soil Pollut. 227 (2016) 247. doi:10.1007/s11270-016-2949-1.
- [75] C. Pongener, P. Bhomick, S. Upasana Bora, R.L. Goswamee, A. Supong, D. Sinha, Sand-supported bio-adsorbent column of activated carbon for removal of coliform bacteria and Escherichia coli from water, Int. J. Environ. Sci. Technol. 14 (2017) 1897–1904. doi:10.1007/s13762-017-1274-6.
- [76] C. Peng, X. Bin Yan, R.T. Wang, J.W. Lang, Y.J. Ou, Q.J. Xue, Promising activated carbons derived from waste tea-leaves and their application in high performance supercapacitors electrodes, Electrochim. Acta. 87 (2013) 401–408. doi:10.1016/j.electacta.2012.09.082.
- [77] K.K. Alau, C.E. Gimba, J.A. Kagbu, Preparation of activated carbon from neem (*Azadirachta indica*) husk by chemical activation with H₃PO₄, KOH and ZnCl₂, Arch. Appl. Sci. Res. 2 (2010) 451–455. doi:10.1016/j.cej.2011.07.075.
- [78] D. Mohan, A. Sarswat, V.K. Singh, M. Alexandre-Franco, C.U. Pittman, Development of magnetic activated carbon from almond shells for trinitrophenol removal from water, Chem. Eng. J. 172 (2011) 1111–1125. doi:10.1016/j.cej.2011.06.054.
- [79] C.X. Chen, B. Huang, T. Li, G.F. Wu, Preparation of phosphoric acid activated carbon from sugarcane bagasse by mechanochemical processing, BioResources. (2012).

doi:10.15376/biores.7.4.5109-5116.

- [80] J. Acharya, J.N. Sahu, B.K. Sahoo, C.R. Mohanty, B.C. Meikap, Removal of chromium(VI) from wastewater by activated carbon developed from Tamarind wood activated with zinc chloride, *Chem. Eng. J.* (2009). doi:10.1016/j.cej.2008.11.035.
- [81] D. Prahas, Y. Kartika, N. Indraswati, S. Ismadji, Activated carbon from jackfruit peel waste by H₃PO₄ chemical activation: Pore structure and surface chemistry characterization, *Chem. Eng. J.* (2008). doi:10.1016/j.cej.2007.08.032.
- [82] K. Ramakrishnan, C. Namasivayam, Zinc chloride-activated jatropha husk carbon for removal of phenol from water by adsorption: Equilibrium and kinetic studies, *Toxicol. Environ. Chem.* (2011). doi:10.1080/02772248.2011.575073.
- [83] B.H. Hameed, I.A.W. Tan, A.L. Ahmad, Adsorption isotherm, kinetic modeling and mechanism of 2,4,6-trichlorophenol on coconut husk-based activated carbon, *Chem. Eng. J.* (2008). doi:10.1016/j.cej.2008.01.028.
- [84] R. Malik, D.S. Ramteke, S.R. Wate, Adsorption of malachite green on groundnut shell waste based powdered activated carbon, *Waste Manag.* 27 (2007) 1129–1138. doi:10.1016/j.wasman.2006.06.009.
- [85] N.R. Bishnoi, M. Bajaj, N. Sharma, A. Gupta, Adsorption of Cr(VI) on activated rice husk carbon and activated alumina, *Bioresour. Technol.* 91 (2004) 305–307. doi:10.1016/S0960-8524(03)00204-9.
- [86] Y.X. Wang, H.H. Ngo, W.S. Guo, Preparation of a specific bamboo based activated carbon and its application for ciprofloxacin removal, *Sci. Total Environ.* (2015). doi:10.1016/j.scitotenv.2015.06.087.
- [87] M.S. Shamsuddin, N.R.N. Yusoff, M.A. Sulaiman, Synthesis and Characterization of Activated Carbon Produced from Kenaf Core Fiber Using H₃PO₄ Activation, *Procedia Chem.* (2016). doi:10.1016/j.proche.2016.03.053.
- [88] Y. Huang, Y. Liu, G. Zhao, J.Y. Chen, Sustainable activated carbon fiber from sawdust by reactivation for high-performance supercapacitors, *J. Mater. Sci.* 52 (2017) 478–488. doi:10.1007/s10853-016-0347-0.
- [89] M. Kobya, Removal of Cr(VI) from aqueous solutions by adsorption onto hazelnut shell activated carbon: Kinetic and equilibrium studies, *Bioresour. Technol.* (2004). doi:10.1016/j.biortech.2003.07.001.
- [90] U.D. Hamza, N.S. Nasri, N.S. Amin, J. Mohammed, H.M. Zain, Characteristics of oil palm shell biochar and activated carbon prepared at different carbonization times, *Desalin. Water Treat.* 57 (2016) 7999–8006. doi:10.1080/19443994.2015.1042068.
- [91] I.I. Gurten, M. Ozmak, E. Yagmur, Z. Aktas, Preparation and characterisation of activated carbon from waste tea using K₂CO₃, *Biomass and Bioenergy.* 37 (2012) 73–81. doi:10.1016/j.biombioe.2011.12.030.
- [92] D. Angin, Production and characterization of activated carbon from sour cherry stones by zinc chloride, *Fuel.* 115 (2014) 804–811. doi:10.1016/j.fuel.2013.04.060.

- [93] M. Açıkyıldız, A. Gürses, S. Karaca, Preparation and characterization of activated carbon from plant wastes with chemical activation, *Microporous Mesoporous Mater.* 198 (2014) 45–49. doi:10.1016/j.micromeso.2014.07.018.
- [94] R.H. Gumus, I. Okpeku, Production of Activated Carbon and Characterization from Snail Shell Waste (*Helix pomatia*), *Adv. Chem. Eng. Sci.* 5 (2015) 51–61. doi:10.4236/aces.2015.51006.
- [95] P.S. Thue, M.A. Adebayo, E.C. Lima, J.M. Sieliechi, F.M. Machado, G.L. Dotto, J.C.P. Vaggetti, S.L.P. Dias, Preparation, characterization and application of microwave-assisted activated carbons from wood chips for removal of phenol from aqueous solution, *J. Mol. Liq.* 223 (2016) 1067–1080. doi:10.1016/j.molliq.2016.09.032.
- [96] C. Cheng, H. Liu, P. Dai, X. Shen, J. Zhan, T. Zhao, Z. Zhu, Microwave-assisted preparation and characterization of mesoporous activated carbon from mushroom roots by phytic acid ($C_6H_{18}O_{24}P_6$) activation, *J. Taiwan Inst. Chem. Eng.* 67 (2016) 532–537. doi:10.1016/j.jtice.2016.08.032.
- [97] J. Matos, C. Nahas, L. Rojas, M. Rosales, Synthesis and characterization of activated carbon from sawdust of Algarroba wood. 1. Physical activation and pyrolysis, *J. Hazard. Mater.* 196 (2011) 360–369. doi:10.1016/j.jhazmat.2011.09.046.
- [98] M. Danish, R. Hashim, M.N.M. Ibrahim, M. Rafatullah, T. Ahmad, O. Sulaiman, Characterization of Acacia mangium wood based activated carbons prepared in the presence of basic activating agents, *BioResources.* 6 (2011) 3019–3033. doi:10.1007/s00114-011-0880-2.
- [99] M. Inyang, B. Gao, W. Ding, P. Pullammanappallil, A.R. Zimmerman, X. Cao, Enhanced lead sorption by biochar derived from anaerobically digested sugarcane bagasse, *Sep. Sci. Technol.* 46 (2011) 1950–1956. doi:10.1080/01496395.2011.584604.
- [100] W. Li, K. Yang, J. Peng, L. Zhang, S. Guo, H. Xia, Effects of carbonization temperatures on characteristics of porosity in coconut shell chars and activated carbons derived from carbonized coconut shell chars, *Ind. Crops Prod.* 28 (2008) 190–198. doi:10.1016/j.indcrop.2008.02.012.
- [101] J. Wang, S. Kaskel, KOH activation of carbon-based materials for energy storage, *J. Mater. Chem.* 22 (2012) 23710–23725. doi:10.1039/c2jm34066f.
- [102] A.U. Rajapaksha, M. Vithanage, M. Ahmad, D.C. Seo, J.S. Cho, S.E. Lee, S.S. Lee, Y.S. Ok, Enhanced sulfamethazine removal by steam-activated invasive plant-derived biochar, *J. Hazard. Mater.* 290 (2015) 43–50. doi:10.1016/j.jhazmat.2015.02.046.
- [103] J.M.V. Nabais, P. Nunes, P.J.M. Carrott, M.M.L. Ribeiro Carrott, A.M. García, M.A. Díaz-Díez, Production of activated carbons from coffee endocarp by CO_2 and steam activation, *Fuel Process. Technol.* 89 (2008) 262–268. doi:10.1016/j.fuproc.2007.11.030.
- [104] T. Zhang, W.P. Walawender, L.T. Fan, M. Fan, D. Dugaard, R.C. Brown, Preparation

- of activated carbon from forest and agricultural residues through CO₂ activation, *Chem. Eng. J.* 105 (2004) 53–59. doi:10.1016/j.cej.2004.06.011.
- [105] N. Radenahmad, A.T. Azad, M. Saghir, J. Taweekun, M.S.A. Bakar, M.S. Reza, A.K. Azad, A review on biomass derived syngas for SOFC based combined heat and power application, *Renew. Sustain. Energy Rev.* (2020). doi:10.1016/j.rser.2019.109560.
- [106] C. Bouchelta, M. Salah, O. Bertrand, J. Bellat, Preparation and characterization of activated carbon from date stones by physical activation with steam, 82 (2008) 70–77. doi:10.1016/j.jaap.2007.12.009.
- [107] N. Byamba-Ochir, W.G. Shim, M.S. Balathanigaimani, H. Moon, Highly porous activated carbons prepared from carbon rich Mongolian anthracite by direct NaOH activation, *Appl. Surf. Sci.* (2016). doi:10.1016/j.apsusc.2016.04.082.
- [108] J. Pallarés, A. González-Cencerrado, I. Arauzo, Production and characterization of activated carbon from barley straw by physical activation with carbon dioxide and steam, *Biomass and Bioenergy*. (2018). doi:10.1016/j.biombioe.2018.04.015.
- [109] W. Ao, J. Fu, X. Mao, Q. Kang, C. Ran, Y. Liu, H. Zhang, Z. Gao, J. Li, G. Liu, J. Dai, Microwave assisted preparation of activated carbon from biomass: A review, *Renew. Sustain. Energy Rev.* (2018). doi:10.1016/j.rser.2018.04.051.
- [110] A. Ahmadpour, D.D. Do, The preparation of activated carbon from macadamia nutshell by chemical activation, *Carbon N. Y.* (1997). doi:10.1016/S0008-6223(97)00127-9.
- [111] Y. Sudaryanto, S.B. Hartono, W. Irawaty, H. Hindarso, S. Ismadji, High surface area activated carbon prepared from cassava peel by chemical activation, *Bioresour. Technol.* 97 (2006) 734–739. doi:10.1016/j.biortech.2005.04.029.
- [112] A.A. Arie, Vincent, A. Putranto, Activated carbons from KOH-activation of salacca peels as low cost potential adsorbents for dye removal, *Adv. Mater. Lett.* 7 (2016) 226–229. doi:10.5185/amlett.2016.6194.
- [113] A. Elmouwahidi, Z. Zapata-Benabithé, F. Carrasco-Marín, C. Moreno-Castilla, Activated carbons from KOH-activation of argan (*Argania spinosa*) seed shells as supercapacitor electrodes, *Bioresour. Technol.* 111 (2012) 185–190. doi:10.1016/j.biortech.2012.02.010.
- [114] H. Saygılı, G.A. Saygılı, Optimized preparation for bimodal porous carbon from lentil processing waste by microwave-assisted K₂CO₃ activation: Spectroscopic characterization and dye decolorization activity, *J. Clean. Prod.* (2019). doi:10.1016/j.jclepro.2019.04.121.
- [115] L. Wang, F. Sun, F. Hao, Z. Qu, J. Gao, M. Liu, K. Wang, G. Zhao, Y. Qin, A green trace K₂CO₃ induced catalytic activation strategy for developing coal-converted activated carbon as advanced candidate for CO₂ adsorption and supercapacitors, *Chem. Eng. J.* (2020). doi:10.1016/j.cej.2019.123205.
- [116] Y. Mao, H. Xie, X. Chen, Y. Zhao, J. Qu, Q. Song, Z. Ning, P. Xing, H. Yin, A combined leaching and electrochemical activation approach to converting coal to capacitive carbon in molten carbonates, *J. Clean. Prod.* (2020).

- doi:10.1016/j.jclepro.2019.119218.
- [117] N. Tsubouchi, M. Nishio, Y. Shinohara, J. Bud, Y. Mochizuki, Production of activated carbon from peat by with natural soda ash and effect of nitrogen addition on the development of surface area, *Fuel Process. Technol.* (2018). doi:10.1016/j.fuproc.2018.03.014.
- [118] Y. Gokce, Z. Aktas, Nitric acid modification of activated carbon produced from waste tea and adsorption of methylene blue and phenol, *Appl. Surf. Sci.* 313 (2014) 352–359. doi:10.1016/j.apsusc.2014.05.214.
- [119] A. Kumar, H.M. Jena, Removal of methylene blue and phenol onto prepared activated carbon from Fox nutshell by chemical activation in batch and fixed-bed column, *J. Clean. Prod.* 137 (2016) 1246–1259. doi:10.1016/j.jclepro.2016.07.177.
- [120] M.J.P. Brito, C.M. Veloso, L.S. Santos, R.C.F. Bonomo, R. da C.I. Fontan, Adsorption of the textile dye Dianix® royal blue CC onto carbons obtained from yellow mombin fruit stones and activated with KOH and H₃PO₄: kinetics, adsorption equilibrium and thermodynamic studies, *Powder Technol.* 339 (2018) 334–343. doi:10.1016/j.powtec.2018.08.017.
- [121] L. Cao, I.K.M. Yu, D.C.W. Tsang, S. Zhang, Y.S. Ok, E.E. Kwon, H. Song, C.S. Poon, Phosphoric acid-activated wood biochar for catalytic conversion of starch-rich food waste into glucose and 5-hydroxymethylfurfural, *Bioresour. Technol.* 267 (2018) 242–248. doi:10.1016/j.biortech.2018.07.048.
- [122] K. Legrouiri, E. Khouya, M. Ezzine, H. Hannache, R. Denoyel, R. Pallier, R. Naslain, Production of activated carbon from a new precursor molasses by activation with sulphuric acid, *J. Hazard. Mater.* 118 (2005) 259–263. doi:10.1016/j.jhazmat.2004.11.004.
- [123] J.M. Ketcha, D.J.D. Dina, H.M. Ngomo, N.J. Ndi, Preparation and Characterization of Activated Carbons Obtained from Maize Cobs by Zinc Chloride Activation, *Am. Chem. Sci. J.* 2 (2012) 136–160. doi:http://dx.doi.org/10.9734/acsj.
- [124] B. Wanassi, I. Ben Hariz, C.M. Ghimbeu, C. Vaultot, M. Ben Hassen, M. Jeguirim, Carbonaceous adsorbents derived from textile cotton waste for the removal of Alizarin S dye from aqueous effluent: kinetic and equilibrium studies, *Environ. Sci. Pollut. Res.* 24 (2017) 10041–10055. doi:10.1007/s11356-017-8410-1.
- [125] Z. Xu, Z. Yuan, D. Zhang, W. Chen, Y. Huang, T. Zhang, D. Tian, H. Deng, Y. Zhou, Z. Sun, Highly mesoporous activated carbon synthesized by pyrolysis of waste polyester textiles and MgCl₂: Physiochemical characteristics and pore-forming mechanism, *J. Clean. Prod.* (2018). doi:10.1016/j.jclepro.2018.05.007.
- [126] H. Saygili, F. Güzel, High surface area mesoporous activated carbon from tomato processing solid waste by zinc chloride activation: Process optimization, characterization and dyes adsorption, *J. Clean. Prod.* 113 (2016) 995–1004. doi:10.1016/j.jclepro.2015.12.055.
- [127] A. Siddique, A.K. Nayak, J. Singh, Synthesis of FeCl₃-activated carbon derived from

- waste Citrus limetta peels for removal of fluoride: An eco-friendly approach for the treatment of groundwater and bio-waste collectively, *Groundw. Sustain. Dev.* (2020). doi:10.1016/j.gsd.2020.100339.
- [128] M. Molina-Sabio, F. Rodríguez-Reinoso, Role of chemical activation in the development of carbon porosity, in: *Colloids Surfaces A Physicochem. Eng. Asp.*, 2004. doi:10.1016/j.colsurfa.2004.04.007.
- [129] M.K.B. Gratio, T. Panyathanmaporn, R.A. Chumnanklang, N. Sirinuntawittaya, A. Dutta, Production of activated carbon from coconut shell: Optimization using response surface methodology, *Bioresour. Technol.* (2008). doi:10.1016/j.biortech.2007.09.042.
- [130] Y. Gao, Q. Yue, B. Gao, A. Li, Insight into activated carbon from different kinds of chemical activating agents: A review, *Sci. Total Environ.* 746 (2020). doi:10.1016/j.scitotenv.2020.141094.
- [131] X.Y. Cui, F. Jia, Y.X. Chen, J. Gan, Influence of single-walled carbon nanotubes on microbial availability of phenanthrene in sediment, *Ecotoxicology*. 20 (2011) 1277–1285. doi:10.1007/s10646-011-0684-3.
- [132] N. Rambabu, B.V.S.K. Rao, V.R. Surisetty, U. Das, A.K. Dalai, Production, characterization, and evaluation of activated carbons from de-oiled canola meal for environmental applications, *Ind. Crops Prod.* (2015). doi:10.1016/j.indcrop.2014.09.046.
- [133] J. Lee, J. Kim, T. Hyeon, Recent progress in the synthesis of porous carbon materials, *Adv. Mater.* (2006). doi:10.1002/adma.200501576.
- [134] C.Y. Yin, M.K. Aroua, W.M.A.W. Daud, Review of modifications of activated carbon for enhancing contaminant uptakes from aqueous solutions, *Sep. Purif. Technol.* (2007). doi:10.1016/j.seppur.2006.06.009.
- [135] J. Rivera-Utrilla, M. Sánchez-Polo, V. Gómez-Serrano, P.M. Álvarez, M.C.M. Alvim-Ferraz, J.M. Dias, Activated carbon modifications to enhance its water treatment applications. An overview, *J. Hazard. Mater.* (2011). doi:10.1016/j.jhazmat.2011.01.033.
- [136] M.S. Shafeeyan, W.M.A.W. Daud, A. Houshmand, A. Shamiri, A review on surface modification of activated carbon for carbon dioxide adsorption, *J. Anal. Appl. Pyrolysis*. (2010). doi:10.1016/j.jaap.2010.07.006.
- [137] J.M. Dias, M.C.M. Alvim-Ferraz, M.F. Almeida, J. Rivera-Utrilla, M. Sánchez-Polo, Waste materials for activated carbon preparation and its use in aqueous-phase treatment: A review, *J. Environ. Manage.* (2007). doi:10.1016/j.jenvman.2007.07.031.
- [138] J.Y. Lai, L.H. Ngu, S.S. Hashim, J.J. Chew, J. Sunarso, Review of oil palm-derived activated carbon for CO₂ capture, *Carbon Lett.* (2021). doi:10.1007/s42823-020-00206-1.
- [139] W. Yantasee, Y. Lin, G.E. Fryxell, K.L. Alford, B.J. Busche, C.D. Johnson, Selective removal of copper(II) from aqueous solutions using fine-grained activated carbon functionalized with amine, *Ind. Eng. Chem. Res.* 43 (2004) 2759–2764.

doi:10.1021/ie030182g.

- [140] D. Aggarwal, M. Goyal, R.C. Bansal, Adsorption of chromium by activated carbon from aqueous solution, *Carbon N. Y.* (1999). doi:10.1016/S0008-6223(99)00072-X.
- [141] H. Bin Hoang, H.J. Abanto-Chavez, I.A. Kozhemyakina, K.B. Hoang, O.N. Temkin, Adsorption of $\text{Zn}(\text{OAc})_2$ from aqueous solutions on the surface of activated carbons modified with acetic acid, *Russ. J. Appl. Chem.* 76 (2003) 1418–1422. doi:10.1023/B:RJAC.0000012660.74112.e2.
- [142] R.R.A. Rios, D.E. Alves, I. Dalmázio, S.F.V. Bento, C.L. Donnici, R.M. Lago, Tailoring activated carbon by surface chemical modification with O, S, and N containing molecules, *Mater. Res.* 6 (2003) 129–135. doi:10.1590/s1516-14392003000200004.
- [143] M.M. Maroto-Valer, I. Dranca, T. Lupascu, R. Nastas, Effect of adsorbate polarity on thermodesorption profiles from oxidized and metal-impregnated activated carbons, *Carbon N. Y.* 42 (2004) 2655–2659. doi:10.1016/j.carbon.2004.06.007.
- [144] A. Aburub, D.E. Wurster, Phenobarbital interactions with derivatized activated carbon surfaces, *J. Colloid Interface Sci.* 296 (2006) 79–85. doi:10.1016/j.jcis.2005.08.035.
- [145] A. Bhatnagar, W. Hogland, M. Marques, M. Sillanpää, An overview of the modification methods of activated carbon for its water treatment applications, *Chem. Eng. J.* (2013). doi:10.1016/j.cej.2012.12.038.
- [146] J.A. Menéndez, J. Phillips, B. Xia, L.R. Radovic, On the modification and characterization of chemical surface properties of activated carbon: In the search of carbons with stable basic properties, *Langmuir.* (1996). doi:10.1021/la9602022.
- [147] P.C.C. Faria, J.J.M. Órfão, M.F.R. Pereira, Adsorption of anionic and cationic dyes on activated carbons with different surface chemistries, *Water Res.* (2004). doi:10.1016/j.watres.2004.01.034.
- [148] S. Biniak, G. Szymański, J. Siedlewski, A. Świątkoski, The characterization of activated carbons with oxygen and nitrogen surface groups, *Carbon N. Y.* (1997). doi:10.1016/S0008-6223(97)00096-1.
- [149] F.W. Shaarani, B.H. Hameed, Ammonia-modified activated carbon for the adsorption of 2,4-dichlorophenol, *Chem. Eng. J.* (2011). doi:10.1016/j.cej.2011.03.002.
- [150] H.L. Chiang, C.P. Huang, P.C. Chiang, The surface characteristics of activated carbon as affected by ozone and alkaline treatment, *Chemosphere.* (2002). doi:10.1016/S0045-6535(01)00215-6.
- [151] K.D. Henning, S. Schäfer, Impregnated activated carbon for environmental protection, *Gas Sep. Purif.* 7 (1993) 235–240. doi:10.1016/0950-4214(93)80023-P.
- [152] L. Monser, N. Adhoum, Modified activated carbon for the removal of copper, zinc, chromium and cyanide from wastewater, *Sep. Purif. Technol.* (2002). doi:10.1016/S1383-5866(01)00155-1.

- [153] N. Adhoum, L. Monser, Removal of cyanide from aqueous solution using impregnated activated carbon, *Chem. Eng. Process.* (2002). doi:10.1016/S0255-2701(00)00156-2.
- [154] N. Adhoum, L. Monser, Removal of phthalate on modified activated carbon: Application to the treatment of industrial wastewater, *Sep. Purif. Technol.* 38 (2004) 233–239. doi:10.1016/j.seppur.2003.11.011.
- [155] C.P. Huang, L.M. Vane, Enhancing As⁵⁺ removal by a Fe²⁺-treated activated carbon, *Res. J. Water Pollut. Control Fed.* 61 (1989) 1596–1603.
- [156] R. Leyva Ramos, J. Ovalle-Turrubiarres, M.A. Sanchez-Castillo, Adsorption of fluoride from aqueous solution on aluminum-impregnated carbon, *Carbon N. Y.* (1999). doi:10.1016/S0008-6223(98)00231-0.
- [157] S.A. Dastgheib, T. Karanfil, W. Cheng, Tailoring activated carbons for enhanced removal of natural organic matter from natural waters, *Carbon N. Y.* 42 (2004) 547–557. doi:10.1016/j.carbon.2003.12.062.
- [158] A.R. Yeddou, S. Chergui, A. Chergui, F. Halet, A. Hamza, B. Nadjemi, A. Ould-Dris, J. Belkouch, Removal of cyanide in aqueous solution by oxidation with hydrogen peroxide in presence of copper-impregnated activated carbon, *Miner. Eng.* (2011). doi:10.1016/j.mineng.2011.02.012.
- [159] Y. Zhao, Z.Q. Wang, X. Zhao, W. Li, S.X. Liu, Antibacterial action of silver-doped activated carbon prepared by vacuum impregnation, *Appl. Surf. Sci.* 266 (2013) 67–72. doi:10.1016/j.apsusc.2012.11.084.
- [160] F.S. Arakawa, Q.L. Shimabuku-Biadola, S. de Lima Bazana, M.F. Silva, B.A. de Abreu Filho, R. Bergamasco, Activated carbon impregnation with ag and cu composed nanoparticles for escherichia coli contaminated water treatment, *Can. J. Chem. Eng.* (2019). doi:10.1002/cjce.23471.
- [161] P. Biswas, R. Bandyopadhyaya, Synergistic antibacterial activity of a combination of silver and copper nanoparticle impregnated activated carbon for water disinfection, *Environ. Sci. Nano.* (2017). doi:10.1039/c7en00427c.
- [162] Z. Shi, K.G. Neoh, E.T. Kang, Antibacterial and adsorption characteristics of activated carbon functionalized with quaternary ammonium moieties, *Ind. Eng. Chem. Res.* 46 (2007) 439–445. doi:10.1021/ie0608096.
- [163] G.J.F. Cruz, M.M. Gómez, J.L. Solis, J. Rimaycuna, R.L. Solis, J.F. Cruz, B. Rathnayake, R.L. Keiski, Composites of ZnO nanoparticles and biomass based activated carbon: Adsorption, photocatalytic and antibacterial capacities, *Water Sci. Technol.* 2017 (2017) 492–508. doi:10.2166/wst.2018.176.
- [164] E. Altintig, G. Arabaci, H. Altundag, Preparation and characterization of the antibacterial efficiency of silver loaded activated carbon from corncobs, *Surf. Coatings Technol.* 304 (2016) 63–67. doi:10.1016/j.surfcoat.2016.06.077.
- [165] P.A.S. Vivekanand Gaur, Surface Modification of Activated Carbon for the Removal of Water Impurities, *Water Cond. Purif.* (2008).

- [166] P. Pietrowski, I. Ludwiczak, J. Tyczkowski, Activated carbons modified by Ar and CO₂ plasmas - Acetone and cyclohexane adsorption, *Medziagotyra*. (2012). doi:10.5755/j01.ms.18.2.1919.
- [167] G. Singh, I.Y. Kim, K.S. Lakhi, P. Srivastava, R. Naidu, A. Vinu, Single step synthesis of activated bio-carbons with a high surface area and their excellent CO₂ adsorption capacity, *Carbon N. Y.* 116 (2017) 448–455. doi:10.1016/j.carbon.2017.02.015.
- [168] A. Nayak, B. Bhushan, V. Gupta, P. Sharma, Chemically activated carbon from lignocellulosic wastes for heavy metal wastewater remediation: Effect of activation conditions, *J. Colloid Interface Sci.* 493 (2017) 228–240. doi:10.1016/j.jcis.2017.01.031.
- [169] T. Tay, S. Ucar, S. Karagöz, Preparation and characterization of activated carbon from waste biomass, *J. Hazard. Mater.* 165 (2009) 481–485. doi:10.1016/j.jhazmat.2008.10.011.
- [170] T. Budinova, E. Ekinici, F. Yardim, A. Grimm, E. Björnbom, V. Minkova, M. Goranova, Characterization and application of activated carbon produced by H₃PO₄ and water vapor activation, *Fuel Process. Technol.* 87 (2006) 899–905. doi:10.1016/j.fuproc.2006.06.005.
- [171] J. Donald, Y. Ohtsuka, C.C. Xu, Effects of activation agents and intrinsic minerals on pore development in activated carbons derived from a Canadian peat, *Mater. Lett.* 65 (2011) 744–747. doi:10.1016/j.matlet.2010.11.049.
- [172] S. Yorgun, D. Yildiz, Preparation and characterization of activated carbons from Paulownia wood by chemical activation with H₃PO₄, *J. Taiwan Inst. Chem. Eng.* 53 (2015) 122–131. doi:10.1016/j.jtice.2015.02.032.
- [173] S.M. Yakout, G. Sharaf El-Deen, Characterization of activated carbon prepared by phosphoric acid activation of olive stones, *Arab. J. Chem.* 9 (2016) S1155–S1162. doi:10.1016/j.arabjc.2011.12.002.
- [174] G. Singh, K.S. Lakhi, I.Y. Kim, P. Srivastava, R. Naidu, A. Vinu, Highly efficient method for the synthesis of activated mesoporous biocarbons with extremely high surface area for high pressure CO₂ adsorption, *ACS Appl. Mater. Interfaces.* 9 (2017) 29782–29793. doi:10.1021/acsami.7b08797.
- [175] A. Bin Noor, M. Asri, B. Mohd, Textural Characteristics of Activated Carbons Prepared from Oil Palm Shells Activated with ZnCl₂ and Pyrolysis Under Nitrogen and Carbon Dioxide, *J. Phys. Sci.* 19 (2008) 93–104.
- [176] D. Lozano-Castelló, J.M. Calo, D. Cazorla-Amorós, A. Linares-Solano, Carbon activation with KOH as explored by temperature programmed techniques, and the effects of hydrogen, *Carbon N. Y.* 45 (2007) 2529–2536. doi:10.1016/j.carbon.2007.08.021.
- [177] A.-N.A. El-Hendawy, An insight into the KOH activation mechanism through the production of microporous activated carbon for the removal of Pb²⁺ cations, *Appl. Surf. Sci.* 255 (2009) 3723–3730. doi:10.1016/j.apsusc.2008.10.034.

- [178] H. Deng, G. Li, H. Yang, J. Tang, J. Tang, Preparation of activated carbons from cotton stalk by microwave assisted KOH and K_2CO_3 activation, *Chem. Eng. J.* 163 (2010) 373–381. doi:10.1016/j.cej.2010.08.019.
- [179] L. Giraldo, J.C. Moreno-Pirajan, Synthesis of activated carbon mesoporous from coffee waste and its application in adsorption zinc and mercury ions from aqueous solution, *E-Journal Chem.* (2012). doi:10.1155/2012/120763.
- [180] H. Sayili, F. Güzel, Y. Önal, Conversion of grape industrial processing waste to activated carbon sorbent and its performance in cationic and anionic dyes adsorption, *J. Clean. Prod.* (2015). doi:10.1016/j.jclepro.2015.01.009.
- [181] S. Timur, I.C. Kantarli, E. Ikizoglu, J. Yanik, Preparation of activated carbons from Oreganum stalks by chemical activation, *Energy and Fuels.* (2006). doi:10.1021/ef060219k.
- [182] G.D. Akpen, I.L. Nwaogazie, T.G. Leton, Optimum conditions for the removal of colour from waste water by mango seed shell based activated carbon, *Indian J. Sci. Technol.* (2011). doi:10.17485/ijst/2011/v4i8/30889.
- [183] S. Uçar, M. Erdem, T. Tay, S. Karagöz, Preparation and characterization of activated carbon produced from pomegranate seeds by $ZnCl_2$ activation, *Appl. Surf. Sci.* (2009). doi:10.1016/j.apsusc.2009.06.080.
- [184] G.A. Adebisi, Z.Z. Chowdhury, P.A. Alaba, Equilibrium, kinetic, and thermodynamic studies of lead ion and zinc ion adsorption from aqueous solution onto activated carbon prepared from palm oil mill effluent, *J. Clean. Prod.* 148 (2017) 958–968. doi:10.1016/j.jclepro.2017.02.047.
- [185] Q. Liang, Y. Liu, M. Chen, L. Ma, B. Yang, L. Li, Q. Liu, Optimized preparation of activated carbon from coconut shell and municipal sludge, *Mater. Chem. Phys.* (2020). doi:10.1016/j.matchemphys.2019.122327.
- [186] R.T. Ayinla, J.O. Dennis, H.M. Zaid, Y.K. Sanusi, F. Usman, L.L. Adebayo, A review of technical advances of recent palm bio-waste conversion to activated carbon for energy storage, *J. Clean. Prod.* 229 (2019) 1427–1442. doi:10.1016/j.jclepro.2019.04.116.
- [187] E. Redondo, J. Carretero-González, E. Goikolea, J. Ségalini, R. Mysyk, Effect of pore texture on performance of activated carbon supercapacitor electrodes derived from olive pits, *Electrochim. Acta.* 160 (2015) 178–184. doi:10.1016/j.electacta.2015.02.006.
- [188] D.P. Wilcox, E. Chang, K.L. Dickson, K.R. Johansson, Microbial growth associated with granular activated carbon in a pilot water treatment facility, *Appl. Environ. Microbiol.* (1983). doi:10.1128/aem.46.2.406-416.1983.
- [189] S.R. Ha, S. Vinitnantharat, Competitive removal of phenol and 2,4-dichlorophenol in biological activated carbon system, *Environ. Technol. (United Kingdom)*. 21 (2000) 387–396. doi:10.1080/09593332108618107.
- [190] H. Treviño-Cordero, L.G. Juárez-Aguilar, D.I. Mendoza-Castillo, V. Hernández-

- Montoya, A. Bonilla-Petriciolet, M.A. Montes-Morán, Synthesis and adsorption properties of activated carbons from biomass of *Prunus domestica* and *Jacaranda mimosifolia* for the removal of heavy metals and dyes from water, *Ind. Crops Prod.* 42 (2013) 315–323. doi:10.1016/j.indcrop.2012.05.029.
- [191] J. Liu, J. Yu, D. Li, Y. Zhang, M. Yang, Reduction of bromate in a biological activated carbon filter under high bulk dissolved oxygen conditions and characterization of bromate-reducing isolates, *Biochem. Eng. J.* (2012). doi:10.1016/j.bej.2012.04.004.
- [192] J.D. Lowry, C.E. Burkhead, The role of adsorption in biologically extended activated carbon columns, *J. Water Pollut. Control Fed.* (1980).
- [193] D.O. Cooney, *Activated Charcoal in Medical Applications*, 2nd ed., CRC Press, Boca Raton, Florida, 1995. doi:10.1177/106002809502901129.
- [194] A. Dobashi, Y. Shu, T. Hasegawa, J. Maruyama, S. Iwasaki, Y. Shen, H. Uyama, Preparation of activated carbon by KOH activation from *Amygdalus pedunculata* shell and its application for electric double-layer capacitor, *Electrochemistry.* 83 (2015) 351–353. doi:10.5796/electrochemistry.83.351.
- [195] X. Li, W. Xing, S. Zhuo, J. Zhou, F. Li, S.Z. Qiao, G.Q. Lu, Preparation of capacitor's electrode from sunflower seed shell, *Bioresour. Technol.* 102 (2011) 1118–1123. doi:10.1016/j.biortech.2010.08.110.
- [196] H. Wang, R. Xie, J. Zhang, J. Zhao, Preparation and characterization of distillers' grain based activated carbon as low cost methylene blue adsorbent: Mass transfer and equilibrium modeling, *Adv. Powder Technol.* (2018). doi:10.1016/j.appt.2017.09.027.
- [197] M. Danish, R. Hashim, M.N. Mohamad Ibrahim, O. Sulaiman, Response surface methodology approach for methyl orange dye removal using optimized *Acacia mangium* wood activated carbon, *Wood Sci. Technol.* (2014). doi:10.1007/s00226-014-0659-7.
- [198] B. Dass, P. Jha, Batch adsorption of phenol by improved activated *Acacia nilotica* branches char: Equilibrium, kinetic and thermodynamic studies, *Int. J. ChemTech Res.* (2015).
- [199] M. Zbair, K. Ainassaari, A. Drif, S. Ojala, M. Bottlinger, M. Pirilä, R.L. Keiski, M. Bensitel, R. Brahmi, Toward new benchmark adsorbents: preparation and characterization of activated carbon from argan nut shell for bisphenol A removal, *Environ. Sci. Pollut. Res.* 25 (2018) 1869–1882. doi:10.1007/s11356-017-0634-6.
- [200] M.J. Ahmed, Preparation of activated carbons from date (*Phoenix dactylifera* L.) palm stones and application for wastewater treatments: Review, *Process Saf. Environ. Prot.* (2016). doi:10.1016/j.psep.2016.03.010.
- [201] J.M. Salman, K.A. Al-Saad, Adsorption of 2, 4-dichlorophenoxyacetic acid onto date seeds activated carbon: Equilibrium, kinetic and thermodynamic studies, *Int. J. Chem. Sci.* 10 (2012) 677–690.
- [202] J.M. Salman, V.O. Njoku, B.H. Hameed, Bentazon and carbofuran adsorption onto date seed activated carbon: Kinetics and equilibrium, *Chem. Eng. J.* 173 (2011) 361–

368. doi:10.1016/j.cej.2011.07.066.
- [203] H. El Bakouri, J. Usero, J. Morillo, R. Rojas, A. Ouassini, Drin pesticides removal from aqueous solutions using acid-treated date stones, *Bioresour. Technol.* (2009). doi:10.1016/j.biortech.2008.12.051.
- [204] L. Khezami, R. Capart, Removal of chromium (VI) from aqueous solution by activated carbons: Kinetic and equilibrium studies, *J. Hazard. Mater.* 123 (2005) 223–231. doi:10.1016/j.jhazmat.2005.04.012.
- [205] M.S. Reza, C.S. Yun, S. Afroze, N. Radenahmad, M.S.A. Bakar, R. Saidur, J. Taweekun, A.K. Azad, Preparation of activated carbon from biomass and its' applications in water and gas purification, a review, *Arab J. Basic Appl. Sci.* 27 (2020) 208–238. doi:10.1080/25765299.2020.1766799.
- [206] F.Y. Wang, H. Wang, J.W. Ma, Adsorption of cadmium (II) ions from aqueous solution by a new low-cost adsorbent-Bamboo charcoal, *J. Hazard. Mater.* 177 (2010) 300–306. doi:10.1016/j.jhazmat.2009.12.032.
- [207] N. Rani, A. Gupta, A.K. Yadav, Removal of Cr (VI) form aqueous solutions by *Acacia nilotica* bark, *Environ. Technol.* (2006). doi:10.1080/09593332708618672.
- [208] L. Wang, J. Zhang, R. Zhao, Y. Li, C. Li, C. Zhang, Adsorption of Pb (II) on activated carbon prepared from *Polygonum orientale* Linn.: Kinetics, isotherms, pH, and ionic strength studies, *Bioresour. Technol.* 101 (2010) 5808–5814. doi:10.1016/j.biortech.2010.02.099.
- [209] G. Alagumuthu, M. Rajan, Equilibrium and kinetics of adsorption of fluoride onto zirconium impregnated cashew nut shell carbon, *Chem. Eng. J.* (2010). doi:10.1016/j.cej.2010.01.017.
- [210] C. Namasivayam, D. Sangeetha, Equilibrium and kinetic studies of adsorption of phosphate onto ZnCl₂ activated coir pith carbon, *J. Colloid Interface Sci.* 280 (2004) 359–365. doi:10.1016/j.jcis.2004.08.015.
- [211] C. Namasivayam, D. Sangeetha, Kinetic studies of adsorption of thiocyanate onto ZnCl₂ activated carbon from coir pith, an agricultural solid waste, *Chemosphere.* (2005). doi:10.1016/j.chemosphere.2005.02.051.
- [212] C. Namasivayam, D. Sangeetha, Removal of molybdate from water by adsorption onto ZnCl₂ activated coir pith carbon, *Bioresour. Technol.* (2006). doi:10.1016/j.biortech.2005.05.008.
- [213] M.C. Macías-Pérez, A. Bueno-López, M.A. Lillo-Ródenas, C. Salinas-Martínez de Lecea, A. Linares-Solano, SO₂ retention on CaO/activated carbon sorbents. Part I: Importance of calcium loading and dispersion, *Fuel.* 86 (2007) 677–683. doi:10.1016/j.fuel.2006.09.004.
- [214] Yuliusman, M.P. Ayu, A. Hanafi, A.R. Nafisah, Adsorption of carbon monoxide and hydrocarbon components in motor vehicle exhaust emission using magnesium oxide loaded on durian peel activated carbon, in: *AIP Conf. Proc.*, 2020. doi:10.1063/5.0002351.

- [215] I. Ghouma, M. Jeguirim, S. Dorge, L. Limousy, C. Matei Ghimbeu, A. Ouederni, Activated carbon prepared by physical activation of olive stones for the removal of NO₂ at ambient temperature, *Comptes Rendus Chim.* 18 (2015) 63–74. doi:10.1016/j.crci.2014.05.006.
- [216] H. Nam, S. Wang, H.R. Jeong, TMA and H₂S gas removals using metal loaded on rice husk activated carbon for indoor air purification, *Fuel*. 213 (2018) 186–194. doi:10.1016/j.fuel.2017.10.089.
- [217] X. Zhang, B. Gao, A.E. Creamer, C. Cao, Y. Li, Adsorption of VOCs onto engineered carbon materials: A review, *J. Hazard. Mater.* 338 (2017) 102–123. doi:10.1016/j.jhazmat.2017.05.013.
- [218] A.J. Fletcher, M.J. Kennedy, X.B. Zhao, J.B. Bell, K.M. Thomas, Adsorption of Organic Vapour Pollutants on Activated Carbon, in: *Recent Adv. Adsorpt. Process. Environ. Prot. Secur.*, 2007. doi:10.1007/978-1-4020-6805-8_4.
- [219] H.J. Busscher, R.J.B. Dijkstra, E. Engels, D.E. Langworthy, D.I. Collias, D.W. Bjorkquist, M.D. Mitchell, H.C. Van Der Mei, Removal of two waterborne pathogenic bacterial strains by activated carbon particles prior to and after charge modification, *Environ. Sci. Technol.* 40 (2006) 6799–6804. doi:10.1021/es061282r.
- [220] Y.L. Li, A. Deletic, D.T. McCarthy, Removal of E. coli from urban stormwater using antimicrobial-modified filter media, *J. Hazard. Mater.* (2014). doi:10.1016/j.jhazmat.2014.01.057.
- [221] P. Biswas, R. Bandyopadhyaya, Water disinfection using silver nanoparticle impregnated activated carbon: Escherichia coli cell-killing in batch and continuous packed column operation over a long duration, *Water Res.* (2016). doi:10.1016/j.watres.2016.04.048.
- [222] H. Qiu, L. Lv, B.C. Pan, Q.J. Zhang, W.M. Zhang, Q.X. Zhang, Critical review in adsorption kinetic models, *J. Zhejiang Univ. Sci. A*. 10 (2009) 716–724. doi:10.1631/jzus.A0820524.
- [223] P.C. Bhomick, A. Supong, M. Baruah, C. Pongener, D. Sinha, Pine Cone biomass as an efficient precursor for the synthesis of activated biocarbon for adsorption of anionic dye from aqueous solution: Isotherm, kinetic, thermodynamic and regeneration studies, *Sustain. Chem. Pharm.* 10 (2018) 41–49. doi:10.1016/j.scp.2018.09.001.
- [224] A.H. Sulaymon, T.J. Mohammed, J. Al-najar, Equilibrium and kinetics studies of adsorption of heavy metals onto activated carbon, *Can. J. Chem. Eng. Technol.* 3 (2012) 86–92.

CHAPTER 2

MATERIALS AND METHODS

This chapter describes the materials and methods used in the current research work. The chapter also presents a brief discussion on the various analytical techniques used for this study. The adsorption isotherm models, adsorption kinetic models, and thermodynamic parameters used for understanding the adsorption process is also discussed in detail.

2.1 Raw precursor for the preparation of activated carbon

For the present study, the raw precursors were selected based on their availability, abundance and eco-friendly nature. Two locally available biomass materials, *Tithonia diversifolia* and *Saccharum Ravenna* were selected as the raw precursors for the preparation of the activated carbon. The raw precursors were collected locally at 26° 13' 29.60" N | 94° 28' 35.0" E for *Tithonia diversifolia* and at 26° 16' 23" N | 94° 27' 55" E for Ravenna grass. The plants were cut into small pieces, washed and dried in an oven at 110°C for 48 hours. The dried biomasses were then subjected to chemical activation for the synthesis of activated carbon. A brief description of the biomasses used in the present study is given below.

2.1.1 *Tithonia diversifolia*

Tithonia diversifolia is a flowering plant that belongs to the family Asteraceae. It is commonly known as the tree marigold, Japanese sunflower, Mexican sunflower or Nitobe chrysanthemum. It is a woody herb, annual or perennial and can grow up to 2-3 meters in height. *Tithonia diversifolia* has been regarded as an invasive alien species (Global Invasive Species Database, GISD) which threatens agricultural habitat and is considered as a severe weed of arable land, plantations and waste areas [1]. The plant grows widely in dense populations throughout the humid and sub-humid tropics in Central and South America, Asia and Africa [2] and is usually discarded without proper utilization. The plant's invasive nature, dense and widely distributed population, fast growth and recultivation using the stem cutting method and lightweight seeds [1], makes the plant a renewable, cheaper, reliable and consistent optional precursor for the production of value-added products such as activated carbon. The present study thus explored the use of *Tithonia diversifolia* (Figure 2.1) as a potential precursor for the production of activated carbon[3].



Figure 2.1 Picture showing *Tithonia diversifolia* plant

2.1.2 *Saccharum ravennae*

Saccharum ravennae is a perennial grass and belong to the family Poaceae. It is commonly known as Ravenna grass, elephant grass, hardy pampas grass or plume grass. The plant grows as a large aggressive grass with bamboo-like stems and can attain a height of 4 meters[4]. *Saccharum ravennae* is native to Northern India, Northern Africa and parts of Europe and Asia[5]. The plant grows and spreads rapidly, is highly competitive, and can out-compete and displace native plant species. The plant is generally treated as a noxious weed and has all the characteristics of an invasive species. The plant can grow on a variety of soils and climatic conditions with considerable resistance to drought and frost. Therefore, considering the vast availability, low-cost cultivation, renewability and non-competitive use of *Saccharum ravennae*, the present study explored the use of *Saccharum ravennae* (Figure 2.2) as a raw precursor for the production of activated carbon.



Figure 2.2 Picture showing *Saccharum Ravenna* plant

2.2 Preparation and modification of activated carbon

For the present study, the activated carbon was prepared by following two-step activation processes. First, the raw material was carbonized and second, the carbonized material was activated using KOH at desired temperatures. Further, the textural and chemical properties of the activated carbon were enhanced by following different techniques such as variation of impregnation ratio, variation of activation temperature, or chemical impregnation using nitric acid and cetyltrimethylammonium tribromide (CTMATB). Thus, depending on the requirement, different precursors and different activating/modifying agents were used for synthesizing the activated carbon with desired surface properties. The detailed preparation and modification procedures are described in Chapter 3, 5 and 6.

2.3 Characterisation of activated carbon

The characterization of the activated carbon is an important step to be taken before its application for any purpose. In the current work, the physical and chemical properties of prepared activated carbon were determined using a variety of techniques and analytical instruments. The proximate analysis for the determination of moisture content, ash content, volatile matter and fixed carbon was done according to the guidelines of the American Society for Testing and Materials[6]. Ultimate analysis was also done for the determination of elemental composition. The zero-point charge of the carbon sample was determined by the batch equilibrium method. Further, different analytical instruments were used to fully characterize the prepared activated carbon.

Proximate analysis

The proximate analysis involves heating the activated carbon at variable temperatures to determine the moisture content, volatile matter, fixed carbon and ash content. The detailed experimental procedures of the tests are discussed below.

Moisture Content

A silica crucible was pre-heated at 110°C for 1 h and cooled to room temperature in a desiccator. Then, 1g of the activated carbon sample was placed in the pre-weighed silica crucible and dried at a drier temperature continuously. The drying sample was constantly reweighed at 10 min intervals until a constant weight was obtained. The ratio of change in original weight expressed in percentage gives the moisture content and is calculated using the equation given below[6].

$$\text{Moisture content \%} = \frac{(C - D)}{(C - B)} \times 100$$

where B= Crucible mass(g), C= Crucible mass with original sample(g) and D = Crucible mass after sample heating(g).

Ash Content

A silica crucible was pre-heated in a muffle furnace at 650°C for 1 hour and cooled to room temperature in a desiccator. Thereafter, 1g of activated carbon was placed in the pre-weighed crucible and heated at 650°C in the furnace. The sample was weighed every 3 hours until a constant weight was achieved [7].

$$\text{Ash content \%} = \frac{(D - B)}{(C - B)} \times 100$$

where B = Crucible mass (g), C= Crucible mass with original sample (g), and D= Crucible mass after sample heating(g).

Volatile Matter

A silica crucible was pre-heated at 900°C in a muffle furnace for 10 minutes and cooled to room temperature in a desiccator. Then, 1g of the activated carbon was placed in the pre-heated silica crucible and was further heated at 900°C for 10 minutes with the lid partially closed. The crucible with the sample was collected and cooled in a desiccator for 1 h[6]. The volatile matter was calculated by the equation below.

$$\text{Volatile Matter \%} = \frac{(C - D)}{(C - B)} \times 100$$

where B= Crucible mass(g), C= Crucible mass with original sample(g) and D = Crucible mass after sample heating(g).

Fixed Carbon

The fixed carbon in percentage was obtained by subtracting the sum of percentage composition of volatile matter, moisture content, and ash content from 100 per cent. Fixed carbon of the activated carbon was obtained using the following equation.

$$\text{Fixed Carbon (\%)} = 100 - (\text{volatile matter \%} + \text{ash content \%} + \text{moisture content \%})$$

Ultimate analysis

The ultimate analysis involves the determination of carbon, hydrogen, nitrogen and oxygen in the activated carbon sample. In the present study, CHN elemental analyser was used for the ultimate analysis of all the prepared samples (Model: PE 2400 Series II, Made: Perkin Elmer).

Zero-point charge (pH_{zpc})

Zero-point charge (pH_{zpc}) is the pH at which the net electrical charge of the activated carbon is zero. If the pH of a solution is lower than the zero-point charge of the activated carbon, then the surface of activated carbon would acquire a positive charge (pH < pH_{zpc}) while if the pH is higher than the zero-point charge, the surface would be occupied by negative charges (pH > pH_{zpc})[8].

The batch equilibrium method was used to measure the zero-point charge of the prepared activated carbon samples[9]. For the experiment, 0.1 g of activated carbon was added to different sets of Erlenmeyer flask containing 50 ml of 0.1 M KNO₃ solution. The initial pH values of the mixtures were adjusted between 2 and 12 with 0.1N HNO₃ or 0.1N KOH. The mixture was then sealed and agitated on a shaker for 24 hours after which the final pH values were measured. The difference between the initial pH and final pH values ($\Delta\text{pH} = \text{pH}_{\text{initial}} - \text{pH}_{\text{final}}$) were plotted against the pH_{initial}. The pH_{zpc} occurred when there was no change in the

pH after adsorption. The pH_{zpc} is the point where the plot of ΔpH vs $\text{pH}_{\text{initial}}$ crosses the baseline in the graph.

2.4 Analytical instruments used for characterisation

Different analytical instruments such as Scanning Electron Microscopy with Energy Dispersive X-ray analysis (SEM/EDX), Fourier Transform Infra-Red Spectroscopy (FTIR), X-Ray Diffractometer (XRD), BET surface area Analyser, Thermogravimetric Analyser (TGA) and X-ray photoelectron spectroscopy (XPS) were used for the characterization of the prepared activated carbon samples. Brief descriptions of the different instruments used in the present study are given below.

Scanning Electron Microscopy and Energy Dispersive X-ray analysis (SEM-EDX)

Scanning Electron Microscopy provides useful information on the surface morphological characteristics of any material. Since surface morphology of the activated carbon plays an important role in the adsorbent-adsorbate interaction, Scanning Electron Microscopy (SEM-JEOL/ JSM-6360) was used in the present study to study the morphological structure of the activated carbon. Further, Energy Dispersive X-ray analysis (EDX) was carried out in conjunction with SEM to determine the elemental composition of the activated carbon. EDX systems are generally attached to electron microscopy such as SEM and can identify and quantify each element present in the sample.

Fourier Transform Infra-Red Spectroscopy (FT-IR)

Fourier Transform Infra-Red Spectroscopy (FT-IR) is an important technique to identify the surface chemical functional groups. Thus, the FT-IR spectra of the carbon samples were taken to identify the different functional groups. To record the FT-IR spectra of the samples, pellets were prepared by mixing the activated carbon with KBr in a 1:100 ratio, followed by pressing using a hydraulic pellet press. The FT-IR spectra of the sample pellets were then obtained using the FT-IR spectrometer (Spectrum Two, Perkin Elmer) at a spectral range of 4000 to 400 cm^{-1} and 4 cm^{-1} spectral resolution.

X-Ray Diffractometer (XRD)

X-ray diffraction (XRD) analysis is an important technique to determine the degree of crystallinity of a material based on its diffraction pattern. The method is performed by directing an X-ray beam at the sample and then measuring the intensities and scattering angles of the X-rays leaving the sample. The present work used Powder X-ray diffractometry in which the diffraction pattern is obtained from a powder of the sample. The diffraction patterns

were used to determine the crystalline or amorphous nature of the activated carbon-based on a database of diffraction patterns. The Powder X-ray Diffraction analysis was done using an XRD diffractometer (Model Rigaky-Ultima iv Japan) using $\text{CuK}\alpha$ radiation at the scan rate of 0.2 degrees per minute.

BET Surface Area and Total Pore Volume

Brunauer, Emmett and Teller (BET) analyser is an instrument that measures the specific surface area of a sample, including the pore size distribution. BET measures surface area based on multilayer gas adsorption. In the current study, BET surface area Analyser namely Smart instrument, model no. SS93/02 was used to determine the surface area and pore volume of the activated carbon by measuring N_2 adsorption-desorption isotherm at liquid nitrogen temperature (-195.79°C) by degassing at 300°C for 60 minutes.

Thermogravimetric Analyser (TGA)

Thermogravimetric analysis was employed to understand the thermal stability and examine the decomposition pattern of the carbon samples. The thermogravimetric analysis was done using Thermogravimetric Analyser (Model STA 6000, Make: Perkin Elmer) at a heating rate of $20^\circ\text{C}/\text{min}$ under a nitrogen atmosphere at $20.0\text{ ml}/\text{min}$.

X-ray photoelectron spectroscopy (XPS)

X-ray Photoelectron Spectroscopy (XPS) also known as Electron Spectroscopy for Chemical Analysis (ESCA) is a quantitative technique for measuring the surface elemental composition of a material and also determining the chemical bonding state of the elements. XPS is typically accomplished by irradiating the sample surface with X-rays causing photoelectrons to be emitted from the sample surface. The kinetic energy of the emitted photoelectrons is then measured by an electron energy analyzer. The binding energy and the intensity of the photoelectron peak determine the elemental identity, binding state and quantity of a detected element. In the current work, X-ray photoelectron spectroscopy (XPS) (Model: ESCALAB Xi+ Make: Thermo Fisher Scientific Pvt. Ltd., UK) was used to determine the chemical bonding nature of the elements.

2.5 Application of the prepared activated carbon

The activated carbons prepared in the current work were used for the removal of organic pollutants such as phenolic compounds and biological pollutants from water. The phenolic compounds considered for the current work included phenol, 4-nitrophenol, 2,4-dinitrophenol and Bisphenol A. Batch mode adsorption experiments were conducted for the removal of

these phenolic compounds from water. In each batch experiment, a required dose of adsorbent was placed in a conical flask containing a certain volume of the desired concentration of the phenolic solution. The solution pH was adjusted using NaOH and HCl. The mixtures were then shaken using a rotary shaker at 180 rpm under controlled temperature for the required amount of time. The solution was then filtered and the residual phenolic concentration was determined using UV-Visible Spectrophotometer (Model: lambda 35, Make: Perkin Elmer). The removal percentage of the phenolic compounds and activated carbon adsorption capacity was calculated using equations 1 and 2 respectively,

$$\text{Removal percentage} = \frac{C_0 - C_e}{C_0} \times 100 \quad (1)$$

$$q_e = \frac{(C_0 - C_e)}{M} V \quad (2)$$

where C_0 is the initial phenol concentration (mg L^{-1}), C_e is the phenol concentration at equilibrium (mg L^{-1}), q_e is the amount of adsorbate adsorbed at equilibrium (mg g^{-1}), M is the mass of activated carbon (g) and V is the volume of the solution (L).

The detailed batch mode experiments for the removal of phenolic compounds are discussed in Chapters 3 and 5.

The water-borne pathogens considered for the current study were coliform bacteria and *Escherichia coli* bacteria. Fixed bed method was used for the removal of these pathogens from water. The activated carbon was tightly packed in glass columns of 2cm in diameter and 30 cm in length. Bacterial solutions were then allowed to run through the column at a flow rate of 1mL /min. The bacterial concentrations were determined at various time intervals at the outlet of the activated carbon column and the standard plate count method was used for the determination of bacterial concentration. The log reduction of the bacteria by the filter column was determined using equation 3,

$$\log_{10} \text{reduction} = -\log_{10} \left(\frac{N}{N_0} \right) \quad (3)$$

where N and N_0 are the final and initial bacterial concentration in CFU/ml respectively.

The detailed experimental set up for the removal of coliform and *Escherichia coli* bacteria are described in Chapter 4.

2.6 Description of pollutants considered for the present study

A brief description of the different pollutants considered for the current work is presented in the following section.

Phenolic compounds

Phenolic compounds are a group of organic compounds with one or more hydroxyl groups directly bonded to the carbon atom of aromatic rings. These compounds enter into water bodies through natural, agricultural, industrial and domestic activities. Phenolic compounds are highly toxic and inflict both severe and long-lasting effects on both humans and animals. Because of their toxicity, poor biodegradability and persistence in the environment, phenolic compounds have been enlisted by the United States Environmental Protection Agency (USEPA) and the European Union (EU) as pollutants of priority concern[10]. The current work thus focused on the removal of four phenolic compounds from water, *Viz.*, Phenol, 4-Nitrophenol, 2,4-Dinitrophenol and Bisphenol-A.

Phenol

Phenol is an aromatic organic compound with the molecular formula C_6H_5OH and 94.11 g/mol molecular weight. The molecule consists of a phenyl group ($-C_6H_5$) bonded to a hydroxy group ($-OH$) (Figure 2.3). Phenol occurs either as a white crystalline solid or colourless liquid at room temperature. Phenol is used in the manufacturing of plastics, fertilizers, rubber, adhesives and paper etc. It is also used in the production of other commercially important materials such as slimicides, general disinfectants, mouthwashes, antiseptic solutions, etc[11]. The most common sources of phenol in natural water include wastewaters from the manufacturing industries and effluents from synthetic fuel manufacturing units.

Human exposure to phenol may irritate the throat, eyes, skin, nose, and nervous system. It can also cause detrimental health effects including nausea, vomiting, headache, pancreas damage, liver and kidney injury, cancer, skin burns, diarrhoea, tissue erosion, protein degeneration and nervous system paralysis [4–6].

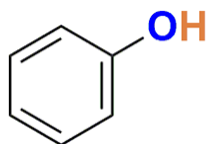


Figure 2.3 Chemical structure of phenol

4-Nitrophenol

4-Nitrophenol is a phenolic compound that has a nitro group (NO_2) at the para position of the hydroxyl group on the benzene ring (Figure 2.4). The chemical formula for 4-nitrophenol is $\text{C}_6\text{H}_5\text{NO}_3$ and the molecular weight is 139.11 g/mol. It appears as a white to light yellow solid with no odour. 4-Nitrophenol is used in manufacturing drugs, insecticides, fungicides, and dyes and to darken leather. The main cause of pollution by 4-nitrophenol in waterbodies is the untreated effluent discharged from these manufacturing industries. Acute ingestion or inhalation of 4-nitrophenol in humans causes headaches, drowsiness, nausea, and cyanosis. Contact with eyes and skin causes may cause severe irritation[12]. Long term exposure to 4-nitrophenol may leave chronic impacts such as damage to kidney, liver, and gastrointestinal tract, cardiovascular diseases, protein degeneration, central nervous system disorder, tissue erosion, muscle weakening and vertigo etc [13–16].

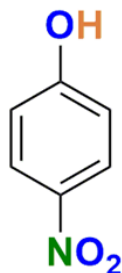


Figure 2.4 Chemical structure of 4-nitrophenol

2,4-dinitrophenol

2,4-dinitrophenol is an organic aromatic compound containing a benzene ring that carries a single hydroxyl group and two nitro groups (Figure 2.5). It appears as solid white crystals with the chemical formula $\text{C}_6\text{H}_4\text{N}_2\text{O}_5$ and 184.11 g/mol molecular weight. 2,4-Dinitrophenol is mainly used as pesticides, fungicides, herbicides, and insecticides and in the manufacture of dyes, wood preservatives[17]. The acute effects of 2,4-dinitrophenol in humans through oral exposure are vomiting, fatigue, nausea, sweating, headaches and dizziness. Contact with skin and eyes can cause severe irritation and burns. Long-term exposure to 2,4-dinitrophenol may damage the eyes causing cataracts, liver, kidney, blood cells and central nervous system[18].

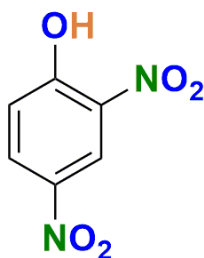


Figure 2.5 Chemical structure of 2,4-dinitrophenol

Bisphenol A

Bisphenol A (BPA) is an organic synthetic compound with two hydroxyphenyl groups and has the chemical formula $(\text{CH}_3)_2\text{C}(\text{C}_6\text{H}_4\text{OH})_2$ (Figure 2.6). Its molecular weight is 228.29 g/mol and is a colourless solid that is soluble in organic solvents, but poorly soluble in water. Bisphenol A is primarily used in the production of polycarbonate plastics and epoxy resins. It is also used as a preservative, in medicine and the manufacture of pesticides [19]. Most BPA pollutants are introduced into the aquatic environment primarily through discharges from domestic and industrial wastewater treatment plants [20]. Bisphenol A is an estrogen-like endocrine-disrupting chemical that is highly toxic, mutagenic and carcinogenic to humans [21]. Humans' exposure to BPA can cause prolonged adverse effects such as reproductive system malfunction, disruption of thyroid function, hypertension, diabetes mellitus, insulin resistance, cardiovascular diseases, blood disorders and hormone-dependent cancer [22,23].

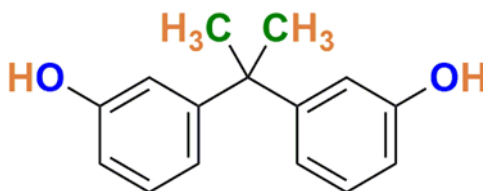


Figure 2.6 Chemical structure of Bisphenol A

Biological pollutants

Biological pollutants include bacteria, viruses, and parasites that are responsible for waterborne diseases, such as cholera, typhoid fever, polio, hepatitis, dysentery and schistosomiasis[24]. The major sources of these pollutants in water are discharge of untreated or partially treated municipal wastewater, poor sanitation and hygiene, open defecation, industrial and agricultural waste, and solid or semisolid refuse[25]. The biological pollutants considered for the current work include coliform bacteria and *Escherichia coli*.

Coliform bacteria include a large group of many types of bacteria, belonging to the genera *Enterobacter*, *Klebsiella*, *Escherichia*, *Hafnia* and certain strains of *Citrobacter*. They are Gram-negative, non-spore-forming, rod-shaped bacteria capable of growing at 35-37°C and ferment lactose with the production of acid and gas[26]. Coliform bacteria are present in the faeces of warm-blooded animals/humans and also in the environment (soil and vegetation). The presence of coliforms in water may not necessarily indicate faecal contamination, as it can also be caused by the entry of soil or organic matter into the water or by conditions suitable for the growth of other types of coliform. However, their detection in water indicates the likelihood of the presence of other harmful pathogens.

Among the coliform bacteria, the detection of *Escherichia coli* in water is significant as it serves as definitive proof of faecal contamination[27]. *Escherichia coli* is a gram-negative rod-shaped bacterium that can grow at 44-45°C and ferments lactose with the production of acid and gas. *Escherichia coli* is found in abundance in the faeces of animals and humans, therefore, the presence of *Escherichia coli* in water is a clear indication of recent faecal contamination. The consumption of *Escherichia coli* contaminated water can cause severe illnesses such as diarrhoea, respiratory illness, urinary tract infections, pneumonia, especially among children and the elderly population[28].

2.7 Adsorption models

Adsorption models provide valuable information on the efficiency of an adsorbent, the rate at which the adsorbent removes a target pollutant and the thermodynamic nature of the adsorption system[29]. Furthermore, these models help in determining the mechanism of the adsorption process. Therefore, in the current work, the experimental adsorption data were fitted to different established mathematical equations and models to understand the adsorption process. The different isotherm models, kinetic models and thermodynamic equations that were used are discussed below.

2.7.1 Adsorption isotherms

Adsorption isotherms are essential to describe the interaction of pollutants with adsorbent surfaces and are useful to optimize the design of the adsorption system for the removal of pollutants from aqueous solutions[30]. Adsorption isotherms are invaluable tools that provide information on the surface properties of the adsorbent, adsorption mechanisms and adsorption affinities.

Adsorption isotherms represent the equilibrium concentration of the adsorbate on the surface of an adsorbent (q_e), as a function of the concentration of the adsorbate in solution (C_e), at a constant temperature. The relationship between these ' q_e ' and ' C_e ' are normally fitted to one or more equilibrium isotherm models. Several isotherm models are available for analysing the experimental adsorption parameters and the most common isotherm models used for the application of activated carbon in water include Langmuir, Freundlich, Temkin and Elovich models.

(a) Langmuir isotherm model

Langmuir isotherm model, proposed by Irving Langmuir assumes that adsorption takes place on a homogeneous active site and no interactions occur between two adsorbate molecules on

adjacent sites[31]. It corresponds to monolayer coverage of the adsorbate at the surface of the adsorbent and indicates chemisorption. The linear form of the Langmuir isotherm model is given by equation 4.

$$\frac{C_e}{q_e} = \frac{1}{q_m} C_e + \frac{1}{q_m K_L} \quad (4)$$

where C_e = adsorbate concentration at equilibrium (mg L^{-1}), q_e = amount of adsorbate per gram of adsorbent at equilibrium (mg g^{-1}), K_L = Langmuir isotherm constant (L mg^{-1}), q_m = maximum adsorption capacity of the adsorbent (mg g^{-1}).

Another important parameter of Langmuir isotherm is the dimensionless separation factor (R_L), which determines the favourability of the adsorption process [32]. The R_L is given by equation 5,

$$R_L = \frac{1}{1 + K_L C_0} \quad (5)$$

The value of R_L indicates the adsorption process to be either unfavourable ($R_L > 1$), favourable ($0 < R_L < 1$), linear ($R_L = 1$) or irreversible ($R_L = 0$) [33].

(b) Freundlich isotherm model

Freundlich model describes a heterogeneous system with non-uniform distribution of adsorption heat on the surface of the adsorbent and applies to multilayer adsorption processes [34]. The linear form of the Freundlich adsorption isotherm model is given by equation 6.

$$\log q_e = \log K_F + \frac{1}{n} \log C_e \quad (6)$$

where C_e = adsorbate concentration at equilibrium (mg L^{-1}), q_e = amount of adsorbate per gram of adsorbent at equilibrium (mg g^{-1}), K_F = Freundlich adsorption capacity constant (mg g^{-1}) (L mg^{-1}) $^{1/n}$ and n = Freundlich adsorption intensity.

The Freundlich adsorption intensity ‘ n ’ describes the adsorption intensity. The higher the ‘ n ’ value, the stronger will be the adsorption intensity. Also, if the value of ‘ $1/n$ ’ is less than unity, the adsorption process is said to follow a normal Langmuir isotherm and if $1/n$ is greater than unity, it specifies the cooperative nature of the adsorption process[34].

(c) Temkin isotherm model

Temkin isotherm assumes that the adsorption heat decreases linearly with surface coverage because of adsorbate-adsorbent interaction and the adsorption is characterized by a uniform

distribution of binding energies [35]. The linear form of the Temkin isotherm model is given by equation 7.

$$q_e = B_T \ln C_e + B_T \ln A_T \quad (7)$$

$$B_T = \frac{RT}{b_T} \quad (8)$$

where B_T is the Temkin constant related to the heat of sorption (J mol^{-1}), A_T = Temkin isotherm equilibrium binding constant (L mg^{-1}), b_T = Temkin isotherm constant (kJ mol^{-1}), R = universal gas constant ($8.314 \text{ J mol}^{-1} \text{ K}^{-1}$) and T = Temperature at 298 K

(d) Dubinin–Radushkevich (D-R) isotherm model

The Dubinin–Radushkevich (D-R) isotherm model helps in determining the porosity apparent free energy and the characteristic of adsorption [36]. The Dubinin–Radushkevich (D-R) helps in determining whether the adsorption proceeds through a physical or chemical process. The mean free energy (E) obtained from the D-R model gives information about the adsorption mechanism, its value in the range of $1\text{--}8 \text{ kJ mol}^{-1}$ is indicative of physical adsorption, while the value between $8\text{--}16 \text{ kJ mol}^{-1}$ indicates chemical adsorption [37].

The linear form of the D-R isotherm model is given by equation 9.

$$\ln q_e = \ln q_{DR} - \beta \epsilon^2 \quad (9)$$

$$\epsilon = RT \ln \left(1 + \frac{1}{C_e} \right) \quad (10)$$

Further, the mean free energy is calculated by using equation 11.

$$E = \frac{1}{(2\beta)^{\frac{1}{2}}} \quad (11)$$

where q_e = amount of adsorbate per gram of adsorbent at equilibrium (mg g^{-1}), q_{DR} = theoretical monolayer adsorption capacity (mg g^{-1}), β = D-R constant, ϵ = Polanyi potential, E = mean free energy (kJ mol^{-1}), R = universal gas constant ($8.314 \text{ J mol}^{-1} \text{ K}^{-1}$) and T = Temperature at 298 K.

2.7.2 Adsorption kinetics

The adsorption kinetics studies aid in assessing the adsorption mechanisms in terms of order and rate constants and provides useful information on possible rate-controlling steps [38]. Four kinetic models namely pseudo-first-order, pseudo-second-order, intraparticle diffusion and Elovich model were employed to examine the kinetics of the adsorption processes in the current study.

(a) Pseudo-first-order model

The pseudo-first-order kinetic model proposed by Lagergren gives a simple kinetic evaluation of the adsorption of adsorbate from a liquid phase to a solid phase[39]. The pseudo-first-order model assumes that physical interactions such as van der Waals forces, π - π type of interactions and hydrogen bonding are the rate-limiting step [40]. The linear form of the pseudo-first-order model is given by equation 12.

$$\log(q_e - q_t) = \log q_e - \frac{k_1}{2.303} t \quad (12)$$

where q_e = equilibrium adsorption capacity (mg g^{-1}), q_t = adsorption capacity at time t (mg g^{-1}), k_1 = rate constant of pseudo-first-order (min^{-1}).

(b) Pseudo-second-order model

The pseudo-second-order model is based on adsorption equilibrium capacity and describes the chemisorptive behaviour of the adsorption process (Ho and McKay, 2000). The pseudo-second-order assumes that the rate constant is proportional to the occupied active adsorption sites[41]. The linear form of the pseudo-second-order rate model is expressed by equation 13.

$$\frac{t}{q_t} = \frac{1}{k_2 q_e^2} + \frac{1}{q_e} t \quad (13)$$

where q_e = equilibrium adsorption capacity (mg g^{-1}), q_t = adsorption capacity at time t (mg g^{-1}), k_2 = rate constant of pseudo-second-order (min^{-1}).

(c) Elovich model

The Elovich model developed by Zeldowitsch is used to further understand the kinetics of chemisorption of the adsorbate on the solid surface of the adsorbent. The Elovich model helps in the prediction of mass and surface diffusion as well as activation and deactivation energy of a system. The model assumes that the rate of adsorption of solute decreases exponentially as the amount of adsorbed solute increase[42]. The linear form of the Elovich model is given by equation 14.

$$q_t = \frac{1}{b} \ln(ab) + \frac{1}{b} \ln t \quad (14)$$

where q_t is the amount of adsorption at any time, t is the time, a = initial adsorption coefficient ($\text{mg g}^{-1} \text{min}^{-1}$), b = desorption coefficient (g mg^{-1})

(d) Intraparticle diffusion model

The Intra-particle diffusion model proposed by Weber and Morris (1963)[43] was used to identify the diffusion mechanism and the rate-limiting step. The intraparticle diffusion model

divides the adsorption into two main stages including the migration of adsorbate from aqueous solution to the surface of the adsorbent and the diffusion of adsorbate molecules into the inner pores of the adsorbent [44]. The expression for the intraparticle diffusion model [43] is given by equation 15.

$$q_t = k_p t^{1/2} + C \quad (15)$$

where q_t is the amount of adsorption at any time, t is the time, k_p = intra-particle diffusion rate constant ($\text{mg g}^{-1} \text{min}^{1/2}$) and C = thickness of the boundary layer.

In the intraparticle diffusion model, q_t is plotted against the square root of time $t^{1/2}$. If the plot gives a linear curve then the intraparticle diffusion is involved in the adsorption process and if the lines pass through the origin then intraparticle diffusion is the rate-limiting step.

2.7.3 Validation of the adsorption models

Chi-squared test (χ^2) and Residual root mean square (RMSE) analysis were employed to determine the most favourable fit of adsorption isotherm and kinetic models to the experimental data. The Chi-square test is given by the equation 16[45].

$$\chi^2 = \sum_{i=1}^n \frac{(q_{e(\text{exp})} - q_{e(\text{cal})})^2}{q_{e(\text{cal})}} \quad (16)$$

The similarity of data obtained from various isotherm and kinetic models to the experimental data would result in a smaller χ^2 value wherein, the χ^2 will be a large number if there is a variation between the data obtained from the model and the experimental data.

RMSE can be defined as [46].

$$RMSE = \sqrt{\frac{1}{n-2} \sum_{i=1}^n (q_{e(\text{exp})} - q_{e(\text{cal})})^2} \quad (17)$$

The smaller value of RMSE would give rise to better-fitting of the curve. The subscripts “exp” and “cal” correspond to the experimental and calculated values respectively while n represents the number of observations.

2.8 Thermodynamic studies

Thermodynamic studies were done to determine the effect of temperature on the adsorption process. The adsorption thermodynamics study provides more knowledge about the internal energy changes during the adsorption process. The important parameters such as Gibbs free energy change (ΔG), enthalpy change (ΔH) and entropy change (ΔS) were determined to

understand the thermodynamics of the adsorption process. The standard enthalpy change (ΔH) and the standard entropy change (ΔS) were calculated by the Van't Hoff equation,

$$\ln K_d = \frac{\Delta S}{R} - \frac{\Delta H}{RT} \quad (18)$$

while the distribution adsorption coefficient (K_d) and Gibbs free energy change (ΔG) was deduced by equation 19 and 20 respectively.

$$K_d = \frac{q_e}{C_e} \quad (19)$$

$$\Delta G = \Delta H - T\Delta S \quad (20)$$

where K_d = distribution adsorption coefficient, T is the absolute temperature (K), q_e is the adsorbed concentration of BPA on the adsorbent (mg/g), C_e is the adsorbate concentration at equilibrium (mg/L), ΔS corresponds to entropy change (J/mol/K), ΔH represents the enthalpy change (J/mol), ΔG (J/mol) is Gibbs free energy change and R corresponds to the universal gas constant (8.314 J/mol K)

2.9 Density Functional theory (DFT) studies

Theoretical study using the density functional theory calculation was used to further understand the possible interaction of adsorbate and activated carbon at the molecular level. Density Functional Theory was implemented because of its simplicity and computational efficiency. All the geometry optimizations, as well as frequency and energy calculations, were performed on the Gaussian 09W[47] program package using DFT employing the B3LYP hybrid functional at basis set 6-31g level of theory in a dielectric medium of $\epsilon = 80$ (corresponding to water). Different activated carbon models were considered and Gauss View 05 was used to produce all the structures which were optimized in their electronic ground state. The adsorption energy (E_{adsorp}) of an adsorbate on the carbon surface was calculated using equation 21.

$$E_{\text{adsorp}} = E_{xy} - (E_x + E_y) \quad (21)$$

where E_{xy} is the total energy of the adsorbate and activated carbon in an equilibrium state, E_x is the total energy of the adsorbate molecule and E_y is the total energy of the activated carbon. Generally, the higher the negative value of E_{adsorp} the stronger the adsorption. Usually, if E_{adsorp} is less than -30 KJ mol^{-1} , the interactions belong to physisorption; whereas, if E_{adsorp} is greater than -50 KJ mol^{-1} , the interactions belong to chemisorption [48].

The application of Density Functional theory in adsorption studies would provide a clear understanding of the adsorption phenomenon under study. Such studies could not only improve our understanding of the bonding and reactivity between the adsorbate and adsorbent but also help in designing an effective adsorbent for a specific adsorbate removal.

References

- [1] J.I. Muoghalu, Growth, reproduction and resource allocation of *Tithonia diversifolia* and *Tithonia rotundifolia*, *Weed Res.* 48 (2008) 157–162. doi:10.1111/j.1365-3180.2007.00613.x.
- [2] B. Jama, C. Palm, R. Buresh, A. Niang, C. Gachengo, G. Nziguheba, B. Amadalo, *Tithonia diversifolia* as a green manure for soil fertility improvement in western Kenya: A review, *Agrofor. Syst.* 49 (2000) 201–221. doi:10.1023/A:1006339025728.
- [3] R. Gualberto, O.F. Souza Júnior, N.R. Costa, C.D. Braccialli, L.A. Gaion, Influence of space and plant development stadium on the production of biomass and nutritional value of *Tithonia diversifolia* (HEMSL.) Gray, *Nucleus.* (2011). doi:10.3738/1982.2278.362.
- [4] M.A. VINCENT, R.L. GARDNER, Spread of the Invasive Ravenna Grass (*Tripsidium Ravennae*, Poaceae) in Ohio, *Phytoneuron.* 78 (2016) 1–9.
- [5] USDA-GRIN, Germplasm Resources Information Network (GRIN)., Germplasm Resour. Inf. Network, Natl. Germplasm Resour. Lab. Beltsville, Maryland. (2015).
- [6] ASTM, Standard method for chemical analysis of wood charcoal, *Am. Soc. Test. Mater.* (1990) 292–293.
- [7] ASTM D 2866 –94, Standard Test Method for Total Ash Content of Activated Carbon, *Current.* 15 (2004) 1–2. doi:10.1520/D2866-11.2.
- [8] B. Wanassi, I. Ben Hariz, C.M. Ghimbeu, C. Vaultot, M. Ben Hassen, M. Jeguirim, Carbonaceous adsorbents derived from textile cotton waste for the removal of Alizarin S dye from aqueous effluent: kinetic and equilibrium studies, *Environ. Sci. Pollut. Res.* 24 (2017) 10041–10055. doi:10.1007/s11356-017-8410-1.
- [9] B.M. Babic, S.K. Milonjic, M.J. Polovina, B. V. Kaludierovic, Point of zero charge and intrinsic equilibrium constants of activated carbon cloth, *Carbon N. Y.* 37 (1999) 477–481. doi:10.1016/S0008-6223(98)00216-4.
- [10] C. Mahugo-Santana, Z. Sosa-Ferrera, M.E. Torres-Padrón, J.J. Santana-Rodríguez, Analytical methodologies for the determination of nitroimidazole residues in biological and environmental liquid samples: A review, *Anal. Chim. Acta.* (2010). doi:10.1016/j.aca.2010.03.022.
- [11] M. Abdollahi, S. Hassani, M. Derakhshani, Phenol, in: *Encycl. Toxicol.* Third Ed., 2014. doi:10.1016/B978-0-12-386454-3.00420-6.
- [12] M. Abdollahi, A. Mohammadirad, Nitrophenol, 4-, in: *Encycl. Toxicol.* Third Ed., 2014. doi:10.1016/B978-0-12-386454-3.01143-X.
- [13] R.R. Karri, J.N. Sahu, N.S. Jayakumar, Optimal isotherm parameters for phenol adsorption from aqueous solutions onto coconut shell based activated carbon: Error analysis of linear and non-linear methods, *J. Taiwan Inst. Chem. Eng.* 80 (2017) 472–487. doi:10.1016/j.jtice.2017.08.004.
- [14] E. Z-Flores, M. Abatal, A. Bassam, L. Trujillo, P. Juárez-Smith, Y. El Hamzaoui, Modeling the adsorption of phenols and nitrophenols by activated carbon using genetic programming, *J. Clean. Prod.* 161 (2017) 860–870. doi:10.1016/j.jclepro.2017.05.192.

- [15] A. Sukan, S. Sargin, Enzymatic Removal of Phenol from Industrial Wastewaters, *J. Biomater. Nanobiotechnol.* 04 (2013) 300–307. doi:10.4236/jbnb.2013.43038.
- [16] L.G.C. Villegas, N. Mashhadi, M. Chen, D. Mukherjee, K.E. Taylor, N. Biswas, A Short Review of Techniques for Phenol Removal from Wastewater, *Curr. Pollut. Reports.* 2 (2016) 157–167. doi:10.1007/s40726-016-0035-3.
- [17] D. Janz, Dinitrophenols, in: *Encycl. Toxicol.*, 2005. doi:10.1016/B0-12-369400-0/00336-7.
- [18] D.M. Janz, Dinitrophenols, in: *Encycl. Toxicol. Third Ed.*, 2014. doi:10.1016/B978-0-12-386454-3.00135-4.
- [19] J. Reddy, L. Prasanna, J. Singh, K. Choo, Effective removal of bisphenol A (BPA) from water using a goethite / activated carbon composite, *Process Saf. Environ. Prot.* 103 (2016) 87–96. doi:10.1016/j.psep.2016.06.038.
- [20] A.O. Ifelebuegu, J.E. Ukpebor, C.C. Obidiegwu, B.C. Kwofi, Comparative potential of black tea leaves waste to granular activated carbon in adsorption of endocrine disrupting compounds from aqueous solution, *Glob. J. Environ. Sci. Manag.* 1 (2015) 205–214. doi:10.7508/GJESM.2015.03.003.
- [21] R. Wirasnita, T. Hadibarata, A.R.M. Yusoff, Z. Yusop, Removal of bisphenol a from aqueous solution by activated carbon derived from oil palm empty fruit bunch, *Water. Air. Soil Pollut.* 225 (2014) 2148. doi:10.1007/s11270-014-2148-x.
- [22] J.R. Kim, S.G. Huling, E. Kan, Effects of temperature on adsorption and oxidative degradation of bisphenol A in an acid-treated iron-amended granular activated carbon, *Chem. Eng. J.* 262 (2015) 1260–1267. doi:10.1016/j.cej.2014.10.065.
- [23] M.H. Dehghani, M. Ghadermazi, A. Bhatnagar, P. Sadighara, G. Jahed-Khaniki, B. Heibati, G. McKay, Adsorptive removal of endocrine disrupting bisphenol A from aqueous solution using chitosan, *J. Environ. Chem. Eng.* 4 (2016) 2647–2655. doi:10.1016/j.jece.2016.05.011.
- [24] C. Postigo, D.E. Martinez, S. Grondona, K.S.B. Miglioranza, Groundwater pollution: Sources, mechanisms, and prevention, in: *Encycl. Anthr.*, 2017. doi:10.1016/B978-0-12-809665-9.09880-3.
- [25] U. Kannan, S. Krishna Prashanth, S. M. Maliyekkal, Measurement, Analysis, and Remediation of Biological Pollutants in Water, in: 2020. doi:10.1007/978-981-15-0540-9_11.
- [26] J. Bartram, S. Pedley, *Water Quality Monitoring- A Practical Guide to the Design and Implementation of Freshwater Quality Studies and Monitoring Programmes*, United Nations Environ. Program. World Heal. Organ. (1996). doi:10.1002/ejoc.201200111.
- [27] S. Verhille, Understanding microbial indicators for drinking water assessment: interpretation of test results and public health significance, *NCCEH Rev.* (2013).
- [28] V. V. Goncharuk, M.R. Vergolyas, Toxic impact of *Escherichia coli* bacteria depending on their content in water on test organisms, *J. Water Chem. Technol.* (2014). doi:10.3103/S1063455X1401007X.
- [29] E.I. Unuabonah, M.O. Omorogie, N.A. Oladoja, Modeling in adsorption: Fundamentals and applications, in: *Compos. Nanoadsorbents*, 2018. doi:10.1016/B978-0-12-814132-

- 8.00005-8.
- [30] R.K. Gautam, M.C. Chattopadhyaya, Kinetics and Equilibrium Isotherm Modeling: Graphene-Based Nanomaterials for the Removal of Heavy Metals From Water, in: *Nanomater. Wastewater Remediat.*, 2016. doi:10.1016/b978-0-12-804609-8.00005-4.
- [31] I. Langmuir, The adsorption of gases on plane surfaces of glass, mica and platinum, *J. Am. Chem. Soc.* 40 (1918) 1361–1403. doi:10.1021/ja02242a004.
- [32] K.R. Hall, L.C. Eagleton, A. Acrivos, T. Vermeulen, Pore- and solid-diffusion kinetics in fixed-bed adsorption under constant-pattern conditions, *Ind. Eng. Chem. Fund.* 5 (1966) 212–223. doi:10.1021/i160018a011.
- [33] O.S. Amuda, A.A. Giwa, I.A. Bello, Removal of heavy metal from industrial wastewater using modified activated coconut shell carbon, *Biochem. Eng. J.* 36 (2007) 174–181. doi:10.1016/j.bej.2007.02.013.
- [34] H.M.. Freundlich, Over the adsorption in solution, *J. Phys. Chem.* 57 (1906) 385–470. doi:10.3390/ijerph9030970.
- [35] M.I. Temkin, Adsorption Equilibrium and the Kinetics of Processes on Nonhomogeneous Surfaces and in the Interaction between Adsorbed Molecules, *Zh. Fiz. Khim.* 15 (1941) 296–332. doi:10.1016/j.micromeso.2017.02.015.
- [36] M.M. Dubinin, the Potential Theory of Adsorption of Gases and Vapors, *Adsorpt. J. Int. Adsorpt. Soc.* (1969).
- [37] H. Demiral, C. Güngör, Adsorption of copper(II) from aqueous solutions on activated carbon prepared from grape bagasse, *J. Clean. Prod.* 124 (2016) 103–113. doi:10.1016/j.jclepro.2016.02.084.
- [38] D. Gialamoudis, M. Mitrakas, M. Liakopoulou-Kyriakides, Equilibrium, thermodynamic and kinetic studies on biosorption of Mn(II) from aqueous solution by *Pseudomonas* sp., *Staphylococcus xylosus* and *Blakeslea trispora* cells, *J. Hazard. Mater.* 182 (2010) 672–680. doi:10.1016/j.jhazmat.2010.06.084.
- [39] S.Y. Lagergren, Zur Theorie der sogenannten Adsorption gelöster Stoffe, *K. Sven. Vetenskapsakad. Handl.* 24 (1898) 1–39. doi:10.1371/journal.pone.0167428.
- [40] J. Chang, J. Ma, Q. Ma, D. Zhang, N. Qiao, M. Hu, H. Ma, Adsorption of methylene blue onto Fe₃O₄/activated montmorillonite nanocomposite, *Appl. Clay Sci.* 119 (2015) 132–140. doi:10.1016/j.clay.2015.06.038.
- [41] Y.S. Ho, G. McKay, Pseudo-second order model for sorption processes, *Process Biochem.* 34 (1999) 451–465. doi:10.1016/S0032-9592(98)00112-5.
- [42] G. William Kajjumba, S. Emik, A. Öngen, H. Kurtulus Özcan, S. Aydın, Modelling of Adsorption Kinetic Processes—Errors, Theory and Application, in: *Adv. Sorption Process Appl.*, 2019. doi:10.5772/intechopen.80495.
- [43] W.J. Weber, J.C. Morris, Kinetics of Adsorption on Carbon from Solution, *J. Sanit. Eng. Div.* 89 (1963) 31–60. doi:10.1080/002689796173345.
- [44] Y. Kuang, X. Zhang, S. Zhou, Adsorption of methylene blue in water onto activated carbon by surfactant modification, *Water (Switzerland)*. (2020). doi:10.3390/w12020587.

- [45] Y.S. Ho, G. McKay, D.A.J. Wase, C.F. Forster, Study of the Sorption of Divalent Metal Ions on to Peat, *Adsorpt. Sci. Technol.* 18 (2000) 639–650. doi:10.1260/0263617001493693.
- [46] K. Vijayaraghavan, T.V.N. Padmesh, K. Palanivelu, M. Velan, Biosorption of nickel(II) ions onto *Sargassum wightii*: Application of two-parameter and three-parameter isotherm models, *J. Hazard. Mater.* 133 (2006) 304–308. doi:10.1016/j.jhazmat.2005.10.016.
- [47] M.J. Frisch, G.W. Trucks, H.B. Schlegel, G.E. Scuseria, M.A. Robb, J.R. Cheeseman, G. Scalmani, V. Barone, B. Mennucci, G.A. Petersson, H. Nakatsuji, M. Caricato, X. Li, H.P. Hratchian, A.F. Izmaylov, J. Bloino, G. Zheng, J.L. Sonnenberg, M. Hada, M. Ehara, K. Toyota, R. Fukuda, J. Hasegawa, M. Ishida, T. Nakajima, Y. Honda, O. Kitao, H. Nakai, T. Vreven, J.A. Montgomery Jr., J.E. Peralta, F. Ogliaro, M. Bearpark, J.J. Heyd, E. Brothers, K.N. Kudin, V.N. Staroverov, R. Kobayashi, J. Normand, K. Raghavachari, A. Rendell, J.C. Burant, S.S. Iyengar, J. Tomasi, M. Cossi, N. Rega, J.M. Millam, M. Klene, J.E. Knox, J.B. Cross, V. Bakken, C. Adamo, J. Jaramillo, R. Gomperts, R.E. Stratmann, O. Yazyev, A.J. Austin, R. Cammi, C. Pomelli, J.W. Ochterski, R.L. Martin, K. Morokuma, V.G. Zakrzewski, G.A. Voth, P. Salvador, J.J. Dannenberg, S. Dapprich, A.D. Daniels, Ö. Farkas, J.B. Foresman, J. V. Ortiz, J. Cioslowski, D.J. Fox, *Gaussian 09, Rev. A.02*, Gaussian Inc., Wallingford CT. (2009) Wallingford CT. doi:10.1159/000348293.
- [48] F. Shen, J. Liu, Z. Zhang, Y. Dong, C. Gu, Density functional study of hydrogen sulfide adsorption mechanism on activated carbon, *Fuel Process. Technol.* 171 (2018) 258–264. doi:10.1016/j.fuproc.2017.11.026.

CHAPTER 3

REMOVAL OF PHENOLS USING ACTIVATED CARBON SYNTHESIZED FROM *Tithonia diversifolia*^{1,2}

This chapter deals with the preparation of activated carbon from Tithonia diversifolia biomass by chemical activation using potassium hydroxide as the activating agent. The physicochemical characteristics of the activated carbon were modified by varying the activating conditions such as the chemical impregnation ratio and activation temperature. Statistical Taguchi design of experiment was used to select the optimum preparation conditions. The prepared carbon samples were characterized and used for the removal of phenolic compounds from aqueous media. Adsorption isotherm, kinetics, and thermodynamics studies were carried out to understand the adsorption behaviour of phenols. Theoretical density functional theory (DFT) studies were also performed to gain an insight into the adsorption mechanism of phenols onto the activated carbon at the molecular level. This chapter also discusses the regeneration studies of the spent carbon to determine the reusability of the adsorbent.

The applications of the prepared activated carbon are divided into two sections, section A describes the removal of Bisphenol A, while section B discusses the removal of phenol and 4-dinitrophenol from aqueous media using the prepared activated carbon.

¹The text of this chapter has been published as:

A. Supong, P.C. Bhomick, M. Baruah, C. Pongener, U.B. Sinha, D. Sinha, Adsorptive removal of Bisphenol A by biomass activated carbon and insights into the adsorption mechanism through density functional theory calculations. *Sustainable chemistry and pharmacy*, 13, 2019, 2352-5541. <https://doi.org/10.1016/j.scp.2019.1001599>.

²**A. Supong, P.C. Bhomick, R. Karmaker, S.L. Ezung, L. Jamir, U.B. Sinha, D. Sinha, Soremo L Ezung, Latonglila Jamir, Upasana Bora Sinha, Dipak Sinha, Experimental and theoretical insight into the adsorption of phenol and 2,4-dinitrophenol onto Tithonia diversifolia activated carbon.** *Applied surface science*, 529, 2020, 147046. <https://doi.org/10.1016/j.apsusc.2020.147046>.

3.1 Introduction^{1,2}

In the last decades, the widespread occurrence of harmful pollutants in water bodies and their continuous detection even in treated water has raised serious concerns among the scientific community. Rapid industrialization is one of the main reasons that has resulted in the increasing discharge of these undesirable substances into water sources[1]. Phenolic compounds such as phenol, 2,4-dinitrophenol (DNP) and Bisphenol A (BPA) are common constituents of industrial effluents with distinct attributes of being highly toxic even at low concentrations, and therefore the United States environmental protection agency (USEPA) has listed these phenolic compounds as priority pollutants [2]. These pollutants pose a severe peril to both humans and the environment due to their high levels of toxicity, poor biodegradability, and biological accumulation [3]. Humans' exposure to these chemicals can cause detrimental health effects including nausea, vomiting, headache, pancreas damage, liver and kidney injury, skin burns, diarrhoea, tissue erosion, protein degeneration, nervous system paralysis, reproductive system malfunction, disruption of thyroid function, hypertension, diabetes mellitus, insulin resistance, cardiovascular diseases, blood disorders and hormone-dependent cancer [4–6]. Therefore, increasing concern over the ill effects of these pollutants on the environment and human health has prompted researchers to establish technologies for removing these harmful phenolic compounds from wastewater. In this regard, multiple approaches have been developed for removing phenolic compounds from wastewater including reverse osmosis [7], ozonation [8], chemical coagulation [9], ultrafiltration [10], chlorination [11], microbial degradation [12,13] electrochemical degradation [14], chemical oxidation [15], photocatalytic degradation [16], enzymatic treatment [17], solvent-based extraction [18], membrane [19] and advanced oxidation [20,21]. Despite the advantages of these methods, there are certain drawbacks such as large waste production, high chemical consumption, low efficiency, complicated operational techniques, and generation of toxic by-products that limits their widespread application. However, in contrast to the methods discussed above, adsorption is considered a promising technology because of its simplicity, low-cost, versatility, and easy operation. Various adsorbents have been used for phenol

¹A. Supong, P.C. Bhomick, M. Baruah, C. Pongener, U.B. Sinha, D. Sinha, **Adsorptive removal of Bisphenol A by biomass activated carbon and insights into the adsorption mechanism through density functional theory calculations.** *Sustainable chemistry and pharmacy*, 13, 2019, 2352-5541. <https://doi.org/10.1016/j.scp.2019.100159>

²A. Supong, P.C. Bhomick, R. Karmaker, S.L. Ezung, L. Jamir, U.B. Sinha, D. Sinha, Soremo L Ezung, Latonglila Jamir, Upasana Bora Sinha, Dipak Sinha, **Experimental and theoretical insight into the adsorption of phenol and 2,4-dinitrophenol onto *Tithonia diversifolia* activated carbon.** *Applied surface science*, 529, 2020, 147046. <https://doi.org/10.1016/j.apsusc.2020.147046>

adsorption processes such as graphene[22], carbon[23], chitosan[24], bio-adsorbents [25], zeolites[26], composites[27], and polymers[28], and among them, activated carbon has gained significant attention because of its high surface area, variable surface chemistry, large pore volume and ability to adsorb multiple pollutants simultaneously[29]. In particular, biomass-derived activated carbon has emerged as a viable alternative to the expensive commercial activated carbon, as biomass materials are renewable, abundant, and economical[30,31]. In acknowledgement of the advantages of biomass-based activated carbon, the present study focuses on the utilization of *Tithonia diversifolia* biomass to prepare porous activated carbon for the removal of phenol, DNP and BPA from water.

The production of activated carbon from *Tithonia diversifolia* biomass was achieved by chemical activation method, and potassium hydroxide (KOH) was used as the activating agent owing to its effectiveness in producing activated carbon with large surface area and well-developed porosity. Experimental parameters such as chemical impregnation ratio and activation temperature were considered for the modification of the activated carbon since these parameters are known to have a large influence on the textural characteristics of the activated carbon. In recent years, several statistical experimental designs have been applied to optimize the experimental parameters and examine the contributing influence of each on the resulting activated carbon characteristics. The Taguchi methodology is one of the most reliable statistical techniques and has frequently been used for the design and optimization of experiments. The Taguchi method was therefore applied to design the experiment and identify the best-operating conditions for preparing activated carbon. The use of this statistical experimental design facilitates proper resource management and reduced production cost and time, which ultimately results in sustainable activated carbon production.

In addition to the textural characteristics of activated carbon such as pore volume and surface area, the surface chemistry of activated carbon is another critical characteristic of the adsorption process, as the adsorbent-adsorbate interaction varies significantly depending on the functional group present on the activated carbon surface. The surface functional groups on the activated carbon largely depend on the chemical agent used for the activation process[32]. The activation process using potassium hydroxide is mainly responsible for the introduction of oxygenated functional groups such as carboxyl, hydroxyl, carbonyl and acid anhydride on the activated carbon surface[33]. It is widely reported that these oxygenated functional groups significantly affect the adsorption capacity of activated carbon [34–37]. The influence of such oxygenated functional groups on the adsorption of phenolic compounds has been a contentious issue among researchers. Various studies have reported that the presence

of oxygenated functional group on activated carbon decreases the adsorption of phenolic compounds [38–40], on the contrary, some other findings reported the positive influence of oxygenated functional groups on phenol uptake [32,41,42]. A clear understanding of the interaction of oxygenated groups with the phenolic compound is thus essential to resolve these fundamental issues. Therefore, the present study attempted to shed more light on the relation between the phenolic compound and oxygenated functional groups by studying the influence of three main oxygenated functional groups (-COOH, -OH and -CHO) on the phenol, DNP and BPA adsorption using density functional theory (DFT) calculations. DFT studies are expected to give a clear picture of the adsorption process and facilitate the design of activated carbon with a maximum affinity for these pollutants. The study proposed several interactive mechanisms and reported the comparative favorability of different adsorptive interactions that occur between the adsorbate and functionalized activated carbon. The findings of this study are expected to provide valuable guidance for future experimental studies in designing specialized and efficient activated carbon.

Thus, for the first time, the present research reports the utilization of *Tithonia diversifolia* biomass for the preparation of activated carbon by KOH activation. The surface characteristics of the activated carbon were modified by subjecting to different chemical impregnation ratio and activation temperature. Taguchi methodology was incorporated to design the experiment and optimize the experimental operating factors. The prepared carbon was characterized to understand its physio-chemical properties using various characterization techniques. The carbon produced was subsequently used for phenol, DNP and BPA removal from aqueous solution and various experimental data were used to examine the adsorption isotherms, kinetic models and thermodynamic parameters. Also, density functional theory (DFT) studies were performed to elucidate the adsorption mechanism. The cost analysis and the regeneration studies were also investigated.

3.2 Materials and methods

The *Tithonia diversifolia* (Tree marigold) biomass used as a raw precursor for this study to prepare activated carbon was collected locally from the vicinity of Nagaland University, Lumami campus (26° 13' 29.60" N | 94 ° 28' 35.0" E). The raw material was manually cut into pieces, washed with water and dried in a hot air oven at 110°C for 48 hours. All the chemicals used in the present work were of analytical grade.

3.2.1 Taguchi design of experiment

Taguchi experimental design uses an orthogonal array method that sorts out the best set of parameters and minimizes the number of experimental runs. Additionally, the optimum level of each operating parameter for achieving the best-desired characteristics of the product can be attained using this methodology.

Taguchi experimental design first requires the selection of control factors and the levels corresponding to each factor. For this study, two control factors, *viz.*, impregnation ratio and activation temperature were selected and four levels were considered for each factor, as shown in Table 3.1. As suggested by the Taguchi method, an L_{16} orthogonal array was selected and sixteen experimental runs were carried out. Evaluating the experimental results requires an analysis of the signal-to-noise ratio(S/N). There exist three types of S/N ratio, ‘larger the better’, ‘nominal the better’ and ‘smaller the better’, and the appropriate S/N ratio is selected depending on the response variable. In the present study, surface area was considered as the response variable since it is one of the most important characteristics of activated carbon and has a direct relationship with other properties such as adsorption capacity and pore volume. The ‘larger the better’ S/N ratio was applied as a larger surface area would account for better adsorbent performance. According to the S/N ratio, the optimum levels of the factors (impregnation ratio and temperature) for obtaining the maximum response variable (surface area) were determined using Equation 3.1.

$$S/N = -10 \log \left(\frac{1}{n} \sum_{i=1}^n \frac{1}{y_i^2} \right) \quad (3.1)$$

where S/N is the calculated signal-to-noise ratio for the experiment of the L_{16} orthogonal array, n is the number of experiments and y_i represents the BET surface area.

Table 3.1 Control variables and their respective levels				
Control variables	Level 1	Level 2	Level 3	Level 4
Impregnation ratio	0.5:1	1:1	2:1	3:1
Activation temperature	500	600	700	800

ANOVA test

The ANOVA technique helps in understanding the relative contribution of each factor on the response variable. The ANOVA table comprises various statistical variables, such as degrees of freedom (DF), P-value, F-value, sequential sums of squares (Seq SS), adjusted sums of squares (Adj SS), adjusted mean square, and relative percentage contribution (%). The factor having the highest F-value and a P-value less than 0.05 would have the most significant

influence on the response variable. Larger percentage contribution values signify a larger influence of the factor on the response variable.

3.2.2 Preparation of activated carbon

The activated carbon was prepared by following a two-step activation process. First, the raw material was carbonized and second, the carbonized material was activated using KOH at the desired temperature. Dried samples were carbonized at 600°C for 1 hour using a muffle furnace. The carbonized sample was pulverized into a fine, uniform-size powder using a planetary ball mill at 600 rpm for around 15 minutes. The resulting powdered carbonized sample was labelled TUC and was further subjected to KOH activation. For this activation, 20 g of KOH was dissolved in a beaker containing 250 mL distilled water. Subsequently, impregnation was done by mixing an appropriate quantity of carbonized samples (TUC) with the prepared KOH solution at different impregnation ratios (KOH:TUC) of 0.5:1, 1:1, 2:1 and 3:1. The mixture was magnetically stirred for 1 hour and oven-dried at 105°C until a constant weight was obtained. The KOH-impregnated carbon samples were further pyrolyzed at an activation temperature ranging from 500–800°C in a muffle furnace for 2 hours under the atmosphere generated by the furnace. The produced activated carbon was then washed with 0.1M HCl and a sufficient amount of distilled water until the filtrate attained a neutral pH. The obtained samples were further subjected to drying in a hot air oven at 105°C for 12 hours and were stored in airtight containers for subsequent analysis. The synthesized activated carbon was denoted as xTAKy where TAK stands for *Tithonia diversifolia* KOH activated carbon, x stands for impregnation ratio of KOH and y is the activation temperature. The yield percentage of the prepared carbon is given by Equation (3.2).

$$\text{Yield, \%} = \frac{W_1}{W_2} \times 100 \quad (3.2)$$

where W_1 is the final weight of the prepared carbon and W_2 is the initial weight of dried raw biomass (*Tithonia diversifolia*).

3.2.3. Characterization of Carbon samples

Characterization of the prepared carbon samples was done using different techniques. The proximate analyses of both the raw material and activated carbon were done according to the guidelines of the American Society for Testing and Materials[43]. The carbon, nitrogen and hydrogen content were analyzed using a CHN elemental Analyzer (Model: PE 2400 Series II, Make: Perkin Elmer). A BET surface area analyzer (Smart instrument, SS93/02) was used to determine the surface area and pore volume. The surface morphology of the activated carbon

was examined using scanning electron microscopy (JEOL/ JSM-6360). Fourier transform infrared spectroscopy (Spectrum Two, Perkin Elmer) was used to study the different functional groups. X-ray diffraction analysis was carried out using an XRD (Model Rigaky-Ultimaiv Japan) at a scan rate of 0.2 degrees per minute using CuK α radiation. Thermal analysis was carried out using TGA equipment (Perkin Elmer/STA-3000).

3.2.4 Theoretical study

A theoretical study using DFT calculations was conducted to further understand the possible interaction of phenols and activated carbon. All the geometry optimizations and energy calculations were performed on the Gaussian 09W program package using DFT employing the B3LYP hybrid functional at basis set 6-31g level of theory in a dielectric medium of $\epsilon = 80$ (corresponding to water). Gauss View 05 was used to produce all the structures which were optimized in their electronic ground state. The adsorption energy (E_{adsorp}) of phenols on the carbon surface was calculated using equation 21 as described in chapter 2.

3.3 Results and discussions

3.3.1 Taguchi design of experiments

A set of 16 different experiments were done according to the Taguchi orthogonal array and different types of activated carbon with specific characteristic properties were obtained. The layout of the orthogonal design and the experimentally obtained results are given in Table 3.2.

Taguchi L₁₆ array		S_{BET} (m²g⁻¹)	V_{Total} (cm³g⁻¹)	Yield (%)	Elemental composition, %			
Activation Temperature (°C)	Impregnation ratio (KOH: TUC)				Carbon	Hydrogen	Nitrogen	Oxygen*
500	0.5:1	222.49	0.125	30.8	62.36	2.72	1.23	33.69
500	1:1	347.37	0.205	26.6	67.44	2.05	1.50	29.01
500	2:1	629.65	0.291	21.1	72.11	1.68	1.53	24.68
500	3:1	584.32	0.257	15.6	73.30	1.39	1.61	23.70
600	0.5:1	315.69	0.182	28.5	75.22	2.51	1.29	20.98
600	1:1	572.15	0.267	24.1	76.55	1.28	1.42	20.75
600	2:1	729.83	0.319	19.2	79.81	1.07	1.49	17.63
600	3:1	637.25	0.300	14.4	80.44	1.01	1.52	17.03
700	0.5:1	411.83	0.222	28.2	81.15	1.80	1.59	15.46
700	1:1	836.50	0.434	23.6	82.64	1.16	1.57	14.63
700	2:1	854.44	0.445	18.3	84.66	0.95	1.62	12.77
700	3:1	726.21	0.323	13.9	87.33	0.88	1.62	10.17
800	0.5:1	398.45	0.219	25.7	83.82	1.48	1.65	13.05
800	1:1	749.44	0.347	22.5	86.57	0.79	1.57	11.07
800	2:1	812.50	0.408	15.5	86.91	0.75	1.69	10.65
800	3:1	673.62	0.311	12.1	89.45	0.70	1.56	8.29
*by difference								

S/N ratio analysis

The experimental data obtained by the Taguchi methodology were analyzed in the form of the S/N ratio. Figure 3.1 represents the effect of the control factor on the mean S/N ratio. Four-factor levels each for temperature (500, 600, 700 and 800°C) and impregnation ratio (0.5:1, 1:1, 2:1 and 3:1) were considered and the factor level with the highest S/N ratio was selected as the optimum parameter responsible for generating the maximum surface area. As seen in Figure 3.1, temperature level 3 gave the highest S/N ratio of 56.65 indicating that the optimum temperature for obtaining maximum surface area was 700°C. Additionally, the largest S/N ratio of 57.52 was obtained at impregnation ratio level 3 which corresponded to a 2:1 impregnation ratio. The results indicated that the optimum parameters for obtaining activated carbon with the largest surface area corresponded to 700°C temperature and a 2:1 impregnation ratio. The surface area was found to be 854.44 m² g⁻¹ at these optimum conditions.

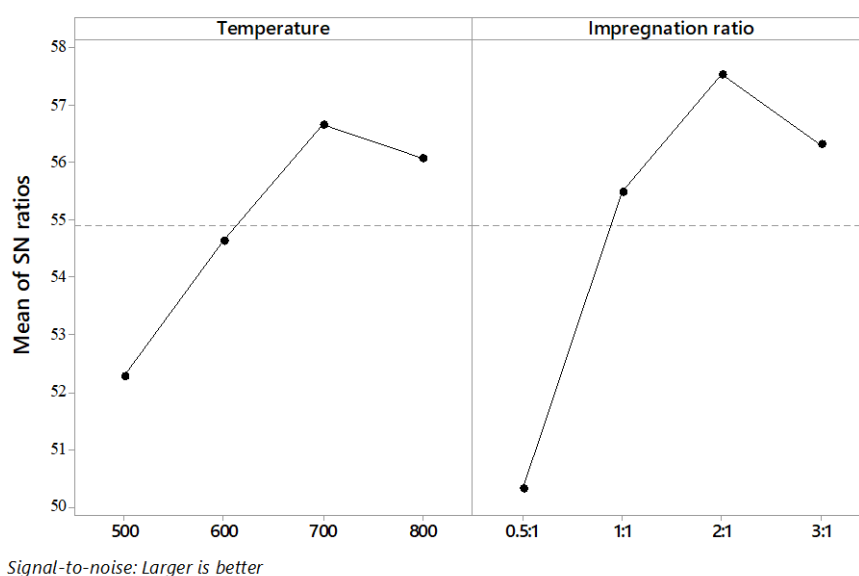


Figure 3.1 Graphical representation of the effect of control factors on the S/N ratio of BET surface area

ANOVA test

ANOVA test helps in determining the statistical significance of the control parameters and to identify the most influential parameter in the production process. The ANOVA results are given in Table 3.3. According to the ANOVA data, both the impregnation ratio and activation temperature give a P-value less than 0.05; these results indicate that both the control factors have a significant association with the response variable. The F-values of the impregnation ratio and activation temperature were 10.86 and 26.5, respectively. The larger F-value and

higher percentage contribution of the impregnation ratio indicate that the KOH impregnation ratio has a larger influence on the surface area compared to the activation temperature.

Table 3.3 Results of ANOVA							
Source	DF	Seq SS	Adj SS	Adj MS	F-Value	P-Value	Contribution
Temperature	3	159271	159271	53090	10.86	0.002	26.89%
Impregnation ratio	3	388966	388966	129655	26.51	0.000	65.68%
Error	9	44011	44011	4890			7.43%
Total	15	592248					100.00%

3.3.2 Characterization of activated samples

a) Elemental analysis

The elemental composition of activated carbon samples obtained at varying impregnation ratio and activation temperatures are given in Table 3.2. The elements carbon, nitrogen, oxygen, and hydrogen constitute the activated carbon and the main component is carbon, between 62 and 90%. The carbon content of the prepared carbon increased with increasing impregnation ratio and activation temperature while the hydrogen and oxygen content decreased. This increase in fixed carbon mass may be attributed to the release of volatiles and non-carbon species upon heat treatment and chemical activation [44].

b) BET surface area, pore volume and yield

The impregnation ratio and activation temperature were found to have a prominent effect on the BET surface area, pore volume and yield of the prepared carbon. As can be seen in Table 3.2, the BET surface area and pore volume increased with increasing impregnation ratio and activation temperature reaching a maximum at 700°C and 2:1 KOH/TUC ratio. This enhancement may be due to the progressive elimination of volatiles and the reaction of more carbon atoms with increasing KOH concentration at elevated temperatures. However, a decrease in surface area and pore volume was observed with further increases in temperature and impregnation ratio from 700°C and 2:1, respectively. This could be due to shrinkage of the carbon structure at very high temperature and impregnation ratios, which ultimately destroys the textural development of the activated carbon. The highest BET surface area (854.44 m²/g) and pore volume (0.445cm³/g) were obtained at a temperature of 700°C with KOH:TUC impregnation ratio of 2:1.

The yield of the prepared carbon also progressively decreased with increasing activation temperature and impregnation ratio. This could be attributed to the escape of a large amount

of volatiles and the increasing reaction rate between KOH and surface carbon, leading to excessive carbon burn-off [45].

c) Visual inspection of SEM images

The scanning electron microscopy technique was employed to examine and compare the surface morphology of the unactivated and activated carbon samples. The SEM microphotographs of the unactivated carbon and some of the activated carbon obtained at different preparation conditions are shown in Figure 3.2. The SEM image of unactivated carbon was found to be quite smooth and barely containing any pores and cracks (Figure 3.2a). However, the activated carbon samples displayed an irregular surface with pores of different shapes and sizes. The SEM micrograph (Figure 3.2b–c) reveals that an increase in activation temperature up to 700°C gives rise to more irregularities with an increase in cavities and voids. However, it could be seen that a higher activation temperature (800°C), the carbon matrix disintegrates, destroying the pore structure (Figure 3.3d). The SEM image of carbon samples with a KOH/TUC impregnation ratio of 1:1, 2:1 and 3:1 at a fixed temperature of 700°C are presented in Figure 3.2e, c and f, respectively.

A study of the surface morphology shows that activation of the precursor with a KOH/ TUC ratio of 1:1 and 2:1 gives rise to a more developed pore network. However, as the KOH/TUC ratio increased to 3:1, the number of pores decreased and the porous network become less-prominent, as shown in Figure 3.2f, which may be due to over-activation of the carbon sample with excess KOH.

d) X-ray diffraction analysis (XRD)

X-ray diffraction studies help in determining the degree of crystalline or amorphous nature of activated carbon. Figure 3.3 illustrates the XRD profile of the activated carbon prepared at different activation temperatures and impregnation ratios.

All the prepared samples show two broad peaks at $2\theta = \sim 23^\circ$ and $\sim 43^\circ$, corresponding to the reflection from the (002) plane and (100) plane, respectively, and the occurrence of broad peaks at these 2θ indicates that the activated carbon consists of graphite-like microcrystallites[46]. An increase in sharpness of the $\sim 23^\circ$ peak is seen with the rise in activation temperature from 500°C to 700°C. This signifies a more regular crystal structure at the optimum higher activation temperature of 700°C[47].

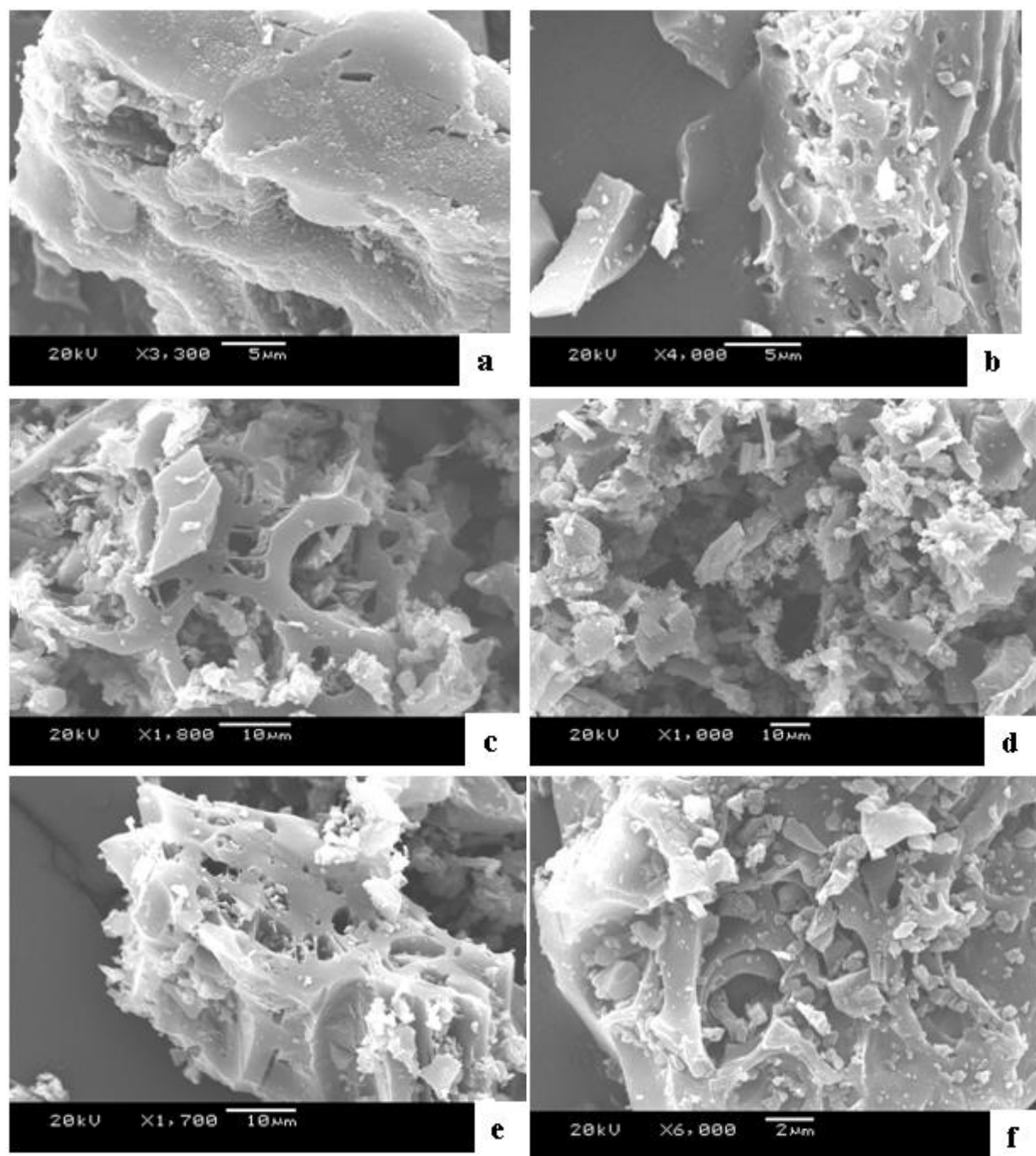


Figure 3.2 SEM micrograph of: (a)TUC (b) 2TAK600 (c) 2TAK700 (d) 2TAK800 (e) 1TAK700 (f) 3TAK700

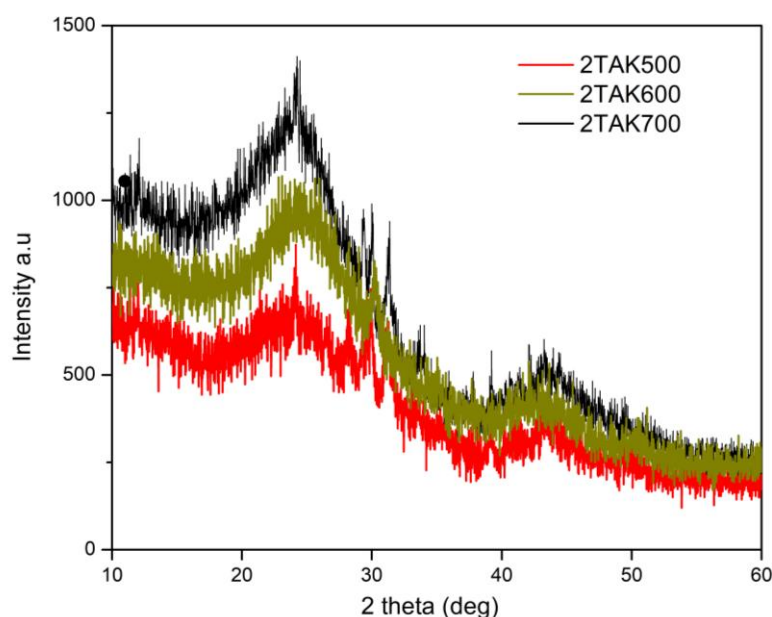


Figure 3.3 XRD patterns of *Tithonia diversifolia* carbons obtained at activation temperature of 500°C, 600 °C, and 700 °C at an impregnation ratio of 2:1

e) Thermogravimetric analysis of activated carbon

Thermogravimetric analysis was employed to understand the thermal stability and examine the decomposition pattern of the carbon samples. Figure 3.4 shows the TGA and DTG curves of some of the activated carbon samples synthesized at different impregnation ratios and temperatures.

It is evident from the TGA curves that there was an initial weight loss at temperatures below 200°C, which could be ascribed to the elimination of moisture adsorbed within the pores of the carbon. A weight loss was observed at a temperature ranging from around 560°C to 650°C, and this phenomenon may be due to the release of volatiles such as CO₂ and CO. Furthermore, no weight loss was observed above 650°C which reflects the thermal stability of the prepared activated carbon samples at relatively high heating temperature up to 900°C. Similar patterns of TGA/DTG curves were obtained for almost all the samples obtained at different activation temperatures and impregnation ratios.

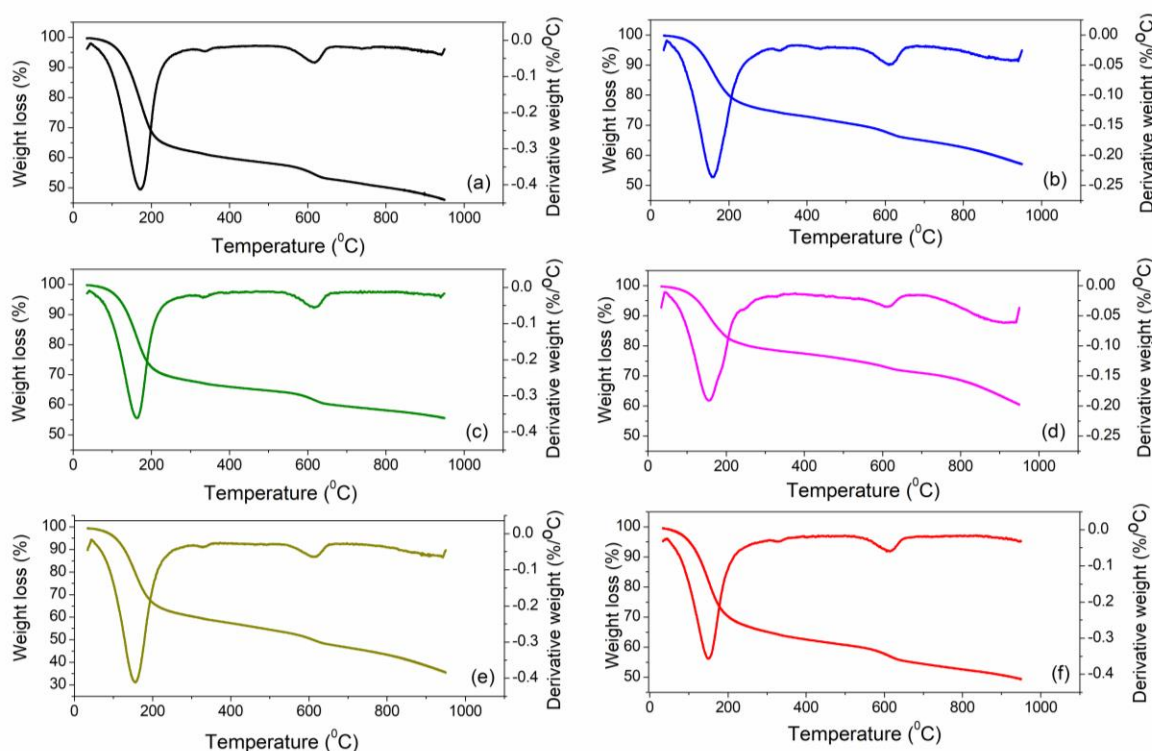


Figure 3.4 TGA/DTG profile of activated carbon samples (a) 2TAK500 (b) 0.5TAK600 (c) 0.5TAK700 (d) 0.5TAK500 (e) 3TAK500 (f) 1TAK500

The appearance of band between $1650\text{--}1620\text{cm}^{-1}$ in both the raw precursor and all the carbon samples could be attributed to olefinic $\text{C}=\text{C}$ stretching vibration, while the skeletal $\text{C}=\text{C}$ vibrations in aromatic rings bands in the $1600\text{--}1400\text{ cm}^{-1}$ region of the spectrum were also observed for all the samples. The transmittance at $1300\text{--}1000\text{ cm}^{-1}$ could be accounted for $\text{C}-\text{O}$ stretching in carboxylic acid or derivatives, alcohols, phenols, ethers or esters group and the appearance of a broader peak at 751.05 cm^{-1} , 758.08 cm^{-1} and 769.07 cm^{-1} attributed to $\text{C}-\text{H}$ out of plane bending vibrations [49]. It could thus be observed from the results that the FTIR spectra of the activated carbon samples prepared at different activating temperature and impregnation ratio showed no visible difference and contained the same functional groups.

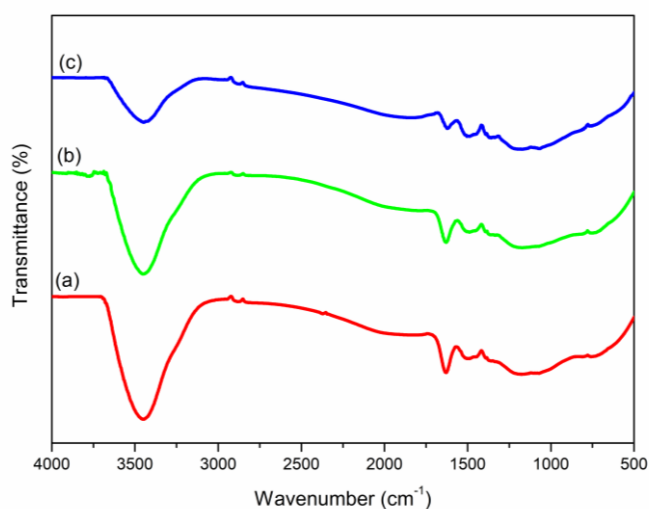


Figure 3.5 FTIR spectra of a) 2TAK500 b) 2TAK600 c) 2TAK800 (impregnation ratio 2:1)

3.3.3 Cost analysis

The approximate logistic cost of harvesting, collection, transportation and processing involved in the production of 250g activated carbon from *Tithonia diversifolia* biomass has been considered and compared with the cost of some of the available commercial activated carbon. Since *Tithonia diversifolia* is widely distributed, invasive and found in abundance in wastelands particularly in the present study area, the stems, leaves and flowers of the plant can directly be collected from these lands and therefore, would not require planting of the biomass. The acquisition cost of the weed would be very low or sometimes near zero because of its wide availability. Recultivation of these plants manually would also not be required as the plant reproduce rapidly by vegetative propagation. However, the cost involved in the harvesting, collection, transportation and processing of the biomass were considered for this study and is given in Table 3.4. The harvesting, collection and transportation cost were estimated according to the cost prevailing in the present study area. The processing process of biomass included the price of KOH, electricity, water, HCl and raw precursor. The resulting production cost was subsequently compared with that of commercially available carbon to make a comparison with regard to economic feasibility. The combined logistic cost of 250g activated carbon was found to be ₹ 540.3 without considering the cost involved in labour income, initial investment, working capital, manufacturer's profits, recovery and reuse of KOH etc. The overall cost might vary from region to region and is expected to reduce in scaling up from laboratory experiments to industrial scale. In the present study, the cost of 250g activated carbon was found to be lower than that of commercial activated carbon.

Therefore, this study suggests that *Tithonia diversifolia* biomass can be used as an optional precursor for the production of low cost activated carbon.

Table 3.4. Cost estimates for production of 250g <i>Tithonia diversifolia</i> activated carbon		
Materials	Consumption(approx.)	Cost (approx.)
Harvesting and collection (manually)	1.4kg	₹ 2
Transportation Truck- Front single axle: Full Load- 9000kg Cost: ₹ 200/km	10 km (approximate)	₹0.03 for 1.4kg
KOH	500g	₹480
HCl	200 ml of 0.1M HCl	₹1 (₹265/500ml)
Raw precursor	1.4 kg	₹ 0
Electricity	14 kWh	₹ 42
Water	50 L	₹ 15
Total Cost/250g (in Rupees)	-	₹ 540.03

Section A

Removal of Bisphenol A using *Tithonia diversifolia* activated carbon¹

The section describes the application of *Tithonia diversifolia* activated carbon for the removal of Bisphenol A from an aqueous medium. The study utilized the 2TAK700 activated carbon, where TAK stands for *Tithonia diversifolia* KOH activated carbon, 2 corresponds to the 2:1 impregnation ratio of KOH/char and 700 is the activation temperature at 700°C. The 2TAK700 activated carbon possessed the highest surface area 854.44 m²g⁻¹ and pore volume 0.445 cm³g⁻¹, and since these properties have a direct relationship with the overall adsorption capacity, the 2TAK700 activated carbon was chosen for the removal of BPA in this study. The effect of process parameters like adsorbent dosage, pH, initial concentration, and contact time were determined using batch adsorption experiments. Adsorption isotherms and kinetics were fitted with the experimental data, and the validation of the models was assessed by applying Chi-Squared Test (χ^2) and Sum of the Square of the Errors (SSE). Thermodynamic studies on the adsorption data were also conducted. Also, density functional theory (DFT) studies were performed to further elucidate the adsorption mechanism of BPA onto the activated carbon.

3.3.4 Adsorption studies of Bisphenol A

For this present study, Bisphenol A (BPA) was purchased from Hi-media, India. A 1000 mg L⁻¹ stock solution of BPA was prepared by dissolving 1g of BPA in a minimum quantity of ethanol and further diluted to 1000ml using distilled water. The working solutions (10 mg L⁻¹ to 100 mg L⁻¹) were further obtained by appropriate dilution of the stock solution with distilled water. Batch mode adsorption experiments provide invaluable information about the different experimental parameters and help in defining the optimum conditions for the process to run efficiently. Thus, the effect of varying adsorbent dose (0.1 to 1g), initial BPA concentration (10 mg L⁻¹ to 100 mg L⁻¹), pH (1 to 12) and contact time (5 min to 200 min) on BPA adsorption were studied by using batch adsorption method, and the optimum process condition was obtained. In each batch experiment, a required dose of adsorbent was placed in a conical flask containing 50 mL of the desired concentration of BPA solution. The solution pH was adjusted using NaOH and HCl. The mixtures were then shaken using a rotary shaker at 180 rpm under controlled temperature for the required amount of time. The solution was

¹A. Supong, P.C. Bhomick, M. Baruah, C. Pongener, U.B. Sinha, D. Sinha, **Adsorptive removal of Bisphenol A by biomass activated carbon and insights into the adsorption mechanism through density functional theory calculations**. *Sustainable chemistry and pharmacy*, 13, 2019, 2352-5541. <https://doi.org/10.1016/j.scp.2019.1001599>.

then filtered and the remaining BPA concentration in the filtrate was determined by measuring absorbance at 276 nm using UV-Visible Spectrophotometer (lambda 35, Perkin Elmer). All the adsorption experiments were run in triplicate. The percentage removal of BPA and adsorption capacity of the prepared carbon (mg g^{-1}) was calculated by using equation 1 and 2 respectively, as described in chapter 2.

The experimental data obtained were fitted into different adsorption isotherm models: Langmuir, Freundlich, Temkin, and Dubinin–Radushkevich. The adsorption mechanisms and rate-limiting steps were analyzed by fitting the obtained data into four kinetic models, *viz.*, pseudo-first-order, pseudo-second-order, intraparticle diffusion, and Elovich.

a) Effect of adsorbent dose

Adsorbent dose is one of the vital parameters in adsorption experiments since it helps in determining the uptake capacities of an adsorbent for a given adsorbate. The effect of adsorbent dose on the adsorption of BPA onto *Tithonia diversifolia* activated carbon was determined by varying the amount of activated carbon from 0.1 to 1 g at initial BPA concentration of 40 mg L^{-1} , pH of 7 and temperature of 25°C . It can be seen from Figure 3.6a that the removal percentage of the BPA increased up to a maximum removal efficiency of 95%, with increasing adsorbent dose from 0.1g to 1g. This is attributed to the availability of more adsorption sites at increased adsorbent dose [50]. By comparing the removal percentage and adsorption capacity, an optimum adsorbent dose of 0.2g was selected for further studies.

b) Effect of contact time

The contact time determines the necessary equilibrium time of the adsorption process. The effect of contact time on removal efficiency and adsorption capacity was evaluated by variation of contact time (5 to 200 min) at constant adsorbent dosage (0.2g), initial BPA concentration of 40 mg/L , solution pH-7 and temperature of 25°C . A plot of removal efficiency (%) and adsorption capacity(q_e) of the *Tithonia diversifolia* activated carbon versus contact time is shown in Figure 3.6b. It is apparent from the figure that the adsorption rate of BPA progressed rapidly at the initial stage, proceeded at a slower uptake rate and finally attained equilibrium. The significant increase in adsorption rate in the initial stages is associated with the presence of higher available surface area and ample vacant sites of activated carbon. However, with the progression of contact time, the removal rate became slow and finally, the system reached equilibrium after around 80 minutes. This is because the remaining vacant surface sites become less accessible as time precedes due to repulsive forces between the BPA molecules on the solid and bulk phases [51,52].

c) Effect of initial concentration

The effect of initial concentration was investigated at different BPA concentrations ranging from 10mg/L to 100 mg/L while other parameters i.e., adsorbent dose, contact time, temperature and pH were fixed at 0.2g, 80 minutes, 25°C and 7, respectively. The effect of initial concentration of BPA on the adsorption process was evaluated by varying the concentration from 10 mg L⁻¹ to 100 mg L⁻¹. Figure 3.6c gives the removal efficiency and adsorption capacity of BPA with an increase in the initial concentration. The removal efficiency of BPA declined with an increasing initial concentration of the solution from 10 mg L⁻¹ to 100 mg L⁻¹. The higher removal percentage at lower BPA concentrations may be due to the availability of more adsorption sites on the surface of the adsorbent than the number of adsorbate molecules (BPA) present in the solution. However, at higher concentrations, the number of BPA molecules competing for the same number of adsorption sites were higher, thus decreasing the removal efficiency [53]. The adsorption capacity(q_e)increased from 2.40 to 15.35 mg/g with an increased in initial BPA concentration from 10mg/L to 100mg/L.

d) Effect of pH

The pH of the working solution plays an important role in the uptake capacity of BPA by the prepared carbon. For the present study, the pH was varied from 2 to 12 and the removal efficiency of BPA under these conditions was studied. The initial concentration, contact time, adsorbent dose and temperature were kept constant at 40 mg L⁻¹, 80 minutes, 0.2 g, and 25°C, respectively. A relatively constant value of removal efficiency and adsorption capacity was observed on increasing the pH from 2 to 9; however, at a higher pH ranging from 9 to 12, BPA adsorption exhibited a decreasing trend. The pKa value of BPA ranges from 9.6 to 10.2 [54] so at pH >pKa, the BPA molecule may undergo ionization to form a bisphenolate anion, resulting in electrostatic repulsion between the negatively charged carbon surface and the bisphenolate anion, thereby reducing BPA adsorption onto the activated carbon. However, at pH<pKa, the adsorption of BPA remained at a maximum and almost constant because BPA was undissociated and the adsorptive interaction between the molecular BPA and the adsorbent predominated. The highest removal efficiency (95.92%) and adsorption capacity (9.59 mg g⁻¹) was obtained at pH 7. Figure 3.6d presents the effect of pH on the removal efficiency and adsorption capacity.

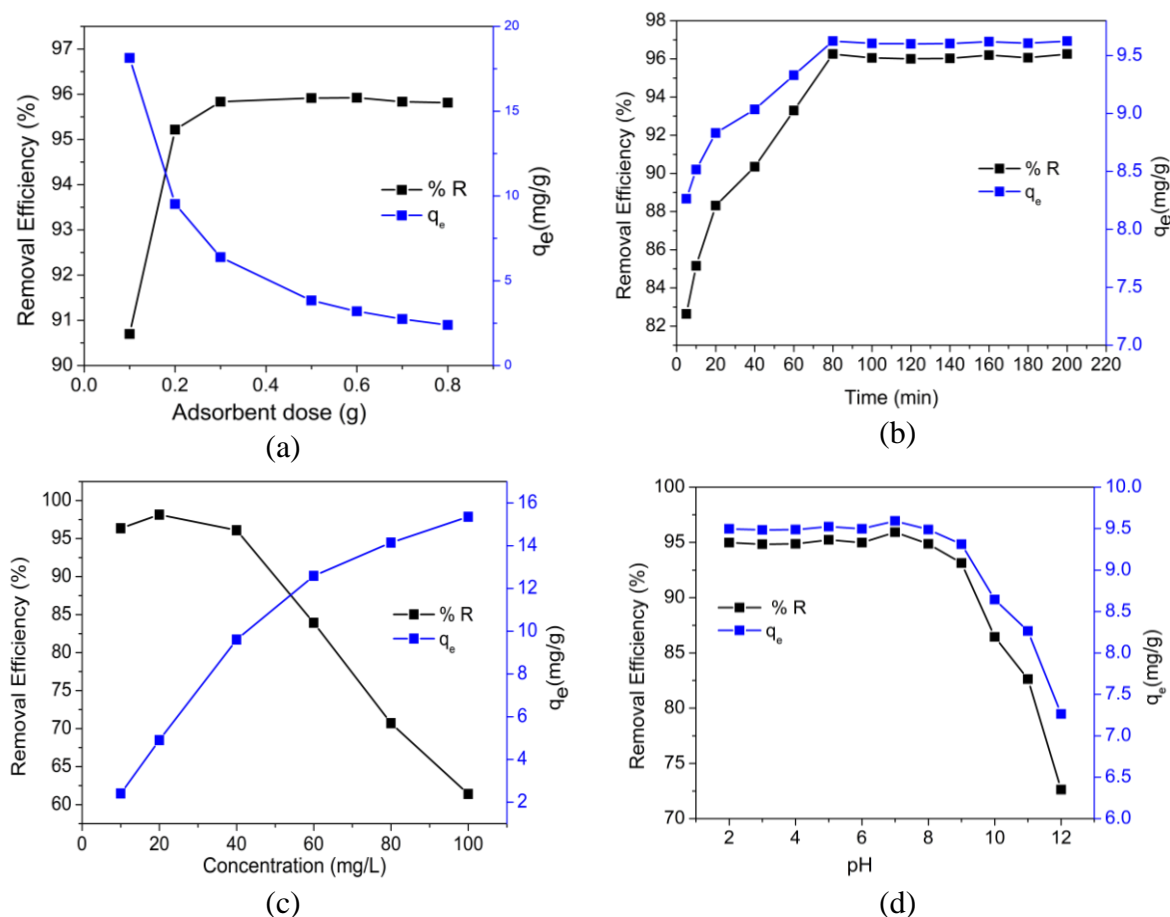


Figure 3.6 Effect of (a) adsorbent dose (b) contact time (c) initial BPA concentration and (d) pH on BPA adsorption

3.3.5 Adsorption Isotherms studies

Adsorption isotherms are useful tools that help in determining the distribution of adsorbate concentration between the solid phase and the liquid phase at equilibrium. In this study, conventional isotherm models, Langmuir, Freundlich, Temkin, and Dubinin-Radushkevich were employed to understand the adsorptive behaviour of BPA onto the *Tithonia diversifolia* carbon. The adsorption isotherm graphs obtained are depicted in Figure 3.7 whereas the obtained plot parameters are presented in Table 3.5.

The Langmuir isotherm was studied using equation 4 of chapter 2. The parameters for the Langmuir model were obtained by plotting C_e/q_e vs. C_e as shown in Figure 3.7 (a). A high correlation factor ($R^2 = 0.99$) signifies that the Langmuir model provides a good fit with a q_m value of 15.69 mg g^{-1} . The dimensionless separation factor (R_L) is another important parameter in Langmuir isotherm. The value of R_L indicates the adsorption process to be unfavourable ($R_L > 1$), favourable ($0 < R_L < 1$) and irreversible ($R_L = 1$). The value of the dimensionless separation factor ($R_L = 0.9389$) confirmed favourable adsorption.

Table 3.5 Adsorption isotherm parameters and correlation coefficients				
Isotherm	Parameters	R²	χ²	RMSE
Langmuir	q _m = 15.69 K _L = 0.0065 R _L = 0.9389	0.9967	0.0033	0.0574
Freundlich	$\frac{1}{n}$ = 0.319 n = 3.13 K _F = 1.19	0.7644	0.0236	0.1538
Temkin	b _T = 1.005 A _T = 15.45	0.9332	1.8174	1.3481
Dubinin–Radushkevich (D-R)	q _{DR} =13.47 β = 1.3 x 10 ⁻⁷ E=1.96	0.8667	0.0709	0.2664

For the Freundlich isotherm model, the plotting parameters were obtained from log q_e vs log C_e graph as shown in Figure 3.7(b). The Freundlich constant K_F and n are indicators of adsorption capacity and intensity respectively and their values are shown in Table 3.5. The parameter ‘n’ indicates the nature of adsorption. The ‘n’ value obtained in this study was found to be greater than unity, which signifies that the adsorption process is favourable and follows normal Langmuir isotherm. The lower value of R²= 0.7644 indicates that the model cannot adequately give a detailed explanation of the adsorption process of BPA onto the prepared carbon.

From the isotherm model, the Temkin constant (b_T) relating to the heat of adsorption was calculated and was found to be 1.005 KJ mol⁻¹. The correlation coefficient value (R²) of 0.9332 showed that the Temkin model cannot sufficiently explain the adsorption process.

The theoretical monolayer adsorption capacity, q_{DR} obtained from the plot of lnq_e versus ε² of Dubinin–Radushkevich model was 13.47 mg g⁻¹ (Figure 3.7d). The mean free energy (E) gives information about the adsorption mechanism, and its value was found to be 1.96. The R² value of 0.8667 proves that adsorption data does not fit to D-R isotherm model.

The isotherm models were further validated by conducting the chi-squared test and RMSE analysis, given by equation 17 and 18 respectively in chapter 2. The values of R², χ², and RMSE for the four adsorption isotherm models under study were compared and analyzed (Table 3.5). The highest adjusted correlation coefficient R² = 0.9967 and lowest RMSE (0.0574) and χ² (0.0033) made the Langmuir model the most appropriate adsorption model for BPA adsorption indicating that the adsorption of BPA predominantly proceeds through monolayer coverage.

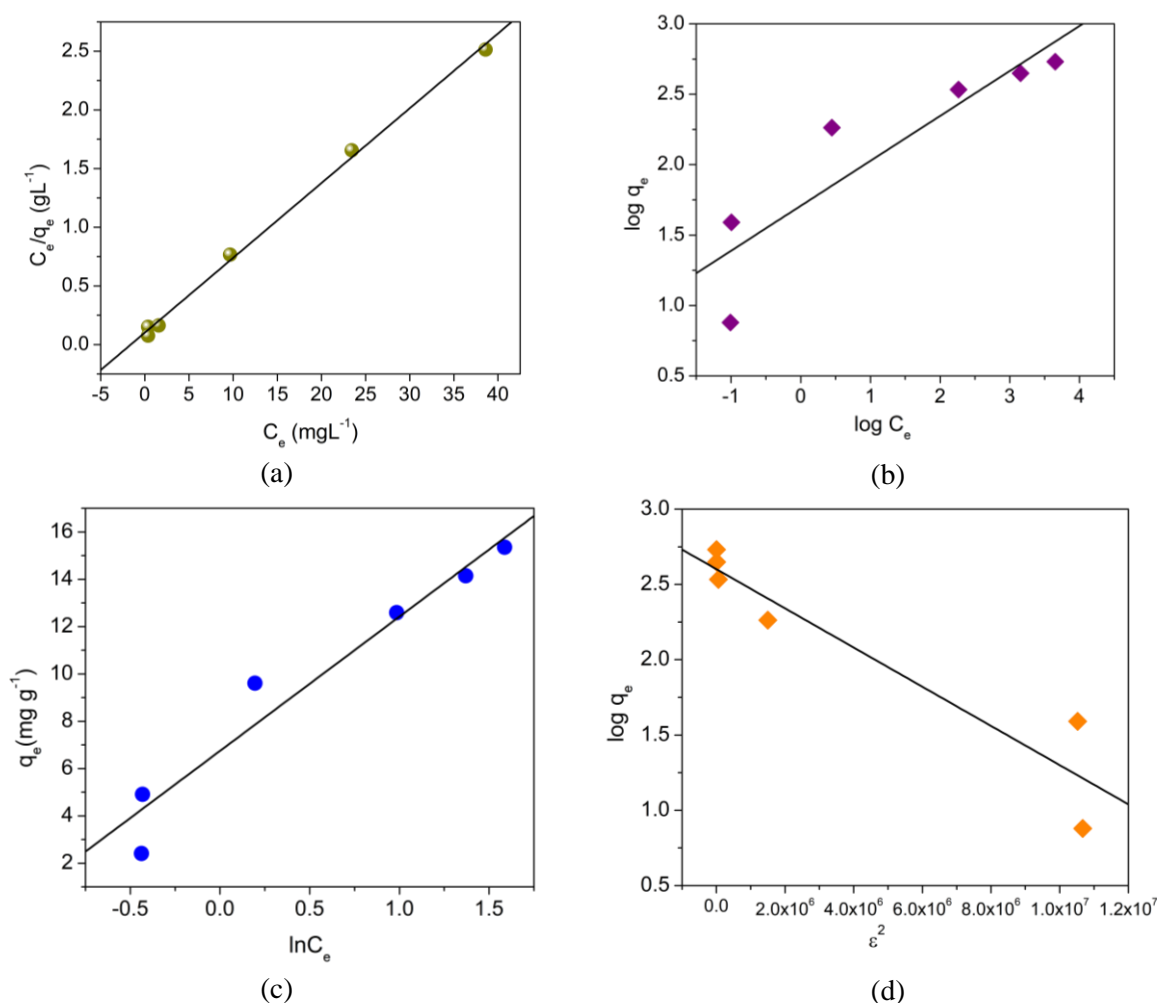


Figure 3.7 Linear fitting of (a) Langmuir (b) Freundlich (c) Temkin and (d) Dubinin–Radushkevich model

3.3.6 Adsorption kinetics studies

Adsorption kinetics studies help in assessing the adsorption mechanisms in terms of order and rate constants and provides useful information on possible rate-controlling steps. Four kinetic models, pseudo-first-order, pseudo-second-order, intraparticle diffusion, and Elovich were used to study the kinetics of the adsorption process. The kinetic graphs obtained are depicted in Figure 3.8 and the plot parameters and are summarised in Table 3.6.

Lagergren's pseudo-first-order kinetic model gives a simple kinetic evaluation of the adsorption of adsorbate between two phases [55]. The first-order rate constant (k_1) and equilibrium capacity (q_e) were determined from the slope and intercept of the linear plots of $\log (q_e - q_t)$ versus time (t) respectively. The linear plot and their corresponding values are given in Figure 3.8a and Table 3.6 respectively. The first-order rate constant (k_1) was found to be 0.031 with a correlation coefficient value (R^2) of 0.895. The experimental adsorption capacity value, $q_{e,(\text{exp})}=9.625$ mg g⁻¹, did not agree with the calculated value, $q_{e,(\text{cal})}=1.396$ mg

g⁻¹. The lower correlation coefficient value and the poor agreement of experimental and calculated adsorption capacity suggest that the pseudo-first-order model is not appropriate to explain the adsorption kinetics of BPA.

The pseudo-second-order model describes the adsorption equilibrium capacity as well as the chemisorptive behaviour of the adsorption process [56]. A plot of t/q_t versus t gives a linear curve as shown in Figure 3.8b, and a high R^2 value of 0.999. Besides, the calculated $q_{e(cal)}=9.716 \text{ mg g}^{-1}$ was found to be close to the experimental data ($q_{e(exp)}=9.625 \text{ mg g}^{-1}$).

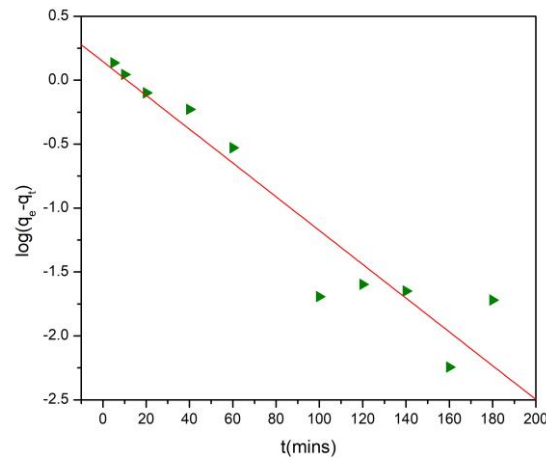
This result implies the pseudo-second-order model best described the adsorption behaviour of BPA onto activated carbon and suggests that the rate-limiting step of the adsorption process is chemical adsorption.

Weber and Morris's intra-particle diffusion model helps identify the diffusion mechanism and the rate-limiting step. The boundary layer thickness(C) and intra-particle diffusion rate constant (k_p) can be deduced from the intercept and slope of the plot of q_t versus the square root of time($t^{1/2}$), respectively. From the plot (Figure 3.8c), it is observed that the adsorption process takes place in two phases. The first phase depicts the rapid adsorption of BPA over a certain period whereas the adsorption rate became slower in the second phase. This could be due to the chemisorptive interactions during the first stages of the adsorption process followed by intraparticle diffusion in the second stage. From Figure 3.8c, the lines failed to pass through the origin, which suggests that intraparticle particle diffusion cannot be considered the rate-limiting step.

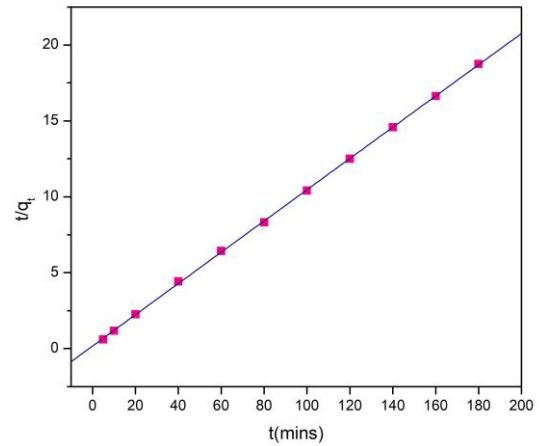
The Elovich model helps in understanding the kinetics of chemisorption of the adsorbate on the solid surface of the adsorbent. The values for a and b are obtained from a plot of q_t versus $\ln t$ (Figure 3.8d), and their values are presented in Table 3.6. The regression coefficient value of Elovich model $R^2 = 0.958$ was higher than for pseudo-first-order but lower than that of the pseudo-second-order and intraparticle diffusion models which indicates the poorer fit of the Elovich model to the experimental data compared to the intraparticle diffusion and pseudo-second-order models.

Table 3.6 Kinetics parameters for the adsorption of BPA				
Kinetics	Parameter	R²	X²	RMSE
Pseudo-first order	$q_{e,(exp)}=9.625$ $q_{e,(cal)}=1.396$ $k_1=0.031$	0.895	0.084	0.290
Pseudo-second order	$q_{e,(exp)}=9.625$ $q_{e,(cal)}=9.716$ $k_2=0.061$	0.999	0.004	0.065
Intraparticle diffusion	$k_p=0.190$ $C=7.888$	0.983	0.005	0.073
Elovich model	$a=4.33 \times 10^7$ $b=2.429$	0.958	0.010	0.102

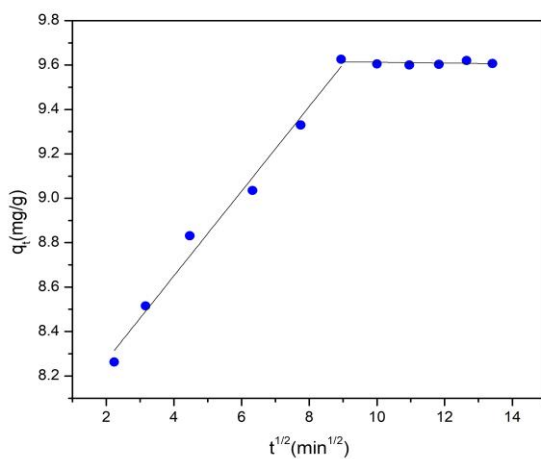
q_e = equilibrium adsorption capacity (mg g^{-1}), q_t = adsorption capacity at time t (mg g^{-1}), k_1 = rate constant of pseudo-first order (min^{-1}), k_2 = rate constant of pseudo-second order ($\text{g mg}^{-1} \text{min}^{-1}$), $q_{e,(cal)}$ = equilibrium calculated BPA concentration (mg g^{-1}), $q_{e,(exp)}$ = experimental BPA concentration at equilibrium (mg g^{-1}); k_p = intra-particle diffusion rate constant ($\text{mg g}^{-1} \text{min}^{1/2}$), C = thickness of the boundary layer, a = initial adsorption coefficient ($\text{mg g}^{-1} \text{min}^{-1}$), b = desorption coefficient (g mg^{-1})



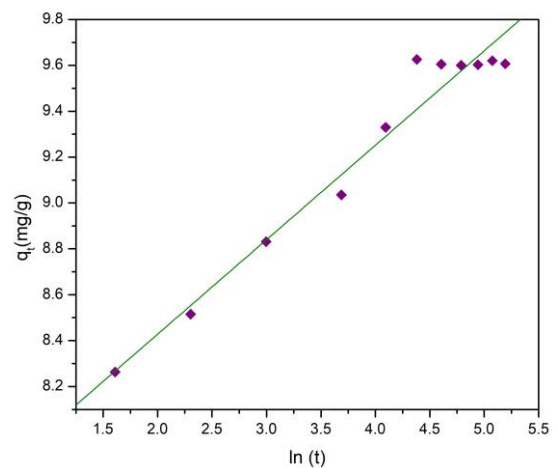
(a)



(b)



(c)



(d)

Figure 3.8 The plots of (a) Pseudo-first-order kinetics model (b) Pseudo-second-order kinetics model (c) Intraparticle diffusion model and (d) Elovich model.

The applicability of the four models was further verified through the root mean square error analyses and chi-squared tests. The R^2 , χ^2 , and RMSE values are given in Table 3.6. It is known that lower values of χ^2 and RMSE and higher values of R^2 indicate the suitability of different kinetic models to the experimental data. The lowest χ^2 and RMSE value and the highest R^2 were obtained for the pseudo-second-order reaction which confirmed the fitness of the model. The fitting of kinetic models based on χ^2 , RMSE, and R^2 follows the following order;

Pseudo-second-order > Intraparticle diffusion > Elovich > Pseudo-first-order model.

3.3.7 Thermodynamic study

The thermodynamic adsorption process of BPA onto *Tithonia diversifolia* activated carbon was carried out by scaling the temperature from 298 K to 318 K wherein the entropy change (ΔS), enthalpy change (ΔH) and Gibbs free energy change (ΔG) were determined. The obtained thermodynamic parameters are given in Table 3.7.

The ΔH and ΔS value were calculated from the plot of $\ln K_d$ versus $1/T$. The positive value of ΔH (64.79 KJ/mol) indicated the endothermic nature and reversibility of the adsorption of BPA while the positive values of ΔS (85.76 J/mol/K) suggested increased randomness at the adsorbate and adsorbent interface during the process of BPA adsorption. The negative ΔG value reflected the spontaneity of the adsorption of BPA.

Table 3.7 Thermodynamic parameters for the adsorption of BPA onto activated carbon					
ΔH (KJ/mol)	ΔS (KJ/mol)	ΔG (KJ/mol)			
		298K	308K	318K	328K
64.79	0.23	-4.74	-7.07	-9.41	-11.74

3.3.8 Computational studies

a) Activated carbon model

For a theoretical study involving the interaction of activated carbon with an adsorbate, the most important requirement is to first establish a correct model for the activated carbon surface. Various authors have considered different models of activated carbon, such as pyrene clusters [57], graphite crystal structures [58], graphene molecular models [59], benzene ring cluster models [60], platelet models [61] and fullerene-related structure of activated carbon [62], for theoretical studies. Various studies have reported that the reactivity of the active sites strongly depended on the local shape of the cluster model rather than on its size [57,63]. Therefore, armchair model consisting of four fused benzene ring clusters ($C_{16}H_6$) with

armchair edge sites was used to simulate the activated carbon surface. The upper side of the carbon atoms in the armchair model was unsaturated to generate an efficient active site while the remaining parts of the cluster were terminated with H atoms. The active site of the cluster was also embedded with different surface functional groups, such as OH, COOH, and CHO, to study the possible effect of these surface functional groups on BPA. The optimized cluster models of activated carbon used for this study are shown in Figure 3.9. The different clusters were named pristine armchair (AC-P), OH embedded armchair (AC-OH), COOH embedded armchair (AC-COOH) and CHO embedded armchair (AC-CHO).

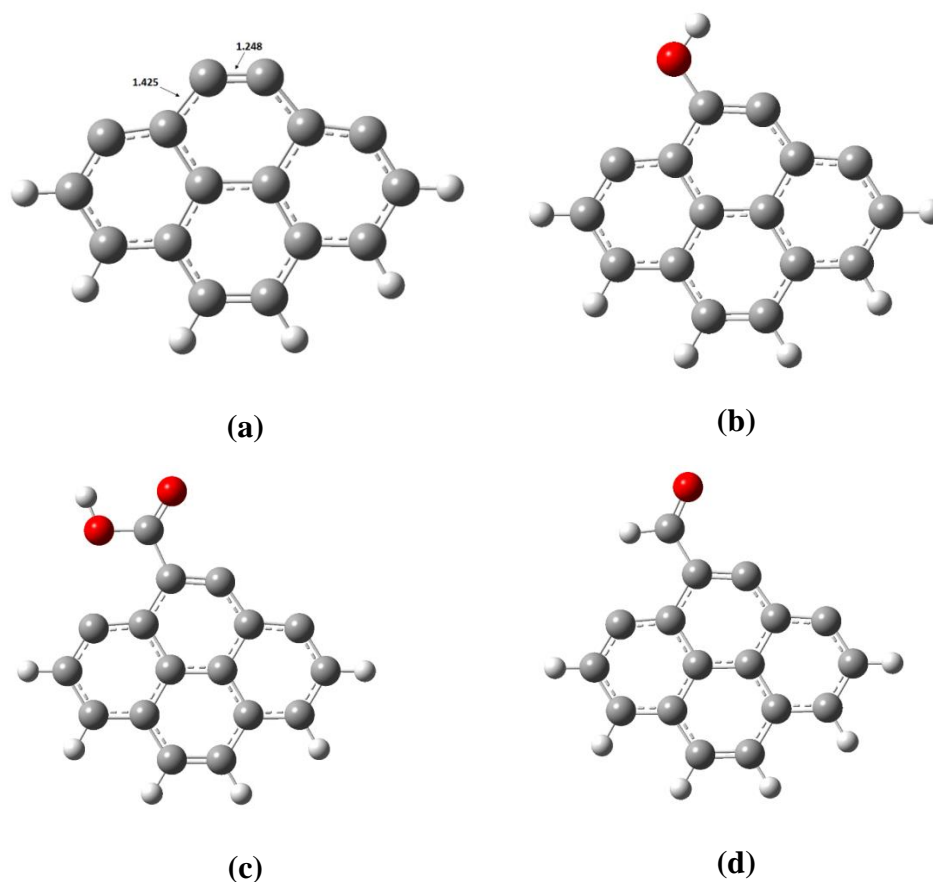


Figure 3.9 Optimized structures of (a) AC-P (b) AC-OH (c) AC-COOH (d) AC-CHO

b) Theoretical calculations

The interaction of BPA with the activated carbon proceeds through chemisorptive interactions i.e π - π bonding, electron donor-acceptor complexes and hydrogen bonding between the oxygen-containing functional groups(-OH,-COOH,-CHO) of activated carbon and the OH group of BPA[64]. Out of the various interactions, the formation of hydrogen bonds between BPA and functionalized activated carbon is an important mode of interaction contributing to the adsorption process [65]. Thus, the effect of hydrogen bond interactions on the adsorptive behaviour of BPA through the DFT approach has been considered for this study. An armchair

model was used to simulate the activated carbon and the interaction of mechanisms of pristine activated carbon and functionalized activated carbon with BPA through hydrogen bonding was studied. Such studies would greatly help in the modification process of activated carbon preparation. Figure 3.10 represents the interaction of BPA adsorption onto pristine and functionalized activated carbon.

BPA adsorption on pristine activated carbon

For the BPA and AC-P system, $(C_{15}H_{15}O)-OH---C(AC)$ mode of interactions were considered for the system where one of the -OH group of BPA was oriented towards the carbon atom of armchair edge site. As can be seen from Figure 3.9a and Figure 3.10a, the adjoining C-C bond lengths of the armchair edge site where an H-atom of BPA was attached elongated from 1.425 Å to 1.453 Å and 1.248 Å to 1.337 Å upon BPA adsorption. This shows that these bonds become weaker because of the electron cloud displacement towards the adsorption site, i.e. the $C_{AC}-H_{BPA}$ bond. Moreover, the E_{adsorp} was found to be $-345.516 \text{ KJ mol}^{-1}$ for the $(C_{15}H_{15}O)-OH---C(AC)$ system which signifies that the interaction between BPA and activated carbon is favourable and chemisorptive in nature.

BPA adsorption on a functionalized activated carbon surface

The surface of activated carbon consists of abundant functional groups that contribute significantly to the adsorption process [66]. The activation of activated carbon using KOH introduces oxygen-containing functional groups into the carbon surface and it is envisaged that these functional groups would interact with the Bisphenol A. Therefore, to get an insight into the interactive mechanism, the possible interactions of three functional groups, -OH, -COOH, -CHO, with the BPA were considered for the study.

The interaction between -OH functionalized activated carbon and BPA was studied by considering two modes of attachment, $(C_{15}H_{15}O)-OH---OH-(AC)$ and $(C_{15}H_{15}O)-HO---HO-(AC)$ (Figure 3.10b and 3.10c). The E_{adsorp} and $H_{BPA}---O_{AC}$ bond length of $(C_{15}H_{15}O)-OH---OH-(AC)$ type of interaction were found to be $-31.9035 \text{ KJ mol}^{-1}$ and 1.766 Å respectively, and for the $(C_{15}H_{15}O)-HO---HO-(AC)$ system, the $O_{BPA}---H_{AC}$ bond distance and E_{adsorp} were found to be 1.656 Å and $-39.0717 \text{ KJ mol}^{-1}$ respectively. The higher negative E_{adsorp} and shorter bond distance of the $(C_{15}H_{15}O)-HO---HO-(AC)$ system indicates the favourability of this type of interaction compared to the $(C_{15}H_{15}O)-OH---OH-(AC)$ system.

For the BPA - AC(COOH) system, two modes of interaction, $(C_{15}H_{15}O)-HO---HOOC-(AC)$ and $(C_{15}H_{15}O)-OH---OHOC-(AC)$, were considered (Figure 3.10d and 3.10e). The E_{adsorp} of

(C₁₅H₁₅O)-HO---HOOC-(AC) was more negative (-55.1855 KJ mol⁻¹.) and the bond length was 1.435 Å shorter than the (C₁₅H₁₅O)-OH---OHOC-(AC) type of interaction. This result implies that the hydrogen bond formed between the oxygen atom of BPA and the hydrogen atom of a COOH group present in activated carbon led to the formation of a more stable conformation, making the adsorption favourable.

With -CHO functionalized AC, the interaction of BPA proceeds through the formation of a hydrogen bond between the H-atom (from the OH group) of BPA and an oxygen atom from a carbonyl group of AC-CHO, as shown in Figure 3.10f. The E_{adsorp} of (C₁₅H₁₅O)-OH---OCH-(AC) was found to be -34.719 KJ mol⁻¹, indicating a weak physisorption interaction.

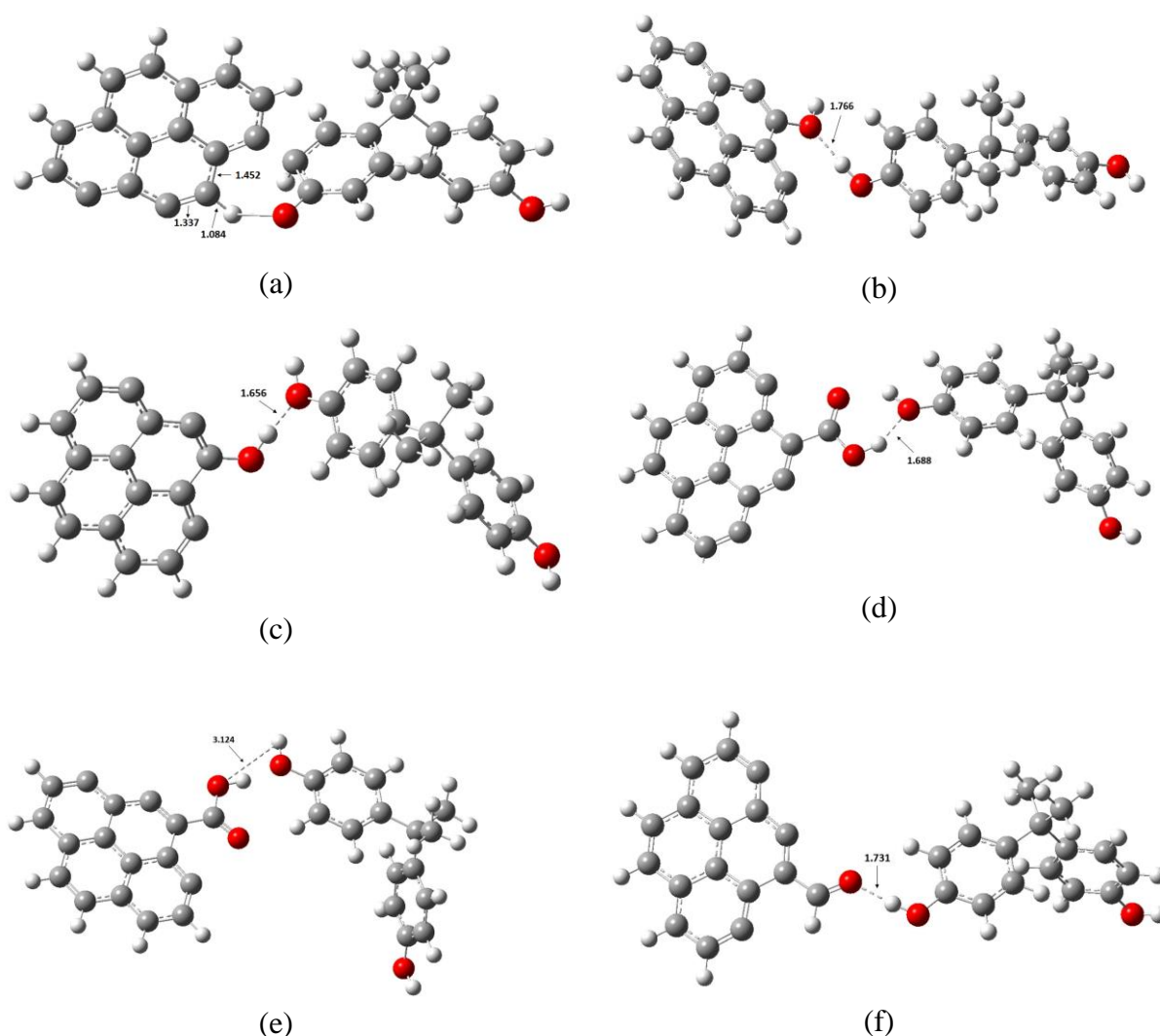


Figure 3.10 Optimized adsorption structure of BPA onto activated carbon(a) (C₁₅H₁₅O)-OH.....C(AC) (b) (C₁₅H₁₅O)-OH.....OH-(AC) (c) (C₁₅H₁₅O)-HO.....HO-(AC) (d) (C₁₅H₁₅O)-OH.....OCH-(AC) (e) (C₁₅H₁₅O)-HO.....HOOC -(AC) (f) (C₁₅H₁₅O)-OH.....OHOC-(AC)

To determine the best possible mode of interaction for the adsorption of BPA onto activated carbon, the relative energies of different optimized configurations of BPA adsorption onto activated carbon were analyzed and are presented in Figure 3.11. The presence of COOH groups on the activated carbon was found to greatly elevate the adsorption process compared to activated carbon functionalized with CHO and OH group. The relative energy and stability of various configurations follow the order:

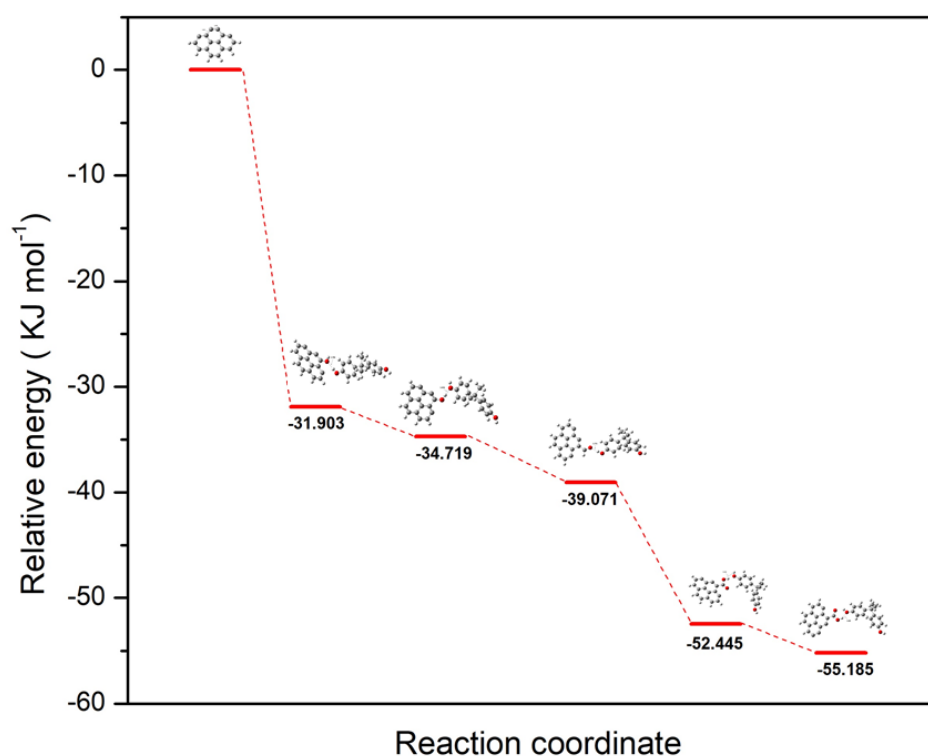
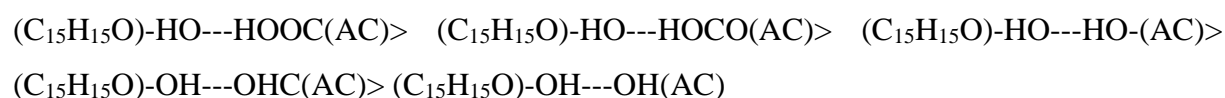


Figure 3.11 Relative energy diagram of adsorption of Bisphenol A onto activated carbon

3.3.9 Comparison of *Tithonia diversifolia* activated carbon with other adsorbent material

To understand the overall efficacy of *Tithonia diversifolia* derived activated carbon obtained in the present work, a comparison was made with some other adsorbents reported in the literature for BPA removal, and the results are listed in Table 3.8. The adsorption capacity of the activated carbon at optimum parameters was considered for comparison. From the results, the *Tithonia diversifolia* derived activated carbon obtained from the present study shows a comparable promising adsorptive capacity with other adsorbents and therefore could be used as an efficient adsorbent for BPA removal.

Table 3.8 Comparison of prepared activated carbon in this study with some other adsorbents reported in the literature for BPA removal

Adsorbent	Surface Area (m ² g ⁻¹)	Pore Volume (m ³ g ⁻¹)	Adsorption capacity for BPA removal q _{max} (mg g ⁻¹)	Source
<i>Tithonia diversifolia</i>	854.44	0.445	15.69	Present Study
<i>Pistacia atlantica</i>	-	-	8	[67]
Coconut Shell-activated carbon	1185	-	23.5	[68]
Modified peat	0.66	-	1.71	[69]
50% CNT/Fe ₃ O ₄	50.6	0.018	43.76	[70]
Rice Husk	--		15.51	[71]
AMBA-sericite	0.93	-	4.816	[72]
Garphene Oxide	20.93	0.99	17.27	[73]
Thermosensitive molecularly imprinted polymer	80.55	0.4776	7.86	[74]
H ₂ SO ₄ -coir pith	-	-	4.31	[75]
H ₂ SO ₄ -coconut shell	4.75	-	4.16	[75]
H ₂ SO ₄ -Durian peel	-	-	4.18	[75]
H ₂ SO ₄ - banana bunches	-	-	4.53	[75]
H ₂ SO ₄ -Coconut bunches	-	-	4.66	[75]
Surfactant modified Zeolite	-	-	6.90	[76]

Section B

Removal of phenol and 2,4-dinitrophenol using *Tithonia diversifolia* activated carbon¹

This section describes the application of *Tithonia diversifolia* activated carbon for the removal of phenol and 2,4-dinitrophenol (DNP) from water. Batch adsorption was used to run the experiments, and the effect of pH, adsorbent dose, initial concentration, temperature, and contact time on the adsorption of phenol and DNP were studied. Adsorption isotherm and kinetics were fitted with the experimental data, and the validation of the models was assessed by applying reduced Chi-Squared Test (χ^2). Thermodynamic studies on the adsorption data were also calculated. DFT calculations were incorporated to understand the adsorptive interaction of the phenolic compound with pristine and functionalized activated carbon. Further, regeneration studies were conducted to test the reusability of the spent adsorbent. The effect of co-ions on removal efficiency was also investigated.

3.4 Adsorption studies of phenol and 2,4-dinitrophenol

Phenol (C_6H_5OH), and 2,4-dinitrophenol ($C_6H_4N_2O_5$) were purchased from Himedia. Stock solutions (1000 mg L^{-1}) of both the adsorbates were prepared, and dilutions were made to obtain the working solutions of various concentrations. All the chemicals used were of analytical grade.

The adsorption of phenol and DNP onto the activated carbon were run in batch experiments. The effect of essential operating factors such as activated carbon dose, pH, contact time, initial adsorbate concentration, and temperature on the adsorption efficiency was studied. For each experiment, 30 ml of adsorbate solution with varying initial concentrations, and the required activated carbon dose was taken and placed in an Erlenmeyer flask. The contents were mixed in a rotary shaker at a constant speed of 180rpm at 298 K for a specific period of time. The contents were then filtered and the residual phenol and DNP concentrations were measured using UV-Visible spectroscopy (lambda 35, Perkin Elmer) at an absorbance of 271 nm for phenol and 358 nm for DNP. Each set of adsorption studies was run in triplicate. The removal efficiency, R% and equilibrium adsorption capacity, q_e were calculated using equation 1 and 2 as described in chapter 2.

¹A. Supong, P.C. Bhomick, R. Karmaker, S.L. Ezung, L. Jamir, U.B. Sinha, D. Sinha, Soremo L. Ezung, Latonglila Jamir, Upasana Bora Sinha, Dipak Sinha, **Experimental and theoretical insight into the adsorption of phenol and 2,4-dinitrophenol onto *Tithonia diversifolia* activated carbon.** *Applied surface science*, 529,2020, 147046. <https://doi.org/10.1016/j.apsusc.2020.147046>.

a) Effect of adsorbent dose

Figure 3.12 represents the removal efficiencies of phenol and DNP as a function of activated carbon dosage. At optimum operating conditions, the removal efficiencies of phenol and DNP significantly increased with increasing dose of activated carbon to a maximum of 99.3% and 97.8% respectively at a dose 0.3g, after which the removal efficiency of phenol and DNP remained almost constant. The increase in removal efficiency at increased adsorbent dose may be attributed to the presence of larger surface area and more binding sites on the activated carbon surface [77]. From the results, 0.3g of activated carbon dose was selected for subsequent experiments.

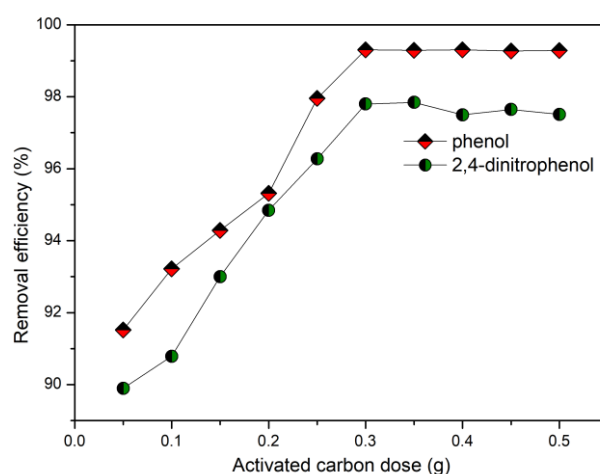


Figure 3.12 Effect of activated carbon dose on removal efficiency (Temperature- 298K; Contact time- 60 mins phenol, 80 mins DNP; pH 8 phenol, pH 6 DNP; Initial concentration- 300 mg L⁻¹ phenol, 200 mg L⁻¹ DNP)

b) Effect of contact time and initial concentration

Figures 3.13 and 3.14 represent the effect of contact time and initial concentration, respectively on the removal efficiency of adsorbates. The optimum initial phenol concentration was found to be 300 mg L⁻¹ at 60 mins equilibrium contact time, and the optimum initial DNP concentration corresponded to 200 mg L⁻¹ at 80 minutes equilibrium contact time.

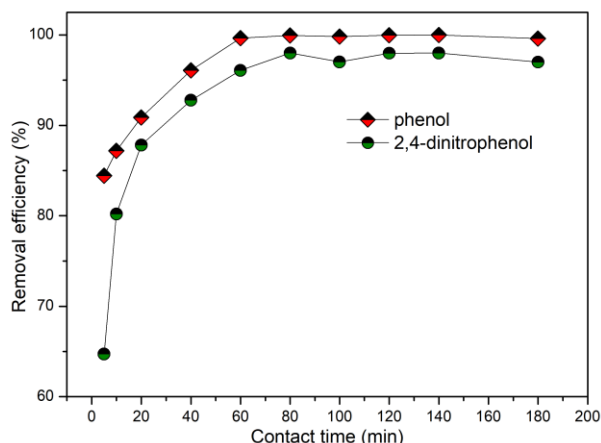


Figure 3.13 Effect of contact time on removal efficiency (Temperature- 298K; pH 8 phenol, pH 6 DNP; Activated carbon dose- 0.3g; Initial concentration- 300 mg L⁻¹phenol, 200 mg L⁻¹ DNP)

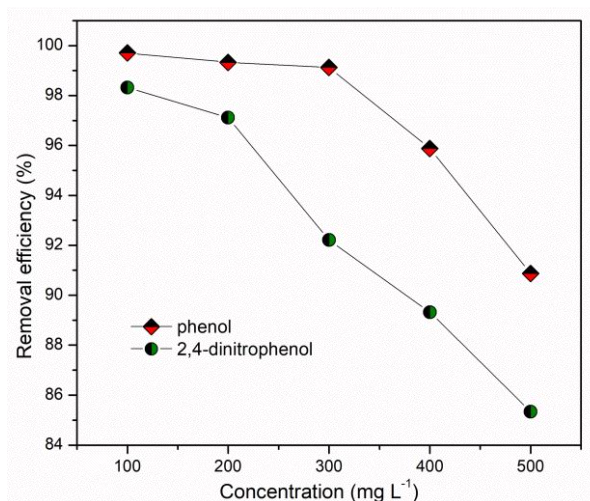


Figure 3.14 Effect of initial concentration on removal efficiency (Temperature- 298K; Activated carbon dose- 0.3g; Contact time- 60 mins phenol, 80 mins DNP; pH 8 phenol, pH 6 DNP)

c) Effect of temperature

Temperature is one of the essential parameters in the adsorption process and has a considerable effect on adsorbent-adsorbate interactive behaviour. The variation in the removal efficiency of phenol and DNP as a function of temperature was studied by increasing the temperature from 298 to 328 K and is shown in Figure 3.15. The adsorption efficiency of phenol and DNP were found to increase with increasing temperature and attained a maximum removal efficiency of 99.99% and 97.82% for phenol and DNP respectively at 328K.

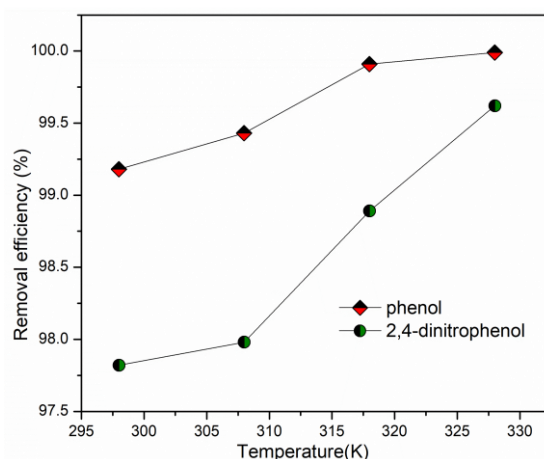


Figure 3.15 Effect of temperature on removal efficiency (Activated carbon dose- 0.3g; pH 8 phenol, pH 6 DNP; Initial concentration- 300 mg L⁻¹phenol, 200 mg L⁻¹ DNP; Contact time- 60 mins phenol, 80 mins DNP)

d) Effect of pH

For any adsorption process, the pH of the aqueous solution is a significant parameter as it affects the chemical properties of the activated carbon and the adsorbate[78]. Generally, adsorbates are neutrally or positively charged at $\text{pH} < \text{pK}_a$ and negatively charged at $\text{pH} > \text{pK}_a$ [79]. Further, if the pH of a solution is lower than the zero-point charge of the activated carbon, then the activated carbon surface acquires a positive charge ($\text{pH} < \text{pH}_{\text{zpc}}$) while if the pH is higher than the zero-point charge, the surface acquires negative charges ($\text{pH} > \text{pH}_{\text{zpc}}$).

The effect of pH was studied over a pH range of 2 to 12 under optimum operating conditions: initial concentration- 300 mg L⁻¹(phenol), 200 mg L⁻¹(DNP); activated carbon dose- 0.3g; contact time- 60 minutes (phenol), 80 minutes (DNP); 298 K temperature. Figure 3.16 presents the effect of pH on phenol and DNP adsorption. For phenol molecule, the removal efficiency raised slightly from 98.29% to 99.45% with an increase in pH from 2 to 8; however, there was a considerable decrease in adsorption efficiency with an increase in pH from 8 to 12. The effect of pH on the removal efficiency could be explained by two important parameters, pK_a values of the phenol and the pH_{zpc} of the adsorbent. The pK_a value of phenol is 9.89, and the pH_{zpc} of activated carbon corresponded to 8.8. Therefore, at pH 2 to 8, the phenol molecule remained undissociated ($\text{pH} < \text{pK}_a$) and the activated carbon surface acquired a positive charge ($\text{pH} < \text{pH}_{\text{zpc}}$). Thus, in this pH range, the attraction between the molecular phenol and the positive carbon surface occurred, resulting in enhanced removal efficiency. However, at higher pH (9 to 12), the phenol molecule dissociated into phenolate anion, and the carbon surface acquired a negative charge ($\text{pH} > \text{pH}_{\text{zpc}}$). Thus, there was repulsion between

the phenolate anion and the negatively charged activated carbon surface, which eventually contributed to low adsorption efficiency.

For DNP, the adsorption favourably occurred over pH 2 to pH 6, and a maximum of 97.72% removal efficiency was attained at pH 6 under optimum operating conditions. At pH 6, the activated carbon acquired positive charge ($\text{pH} < \text{pH}_{\text{zpc}}, 8.8$) and the DNP molecule remained in its anionic form ($\text{pH} > \text{pK}_a, 4.09$), resulting in electrostatic attraction between DNP anion and the positive activated carbon surface. However, at higher pH, the DNP molecule progressively transformed into its phenolate anion ($\text{pH} < \text{pK}_a$), which was repelled by the increasingly negative carbon surface ($\text{pH} > \text{pH}_{\text{zpc}}$) [80]. As a result, the removal of the anionic state of DNP was unfavourable, leading to low removal efficiency at higher pH.

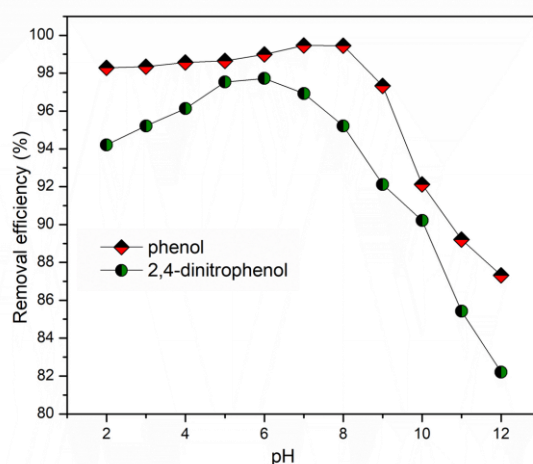


Figure 3.16 Effect of pH on removal efficiency (Contact time- 60 mins phenol, 80 mins DNP; Temperature- 298K; Activated carbon dose- 0.3g; Initial concentration- 300 mg L⁻¹phenol, 200 mg L⁻¹ DNP)

3.4.1 Adsorption isotherm studies

Adsorption isotherms are vital tools for understanding the distribution of an adsorbate between the activated carbon and the aqueous solution at equilibrium. In the present study, three commonly used isotherms, Langmuir, Freundlich, and Temkin were used to study the adsorptive behaviour of phenol and DNP onto the activated carbon. The plot parameters obtained for the isotherm models and chi-squared value (χ^2) are shown in Table 3.9. Based on the correlation coefficient (R^2) and χ^2 value, the Langmuir model best-fitted the experimental adsorption data. The closest fitting of experimental data to the Langmuir model indicated that phenol and DNP adsorption on the activated carbon occurred through monolayer coverage. The maximum adsorption capacity ' q_m ' of phenol (50.552 mg g⁻¹) was higher than 2,4-dinitrophenol (42.607 mg g⁻¹). This could be because of the smaller size of phenol, which

provides a better chance of reaching and occupying the pores of the activated carbon as compared to the larger DNP molecule[32]. The R_L values for phenol and DNP were between 0 and 1 which confirmed the favourability of the Langmuir isotherm for phenol and DNP adsorption onto the activated carbon[81]. From the Freundlich isotherm analysis, the value of 'n' was found to be higher than 1 for both phenol ($n=3.819$) and DNP ($n=4.078$), which indicated that the adsorption of phenol and DNP adsorption onto the activated carbon is favourable [82]. The Temkin constant (b_T) obtained from Temkin isotherm corresponds to the heat of adsorption, and its value was $0.366 \text{ kJ mol}^{-1}$ and $0.440 \text{ kJ mol}^{-1}$ for phenol and DNP respectively. The positive b_T value indicated the adsorption process to be exothermic. The best-fitted isotherm model among the Langmuir, Freundlich, and Temkin was validated from the chi-squared value (χ^2) and correlation coefficient (R^2). The lowest χ^2 and highest R^2 value for the Langmuir isotherm model confirmed its suitability in explaining the equilibrium adsorption of both phenol and DNP onto activated carbon.

Table 3.9 Langmuir, Freundlich and Temkin isotherm parameters		
	Phenol	2,4-dinitrophenol
Langmuir		
q_m	50.352	42.607
K_L	21.825	0.408
R_L	0.0004	0.023
R^2	0.990	0.996
χ^2	1.31×10^{-6}	2.29×10^{-3}
Freundlich		
$1/n$	0.261	0.245
n	3.819	4.078
K_F	50.445	15.865
R^2	0.864	0.922
χ^2	1.02×10^{-2}	4.92×10^{-3}
Temkin		
b_T	0.366	0.440
A_T	10.47	22.705
R^2	0.963	0.986
χ^2	8.992	0.528

3.4.2 Adsorption kinetics study

Adsorption kinetics determine the uptake rate that controls the residence time of adsorbate at the solid-liquid interface[83]. Pseudo-first order, pseudo-second-order, Elovich and intraparticle diffusion models were used for understanding the kinetics of adsorption. The kinetic graphs are given in Figure 3.17 and fitting parameters obtained are shown in Table 3.10.

From the plots, it is clear that the experimental kinetics data for both phenol and DNP could not provide an accurate fit to the pseudo-first-order model. This is indicated by the low correlation factor ($R^2 = 0.895$ for phenol, 0.824 for DNP) and the vast difference in the calculated and experimental q_e values.

For the pseudo-second-order model, the calculated q_e values derived from the pseudo-second-order model were found to be very close to the experimental q_e values, indicating the suitability of the pseudo-second-order model. Besides, the highest correlation factor obtained for both phenol ($R^2 = 0.999$) and DNP ($R^2 = 0.996$) indicated that the pseudo-second-order model is indeed the best-fitted model. The pseudo-second-order rate constant (k_2) of phenol and DNP were found to be 0.04 and 0.01 respectively, the greater k_2 value for phenol indicated that the phenol removal attained a faster equilibrium than DNP[84]. This could be attributed to the smaller size of phenol molecules which allowed them to reach and occupy the active sites/pores of the activated carbon with more ease as compared to the DNP molecule, and subsequently, the activated carbon surface reached saturation faster.

The Elovich model describes the chemical nature of the adsorption process. The 'a' value is related to the initial adsorption rate. The 'a' value for phenol (1.64×10^8) was higher than DNP (1.10×10^4) indicating the fast nature of phenol adsorption compared to DNP. The correlation coefficient (R^2) values for the Elovich kinetic model corresponded to 0.80 and 0.93 for phenol and DNP respectively. The lower R^2 value indicated the poor fitting of the Elovich model to the experimental data.

The mass transfer process of phenol and DNP at the solid-liquid interface was described using the intraparticle diffusion model. The plot of intraparticle diffusion model showed two stages of adsorption, initial and final stage (Figure 3.17d). The first stage of adsorption was due to the boundary layer diffusion and the final stage to the intraparticle diffusion of phenol molecules[6]. The intraparticle diffusion rate constant K_{p1} was greater than K_{p2} , indicating that the intraparticle diffusion rate became slower in the final stage of adsorption. This decrease in diffusion rate may have resulted from the blockage of pores and steric repulsive barrier induced by adsorbed phenol/DNP on the activated carbon surface. The intraparticle diffusion will be the only rate-controlling step if the plot passes through the origin. The linear plots deviated from the origin indicating that intraparticle diffusion is not the only rate-limiting step, but other kinetics mechanisms simultaneously control the adsorption process.

Chi-squared test (χ^2) further validated the kinetic models. The χ^2 value of the pseudo-second-order model was lowest, suggesting that the pseudo-second-order model well elucidated the kinetics of phenol and DNP adsorption.

Table 3.10 Kinetic parameters for the adsorption of phenol and DNP					
Adsorbates	Pseudo-first order model	Pseudo-second order model	Elovich model	Intraparticle diffusion model	
Phenol	$q_{e,(\text{exp})} = 29.52$ $q_{e,(\text{cal})} = 1.39$ $k_1 = 0.03$ $R^2 = 0.89$ $\chi^2 = 8.46 \times 10^{-2}$	$q_{e,(\text{exp})} = 29.52$ $q_{e,(\text{cal})} = 29.70$ $k_2 = 0.04$ $R^2 = 0.99$ $\chi^2 = 7.90 \times 10^{-5}$	$a = 1.64 \times 10^8$ $b = 0.78$ $R^2 = 0.80$ $\chi^2 = 5.30 \times 10^{-1}$	Initial stage $K_{p1} = 1.78$ $C = 20.98$ $R^2 = 0.99$ $\chi^2 = 3.71 \times 10^{-2}$	Final stage $K_{p2} = 0.08$ $C = 28.90$ $R^2 = 0.65$ $\chi^2 = 2.31 \times 10^{-2}$
DNP	$q_{e,(\text{exp})} = 19.34$ $q_{e,(\text{cal})} = 6.29$ $k_1 = 0.03$ $R^2 = 0.82$ $\chi^2 = 9.47 \times 10^{-2}$	$q_{e,(\text{exp})} = 19.345$ $q_{e,(\text{cal})} = 19.821$ $k_2 = 0.01$ $R^2 = 0.99$ $\chi^2 = 1.84 \times 10^{-2}$	$a = 1.10 \times 10^4$ $b = 0.70$ $R^2 = 0.93$ $\chi^2 = 1.77 \times 10^{-1}$	Initial stage $K_{p1} = 0.98$ $C = 12.69$ $R^2 = 0.98$ $\chi^2 = 1.22 \times 10^{-1}$	Final stage $K_{p2} = 0.12$ $C = 17.89$ $R^2 = 0.33$ $\chi^2 = 2.78 \times 10^{-1}$

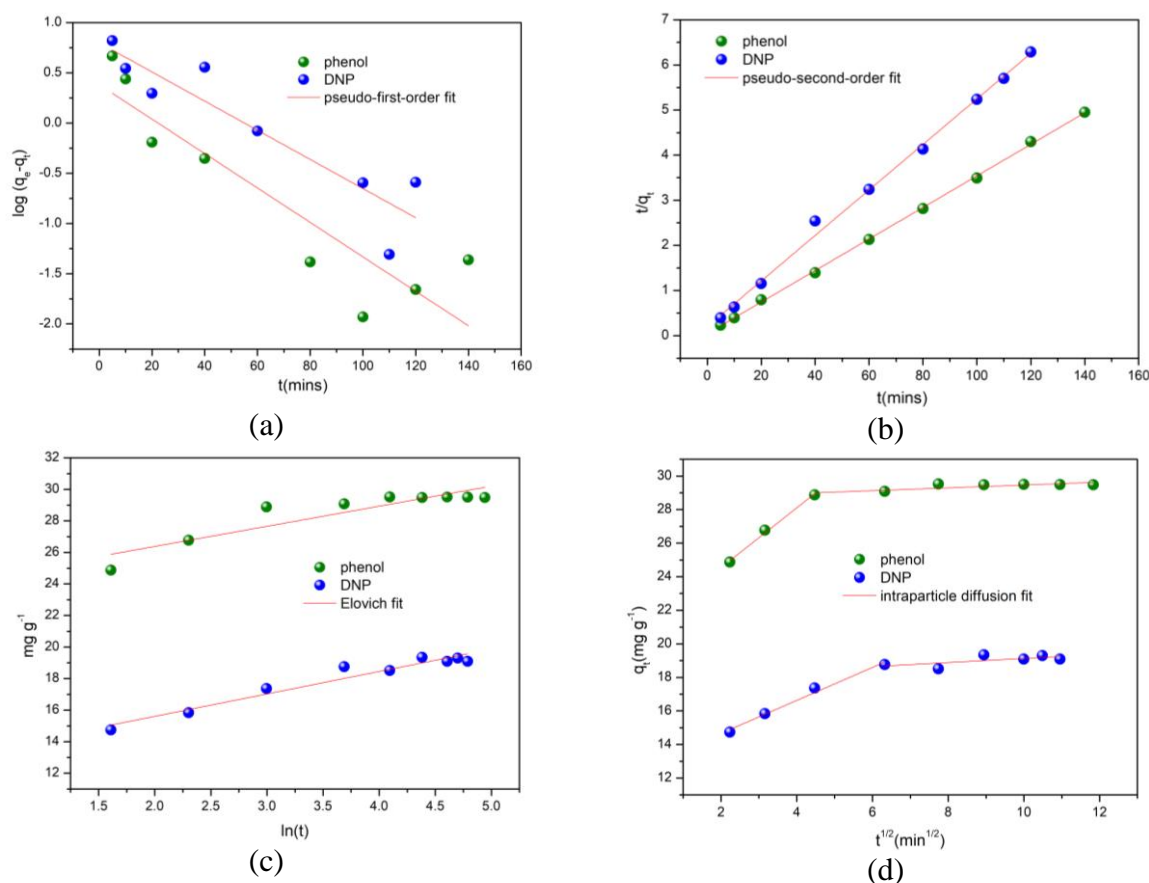


Figure 3.17 (a) pseudo-first-order and (b) pseudo-second-order (c) Elovich and (d) Intraparticle diffusion adsorption kinetics plot for phenol and DNP.

3.4.3 Thermodynamics study

The thermodynamic study of the adsorption of phenol and DNP were conducted over the temperature range 298K to 318 K. The thermodynamic parameters, enthalpy change (ΔH) and entropy change (ΔS) were graphically determined by equations 18, 19 and 20, as described in chapter 2.

The obtained values of various thermodynamic parameters are shown in Table 3.11. The values of ΔH for phenol and DNP adsorption were 121.63 kJ mol⁻¹ and 47.42 kJ mol⁻¹ respectively. The positive ΔH values inferred the endothermic nature of the adsorption process[85]. The positive ΔS value indicated increased randomness at the adsorbate/solution interface during the adsorption process [86] and the negative ΔG values demonstrated the feasibility and spontaneity of the adsorption process. The decrease in ΔG value with an increase in temperature suggested the favourability of the adsorption process at elevated temperatures[87].

Table 3.11. Thermodynamic parameters for phenol and DNP adsorption onto activated carbon					
$\Delta H(\text{kJ/mol})$	$\Delta S(\text{kJ/mol})$	$\Delta G(\text{kJ/mol})$			
		298K	308K	318K	328K
121.63	0.42	-4.82	-9.07	-13.31	-17.56
47.42	0.16	-3.07	-4.76	-6.45	-8.15

3.5 Effect of co-existing ions

Wastewater commonly consists of various inorganic ions and thus, it is essential to study the effect of these co-existing ions on the removal efficiency of phenol and DNP from aqueous solution. Therefore, the adsorption of phenol and DNP in the presence CO_3^{2-} , NO_3^- and Cl^- was investigated. The effect of these ions on phenol and DNP removal efficiency is depicted in Figure 3.18. A decrease in the removal efficiency of phenol and DNP was observed in the presence of the co-ions, which may be due to the competition between the phenols and the ions for the same active sites on the activated carbon surface. The effect of co-ions with respect to removal efficiency of phenol and DNP decreased in the order: $\text{CO}_3^{2-} > \text{NO}_3^- > \text{Cl}^-$. The greater influence of divalent anion, CO_3^{2-} may be attributed to its higher negative charge, which allows it to bind more strongly on the activated carbon surface via electrostatic interaction.

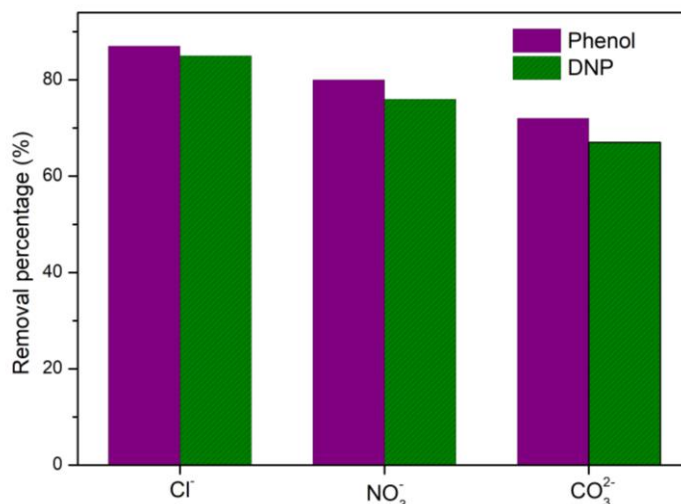


Figure 3.18 Effect of co-existing ions on phenol and DNP adsorption onto activated carbon.

(Conditions: ionic concentration - 0.1 mol/L; activated carbon dose- 0.3g; Initial concentration- 300 mg L⁻¹phenol, 200 mg L⁻¹ DNP; pH 8 phenol, pH 6 DNP; Contact time- 60 mins phenol, 80 mins DNP; Temperature-298K)

3.6 Regeneration studies

Regeneration studies help in evaluating the feasibility of the adsorption process in real practice. The regeneration cycles i.e., the process of adsorption and desorption were carried out up to the fifth cycle, to understand the efficacy and reusability of the regenerated activated carbon. Figure 3.19 presents the removal efficiency of the regenerated activated carbon over five cycles of use. After the first cycle, the removal efficiency of the regenerated carbon was 83.21% and 85.99% for phenol and DNP respectively, and their respective adsorption proficiency slightly decreased to 80.43% and 82.01% after the fifth cycle. The decrease in phenol removal efficiency after the fifth cycle could be due to the inability of NaOH to fully flush/desorb the adsorbate loaded onto the adsorbent surface. Further, due to the adsorption of the regenerant (NaOH) itself on the activated carbon surface[88], permanent loss of active sites takes place [88].

The regeneration of the activated carbon occurred mainly because, in NaOH solution, phenol transforms into phenolate anions, and the carbon surface acquires a negative charge. The phenolate anions repel the negatively charged carbon surface, which results in the desorption of the adsorbate from the saturated activated carbon. Additionally, the reaction of alkaline NaOH with the phenols forms sodium-phenol salt, which further facilitated the desorption of phenol and DNP from the activated carbon surface[89]. These studies indicate that sodium hydroxide could be used for recovery of phenol and DNP loaded activated carbon, and the regenerated carbon could be reused several times with minimal loss in adsorption efficiency,

leading to the sustainability of the overall adsorption process. However, more in-depth regeneration studies are required to optimise the regeneration process parameters and increase the adsorptive capacity and reusability of the spent carbon

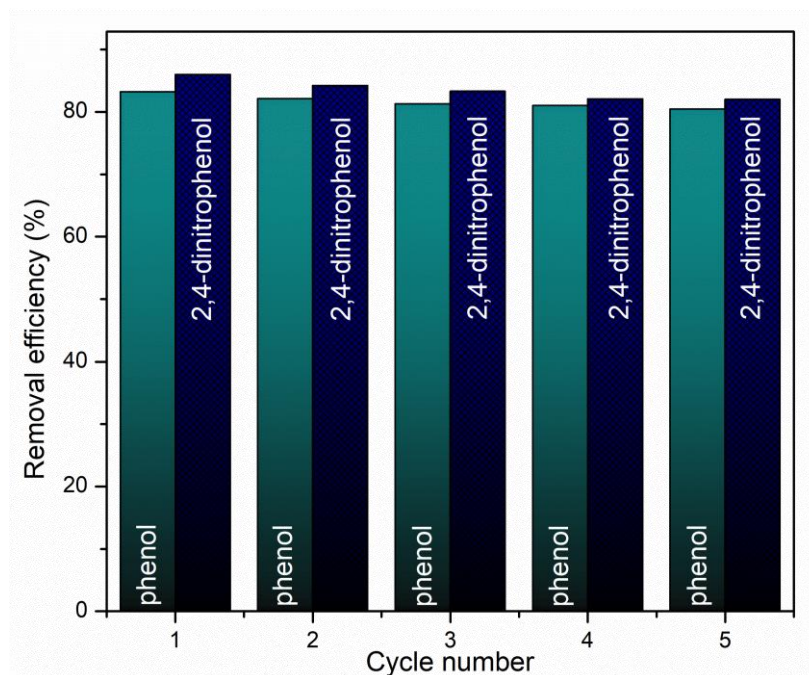


Figure 3.19 Regeneration of activated carbon over five cycles (regenerated carbon dose-0.3g; contact time- 60 minutes (Phenol), 80 minutes (DNP). adsorbate concentration- 300 mg L⁻¹(Phenol), 200 mg L⁻¹ (DNP); 298K temperature.

3.7 Adsorption mechanism

The development of a possible mechanism for phenol and DNP adsorption onto the activated carbon would improve our understanding of the adsorbate-adsorbent interaction. The schematic representation of the possible adsorption mechanism is presented in Figure 3.20. The adsorption of phenol and DNP by activated carbon might take place through various mechanisms like (a) Electrostatic interaction, (b) π - π interaction, (c) Electron donor-acceptor mechanism and (d) Hydrogen bond[1]. A brief explanation for each adsorption mechanism is given below.

Electrostatic interaction

When the pH of the solution is lower than the pH_{zpc} of activated carbon and the pK_a of phenol/DNP, the activated carbon surface will be positively charged and phenol/DNP would remain undissociated under this condition. This will result in an electrostatic attraction between the electron-rich benzene ring of phenol/DNP and the positively charged carbon surface. At pH higher than the pK_a value and pH_{zpc} , the phenol will dissociate into phenolate

anion, and the carbon surface will acquire a negative charge, which would result in electrostatic repulsive interaction between phenolate anion and negatively charged carbon surface. According to our experimental results, electrostatic attractive interaction would occur at solution $\text{pH} < 8$ for phenol, and at $\text{pH} < 6$ for DNP.

π - π interaction

The π - π interaction assumes charge transfer between the π -electrons of the aromatic rings of phenols and the π -electrons of the activated carbon surface[40]. The presence of an electron-withdrawing group would enhance the π - π interaction and reduce the repulsion between consecutive aromatic rings. Therefore, DNP would exhibit stronger π - π interaction as compared to phenol, owing to the presence of two strong electron-withdrawing nitro-functional groups.

Electron donor-acceptor mechanism

Mattson et al.[41] first proposed the electron donor-acceptor complex mechanism. According to this mechanism, the phenol aromatic ring acts as the electron acceptor and the surface functional group of activated carbon acts as an electron donor. The electron-donating groups of activated carbon donate the electrons to the aromatic ring of phenol and DNP, resulting in increased uptake capacity of phenol and DNP onto the activated carbon.

Hydrogen bond

Hydrogen bonding occurs by sharing electrons between the activated carbon and the phenolic compound. It is considered one of the strongest interaction mechanisms of the adsorption process[1]. Hydrogen bond formation may take place between the -OH or -NO₂ group of phenol and DNP and the activated carbon surface at various positions, which enhances the adsorption efficiency.

3.8 Theoretical calculations

a) Activated carbon model

To comprehend the adsorption mechanism of phenol and DNP on the activated carbon at the molecular and theoretical levels, appropriate models simulating the activated carbon surface need to be established. Solid-state ¹³C nuclear magnetic resonance experiments revealed that the activated carbon surface consists of three to seven fused benzene rings[90]. In previous theoretical studies, cluster models consisting of four to seven fused benzene rings were used for simulating the activated carbon surface, and these models proved valuable in understanding the adsorptive interaction of various species with the activated carbon

surface[57,60,91–96]. Therefore, in this study, six fused benzene rings with armchair edge sites simulated the activated carbon surface. The carbon atoms on the upper side were unsaturated to simulate the active sites while the remaining carbon atoms were terminated with hydrogen atoms. The presence of oxygenated functionals on the activated carbon is known to affect the adsorptive properties significantly. Therefore, three oxygenated surface functional groups, -CHO, -OH, and -COOH were attached to the active site of the activated carbon model to understand the influence of these functional groups on the phenol and DNP adsorption process. Figure 3.21 represents the optimised activated carbon models. The activated carbon models were pristine activated carbon (AC), -COOH functionalized activated carbon (COOH-AC), -CHO functionalized activated carbon (CHO-AC), -OH functionalized activated carbon (OH-AC) and -COOH, -OH, -CHO functionalized activated carbon (COOH+OH+CHO-AC)

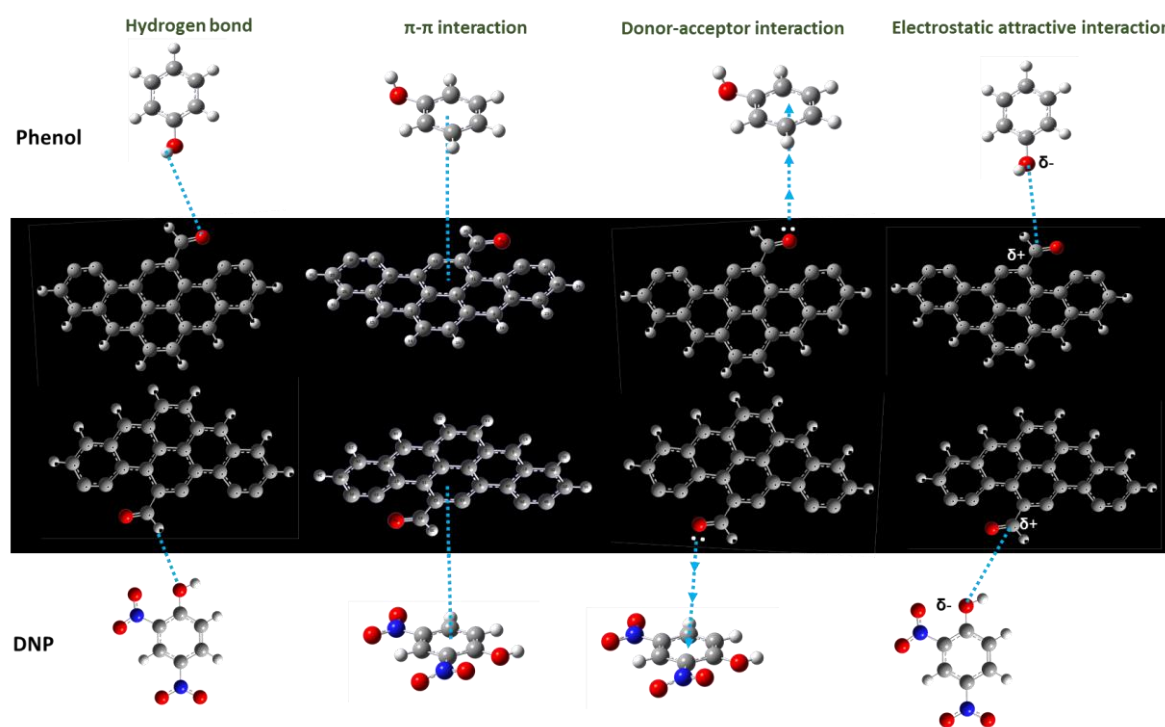


Figure 3.20 Schematic representation of the different mechanism for phenol and DNP adsorption on activated carbon

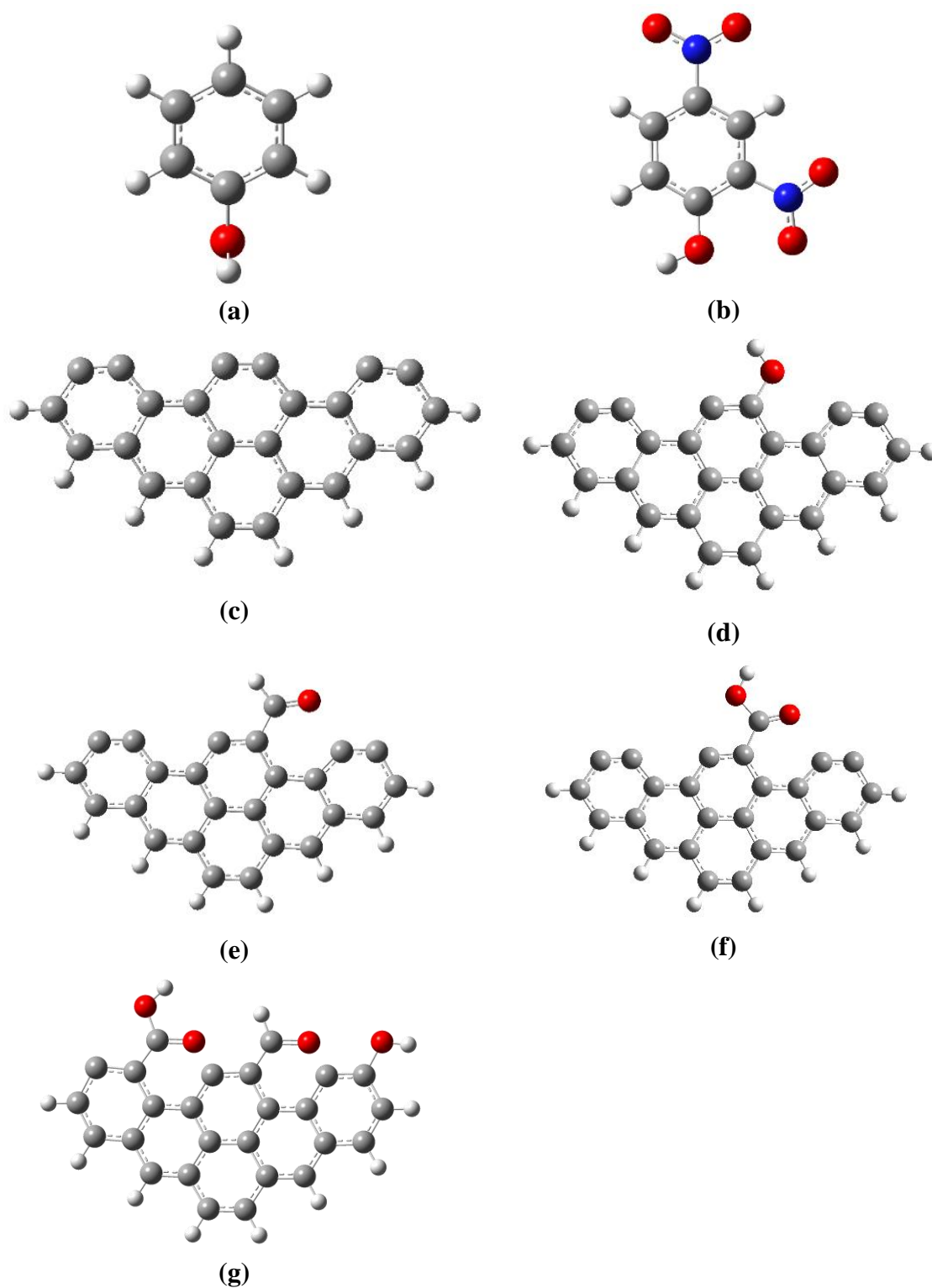


Figure 3.21 Optimised molecular structure of (a) Phenol and (b) 2,4-dinitrophenol (c) AC (d) OH-AC (e) CHO-AC (f) COOH-AC (g) COOH+OH+CHO-AC

b) Theoretical calculations

Amongst the various adsorptive interactions between the phenols and activated carbon surface, hydrogen bonding is one of the most significant modes of interaction that enhances the adsorption process. Therefore, the present study attempted to elucidate the possible modes of hydrogen bond formation between activated carbon and the adsorbate using DFT calculations. The armchair model with six-fused benzene ring simulated the pristine activated carbon surface. Oxygenated surface functional groups, -COOH, -CHO, and -OH were also embedded on the pristine armchair activated carbon model to study the effects of such groups on the adsorption of phenol and DNP.

In most cases, phenolic compounds interact with the carbon surface either through its benzene ring or the hydroxyl group. The present study focused on understanding the possible interaction of hydroxyl groups of phenol and DNP with the pristine and functionalized activated carbon through hydrogen bond formation. The optimised structures representing the adsorbate-adsorbent interactions are represented in Figure 3.22, while the bond distance and adsorption energies obtained for the different interactions are given in Table 3.12.

Adsorption on pristine activated carbon

To comprehend the probable adsorptive interaction of phenol and DNP with the pristine activated carbon surface, hydrogen bond formation between a carbon atom of the activated carbon surface and the hydroxyl oxygen atom in phenol (P-OH) and 2,4-dinitrophenol (DNP-OH) was considered. The optimised structures representing the phenol and pristine activated carbon interaction (P-HO-----C-AC) and DNP and pristine activated carbon interaction (DNP-HO-----C-AC) are shown in Figures 3.22(a) and 3.23(b) respectively. Phenol adsorption onto the pristine activated carbon was found to proceed *via* the dissociation of P-OH into P-O and H leading to the formation of two interactions: H_P-----C-AC and P-O-----C-AC. Similarly, the DNP-OH dissociated into DNP-O and H atom, and these dissociated species interacted with the pristine activated carbon surface resulting in DNP-O-----C-AC and H_{DNP}-----C-AC interactions.

The C-C bond distance of the pristine activated carbon where the oxygen atom of phenolic hydroxyl group was directly attached elongated from 1.24Å to 1.37Å and 1.24Å to 1.36Å upon phenol and DNP adsorption respectively. These observations indicated that the electron density moves towards the adsorption sites and weakens the C-C bond of activated carbon. The adsorption energy of both P-HO-----C-AC and DNP-HO-----C-AC interactions were found to be highly negative, indicating a thermodynamically favourable adsorption process.

On comparing the adsorption energy and O-C bond length of P-O-----C-AC and DNP-O-----C-AC, higher negative adsorption energy and shorter O-C bond distance were observed for phenol. These results suggest that phenol adsorbed more firmly onto the pristine activated carbon surface as compared to DNP, which agrees well with the experimental observation.

Adsorption on OH functionalized activated carbon

To understand the phenol and DNP adsorption onto the OH-functionalized activated carbon, the interactive mechanism involving the formation of a hydrogen bond between the oxygen atom of phenolic hydroxyl group and hydrogen atom of OH-AC was considered. The optimised structures representing the hydrogen bond interaction of phenol with OH functionalized activated carbon (P-HO-----HO-AC) and DNP with OH functionalized activated carbon (DNP-HO-----HO-AC) are given in Figure 3.22(c) and 3.22(d) respectively. The O-H bond distance of OH-AC increased from 0.97 Å to 1.02 Å and 0.97 Å to 0.99 Å upon phenol and DNP adsorption, respectively. This observation indicated that the electron density around the O-H bond of activated carbon shifts towards the adsorption site and results in stronger adsorbate-activated carbon interaction. The negative adsorption energy of -55.03 kJ mol⁻¹ and -31.17 kJ mol⁻¹ for P-HO-----HO-AC and DNP-HO-----HO-AC was obtained, indicating a favourable adsorption process.

The interaction of OH-functionalized activated carbon with phenol was found to be stronger than its interaction with DNP as indicated by the shorter O-H bond distance of P-HO-----HO-AC.

Adsorption on CHO functionalized activated carbon

The probable adsorptive interaction of phenol and DNP with the CHO-AC was examined by considering the hydrogen bond formation between the adsorbate and adsorbent. The hydrogen bond formation between the adsorbate and the CHO-functionalized activated carbon surface occurred in numerous ways. However, the adsorptive interaction involving hydrogen bond formation between the hydrogen of the phenolic hydroxyl group and the oxygen of CHO-AC resulted in the most stable interaction. The minimum energy structure representing the adsorption of phenol onto CHO-AC (P-OH-----OHC-AC) and DNP onto CHO-AC (DNP-OH-----OHC-AC) is given in Figure 3.22(e) and 3.22(f) respectively. For P-OH-----OHC-AC interaction, the C=O bond distance of AC-CHO increased from 1.25 Å to 1.26 Å while the phenol O-H bond distance elongated from 0.97 Å to 0.99 Å upon adsorption. As for DNP-OH-----OHC-AC interaction, the DNP C=O and O-H bond distance of AC-CHO increased from 1.25 Å to 1.26 Å and 0.97 Å to 1.01 Å respectively. These results indicate that the

electron density tends to accumulate more towards the interaction site during the adsorption process and results in greater interaction between the phenol/DNP and adsorbent. The adsorption energy of P-OH-----OHC-AC was $-49.02 \text{ kJ mol}^{-1}$, while for DNP-OH-----OHC-AC, the adsorption energy was $-47.73 \text{ kJ mol}^{-1}$ respectively. The negative adsorption energies indicate the favourability of the adsorption process.

Adsorption on COOH functionalized activated carbon

The interaction of phenol and DNP with the COOH-AC surface proceeded via the simultaneous occurrence of two hydrogen bonds between the adsorbate and AC-COOH. One of the hydrogen bonds were found to exist between oxygen atom of the adsorbate and the hydrogen atom of AC-COOH, while the other hydrogen bond formed between oxygen of AC-COOH and the hydroxyl hydrogen of adsorbate. The optimised interaction structures are given in Figure 3.22(d) and 3.22(h). The hydrogen bond formation between phenol and AC-COOH is represented by P-HO-----HOOC-AC and P-OH-----OHOC-AC. The $O_{\text{P}}\text{-H}_{\text{AC}}$ and $H_{\text{P}}\text{-O}_{\text{AC}}$ bond length corresponded to 1.64 \AA and 2.02 \AA respectively, and the adsorption energy was found to be -63 kJ mol^{-1} for such interactions. Upon adsorption, the electron cloud around the O-H bond of phenol and AC-COOH shifted towards the interaction site, indicating the strengthening of the hydrogen bond formed between phenol and AC-COOH.

In the case of 2,4-dinitrophenol and AC-COOH interaction, the O-H bond distance of DNP and AC-COOH increased from 0.97 \AA to 0.99 \AA and 0.97 \AA to 0.99 \AA respectively upon DNP and AC-COOH bonding. The weakening of the O-H bond leads to the strengthening of the hydrogen bond between DNP and AC-COOH, thus favouring the adsorption process. The bond length for DNP-OH-----OHOC-AC and DNP-HO-----HOOC-AC was 1.80 \AA and 1.76 \AA respectively and the adsorption energy was found to be $-48.75 \text{ kJ mol}^{-1}$. The high negative adsorption energy and the decrease in bond distance indicate the favourability of P-HO-----HOOC-AC and DNP-HO-----HOOC-AC interactions.

Table 3.12 Adsorption energy and bond distance of phenol-AC and DNP-AC system			
System	Interactions	Adsorption energy (kJ mol^{-1})	Bond distance (\AA)
Phenol + activated carbon	P-HO-----C-AC	-355.26	1.39
	P-HO-----HO-AC	-55.03	1.66
	P-OH-----OHC-AC	-49.02	1.77
	P-HO-----HOOC-AC	-63.00	1.64
	P-OH-----OHOC-AC		2.02
DNP + activated carbon	DNP-HO-----C-AC	-323.86	1.42
	DNP-HO-----HO-AC	-31.17	1.93
	DNP-OH-----OHC-AC	-47.73	1.61
	DNP-HO-----HOOC-AC	-48.75	1.80
	DNP-OH-----OHOC-AC		1.76

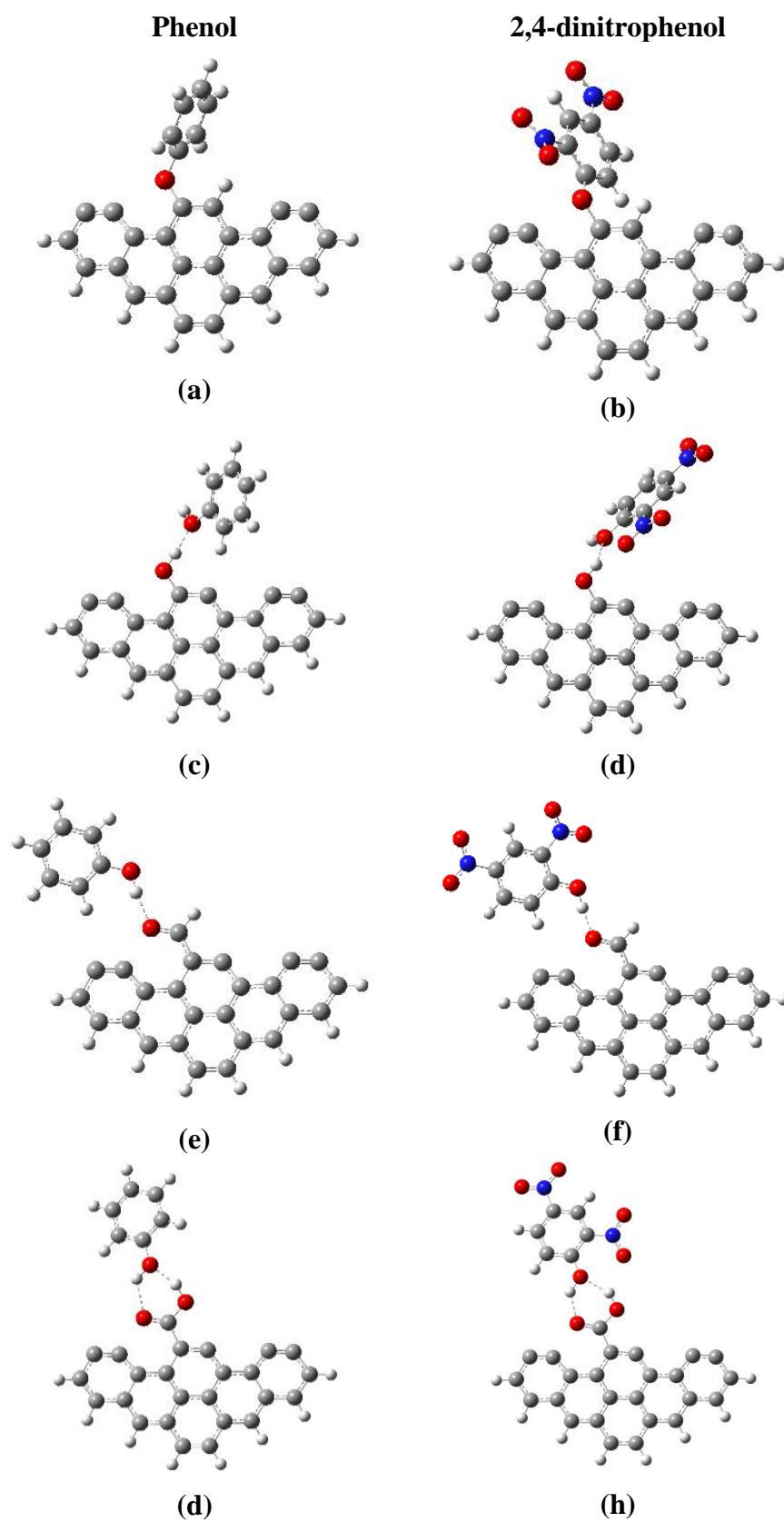


Figure 3.22 Optimised structure representing (a) P-HO----C-AC (b) DNP-HO----C-AC (c) P-HO----HO-AC (d) DNP-HO----HO-AC (e) P-OH----OHC-AC (f) DNP-OH----OHC-AC (g) P-HO----HOOC-AC and (h) DNP-

HO-----HOOC-AC interactions

Relative adsorption energies of phenol and DNP on activated carbon

The energy profile diagrams depicting the relative adsorption energies for adsorptive interaction of phenol and DNP with activated carbon are given in Figure 3.23(a) and 3.23(b) respectively.

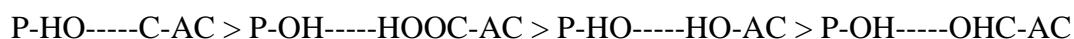
From the energy profile diagram, the adsorption energies of phenol molecule with the pristine and functionalized activated carbon are comparatively higher than DNP, indicating that phenol molecule shows stronger adsorptive interactions with both the pristine and functionalized carbon surface. These results supported the experimental higher removal efficiency and adsorptive capacity of phenol as compared to DNP.

From Figure 3.23(a) and 3.23(b), it can be observed that adsorption energies of phenol and DNP on the pristine activated carbon surface are more negative than their adsorption energies on the functionalized activated carbon surface. This indicates that the presence of oxygenated functional groups on the activated carbon surface less favoured the adsorption of phenol and DNP, compared to their adsorption on pristine activated carbon.

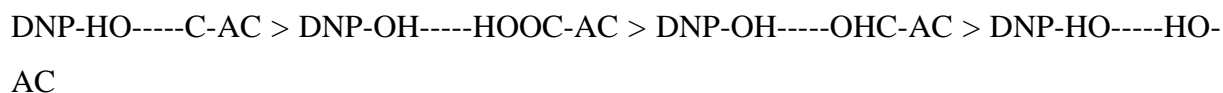
However, among the various oxygenated functional groups, AC-COOH interacted more strongly with both phenol and DNP as compared to AC-OH and AC-CHO. This may be attributed to the simultaneous formation of two hydrogen bonds between AC-COOH and the adsorbate as compared to single hydrogen bond formation with AC-OH and AC-CHO. These theoretical outcomes suggest that the modification of the activated carbon surface with carboxyl group may favour the adsorption of phenol and DNP more as compared to hydroxyl and carbonyl functional groups.

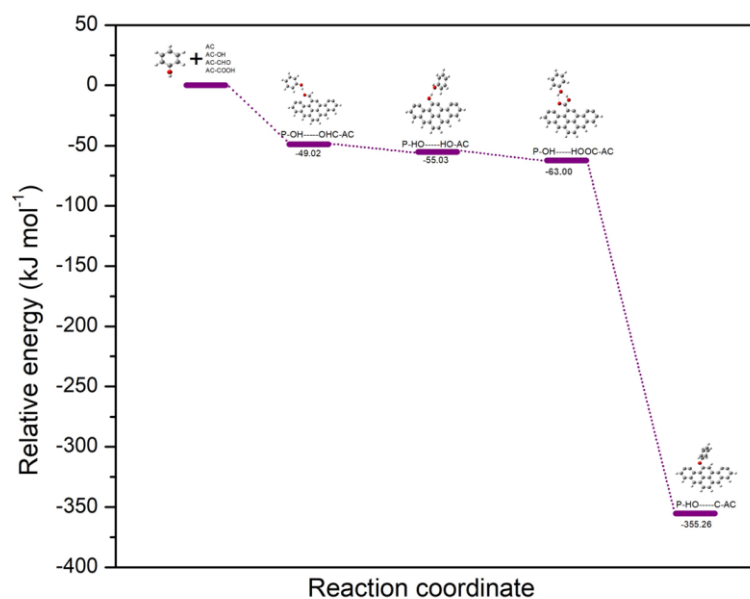
The relative adsorption energies and stability of the different modes of interactions decrease in the following order:

For phenol,

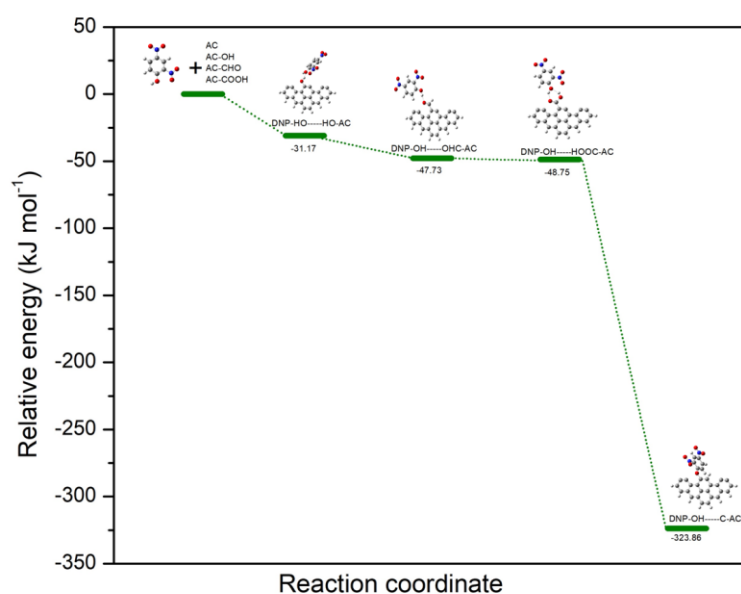


For 2,4-dinitrophenol,





(a)



(b)

Figure 3.23 Energy profile diagram of (a) Phenol and (b) 2,4-dinitrophenol

To examine the net effect of the three oxygenated functional groups on the adsorption of phenol and DNP, -COOH, -OH, and -CHO were embedded together on the active site of the pristine activated carbon and possible interactions were studied. For this study, the activated carbon model was designated as (COOH+OH+CHO-AC). The optimised COOH+OH+CHO-AC structure and its possible interactions with phenol and DNP are given in Figure 3.21(g) and Figure 3.24 respectively. The COOH+OH+CHO-AC preferably interacted with phenol

and DNP by forming hydrogen bond. The hydrogen bonding occurred between the carboxyl hydrogen atom of COOH+OH+CHO-AC and the hydroxyl oxygen atom of phenol molecule, however, for DNP, the hydrogen bond formation occurred between the carboxyl hydrogen atom of COOH+OH+CHO-AC and the oxygen atom belonging to the nitro group of DNP molecule.

The adsorption energy of phenol and COOH+OH+CHO-AC interaction was found to be -70 kJ mol^{-1} , which is more than the adsorption energy obtained for interaction of phenol with different functional groups like COOH-AC, OH-AC, or CHO-AC. However, the adsorption energy of DNP and COOH+OH+CHO-AC interaction was -43 kJ mol^{-1} , which was almost similar to the adsorption energies obtained for interactions of phenol with COOH-AC, OH-AC, or CHO-AC. Thus, the results demonstrated that the net effect of these oxygenated groups on activated carbon surface enhanced the binding of phenol with the activated carbon surface. On the other hand, the presence of all three functional groups on the activated carbon surface did not yield any significant change in the binding of DNP with the activated carbon surface.

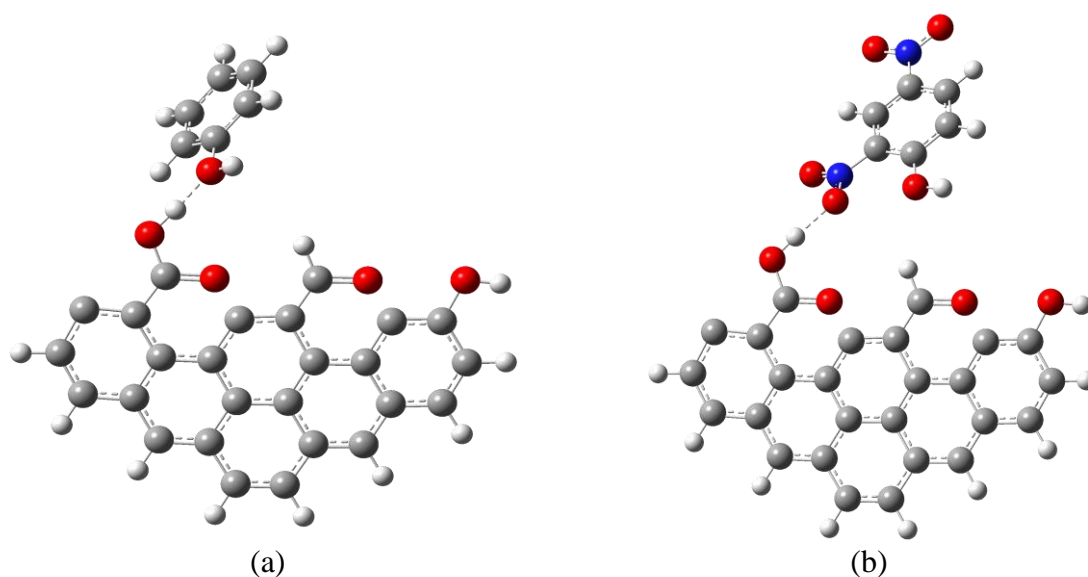


Figure 3.24 (a) Optimised structure of COOH+OH+CHO-AC (b) Interaction between COOH+OH+CHO-AC and phenol (c) Interaction between COOH+OH+CHO-AC and DNP

3.9 Comparative study of adsorption capacity of various adsorbents

A comparative study of the prepared activated carbon with other adsorbents was done to comprehend the relative efficiency of the prepared activated carbon for phenol and DNP removal from water. The maximum adsorption capacity (q_{\max}) of the activated carbon obtained from the Langmuir isotherm was compared with the q_{\max} of some other adsorbents

reported in the literature. The results of the comparison are shown in Table 3.13, and it is observed that the present activated carbon has comparatively higher adsorption capacity for both phenol and 2,4-dinitrophenol, as compared to other adsorbents in literature. Thus, *Tithonia diversifolia* activated carbon could be a potential adsorbent for the effective removal of phenolic compounds from water.

Table 3.13 Comparative study of adsorption capacity of various adsorbents			
Adsorbate	Adsorbent	Adsorption capacity (mg g⁻¹)	Reference
Phenol	<i>Tithonia diversifolia</i> activated carbon	50.552	This study
	Activated coal	1.48	[97]
	Activated carbon-Laboratory grade	24.64	[98]
	Activated carbon-commercial grade	30.21	[98]
	Sugarcane bagasse fly ash	23.83	[98]
	Commercial activated carbon	6.13	[99]
	Activated carbon-K ₂ CO ₃ impregnation	17.83	[100]
	Activated carbon- KOH impregnation	45.49	[100]
	Banyan root activated carbon	26.95	[88]
	Banana Peel activated carbon	48.58	[101]
DNP	<i>Tithonia diversifolia</i> activated carbon	42.607	This study
	Char ash	7.55	[2]
	Cotton cakes activated carbon		
	Impregnation ratios 1:1, concentration 1.5 M	19.273	[102]
		19.691	[102]
	Impregnation ratios 2:1, concentration 1 M	20.424	[102]
	Impregnation ratios 2:1, concentration 1.5 M		
	Cotton cakes and olive stones activated carbon	9.112	[103]
	Olive stone activated carbon	13.867	[103]
	Microbeads	16.2	[104]
	Chemically treated kola nut pod	32.26	[105]
	Carbon nanospheres	32.9	[106]

3.10 Application to real water samples

The practical applicability of the activated carbon was evaluated by conducting the removal of phenol and DNP in real wastewater environment. The real water sample experiments were conducted in triplicates under optimised process conditions (activated carbon dose- 0.3g; pH 8 phenol, pH 6 DNP; contact time- 60 mins phenol, 80 mins DNP; Temperature-298K). The sample was spiked with 100 mg/L initial concentration of phenol and DNP. The removal

efficiency of phenol and DNP in the wastewater environment using activated carbon is depicted in Figure 3.25 while Figure 3.26 showed the image of the wastewater collection site. The mean removal efficiency values corresponded to 85.23% for phenol and 79.31% for DNP.

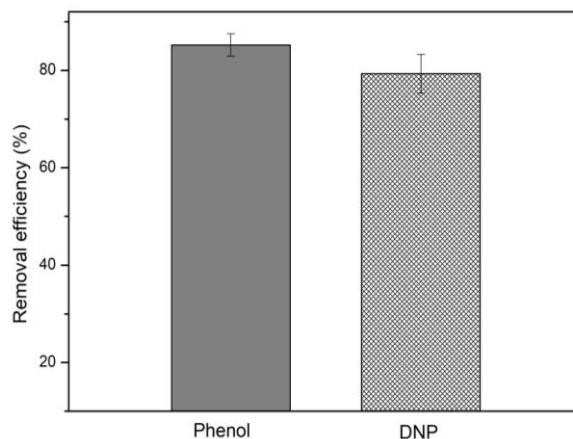


Figure 3.25 Removal efficiency of phenol and DNP in the real water environment



Figure 3.26 Wastewater collection site

3.11 Conclusion

Activated carbon prepared from *Tithonia diversifolia* biomass served as an excellent adsorbent for the removal of phenol, DNP and BPA from aqueous solution. The use of statistical Taguchi approach for designing the experiment helped reduce the use of resources and time. The signal to noise ratios (S/N) obtained from the Taguchi method indicated that 2:1 KOH:TUC impregnation ratio and 700°C activation temperature is the optimum condition for the preparation of activated carbon with maximum surface area. SEM images and XRD analysis indicated the presence of a porous network and graphite-like microcrystallites on the *Tithonia diversifolia* activated carbon. FT-IR revealed the presence of various functional groups such as hydroxyl, carboxyls, carbonyls, ester etc on the activated carbon surface. The

TGA thermogram of all the activated carbon samples was similar and no weight loss was observed above 650°C reflecting the thermal stability of the prepared activated carbon samples at relatively high heating temperature upto 900°C.

The adsorption process was found to be in good agreement with the Langmuir isotherm model with a maximum adsorption capacity(q_m) of 15.69 mg g⁻¹ for BPA, 50.552 mg g⁻¹ for phenol and 42.607 mg g⁻¹ for DNP. The pseudo-second-order kinetic model best described the adsorption kinetics for all the phenols. The thermodynamic parameters revealed the endothermic and spontaneous nature of the adsorption process. DFT studies also indicated the favourability of the adsorption of BPA onto activated carbon, with COOH functional group greatly enhancing the adsorption process. The thermodynamic studies suggest that the adsorption process was endothermic($\Delta H > 0$) and spontaneous ($\Delta G < 0$). Theoretical investigations through density functional theory calculations provided new insights into the adsorption of BPA, phenol and DNP on pristine and functionalized (-COOH, -CHO, -OH) activated carbon. Regeneration studies showed that the regenerated carbon could be used multiple times with considerable removal efficiency.

Thus, from the results obtained in this work, it can be concluded *Tithonia diversifolia* activated carbon could serve as a suitable adsorbent for the removal of BPA, phenol and 2,4-dinitrophenol from aqueous solution. Besides, the results obtained from theoretical studies could potentially aid in the design and preparation of activated carbon with a maximum affinity for these phenolic compounds.

References

- [1] P.Q. Thang, K. Jitae, B.L. Giang, N.M. Viet, P.T. Huong, Potential application of chicken manure biochar towards toxic phenol and 2,4-dinitrophenol in wastewaters, *J. Environ. Manage.* 251 (2019) 109556. doi:10.1016/j.jenvman.2019.109556.
- [2] Y.M. Magdy, H. Altaher, E. ElQada, Removal of three nitrophenols from aqueous solutions by adsorption onto char ash: equilibrium and kinetic modeling, *Appl. Water Sci.* 8 (2018) 1–15. doi:10.1007/s13201-018-0666-1.
- [3] X. Zhou, C. Lai, D. Huang, G. Zeng, L. Chen, L. Qin, P. Xu, M. Cheng, C. Huang, C. Zhang, C. Zhou, Preparation of water-compatible molecularly imprinted thiol-functionalized activated titanium dioxide: Selective adsorption and efficient photodegradation of 2, 4-dinitrophenol in aqueous solution, *J. Hazard. Mater.* 346 (2018) 113–123. doi:10.1016/j.jhazmat.2017.12.032.
- [4] J.R. Kim, S.G. Huling, E. Kan, Effects of temperature on adsorption and oxidative degradation of bisphenol A in an acid-treated iron-amended granular activated carbon, *Chem. Eng. J.* 262 (2015) 1260–1267. doi:10.1016/j.cej.2014.10.065.
- [5] M.H. Dehghani, M. Ghadermazi, A. Bhatnagar, P. Sadighara, G. Jahed-Khaniki, B. Heibati, G. McKay, Adsorptive removal of endocrine disrupting bisphenol A from aqueous solution using chitosan, *J. Environ. Chem. Eng.* 4 (2016) 2647–2655. doi:10.1016/j.jece.2016.05.011.
- [6] L.A. de Sousa Ribeiro, G.P. Thim, M.O. Alvarez-Mendez, A. dos Reis Coutinho, N.P. de Moraes, L.A. Rodrigues, Preparation, characterization, and application of low-cost açai seed-based activated carbon for phenol adsorption, *Int. J. Environ. Res.* 12 (2018) 755–764. doi:10.1007/s41742-018-0128-5.
- [7] Y. Zhang, C. Causserand, P. Aimar, J.P. Cravedi, Removal of bisphenol A by a nanofiltration membrane in view of drinking water production, *Water Res.* 40 (2006) 3793–3799. doi:10.1016/j.watres.2006.09.011.
- [8] M. Umar, F. Roddick, L. Fan, H. Abdul, Chemosphere Application of ozone for the removal of bisphenol A from water and wastewater – A review, *Chemosphere.* 90 (2013) 2197–2207. doi:10.1016/j.chemosphere.2012.09.090.
- [9] L. Joseph, L.K. Boateng, J.R.V. Flora, Y.G. Park, A. Son, M. Badawy, Y. Yoon, Removal of bisphenol A and 17 α -ethinyl estradiol by combined coagulation and adsorption using carbon nanomaterials and powdered activated carbon, *Sep. Purif. Technol.* 107 (2013) 37–47. doi:10.1016/j.seppur.2013.01.012.
- [10] J. Heo, J.R. V Flora, N. Her, Y. Park, J. Cho, A. Son, Y. Yoon, Removal of bisphenol A and 17 b -estradiol in single walled carbon nanotubes – ultrafiltration (SWNTs – UF) membrane systems, *Sep. Purif. Technol.* 90 (2012) 39–52. doi:10.1016/j.seppur.2012.02.007.
- [11] R.F. Lane, C.D. Adams, S.J. Randtke, R.E. Carter, ScienceDirect Chlorination and chloramination of bisphenol A , bisphenol F , and bisphenol A diglycidyl ether in drinking water, *Water Res.* 79 (2015) 68–78. doi:10.1016/j.watres.2015.04.014.
- [12] E.J. Eio, M. Kawai, C. Niwa, M. Ito, S. Yamamoto, T. Toda, Biodegradation of bisphenol A by an algal-bacterial system, *Environ. Sci. Pollut. Res.* 22 (2015) 15145–15153. doi:10.1007/s11356-015-4693-2.

- [13] S.E. Agarry, T.O.K. Audu, B.O. Solomon, Kinetics of batch microbial degradation of phenols by indigenous binary mixed culture of *Pseudomonas aeruginosa* and *Pseudomonas fluorescens*, *Int. J. Environ. Pollut.* 43 (2010) 177–189. doi:10.1504/IJEP.2010.035922.
- [14] J. Zambrano, B. Min, Comparison on efficiency of electrochemical phenol oxidation in two different supporting electrolytes (NaCl and Na₂SO₄) using Pt/Ti electrode, *Environ. Technol. Innov.* 15 (2019) 100382. doi:10.1016/j.eti.2019.100382.
- [15] M. V. Bagal, P.R. Gogate, Degradation of 2,4-dinitrophenol using a combination of hydrodynamic cavitation, chemical and advanced oxidation processes, *Ultrason. Sonochem.* 20 (2013) 1226–1235. doi:10.1016/j.ultsonch.2013.02.004.
- [16] Z. Dong, R. Zhou, L. Xiong, H. Li, Q. Liu, L. Zheng, Z. Guo, Z. Deng, Preparation of a Ti_{0.7}W_{0.3}O₂/TiO₂ nanocomposite interfacial photocatalyst and its photocatalytic degradation of phenol pollutants in wastewater, *Nanoscale Adv.* (2020) 425–437. doi:10.1039/c9na00478e.
- [17] H. Rahmani, A. Lakzian, A. Karimi, A. Halajnia, Efficient removal of 2,4-dinitrophenol from synthetic wastewater and contaminated soil samples using free and immobilized laccases, *J. Environ. Manage.* 256 (2020) 109740. doi:10.1016/j.jenvman.2019.109740.
- [18] X. Yang, Z. Bai, B. Wang, F. Jie, Optimal ternary extractant for phenol removal from wastewater: Modeling and application, *Sep. Sci. Technol.* 54 (2019) 69–78. doi:10.1080/01496395.2018.1501394.
- [19] N.A. Yusof, N.D. Zakaria, N.A.M. Maamor, A.H. Abdullah, M.J. Haron, Synthesis and characterization of molecularly imprinted polymer membrane for the removal of 2,4-dinitrophenol, *Int. J. Mol. Sci.* 14 (2013) 3993–4004. doi:10.3390/ijms14023993.
- [20] Y. Xi, Z. Sun, T. Hreid, G.A. Ayoko, R.L. Frost, Bisphenol A degradation enhanced by air bubbles via advanced oxidation using in situ generated ferrous ions from nano zero-valent iron / palygorskite composite materials, *Chem. Eng. J.* 247 (2014) 66–74. doi:10.1016/j.cej.2014.02.077.
- [21] E. Saputra, X. Duan, J. Armedi Pinem, S. Bahri, S. Wang, Shape-controlled Co₃O₄ catalysts for advanced oxidation of phenolic contaminants in aqueous solutions, *Sep. Purif. Technol.* 186 (2017) 213–217. doi:10.1016/j.seppur.2017.02.057.
- [22] N. Baig, Ihsanullah, M. Sajid, T.A. Saleh, Graphene-based adsorbents for the removal of toxic organic pollutants: A review, *J. Environ. Manage.* 244 (2019) 370–382. doi:10.1016/j.jenvman.2019.05.047.
- [23] B. Kakavandi, A. Raofi, S.M. Peyghambarzadeh, B. Ramavandi, M.H. Niri, M. Ahmadi, Efficient adsorption of cobalt on chemical modified activated carbon: Characterization, optimization and modeling studies, *Desalin. Water Treat.* 111 (2018) 310–321. doi:10.5004/dwt.2018.22238.
- [24] M. Ahmadi, M. Hazrati Niari, B. Kakavandi, Development of maghemite nanoparticles supported on cross-linked chitosan (γ-Fe₂O₃@CS) as a recoverable mesoporous magnetic composite for effective heavy metals removal, *J. Mol. Liq.* 248 (2017) 184–196. doi:10.1016/j.molliq.2017.10.014.
- [25] M. Omidvar Borna, M. Pirsaeheb, M. Vosoughi Niri, R. Khosravi Mashizie, B.

- Kakavandi, M.R. Zare, A. Asadi, Batch and column studies for the adsorption of chromium(VI) on low-cost Hibiscus Cannabinus kenaf, a green adsorbent, *J. Taiwan Inst. Chem. Eng.* 68 (2016) 80–89. doi:10.1016/j.jtice.2016.09.022.
- [26] M. Wołowicz, B. Muir, K. Zieba, T. Bajda, M. Kowalik, W. Franus, Experimental Study on the Removal of VOCs and PAHs by Zeolites and Surfactant-Modified Zeolites, *Energy and Fuels*. 31 (2017) 8803–8812. doi:10.1021/acs.energyfuels.7b01124.
- [27] A. Rajput, P.P. Sharma, V. Yadav, H. Gupta, V. Kulshrestha, Synthesis and characterization of different metal oxide and GO composites for removal of toxic metal ions, *Sep. Sci. Technol.* 54 (2019) 426–433. doi:10.1080/01496395.2018.1500596.
- [28] N. Benosmane, B. Boutemour, S.M. Hamdi, M. Hamdi, Removal of phenol from aqueous solution using polymer inclusion membrane based on mixture of CTA and CA, *Appl. Water Sci.* 8 (2018). doi:10.1007/s13201-018-0643-8.
- [29] N. Ouasfi, M. Zbair, S. Bouzikri, Z. Anfar, M. Bensitel, H. Ait Ahsaine, E. Sabbar, L. Khamliche, Selected pharmaceuticals removal using algae derived porous carbon: experimental, modeling and DFT theoretical insights, *RSC Adv.* 9 (2019) 9792–9808. doi:10.1039/C9RA01086F.
- [30] A. Supong, P.C. Bhomick, U.B. Sinha, D. Sinha, A combined experimental and theoretical investigation of the adsorption of 4-Nitrophenol on activated biocarbon using DFT method, *Korean J. Chem. Eng.* 36 (2019) 2023–2034. doi:10.1007/s11814-019-0382-z.
- [31] O. Article, N. You, J. Li, H. Fan, H. Shen, In-Situ Sampling of Nitrophenols in Industrial Wastewaters Using Diffusive Gradients in Thin Films based on Lignocellulose-derived Activated Carbons, 15 (2018) 77–86. doi:10.1016/j.jare.2018.09.005.
- [32] A.M. Carvajal-Bernal, F. Gómez, L. Giraldo, J.C. Moreno-Piraján, Adsorption of phenol and 2,4-dinitrophenol on activated carbons with surface modifications, *Microporous Mesoporous Mater.* 209 (2015) 150–156. doi:10.1016/j.micromeso.2015.01.052.
- [33] S.J. Park, W.Y. Jung, Effect of KOH activation on the formation of oxygen structure in activated carbons synthesized from polymeric precursor, *J. Colloid Interface Sci.* 250 (2002) 93–98. doi:10.1006/jcis.2002.8309.
- [34] R.C. Bansal, M. Goyal, Activated carbon adsorption, 2005. doi:10.1680/bwtse.63341.147.
- [35] B. Zhang, P. Xu, Y. Qiu, Q. Yu, J. Ma, H. Wu, G. Luo, M. Xu, H. Yao, Increasing oxygen functional groups of activated carbon with non-thermal plasma to enhance mercury removal efficiency for flue gases, *Chem. Eng. J.* 263 (2015) 1–8. doi:10.1016/j.cej.2014.10.090.
- [36] X. Liang, J. Chi, Z. Yang, The influence of the functional group on activated carbon for acetone adsorption property by molecular simulation study, *Microporous Mesoporous Mater.* 262 (2018) 77–88. doi:10.1016/j.micromeso.2017.06.009.
- [37] W. Dilokekunakul, P. Teerachawanwong, N. Klomkliang, S. Supasitmongkol, S. Chaemchuen, Effects of nitrogen and oxygen functional groups and pore width of

- activated carbon on carbon dioxide capture: Temperature dependence, *Chem. Eng. J.* 389 (2020). doi:10.1016/j.cej.2020.124413.
- [38] C.H. Tessmer, R.D. Vidic, L.I. Uranowski, Impact of oxygen-containing surface functional groups on activated carbon adsorption of phenols, *Environ. Sci. Technol.* 31 (1997) 1872–1878. doi:10.1021/es960474r.
- [39] D. Zhang, P. Huo, W. Liu, Behavior of phenol adsorption on thermal modified activated carbon, *Chinese J. Chem. Eng.* 24 (2016) 446–452. doi:10.1016/j.cjche.2015.11.022.
- [40] R.W. Coughlin, F.S. Ezra, Role of Surface Acidity in the Adsorption of Organic Pollutants on the Surface of Carbon, *Environ. Sci. Technol.* 2 (1968) 291–297. doi:10.1021/es60016a002.
- [41] J.A. Mattson, H.B. Mark, M.D. Malbin, W.J. Weber, J.C. Crittenden, Surface chemistry of active carbon: Specific adsorption of phenols, *J. Colloid Interface Sci.* 31 (1969) 116–130. doi:10.1016/0021-9797(69)90089-7.
- [42] M. Franz, H.A. Arafat, N.G. Pinto, Effect of chemical surface heterogeneity on the adsorption mechanism of dissolved aromatics on activated carbon, *Carbon N. Y.* 38 (2000) 1807–1819. doi:10.1016/S0008-6223(00)00012-9.
- [43] ASTM, Standard method for chemical analysis of wood charcoal, *Am. Soc. Test. Mater.* (1990) 292–293.
- [44] U.D. Hamza, N.S. Nasri, N.S. Amin, J. Mohammed, H.M. Zain, Characteristics of oil palm shell biochar and activated carbon prepared at different carbonization times, *Desalin. Water Treat.* 57 (2016) 7999–8006. doi:10.1080/19443994.2015.1042068.
- [45] S. Mopoung, P. Moonsri, W. Palas, S. Khumpai, Characterization and Properties of Activated Carbon Prepared from Tamarind Seeds by KOH Activation for Fe(III) Adsorption from Aqueous Solution, *Sci. World J.* 2015 (2015) 1–9. doi:10.1155/2015/415961.
- [46] S. Li, K. Han, J. Li, M. Li, C. Lu, Preparation and characterization of super activated carbon produced from gulfweed by KOH activation, *Microporous Mesoporous Mater.* 243 (2017) 291–300. doi:10.1016/j.micromeso.2017.02.052.
- [47] T.D. Nguyen, J.I. Moon, J.H. Song, T.N. Kim, Synthesis of activated carbon from rice husk using microwave heating induced KOH activation, *Korean J. Mater. Res.* 22 (2012) 321–327. doi:10.3740/MRSK.2012.22.6.321.
- [48] I.I. Gurten, M. Ozmak, E. Yagmur, Z. Aktas, Preparation and characterisation of activated carbon from waste tea using K₂CO₃, *Biomass and Bioenergy.* 37 (2012) 73–81. doi:10.1016/j.biombioe.2011.12.030.
- [49] B.T.H. Guan, P.A. Latif, T.Y.H. Yap, Physical Preparation of Activated Carbon From Sugarcane Bagasse and Corn Husk and Its Physical and Chemical, *Int. J. Eng. Res. Sci. Technol.* 2 (2013) 1–16.
- [50] H. Soni, P. Padmaja, Palm shell based activated carbon for removal of bisphenol A: An equilibrium, kinetic and thermodynamic study, *J. Porous Mater.* 21 (2014) 275–284. doi:10.1007/s10934-013-9772-5.
- [51] M. Shirzad-Siboni, S.-J. Jafari, M. Farrokhi, J.K. Yang, Removal of Phenol from

- Aqueous Solutions by Activated Red Mud: Equilibrium and Kinetics Studies, *Environ. Eng. Res.* 18 (2013) 247–252. doi:10.4491/eer.2013.18.4.247.
- [52] D. Kavitha, Adsorptive removal of phenol by thermally modified activated carbon: Equilibrium, kinetics and thermodynamics, *J. Environ. Biotechnol. Res.* 3 (2016) 24–34.
- [53] P. Sudhakar, I.D. Mall, V.C. Srivastava, Adsorptive removal of bisphenol-A by rice husk ash and granular activated carbon—A comparative study, *Desalin. Water Treat.* 57 (2016) 12375–12384. doi:10.1080/19443994.2015.1050700.
- [54] W.T. Tsai, C.W. Lai, T.Y. Su, Adsorption of bisphenol-A from aqueous solution onto minerals and carbon adsorbents, *J. Hazard. Mater.* 134 (2006) 169–175. doi:10.1016/j.jhazmat.2005.10.055.
- [55] S. Cermak, M. Kosicek, A. Mladenovic-Djordjevic, K. Smiljanic, S. Kanazir, S. Hecimovic, Loss of cathepsin B and L leads to lysosomal dysfunction, NPC-like cholesterol sequestration and accumulation of the key Alzheimer's proteins, *PLoS One.* 11 (2016) 1–39. doi:10.1371/journal.pone.0167428.
- [56] Y.S. Ho, G. McKay, The kinetics of sorption of divalent metal ions onto sphagnum moss peat, *Water Res.* 34 (2000) 735–742. doi:10.1016/S0043-1354(99)00232-8.
- [57] B. Padak, J. Wilcox, Understanding mercury binding on activated carbon, *Carbon N. Y.* 47 (2009) 2855–2864. doi:10.1016/j.carbon.2009.06.029.
- [58] T. Depci, M. Sarikaya, K.A. Prsbrey, A. Yucel, Computational Chemistry Approach to Interpret the Crystal Violet Adsorption on Golbasi Lignite Activated Carbon, in: *IOP Conf. Ser. Earth Environ. Sci.*, 2016: pp. 1–5. doi:10.1088/1755-1315/44/5/052026.
- [59] Q. Zaib, I.A. Khan, N.B. Saleh, J.R. V. Flora, Y.-G. Park, Y. Yoon, Removal of Bisphenol A and 17 β -Estradiol by Single-Walled Carbon Nanotubes in Aqueous Solution: Adsorption and Molecular Modeling, *Water, Air, Soil Pollut.* 223 (2012) 3281–3293. doi:10.1007/s11270-012-1109-5.
- [60] F. Shen, J. Liu, Z. Zhang, Y. Dong, C. Gu, Density functional study of hydrogen sulfide adsorption mechanism on activated carbon, *Fuel Process. Technol.* 171 (2018) 258–264. doi:10.1016/j.fuproc.2017.11.026.
- [61] J.-C. Liu, P. a. Monson, Molecular Modeling of Adsorption in Activated Carbon: Comparison of Monte Carlo Simulations with Experiment, *Adsorption.* 11 (2005) 5–13. doi:10.1007/s10450-005-1088-6.
- [62] L.M. Cam, L. Van Khu, N.N. Ha, Theoretical study on the adsorption of phenol on activated carbon using density functional theory, *J. Mol. Model.* 19 (2013) 4395–4402. doi:10.1007/s00894-013-1950-5.
- [63] N. Chen, R.T. Yang, Ab initio molecular orbital calculation on graphite: Selection of molecular system and model chemistry, *Carbon N. Y.* 36 (1998) 1061–1070. doi:10.1016/S0008-6223(98)00078-5.
- [64] R. Wirasnita, T. Hadibarata, A.R.M. Yusoff, Z. Yusop, Removal of bisphenol a from aqueous solution by activated carbon derived from oil palm empty fruit bunch, *Water. Air. Soil Pollut.* 225 (2014) 2148. doi:10.1007/s11270-014-2148-x.
- [65] D. Cortés-Arriagada, L. Sanhueza, M. Santander-Nelli, Modeling the physisorption of

- bisphenol A on graphene and graphene oxide, *J. Mol. Model.* 19 (2013) 3569–3580. doi:10.1007/s00894-013-1872-2.
- [66] H. Marsh, F. Rodríguez-Reinoso, *Activated Carbon*, 2006. doi:10.1016/B978-008044463-5/50018-2.
- [67] S. Ahmadi, F.K. Mostafapour, Adsorptive removal of aniline from aqueous solutions by *Pistacia atlantica* (Baneh) shells: isotherm and kinetic studies, *J. Sci. Technol. Environ. Informatics.* 5 (2017) 327–335. doi:10.18801/jstei.050117.35.
- [68] A. Nakanishi, M. Tamai, N. Kawasaki, T. Nakamura, S. Tanada, Adsorption characteristics of bisphenol A onto carbonaceous materials produced from wood chips as organic waste, *J. Colloid Interface Sci.* 252 (2002) 393–396. doi:10.1006/jcis.2002.8387.
- [69] Y. Zhou, P. Lu, J. Lu, Application of natural biosorbent and modified peat for bisphenol a removal from aqueous solutions, *Carbohydr. Polym.* 88 (2012) 502–508. doi:10.1016/j.carbpol.2011.12.034.
- [70] S. Li, Y. Gong, Y. Yang, C. He, L. Hu, L. Zhu, L. Sun, D. Shu, Recyclable CNTs/Fe₃O₄ magnetic nanocomposites as adsorbents to remove bisphenol A from water and their regeneration, *Chem. Eng. J.* 260 (2015) 231–239. doi:10.1016/j.cej.2014.09.032.
- [71] D. Balarak, Kinetics, isotherm and thermodynamics studies on bisphenol a adsorption using barley husk, *Int. J. ChemTech Res.* 9 (2016) 681–690.
- [72] Thanhmingliana, S.M. Lee, D. Tiwari, Use of hybrid materials in the decontamination of bisphenol A from aqueous solutions, *RSC Adv.* 4 (2014) 43921–43930. doi:10.1039/c4ra06793b.
- [73] S. Bele, V. Samanidou, E. Deliyanni, Effect of the reduction degree of graphene oxide on the adsorption of Bisphenol A, *Chem. Eng. Res. Des.* 109 (2016) 573–585. doi:10.1016/j.cherd.2016.03.002.
- [74] R. Dong, J. Li, H. Xiong, W. Lu, H. Peng, L. Chen, Thermosensitive molecularly imprinted polymers on porous carriers: Preparation, characterization and properties as novel adsorbents for bisphenol A, *Talanta.* 130 (2014) 182–191. doi:10.1016/j.talanta.2014.06.055.
- [75] Z.M. Lazim, T. Hadibarata, M.H. Puteh, Z. Yusop, Adsorption characteristics of bisphenol a onto low-cost modified phyto-waste material in aqueous solution, *Water. Air. Soil Pollut.* 226 (2015). doi:10.1007/s11270-015-2318-5.
- [76] N. Genç, Ö. Kılıçoğlu, A.O. Narci, Removal of Bisphenol A aqueous solution using surfactant-modified natural zeolite: Taguchi's experimental design, adsorption kinetic, equilibrium and thermodynamic study, *Environ. Technol. (United Kingdom).* 38 (2017) 424–432. doi:10.1080/21622515.2016.1196739.
- [77] N.S. Kumar, M. Asif, M.I. Al-Hazaa, Adsorptive removal of phenolic compounds from aqueous solutions using pine cone biomass: kinetics and equilibrium studies, *Environ. Sci. Pollut. Res.* 25 (2018) 21949–21960. doi:10.1007/s11356-018-2315-5.
- [78] L.A. Rodrigues, M.L.C.P. da Silva, M.O. Alvarez-Mendes, A. dos R. Coutinho, G.P. Thim, Phenol removal from aqueous solution by activated carbon produced from avocado kernel seeds, *Chem. Eng. J.* 174 (2011) 49–57. doi:10.1016/j.cej.2011.08.027.

- [79] G. Lv, J. Liu, Z. Xiong, Z. Zhang, Z. Guan, Selectivity Adsorptive Mechanism of Different Nitrophenols on UIO-66 and UIO-66-NH₂ in Aqueous Solution, *J. Chem. Eng. Data*. 61 (2016) 3868–3876. doi:10.1021/acs.jced.6b00581.
- [80] N.A.N.M. Sani, N.A. Mazlan, A.H. Mohamed, K.P. Sambasevam, K.A. Jantan, M.R. Ramachandran, J.M. Sapari, Removal of 2,4-dinitrophenol (2,4-DNP) by using magnetic nanoparticles (MNPs) coated with polypyrrole (PPy), in: *IOP Conf. Ser. Mater. Sci. Eng.*, 2018: pp. 2–10. doi:10.1088/1757-899X/458/1/012007.
- [81] K.R. Hall, L.C. Eagleton, A. Acrivos, T. Vermeulen, Pore- and solid-diffusion kinetics in fixed-bed adsorption under constant-pattern conditions, *Ind. Eng. Chem. Fundam.* 5 (1966) 212–223. doi:10.1021/i160018a011.
- [82] X. Ma, H. Peng, X. Zhang, Regeneration of nitrophenol loaded granular activated carbon and its effect on the surface properties of adsorbent, *Desalin. Water Treat.* 57 (2016) 25494–25502. doi:10.1080/19443994.2016.1157523.
- [83] A. Kumar, H.M. Jena, Removal of methylene blue and phenol onto prepared activated carbon from Fox nutshell by chemical activation in batch and fixed-bed column, *J. Clean. Prod.* 137 (2016) 1246–1259. doi:10.1016/j.jclepro.2016.07.177.
- [84] H.N. Tran, H.C. Nguyen, S.H. Woo, T.V. Nguyen, S. Vigneswaran, A. Hosseini-Bandegharaei, J. Rinklebe, A. Kumar Sarmah, A. Ivanets, G.L. Dotto, T.T. Bui, R.S. Juang, H.P. Chao, Removal of various contaminants from water by renewable lignocellulose-derived biosorbents: a comprehensive and critical review, *Crit. Rev. Environ. Sci. Technol.* 49 (2019) 2155–2219. doi:10.1080/10643389.2019.1607442.
- [85] R. Rezaei Kalantry, A.J. Jafari, A. Esrafil, B. Kakavandi, A. Gholizadeh, A. Azari, Optimization and evaluation of reactive dye adsorption on magnetic composite of activated carbon and iron oxide, *Desalin. Water Treat.* 57 (2016) 6411–6422. doi:10.1080/19443994.2015.1011705.
- [86] E. Karimi Pasandideh, B. Kakavandi, S. Nasser, A.H. Mahvi, R. Nabizadeh, A. Esrafil, R. Rezaei Kalantary, Silica-coated magnetite nanoparticles core-shell spheres (Fe₃O₄@SiO₂) for natural organic matter removal, *J. Environ. Heal. Sci. Eng.* 14 (2016) 1–13. doi:10.1186/s40201-016-0262-y.
- [87] M. El Ouardi, M. Laabd, H. Abou Oualid, Y. Brahmi, A. Abaamrane, A. Elouahli, A. Ait Addi, A. Laknifli, Efficient removal of p-nitrophenol from water using montmorillonite clay: insights into the adsorption mechanism, process optimization, and regeneration, *Environ. Sci. Pollut. Res.* 26 (2019) 19615–19631. doi:10.1007/s11356-019-05219-6.
- [88] G. Nirmala, T. Murugesan, K. Rambabu, K. Sathiyarayanan, P.L. Show, Adsorptive removal of phenol using banyan root activated carbon, *Chem. Eng. Commun.* (2019). doi:10.1080/00986445.2019.1674839.
- [89] L.A. Rodrigues, L.A. De Sousa Ribeiro, G.P. Thim, R.R. Ferreira, M.O. Alvarez-Mendez, A.D.R. Coutinho, Activated carbon derived from macadamia nut shells: An effective adsorbent for phenol removal, *J. Porous Mater.* 20 (2013) 619–627. doi:10.1007/s10934-012-9635-5.
- [90] S.T. Perry, E.M. Hambly, T.H. Fletcher, M.S. Solum, R.J. Pugmire, Solid-state ¹³C NMR characterisation of matched tars and chars from rapid coal devolatilization, *Proc. Combust. Inst.* 28 (2000) 2313–2319.

- [91] A. Supong, P.C. Bhomick, M. Baruah, C. Pongener, U.B. Sinha, D. Sinha, Adsorptive removal of Bisphenol A by biomass activated carbon and insights into the adsorption mechanism through density functional theory calculations, *Sustain. Chem. Pharm.* 13 (2019) 100159. doi:10.1016/j.scp.2019.100159.
- [92] P.C. Bhomick, A. Supong, R. Karmaker, M. Baruah, C. Pongener, D. Sinha, Activated carbon synthesized from biomass material using single-step KOH activation for adsorption of fluoride: Experimental and theoretical investigation, *Korean J. Chem. Eng.* 36 (2019) 551–562. doi:10.1007/s11814-019-0234-x.
- [93] J. Liu, W. Qu, C. Zheng, Theoretical studies of mercury-bromine species adsorption mechanism on carbonaceous surface, *Proc. Combust. Inst.* 34 (2013) 2811–2819. doi:10.1016/j.proci.2012.07.028.
- [94] J. Liu, W. Qu, S.W. Joo, C. Zheng, Effect of SO₂ on mercury binding on carbonaceous surfaces, *Chem. Eng. J.* 184 (2012) 163–167. doi:10.1016/j.cej.2012.01.023.
- [95] B. Padak, M. Brunetti, A. Lewis, J. Wilcox, Mercury binding on activated carbon, *Environ. Prog.* 25 (2006) 319–326. doi:10.1002/ep.10165.
- [96] L.R. Radovic, The mechanism of CO₂ chemisorption on zigzag carbon active sites: A computational chemistry study, *Carbon N. Y.* 43 (2005) 907–915. doi:10.1016/j.carbon.2004.11.011.
- [97] I. Vázquez, J. Rodríguez-Iglesias, E. Marañón, L. Castrillón, M. Álvarez, Removal of residual phenols from coke wastewater by adsorption, *J. Hazard. Mater.* 147 (2007) 395–400. doi:10.1016/j.jhazmat.2007.01.019.
- [98] V.C. Srivastava, M.M. Swamy, I.D. Mall, B. Prasad, I.M. Mishra, Adsorptive removal of phenol by bagasse fly ash and activated carbon: Equilibrium, kinetics and thermodynamics, *Colloids Surfaces A Physicochem. Eng. Asp.* 272 (2006) 89–104. doi:10.1016/j.colsurfa.2005.07.016.
- [99] B. Özkaya, Adsorption and desorption of phenol on activated carbon and a comparison of isotherm models, *J. Hazard. Mater.* 129 (2006) 158–163. doi:10.1016/j.jhazmat.2005.08.025.
- [100] M. Kilic, E. Apaydin-Varol, A.E. Pütün, Adsorptive removal of phenol from aqueous solutions on activated carbon prepared from tobacco residues: Equilibrium, kinetics and thermodynamics, *J. Hazard. Mater.* 189 (2011) 397–403. doi:10.1016/j.jhazmat.2011.02.051.
- [101] R.S. Ingole, D.H. Lataye, P.T. Dhorabe, Adsorption of phenol onto Banana Peels Activated Carbon, *KSCE J. Civ. Eng.* 21 (2017) 100–110. doi:10.1007/s12205-016-0101-9.
- [102] B. Aurelien, T.T.D. Raoul, N.G. Ndifor-Angwafor, K.T. Arnaud, A.S. Gabche, Adsorption of 2,4-dinitrophenol on Activated Carbon Prepared from Cotton Cakes: Non-linear Isotherm Modeling, *Chem. Sci. Int. J.* 24 (2018) 1–20. doi:10.9734/csji/2018/43499.
- [103] B. Aurelien, R.T.T. Donald, G.N.-A. Nche, D. Giscard, S.G. Anagho, Non-linear equilibrium and kinetic study of the adsorption of 2,4-dinitrophenol from aqueous solution using activated carbon derived from a olives stones and cotton cake, *African J.*

- Environ. Sci. Technol. 13 (2019) 365–380. doi:10.5897/ajest2019.2717.
- [104] A. Denizli, G. Ökan, M. Uçar, Dye-affinity microbeads for removal of phenols and nitrophenols from aquatic systems, *J. Appl. Polym. Sci.* 83 (2002) 2411–2418. doi:10.1002/app.10199.
- [105] S. Agarry, O. Ogunleye, Chemically treated kola nut pod as low-cost natural adsorbent for the removal of 2,4-dinitrophenol from synthetic wastewater: Batch equilibrium, kinetic, and thermodynamic modelling studies, *Turkish J. Eng. Environ. Sci.* 38 (2014) 11–40. doi:10.3906/muh-1304-24.
- [106] J.C. Lazo-Cannata, A. Nieto-Márquez, A. Jacoby, A.L. Paredes-Doig, A. Romero, M.R. Sun-Kou, J.L. Valverde, Adsorption of phenol and nitrophenols by carbon nanospheres: Effect of pH and ionic strength, *Sep. Purif. Technol.* 80 (2011) 217–224. doi:10.1016/j.seppur.2011.04.029.

CHAPTER 4

REMOVAL OF COLIFORM BACTERIA AND *Escherichia coli* USING ACTIVATED CARBON SYNTHESIZED FROM *Tithonia* *diversifolia*

This chapter deals with the utilization of Tithonia diversifolia activated carbon for the removal of coliform and Escherichia coli bacteria from water. Biofilter columns consisting of activated carbon and supporting medium of either sand, brick or pebbles were constructed and tested for Escherichia coli removal efficiency from synthetic bacterial solution. The breakthrough curve and adsorbent exhaustion rate of all the biofilter columns were investigated and the column with the best performance was used for removal of coliform and Escherichia coli from real wastewater. The colony-forming units of coliform and Escherichia coli in the untreated and treated real water samples were determined using multiple tube fermentation technique. Further, biochemical tests were also carried out to confirm and identify the coliform and Escherichia coli bacteria in the water samples.

4.1 Introduction

Access to safe and affordable drinking water is a fundamental human need and a basic human right. However, according to the World Health Organization (WHO), 785 million people across the globe lack even a basic drinking water source and at least 2 billion people use drinking water from faecal contaminated sources [1]. Faecal contamination is one of the greatest waterborne threat to humans, especially in developing countries where drinking water quality and sanitation is very poor [2,3]. Faecal contaminated water contains a high percentage of pathogens such as bacteria, viruses and protozoa which are capable of causing various water-borne diseases such as giardiasis, cryptosporidiosis, gastroenteritis, cholera, typhoid fever and bacillary dysentery, etc[4].

Among all the pathogens, coliform bacteria are the most frequently encountered in water sources. Coliform bacteria are present in the intestinal flora of human and warm-blooded animals and faecal waste. They include organisms of many genera such as *Escherichia*, *Klebsiella*, *Citrobacter*, *Enterobacter* and *Shigella* etc., and among these, the detection of *Escherichia coli* (*E.coli*) in water sources indicate recent faecal contamination and thus increasing the likelihood of the presence of disease-causing pathogens [5]. These pathogens are transmitted to humans by the consumption of contaminated water and pose an immediate health risk to anyone who consumes the water. Therefore, effective removal of such bacterial pathogens is necessary for safe drinking water.

Over the years, several improved and advanced technologies have been developed for the removal of waterborne pathogens from water such as electrochemical process [6–8], single and catalytic ozonation [9,10], photocatalytic inactivation [11,12], phytoremediation[13,14], chemical disinfection and membrane filtration[15,16]. Also, ceramic filters[17,18], silver nanoparticles[19,20], activated carbon composite[21,22] and magnetic nano composites[23,24] have been employed for the efficient removal of a wide range of waterborne pathogens. Despite the efficiency of the above-mentioned techniques, the practical utilization of these systems particularly in rural areas is unfeasible in many cases, because they often include complicated installation process, high maintenance, high-cost and are difficult to operate. Therefore, there is a need to develop low-tech water treatment systems that are affordable, efficient, easy to maintain and operate, so that people in developing countries, particularly in rural areas, can continuously access safe drinking water. This could be achieved by including more practical options such as using point-of-use (POU) technologies for water purification at the household level. Several household POU technologies are available which include boiling, disinfection, flocculation, coagulation and

filtration. However, these processes have inherent limitations, for example, boiling of contaminated water does not ensure complete removal of pathogens[25], disinfection process generally produces by-products that are toxic and carcinogenic to humans[26], while flocculation and coagulation treatments involve high operating costs and generate increased volume of sludge[27]. In this regard, filtration is particularly promising because of the ease of application, efficiency, affordability and high acceptance rate among users. Several POU filtration system such as ceramic filter, bio sand filter, slow sand filter, biochar filter and activated carbon filter[18,28–32] have been adopted to obtain potable water at household level in remote areas. These household filtration systems are simple and have proven to be effective in purifying highly turbid water and removal of various pathogens from water.

Activated carbon filter is one of the most efficient POU filter systems. The advantages of using activated carbon in filter media lies in its high adsorption capacity and its versatility to remove a wide range of pollutants. Besides, the raw materials for the preparation of activated carbon can be obtained from locally sourced materials.

Keeping this in mind, the present work focusses on the utilization of the activated carbon in a biofilter column for the removal of coliform and *E.coli* from water. The activated carbon was prepared from locally available *Tithonia diversifolia* biomass and was used in the biofilter column as the principal media along with other supporting media. The use of supporting media in the filter column improved the overall efficiency of the column and also prevented the activated carbon from floating. Sand, brick and pebbles were used as different supporting media in the present study in order to provide options depending on the local availability and cost and their comparative efficiency was studied.

This chapter thus explores the use of *Tithonia diversifolia* activated in a biofilter column for the removal of coliform and *E.coli* from water. Altogether, six biofilter columns were constructed, three of the biofilter column were loaded with either sand, brick or pebbles, while the remaining three columns were loaded with activated carbon and supporting medium of either sand, brick or pebbles. The biofilter columns were further tested for their *E.coli* removal efficiency from synthetic bacterial solution. Break-through curve and adsorption exhaustion rate of all the columns were investigated for determining the lifespan and overall efficiency of the biofilter columns. The biofilter column with the best performance in synthetic *E.coli* solution was further used for the removal of coliform and *E.coli* bacteria from a real water sample. The possible presence of bacteria in real water samples was determined by conducting various biochemical tests.

4.2 Materials and methods

For the present study, activated carbon synthesized from *Tithonia diversifolia* was used. The detailed preparation procedure and characterisation of the activated carbon have already been discussed in chapter 4. The present study utilized the 2TAK700 activated carbon, where TAK stands for *Tithonia diversifolia*, KOH activated carbon, 2 corresponds to the 2:1 impregnation ratio of KOH/char and 700 is the activation temperature at 700°C. The 2TAK700 activated carbon possessed the highest surface area and pore volume, and since these properties have a direct relationship with the overall adsorption capacity, the 2TAK700 activated carbon was chosen for the removal of bacteria from water in this study.

The removal of bacteria was studied by constructing biofilter columns using the activated carbon along with supporting media. Different microbiological media such as nutrient agar media, brilliant green bile salt media, single and double strength lactose broth etc were used for the bacteriological studies. All the chemicals and reagents were purchased from Hi-media, India. The detailed experimental procedures are discussed below.

4.2.1 Collection and preparation of supporting media for biofilter column.

Sand, brick and pebbles were used as the supporting media for the biofilter column and were collected from local sources. The sand was sieved to remove the coarse particles while the brick and pebbles were ground manually into smaller pieces. The materials were then washed in deionised water, dried in an oven at 110°C overnight and autoclaved at 121°C, 100kPa for 15 minutes. All the materials were further stored in sterile containers before using for column experiments.

4.2.2 Construction of biofilter column

Altogether, six types of biofilter columns were constructed, namely sand-activated carbon-sand (SAS), brick-activated carbon-brick (BAB), pebble-activated carbon-pebble (PAP), pristine sand (PS), pristine pebble (PP) and pristine brick (PB) biofilter column.

All the biofilter columns were constructed using glass chromatography columns of 30cm length and 2cm diameter. Each SAS biofilter column was first prepared by filling the column with 2g of sand followed by sequential addition of 0.5g of activated carbon and 2g of sand giving rise to an overall bed height of 5cm. The packing materials were tapped manually after the addition of each layer and compacted gently using a glass rod to prevent any air entrapment. A small layer of cotton was packed at the bottom of the column to prevent the materials from eluting out of the column. The column was conditioned by passing 100ml of

phosphate buffer solution (PBS) before passing the bacterial suspension dispersed in the same sterile saline solution.

Similarly, the BAB biofilter column was prepared by the sequential addition of 0.2g brick, 0.5g activated carbon and 0.2g brick resulting in a bed height of 4.5 cm. The PAP biofilter column was also loaded in the same manner with 0.2g pebbles, 0.5g activated carbon and 0.2g pebbles with an overall bed height of 4.5 cm. Further, the PS, PB and PP biofilter columns were constructed and each of the columns was loaded with 4g sand, brick and pebble respectively. The experimental set up of the columns, PS, PP, PB, SAS, BAB, PAP biofilter columns is shown in Figure 4.1.

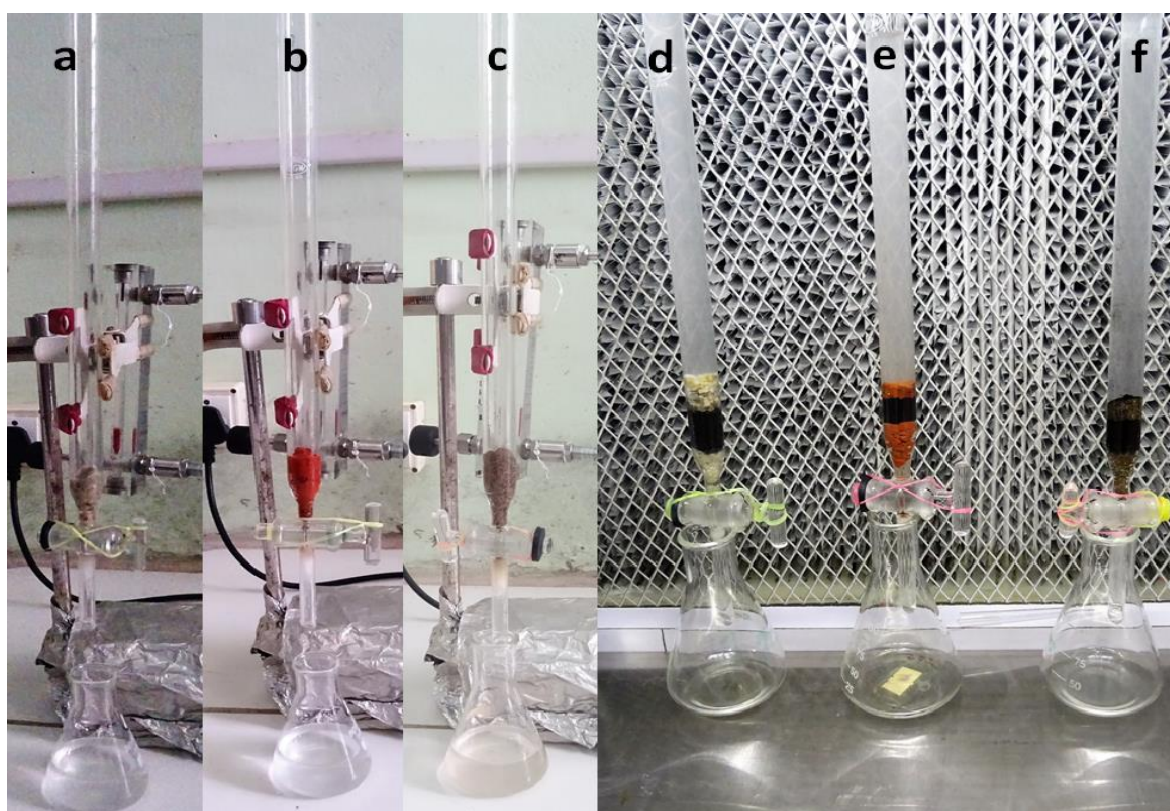


Figure 4.1 Experimental set up of (a) PS (b) PB (c) PP (d) PAP (e) BAB and (f) SAS column for removal of bacterial pathogens

4.2.3 Preparation of bacteria solution

Pure cultures of *Escherichia coli* (MTCC 40) were grown in nutrient broth and incubated at 37°C for 24 hours. Then the bacterial cells were harvested by centrifugation at 3000rpm for 15 minutes. The cells were washed three times with sterile phosphate-buffered solution and resuspended in PBS to produce a cell count of approximately 1×10^8 CFU/mL. The initial estimation of cell count was done using a UV-VIS spectrophotometer (lambda 35, Perkin Elmer) at a wavelength of 600 nm. The absorbance value of approximately 0.1 corresponded

to 10^8 CFU/mL (0.5 Mc Farlands Standard). The initial viable bacterial cells were also measured by plating out various dilutions of the stock solution and counting the colony. The colony-forming units (CFU/mL) was calculated by using the formula

$$\text{CFU/mL} = \frac{\text{no.of colonies} \times \text{dilution factor}}{\text{Volume of culture plate}} \quad (4.1)$$

4.2.4 Removal experiment of *E.coli* by biofilter columns

The removal of *E.coli* by the biofilter columns was performed by allowing a known quantity of *E.coli* solution to flow down the columns at an initial filtration rate of 1mL/min. Initially, 30 ml of known *E.coli* solution (1×10^8 CFU/mL) was fed into the column, followed by continuous addition of the bacterial solution up to 100 mL. The effluent was collected and the bacterial concentration was measured by the standard plate count method. All the experiments were run in triplicates and the mean value was recorded. The log reduction of the bacteria by each filter column was determined using the equation

$$\log_{10} \text{reduction} = -\log_{10} \left(\frac{N}{N_0} \right) \quad (4.2)$$

where N and N_0 are the final and initial bacterial concentration in CFU/ml respectively.

In another experiment, glass columns were loaded with fresh packing materials and used to generate the breakthrough curve. Breakthrough curves refer to the variation of the adsorbate concentration in the column effluent over time. It is obtained by plotting C/C_0 versus time (time taken to run the column), where C is the inlet concentration and C_0 is the outlet concentration. The plot is useful to determine the breakthrough time of the column i.e., the time at which the adsorbate reaches the end of the column and leaves with the effluent. It is an essential tool to determine the lifespan of the column.

The experiments were conducted by allowing the influent to run through the column in two successive phases. In the first phase, 100mL of *E.coli* solution was allowed to run through the column, while in the second phase, 100mL of free *E.coli* free solution was fed into the column. The *E.coli* concentrations in the effluent were measured every 5 minutes interval and the breakthrough curve was plotted.

4.2.5 Real water sample analysis

The performance of the biofilter column in a real-case scenario was determined by running a real water sample through the biofilter column. Among all the biofilter columns, the column with the optimum removal efficiency for synthetic *E.coli* solution was used for the real water

analysis. The water sample was collected from a shallow well, located near a domestic wastewater drain at Mokokchung, Nagaland. An image of the collection site is given in Figure 4.2. The water samples were collected in sterilized sampling bottles and immediately stored in a chilled insulation container to prevent bacteria overgrowth. The samples were analyzed within 1 hour of collection and the possible presence of total heterotrophic, coliform and *E.coli* bacteria in the water sample was determined. Conventional plate count method and Multiple tube fermentation technique were used to determine the bacterial concentration. After the determination of bacteria in the water sample, the sample was allowed to run through the biofilter column and the efficiency of the column in the real water environment was determined. The detailed experimental procedures are discussed below.



Figure 4.2 Wastewater collection site

4.2.5.1 Determination of total heterotrophic bacteria

The heterotrophic group of bacteria encompasses all the bacteria that are capable of growing in an organic carbon-rich medium [33]. Colony counts of heterotrophic bacteria are referred to as heterotrophic plate count (HPC), standard plate count (SPC), aerobic plate count (APC) or total plate count (TPC). The total heterotrophic bacteria plate count (HPC) was done using the pour plate technique to assess the general bacterial content of water. For this, 0.1 mL of each of the water sample was placed in two different sterile Petri dishes. Then, 20 ml of molten cooled agar was poured into each plate, mixed well and the agar was allowed to solidify. One plate was incubated at 22°C and the other at 37°C for 48 hours. After

incubation, the number of colonies formed in both the plates was counted, and the average was reported as CFU/mL of the water sample

4.2.5.2 Determination of total coliform and *E.coli* bacteria

Total coliform refers to a large group of Gram-negative, non-spore-forming, rod-shaped bacteria capable of growing at 35-37°C and ferments lactose with the production of acid and gas [34]. They are present in the faeces of warm-blooded animals/humans and also in the environment (soil and vegetation). Therefore, the presence of coliform in water may not necessarily indicate faecal contamination, as it can also be caused by the entry of soil or organic matter into the water or by conditions suitable for the growth of other types of coliform. As a result, it is often necessary to undertake further testing to confirm the presence of coliform bacteria that are specific to the faecal origin.

E.coli is a subset of coliform bacteria that exist in the intestinal tract and faeces of warm-blooded animals. It can grow at 44-45°C and ferments lactose with the production of acid and gas[35]. It is found in abundance in the faeces of animals and humans, and the presence of *E.coli* in the water sample is definitive proof of faecal contamination. Therefore, testings were done to confirm the presence of *E.coli* in water, which would indicate recent faecal contamination.

Multiple tube fermentation (MTF) technique was used to determine the presence of coliform and *E.coli* bacteria in water [36]. The presence of the bacteria in the water sample is indicated by the production of either gas or acid and turbidity in the culture medium. The results of the MTF are reported in terms of the most probable number (MPN). This number is a statistical estimate of the mean number of coliforms/*E.coli* present in the water sample.

Test for total coliform bacteria

For this study, 5 test tubes containing 10 mL double-strength lactose broth and 10 test tubes containing 10 mL single strength lactose broth were taken and Durham tubes in an inverted position were added to all the test tubes without the formation of air bubbles. The test tubes were sterilized by autoclaving at 15 lbs pressure for 15 minutes. Further, using a sterile pipette, 10 mL of water sample was added to the 5 tubes containing double strength lactose broth (Set A), 1 mL of water sample to 5 tubes containing single strength lactose broth (Set B) and 0.1 mL to the remaining 5 tubes of single strength lactose broth (Set C). All the test tubes were then incubated at 37°C for 48 hours. After incubation, gas and acid production in Durham's tubes was observed. The presence of gas is detected as air bubbles collected inside the inverted Durham tube and the presence of acid is indicated by the colour change of the

medium. The tubes showing both colour change and gas production were recorded as positive tubes, while the tubes without any gas production were recorded as negative and were discarded. The number of total coliform bacteria was determined by counting the number of positive tubes in each set and comparing the pattern of positive results with standard statistical Mc Cardy, MPN table for five-tube dilution.

Test for *E.coli*

For the test of *E.coli*, 3 sets of test tubes set 1, set 2 and set 3, each containing the number of tubes equal to the positive tube of set A, set B and set C respectively were taken and Durham tubes were added to all the tubes. Further, 10 mL of brilliant green bile lactose broth was added to all the tubes and 1 ml of the sample from each positive tubes of set A, B and C were inoculated in respected tubes of set 1, 2 and 3. After incubation of the test tubes at 44 °C for 24 hours, the number of *E.coli* was determined by using the MPN table.

4.2.5.3 Biochemical identification of coliform and *E.coli* bacteria

Biochemical tests were done to further confirm and identify the coliform and *E.coli* bacteria present in the water sample. The water samples were collected in sterilized glass bottles and a volume of 0.1 mL water sample was spread on nutrient agar medium and incubated at 37°C for 48 hours. After incubation, the mixed bacterial colonies formed on the agar plates were streaked and re-streaked on fresh agar plates to obtain discrete bacterial colonies/pure cultures. For pure culture, bacterial incubation was carried out at 37°C for 24 hours. The isolates were further subjected to various biochemical tests to identify and confirm the isolates as either coliform or non-coliform bacteria. The biochemical tests were carried out following standard procedures for water analysis, section 9225A (APHA, 1995)[36] and the results were analysed as per standard protocol [37-39]. The various biochemical tests conducted are listed in Table 4.1 and the detailed experimental procedures are discussed below.

Table 4.1 Biochemical tests and their uses

Biochemical Tests	Uses
Gram staining	To differentiate isolates into gram-positive and gram-negative bacteria
Oxidase test	To identify isolates that produce the enzyme cytochrome oxidase
Catalase test	To identify isolates that produce the enzyme catalase
Motility Test	To determine the motile nature of the isolates
Triple sugar iron test	To determine the ability of the isolates to ferment sugars (glucose, sucrose, dextrose) and their ability to produce hydrogen sulphide gas
IMViC tests	To identify isolates in the coliform group

Gram staining

The coliform and *E.coli* bacteria refer to a broad group of gram-negative rod-shaped bacteria. Therefore, gram staining test was done to differentiate the isolates into coliform (gram-negative) and non-coliform (gram-positive) bacteria. The isolates were mounted on a glass slide and flooded with crystal violet. Bacterial smear for gram staining was prepared by placing a drop of water with the help of a sterilized dropper on a sterilized slide. Then, 18-24 hours old bacteria isolates were transferred to the slide with a heat-sterilized loop and spread by circular motion using an inoculating loop. The smear was allowed to air-dry and heat-fixed by passing the slide through the Bunsen burner flame. The smear was flooded with crystal violet and allowed to stand for 1 minute. The stained slide was washed gently with distilled water followed by flooding with gram's iodine mordant. The slide was allowed to stand for 1 minute and washed with distilled water. This was followed by decolourizing where 95% of ethyl alcohol was added until the slide showed only a blue tinge. The decolourization step was followed by counterstaining with safranin for 0.45 minutes after washing the slide with distilled water. Excess safranin was washed with distilled water and the slide was dried with blotting paper. The slide was examined under a microscope at a resolution of 100X after adding a drop of oil immersion. The Gram-positive bacteria will appear violet under the microscope since they will retain the primary stain (crystal violet) and iodine complex. While gram-negative bacteria will appear pink as they will lose crystal violet and iodine complex upon alcohol washing and retain the pink colouration of safranin counterstain.

Oxidase test

Oxidase test is used to determine the ability of the bacteria to produce the cytochrome oxidase enzyme. For the test, oxidase disc containing tetramethyl-p-phenylenediamine dihydrochloride (TMPD) was soaked in sterilized water and transferred to a sterilized slide. Bacterial isolates from the nutrient broth were then transferred into the disc with the help of a sterilized inoculation loop. The presence of oxidase enzyme is evident by the rapid development of purple colour on the disc which is caused by the oxidation of test reagent by the enzyme, whereas no colour change is observed for a negative test. Coliforms and *E.coli* give negative results for oxidase test.

Catalase test

Catalase tests are done to identify bacteria that produce the enzyme catalase, an enzyme that catalyses the release of oxygen from hydrogen peroxide (H_2O_2). Coliform and *E.coli* bacteria usually show positive results for the catalase test. In order to perform the experiment, a

loopful of 24 old bacteria isolates from the nutrient broth were transferred to a sterilized slide. To this, a drop of 3% H_2O_2 was added and mixed using the loop. The occurrence of effervescence caused by the rapid release of oxygen from H_2O_2 indicated catalase activity of the bacteria.

Motility Test

This test was carried out to determine the motile nature of the bacteria. SIM medium (Sulphide Indole Motility medium) was prepared according to the manufacturer's instruction. Before autoclaving the medium, triphenyl tetrazolium chloride (0.5g/l) was added to enhance the visibility of bacterial growth. Bacterial isolates were inoculated on agar tubes by stabbing the agar with a needle in one straight line through the centre of the medium and the tubes were incubated at 37 °C for 24 hours. The results were recorded as positive if the medium turned red along with an outward projection of the bacterial growth from the inoculation line. The negative results were determined by the confinement of the bacterial growth only to the inoculation line.

Triple sugar iron test

Triple sugar iron test is used to determine the ability of the bacteria to ferment sugars (glucose, sucrose, dextrose) and their ability to produce hydrogen sulphide gas. For the given test, the bacteria isolates were inoculated in slant triple sugar iron agar (TSIA) by first stabbing through the centre of the medium with the help of a straight needle and then streaking on the surface of the TSIA slant. The slant was further incubated at 37°C for 24 hours. After the incubation, the colour change, blackening and cracks in the agar slant were examined. The change in TSIA slant colour from orange-red to yellow indicates the production of acid as a result of the fermentation process, while the production of H_2S is indicated by the blackening of the butt of the media. Some bacteria also produce gas identified by the cracks in the media. *E. coli* is identified by acidic slant/acidic butt(A/A) i.e., yellow/yellow, gas positive and H_2S negative. Likewise, other coliform bacteria are also identified by interpreting their test result.

IMViC tests

The IMViC tests are the most useful and important biochemical tests to identify bacteria in the coliform group. These include four different tests and the term IMViC is an acronym that stands for each of the tests. 'I' is for Indole test, 'M' is for Methyl red test, 'V' is for Voges Proskauer test, lowercase 'i' is added for the ease of pronunciation and 'C' is for citrate

utilization test. The members of the coliform are differentiated into individual species depending on the IMViC test result. For e.g., *E.coli* yields ‘+ + - -’ result with respect to the IMViC test and *Enterobacter* sp., yields ‘- - + +’ result to the IMViC test. Similarly, other coliform species are identified according to their IMViC test result pattern. The detailed tests procedures are discussed below:

Indole test

Each isolate was inoculated in 5 ml of tryptone-water broth and incubated at 37 °C for 24 hours. Following incubation, 0.5 ml of Kovac’s reagent was added to the bacterial broth. Culture tubes with a cherry-red ring on the surface of the bacterial broth indicated a positive reaction while tubes without colour development on the surface of the bacterial broth indicated a negative reaction.

Methyl Red (MR) - Voges Proskauer (VP) test.

For the MR test, a loopful of the isolate was transferred into a 10 ml MR-VP broth (glucose phosphate broth) and incubated at 37 °C for 48 hours. Following incubation, 3-5 drops of methyl red indicator was added to the bacterial broth. Colour change in the upper layer of the broth from yellow to red was recorded in positive isolates while methyl red negative bacteria and control tubes were detected based on no colour change of the culture broth.

For the VP test, a loopful of the isolate was transferred into a 10 ml MR-VP broth (glucose phosphate broth) and incubated at 37°C for 48 hours. Following incubation, Barritt’s reagent A and Barritt’s reagent B were added to the bacterial broth. The test tube was shaken for 3 minutes, allowed to stand at room temperature for 15 minutes. Colour change to pink was recorded in test tubes with positive isolates while no change in colour was observed in VP negative and control tube.

Citrate utilization test

The Simmon-citrate medium was prepared according to the manufacturer’s instructions. The isolate was streaked in Simmon-citrate agar tubes. Incubation was carried out at 37°C for 48-72 hours. Test tubes were recorded for colour change of the medium from deep forest green to a Prussian blue colour. The control tube was maintained without bacterial isolates.

4.2.5.4 Removal of total coliform and *E.coli* from real water sample

The removal of total coliform and *E.coli* from real water sample was studied using the biofilter column that showed the optimum removal efficiency for synthetic *E.coli* solution. For this study, 100 mL of real water sample was allowed to run through the column and the

effluent was collected in a sterilized glass bottle. The total coliform and *E.coli* concentrations in the effluent (treated water) were further determined following the same multiple tube fermentation technique used for untreated water.

4.3 Results and discussion

4.3.1 Removal of synthetic *E.coli* solution by biofilter column with different supporting media

The removal of *E.coli* each by SAS, PAB and BAB column was studied by passing 100 ml of approximately 10^8 CFU/ml of bacterial suspension through the column. The column was gravity-driven and maintained a flow rate of 1ml/min. The removal efficiency of the supporting material i.e. plain sand, brick and pebbles were also evaluated by allowing the bacterial suspension to pass through columns consisting solely of these materials. As seen from Figure 4.3, the columns packed with only the supporting material i.e PB, PP and PS showed low log reduction of 0.77 ± 0.17 , 0.04 ± 0.03 and 0.27 ± 0.22 respectively. However, the biofilter columns amended with the activated carbon i.e., BAB, SAS and PEB achieved high log reduction of 4.45 ± 0.57 , 3.94 ± 0.49 and 3.38 ± 0.90 respectively. Significant differences in the log reduction capacity were observed between the biofilter column amended with activated carbon and the column with only the pure supporting media. The high log reduction of *E.coli* by the activated carbon amended column may be due to the large surface area and porous nature of activated carbon which may have facilitated the attachment of *E.coli* and thereby, preventing their elution from the filter media[40]. Besides, multifunctional groups present on the surface of the activated carbon may also have increased the adsorption of negatively charged *E.coli* onto the activated carbon surface[41].

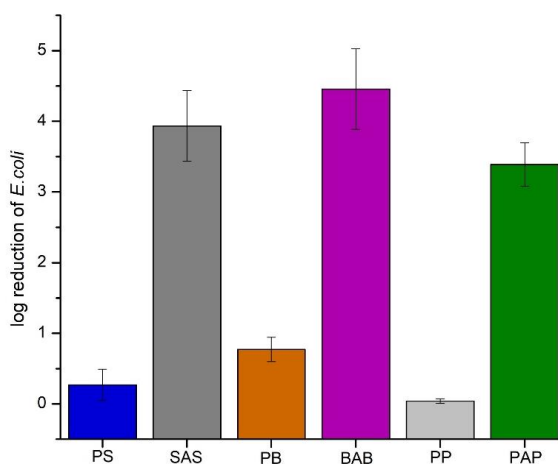


Figure 4.3 Log reduction of *E.coli* (CFU/mL) by different biofilter column (PS-pristine sand, SAS-sand/activated carbon/sand, PB-pristine brick, BAB- brick/activated carbon/brick, PP-pristine pebbles, PAP-pebbles/activated carbon/ pebbles). Error bars represent the standard deviation of average results of triplicate experiments

Among the activated carbon amended biofilter columns, the BAB column removed more *E.coli* than the PAP and SAS biofilters. The high removal rate of the BAB column may be attributed to the combined adsorption effect of the activated carbon and brick powder. Figure 4.4 represents the SEM image of brick, pebbles and sand, and it is observed that the brick powder has a higher porous network as compared to pebbles and sand. Thus, in addition to the large surface area, high porosity and multifunctional groups present in activated carbon, the higher porosity of brick powder may have facilitated the trapping of *E.coli*. Moreover, the EDX analysis (Figure 4.5) of brick, sand and pebbles revealed the presence of a higher percentage of crystalline minerals such as Ca^{2+} , Mg^{2+} , Al^{3+} etc in brick. The presence of such positively charged ions may have further facilitated the overall attachment of the negatively charged *E.coli* [42], thereby increasing the removal efficiency.

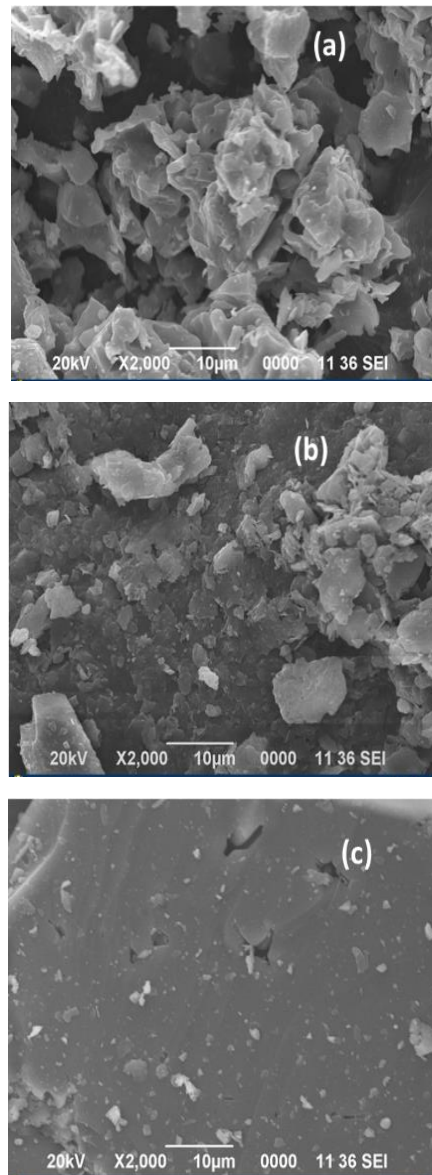


Figure 4.4 SEM image of (a) Brick (b) Sand and (c) Pebbles

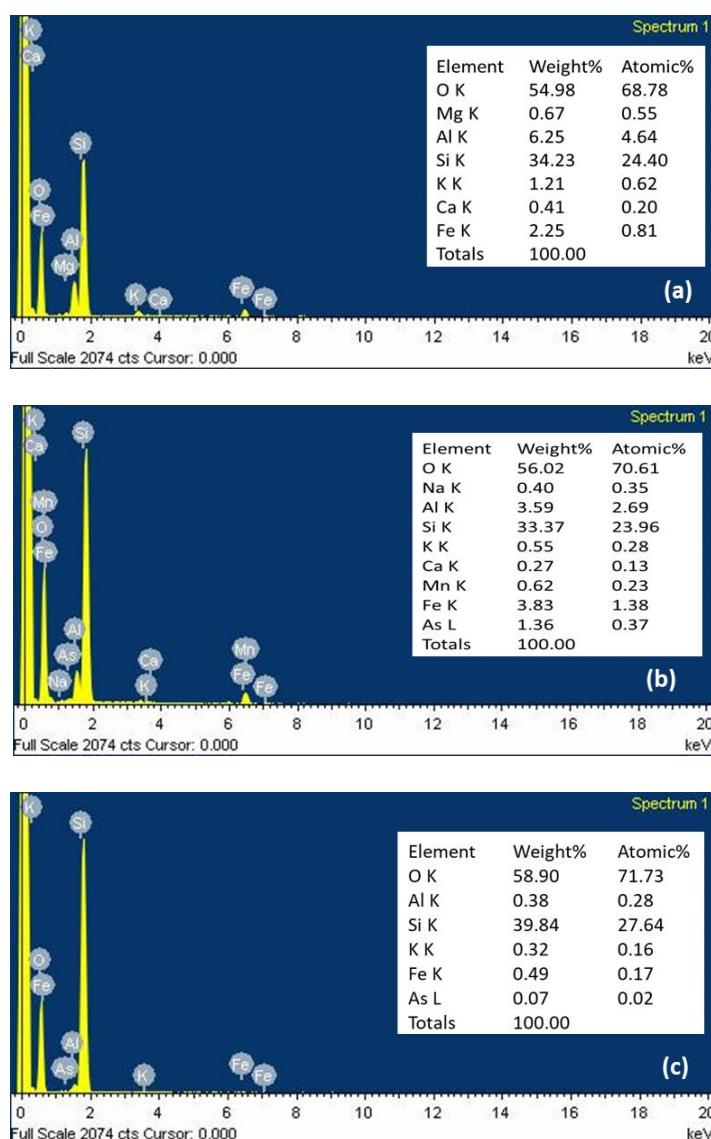


Figure 4.5 EDX of (a) Brick (b) Sand and (c) Pebbles

Breakthrough analysis

Figure 4.6 represents the breakthrough curve of *E.coli* using different biofilter columns. All the breakthrough curves followed a similar pattern consisting of a rising limb, a plateau phase and a declining limb. The biofilter columns PS, PP and PB with only the supporting media resulted in early *E.coli* breakthrough at 15, 5 and 30 minutes respectively. However, the *E.coli* breakthrough in biofilter columns with the activated carbon i.e., SAS, BAB and PAP biofilter columns were observed only after 55, 60 and 55 minutes respectively. It is apparent that the presence of activated carbon in the SAS, BAB and PAP biofilter columns significantly improved the overall biofilter column efficiency. As seen from Figure 4.6, the C/C_0 ratio in the PP and PS plateau phase was similar at ~ 0.9 while that of PB was at ~ 0.7 .

However, the C/C_0 ratios in the plateau phase for the biofilter columns with the activated carbon was only around 0.1, indicating that the *E.coli* colony in the effluent remained less than 10% even after the breakthrough point for BAB, PAP and SAS column.

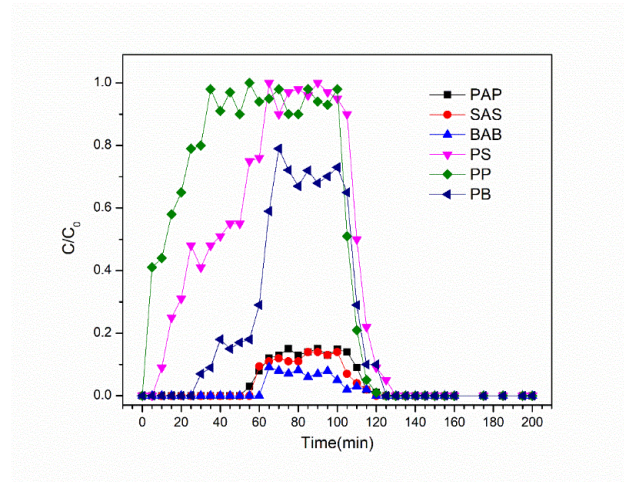


Figure 4.6 Breakthrough curve of *E.coli* using different biofilter column

Adsorption exhaustion rate (AER) was further used to comparatively study the performance of the various columns. It is defined as the mass of adsorbent deactivated per volume of water treated at the breakthrough point and is calculated by using the following equation[43],

$$AER = \frac{\text{Mass of adsorbent (g)}}{\text{Volume of water treated(L)}}$$

The AER value is used as a performance indicator, and a smaller AER value signifies a better performance of the biofilter columns. From the calculated AER value given in Table 4.2 it is observed that the BAB exhibited the lowest AER value among all the biofilter columns, indicating that BAB is more efficient in immobilising the *E.coli*. Based on the calculated AER values, the performance of the columns follow the order;

$$BAB > SAS > PAP > PB > PS > PP$$

Table 4.2 AER value of biofilter columns	
Column	AER value(g/L)
PP	0.8
PS	0.22
PB	0.13
PAP	0.08
SAS	0.07
BAB	0.06

4.3.2 Real water analysis

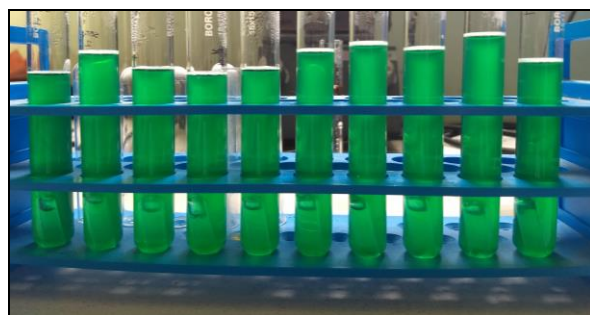
The practical applicability of the BAB biofilter column was further evaluated using real water sample. The water sample was collected and tested for total heterotrophic bacteria, total

coliform bacteria and *E.coli*. After confirming the presence of bacteria in the collected water sample, it was allowed to run through the BAB column. The bacterial concentration in the effluent was further evaluated and the removal efficiency of the BAB column was determined.

The total heterotrophic bacteria of the collected water sample determined by the pour plate technique was found to be around 10^3 CFU/mL. After the confirmation of general bacterial load by HPC, the total coliform bacteria in the water sample was estimated. The multiple tube fermentation experiment carried out in lactose broth indicated the presence of coliform bacteria in the water sample. The positive results were indicated by the formation of bubbles inside the Durham tubes and the colour change of media as shown in Figure 4.7. All the 5 tubes each of set A, set B and set C were tested positive. Thus, the MPN value for (5,5,4) positive tubes was 1600, which indicated that the water sample contained around 1600 coliforms per 100 mL of the sample. Similarly, from the multiple tube fermentation experiment for *E.coli* using brilliant green lactose broth, it was observed that all the 5 tubes of set 1 and set 2 showed positive results, whereas, 3 tubes out of the four tubes were tested positive for set 3. Thus the MPN value for (5,5,3) positive tubes was 920 i.e., the water sample contained an estimated 920 *E.coli* colonies per 100 ml of the water sample.



(a)



(b)

Figure 4.7 Multiple tube fermentation test for (a) total coliform bacteria in lactose broth (b) *E.coli* in brilliant green bile lactose broth

After the confirmation of bacterial activity in the collected water sample, 50 ml of the sample was allowed to run through the BAB column and the HPC, total coliform count and *E.coli* concentration in the effluent were determined. The results showed a significant reduction in the bacterial concentrations after passing through the BAB column. Table 4.3 presents the heterotrophic plate count in treated and untreated water, while Table 4.4 presents the MPN value and the combination of positive tubes for *E.coli* and other coliforms. It was observed

that the heterotrophic plate count in the effluent was 20 CFU/mL, resulting in a 98% reduction of HPC after the filtration process. The total coliform count also decreased considerably from 1600 MPN/100 mL to 9 MPN/100 mL, indicating 99.4% removal efficiency. Similarly, the initial *E.coli* count of 920 MPN/100mL decreased to 2 MPN/100 mL after running through the column, resulting in 99.8% removal efficiency.

Table 4.3 Heterotrophic plate count for treated and untreated water

HPC in Untreated water	HPC in Treated water	Removal percentage(%)
10 ³ CFU/mL	20 CFU/mL	98%

Table 4.4 Total coliform and *E.coli* bacteria count for treated and untreated water

	Untreated water		Treated water		
Bacteria	Combination of positive tubes	MPN/100 mL	Combination of positive tubes	MPN/100mL	Removal percentage (%)
Total coliform count	5-5-4	1600	2-1-1	9	99.4%
<i>E.coli</i>	5-5-3	920	1-0-0	2	99.8%

4.3.3 Biochemical identification *E.coli* bacteria

Although the enumeration of *E.coli* and total coliform is done by standard methods such as multiple tube fermentation technique, an additional biochemical test is often recommended to identify the isolates as *E.coli* bacteria (WHO, 1993) [44]. Therefore, the pure isolates cultured from the collected water sample were subjected to various biochemical tests for the confirmation and identification of the isolates as *E.coli* and other coliform bacteria or non-coliform bacteria.

Altogether, 12 bacteria isolates were isolated from the mixed culture based on their colony and morphological characteristics. Figure 4.8 represent some of the bacteria isolates.

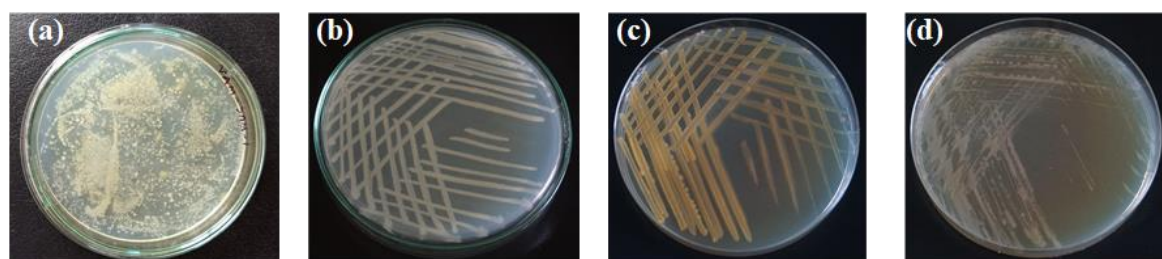


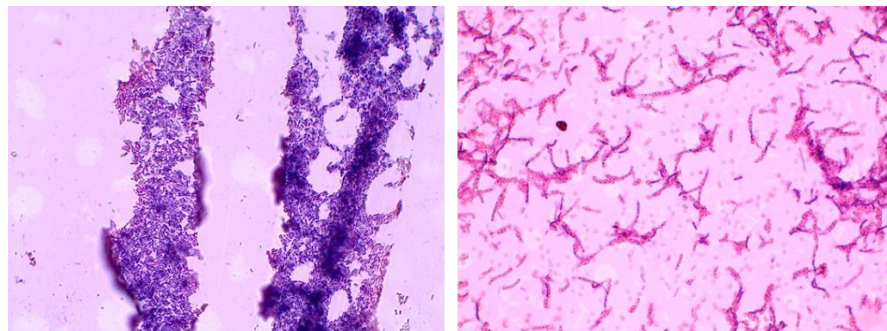
Figure 4.8 (a) Mixed culture of bacteria in the water sample and Pure culture of (b) Isolate 1 (c) Isolate 6 (d) Isolate 9

Depending on the biochemical characters, 9 isolates were identified as coliform bacteria while the remaining 3 isolates were identified as non-coliform bacteria. The test results are given in Table 4.5. Among the coliform isolates, isolate 1, isolate 4 and isolate 12 were identified as

E.coli, given by their gram-negative character, catalase-positive, motile nature, hydrogen sulphide negative, triple sugar iron negative and IMViC pattern “++--” [45]. Besides, other coliform genera such a *Klebsiella*, *Enterobacter*, and *Citrobacter* were also identified by their biochemical characters. Biochemical properties of the isolates thus clearly confirmed the presence of *E.coli* and other coliform species in the water sample. The interpretations of the biochemical tests are given in Figure 4.9.

Table 4.5 Test result of biochemical tests

Isolate No.	Gram character	Catalase	Oxidase	Motility	Indole production	Methyl red	Voges Proskauer	Citrate utilization	Triple sugar iron	Bacterial group
Isolate 1	-ve, Rod	+	-	+	+	+	-	-	A/A Gas	Coliform- <i>E.coli</i> .
Isolate 2	-ve, Rod	+	-	-	-	-	+	+	A/A gas	Coliform- <i>Klebsiella</i> sp.
Isolate 3	-ve, Rod	+	-	+	-	-	+	+	A/A gas	Coliform- <i>Enterobacter</i> sp.
Isolate 4	-ve, Rod	+	-	+	+	+	-	-	A/A gas	Coliform- <i>E.coli</i> .
Isolate 5	+ve, Rod	+	+	+	-	-	+	+	K/K	Non-coliform
Isolate 6	+ve, Rod	+	+	-	-	-	+	-	K/K	Non-coliform
Isolate 7	+ve, Rod	+	-	+	-	+	+	+	A/K +H ₂ S	Non-coliform
Isolate 8	-ve, Rod	+	-	+	+	+	-	-	A/A	Coliform – <i>E.coli</i> sp.
Isolate 9	-ve, Rod	+	-	+	-	-	+	+	A/A gas	Coliform <i>Enterobacter</i> sp.
Isolate 10	-ve, Rod	+	-	+	-	+	-	+	A/A gas +H ₂ S	Coliform <i>Citrobacter</i> sp.
Isolate 11	-ve, Rod	+	-	+	-	-	+	+	A/A gas	Coliform- <i>Enterobacter</i> sp.
Isolate 12	-ve, Rod	+	-	+	+	+	-	-	A/A gas	Coliform- <i>E.coli</i>



Gram Positive bacteria

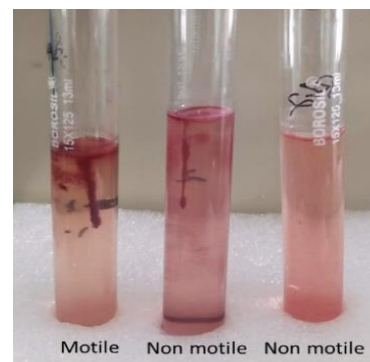
Gram Negative bacteria

(a)



Positive

(b)

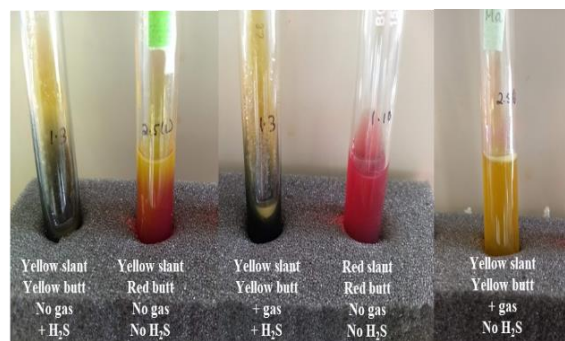


Motile Non motile Non motile

(c)

Positive: Copious bubbles produced
Negative: No bubble produced

Non-motile: Intact straight stab line
Motile: Original stab line diffuse out into the medium



(d)

Alkaline /Alkaline (K/K) i.e., Red slant /Red butt = glucose, lactose and sucrose non-fermenter

Alkaline /Acidic (K/A) i.e., Red slant /Yellow butt = glucose fermentation only

Acidic /Acidic (A/A) i.e., Yellow slant/Yellow butt = glucose, lactose and/or sucrose fermenter gas

Acidic/Alkaline (A/K) i.e., Yellow slant/ Red butt = glucose oxidation

Blackening of the medium: Occurs in the presence of H_2S

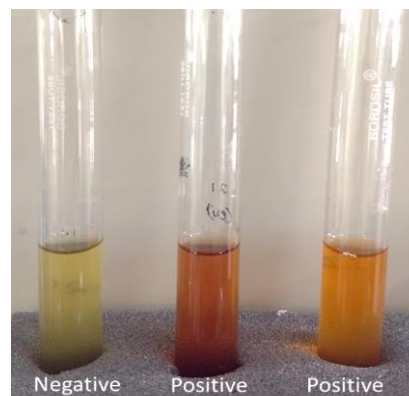
Gas production: Bubbles or cracks in the indicate the production of gas (formation of CO_2 and H_2)



(e)

Positive: Formation of a cherry-red ring on top of the medium after addition of Kovac's reagent

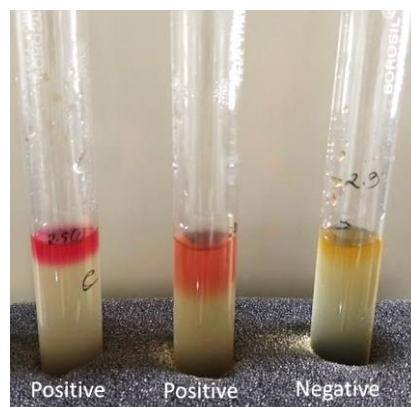
Negative: No colour change observed after addition of Kovac's reagent



(f)

Positive: Colour change from yellow to orange

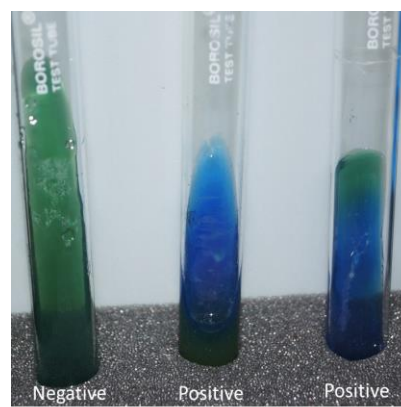
Negative: No colour change observed



(g)

Positive: Pink-red colour at the surface

Negative: Lack of pink-red colour



(h)

Positive: Colour change of the medium from deep forest green to a Prussian blue colour

Negative: No colour change.

Figure 4.9 Result interpretation of biochemical tests (a) Gram character (b) catalase test (c) Motility (d) Triple sugar iron (e) Indole (f) Methyl red (g) Voges Proskauer and (h) Citrate utilization test

4.4 Conclusion

In this study, a simple and efficient activated carbon biofilter column was developed for the treatment of bacteria-contaminated water. The biofilter columns amended with activated carbon i.e., BAB, SAS and PAP achieved a high removal efficiency of *E.coli* from aqueous solution. BAB, SAS and PAP showed high log reduction of *E.coli* corresponding to 4.45 ± 0.57 , 3.94 ± 0.49 and 3.38 ± 0.90 respectively, while the biofilter columns consisting of only the supporting media i.e., PB, PP and PS attained a very low log reduction of 0.77 ± 0.17 , 0.04 ± 0.03 and 0.27 ± 0.22 respectively. Further, the *E.coli* breakthrough in the biofilter column

with only the supporting media was observed in the first 15 minutes. However, the *E.coli* breakthrough in biofilter columns with the activated carbon was observed at a much later stage i.e only after 55 minutes. These results indicated that the presence of activated carbon significantly improved the overall performance of the biofilter columns. Among all the biofilter columns, BAB attained the highest removal efficiency of *E.coli* from aqueous solution. This proves the higher effectiveness of brick powder as a supporting medium compared to sand and pebbles. Further, the BAB column could remove 98% total heterotrophic bacteria, 99.4% total coliform and 99.8 % *E.coli* from a real water sample, indicating the applicability of the BAB column in the real world scenario.

References

- [1] WHO, UNICEF, Progress on household drinking water, sanitation and hygiene 2000-2017 Special focus on inequalities, 2019.
- [2] World Health Organization, Safe water, better health, 2019.
- [3] A. Prüss-Ustün, J. Wolf, J. Bartram, T. Clasen, O. Cumming, M.C. Freeman, B. Gordon, P.R. Hunter, K. Medlicott, R. Johnston, Burden of disease from inadequate water, sanitation and hygiene for selected adverse health outcomes: An updated analysis with a focus on low- and middle-income countries, *Int. J. Hyg. Environ. Health.* 222 (2019) 765–777. doi:10.1016/j.ijheh.2019.05.004.
- [4] T.A. Dankovich, D.G. Gray, Bactericidal paper impregnated with silver nanoparticles for point-of-use water treatment, *Environ. Sci. Technol.* 45 (2011) 1992–1998. doi:10.1021/es103302t.
- [5] J. Jang, H.G. Hur, M.J. Sadowsky, M.N. Byappanahalli, T. Yan, S. Ishii, Environmental *Escherichia coli*: ecology and public health implications—a review, *J. Appl. Microbiol.* (2017). doi:10.1111/jam.13468.
- [6] K.S. Hashim, S.S.M. Ali, J.K. AlRifaie, P. Kot, A. Shaw, R. Al Khaddar, I. Idowu, M. Gkantou, *Escherichia coli* inactivation using a hybrid ultrasonic–electrocoagulation reactor, *Chemosphere.* (2020). doi:10.1016/j.chemosphere.2020.125868.
- [7] D. Ghernaout, Electrocoagulation and Electrooxidation for Disinfecting Water: New Breakthroughs and Implied Mechanisms, *Appl. Eng.* (2019). doi:10.11648/j.ae.20190302.18.
- [8] S. Gholami, M. Naderi, M. Yousefi, M.M. Arjmand, The electrochemical removal of bacteria from drinking water, *Desalin. Water Treat.* (2019). doi:10.5004/dwt.2019.24181.
- [9] I.C. Iakovides, I. Michael-Kordatou, N.F.F. Moreira, A.R. Ribeiro, T. Fernandes, M.F.R. Pereira, O.C. Nunes, C.M. Manaia, A.M.T. Silva, D. Fatta-Kassinos, Continuous ozonation of urban wastewater: Removal of antibiotics, antibiotic-resistant *Escherichia coli* and antibiotic resistance genes and phytotoxicity, *Water Res.* (2019). doi:10.1016/j.watres.2019.05.025.
- [10] J. Gomes, D. Frasson, R.M. Quinta-Ferreira, A. Matos, R.C. Martins, Removal of enteric pathogens from real wastewater using single and catalytic ozonation, *Water (Switzerland).* (2019). doi:10.3390/w11010127.
- [11] A.K. Benabbou, Z. Derriche, C. Felix, P. Lejeune, C. Guillard, Photocatalytic inactivation of *Escherichia coli*. Effect of concentration of TiO₂ and microorganism, nature, and intensity of UV irradiation, *Appl. Catal. B Environ.* (2007). doi:10.1016/j.apcatb.2007.05.026.
- [12] S. Das, N. Ranjana, A.J. Misra, M. Suar, A. Mishra, A.J. Tamhankar, C.S. Lundborg, S.K. Tripathy, Disinfection of the water borne pathogens *Escherichia coli* and *Staphylococcus aureus* by solar photocatalysis using sonochemically synthesized reusable Ag@ZnO core-shell nanoparticles, *Int. J. Environ. Res. Public Health.* (2017).

- doi:10.3390/ijerph14070747.
- [13] S. Neralla, R.W. Weaver, Phytoremediation of domestic wastewater for reducing populations of *Escherichia coli* and MS-2 coliphage, *Environ. Technol.* (2000). doi:10.1080/09593332108618083.
- [14] R. Alufasi, J. Gere, E. Chakauya, P. Lebea, W. Parawira, W. Chingwaru, Mechanisms of pathogen removal by macrophytes in constructed wetlands, *Environ. Technol. Rev.* (2017). doi:10.1080/21622515.2017.1325940.
- [15] C.U. Schwermer, P. Krzeminski, A.C. Wennberg, C. Vogelsang, W. Uhl, Removal of antibiotic resistant *E. coli* in two Norwegian wastewater treatment plants and by nano- and ultra-filtration processes, *Water Sci. Technol.* (2018). doi:10.2166/wst.2017.642.
- [16] M. Hassan, R. Abou-Zeid, E. Hassan, L. Berglund, Y. Aitomäki, K. Oksman, Membranes based on cellulose nanofibers and activated carbon for removal of *Escherichia coli* bacteria from water, *Polymers (Basel)*. (2017). doi:10.3390/polym9080335.
- [17] A. Pérez-Vidal, S.P. Rivera-Sanchez, L.J. Florez-Elvira, J.A. Silva-Leal, J. Diaz-Gomez, L.F. Herrera-Cuero, L.P. Lopez Botero, Removal of *E. coli* and *Salmonella* in pot ceramic filters operating at different filtration rates, *Water Res.* (2019). doi:10.1016/j.watres.2019.05.028.
- [18] C. Farrow, E. McBean, G. Huang, A.L. Yang, Y.C. Wu, Z. Liu, Z.N. Dai, H.Y. Fu, T. Cawte, Y.P. Li, Ceramic water filters: A point-of-use water treatment technology to remove bacteria from drinking water in Longhai City, Fujian Province, China, *J. Environ. Informatics.* (2018). doi:10.3808/jei.201800388.
- [19] W. Che, Z. Xiao, Z. Wang, J. Li, H. Wang, Y. Wang, Y. Xie, Wood-Based Mesoporous Filter Decorated with Silver Nanoparticles for Water Purification, *ACS Sustain. Chem. Eng.* (2019). doi:10.1021/acssuschemeng.8b06001.
- [20] J. Arevalo-Fester, Efficiency Study of Silver Nanoparticles (AgNPs) Supported on Granular Activated Carbon against *Escherichia coli*, *J. Nanomedicine Res.* (2014). doi:10.15406/jnmr.2014.01.00009.
- [21] T. Huang, R. Zhou, J. Cui, J. Zhang, X. Tang, S. Chen, J. Feng, H. Liu, Fast and cost-effective preparation of antimicrobial zinc oxide embedded in activated carbon composite for water purification applications, *Mater. Chem. Phys.* (2018). doi:10.1016/j.matchemphys.2017.11.044.
- [22] F.S. Arakawa, Q.L. Shimabuku-Biadola, S. de Lima Bazana, M.F. Silva, B.A. de Abreu Filho, R. Bergamasco, Activated carbon impregnation with ag and cu composed nanoparticles for *escherichia coli* contaminated water treatment, *Can. J. Chem. Eng.* (2019). doi:10.1002/cjce.23471.
- [23] S. Asadi, F. Moeinpour, Inactivation of *Escherichia coli* in water by silver-coated Ni_{0.5}Zn_{0.5}Fe₂O₄ magnetic nanocomposite: a Box–Behnken design optimization, *Appl. Water Sci.* (2019). doi:10.1007/s13201-019-0901-4.
- [24] S. Zhan, D. Zhu, S. Ma, W. Yu, Y. Jia, Y. Li, H. Yu, Z. Shen, Highly efficient removal

- of pathogenic bacteria with magnetic graphene composite, *ACS Appl. Mater. Interfaces*. (2015). doi:10.1021/am508682s.
- [25] S.Y.I. Sari, A.R. Alfian, T. Respati, D. Agustian, A.S. Raksanagara, Comparison of drinking water quality following boiling, household filtration and water-refill in Urban-Slum Area, *J. Int. Dent. Med. Res.* (2019).
- [26] M. Al-Abri, B. Al-Ghafri, T. Bora, S. Dobretsov, J. Dutta, S. Castelletto, L. Rosa, A. Boretti, Chlorination disadvantages and alternative routes for biofouling control in reverse osmosis desalination, *Npj Clean Water*. (2019). doi:10.1038/s41545-018-0024-8.
- [27] G. Crini, E. Lichtfouse, Advantages and disadvantages of techniques used for wastewater treatment, *Environ. Chem. Lett.* (2019). doi:10.1007/s10311-018-0785-9.
- [28] A. Maurya, M.K. Singh, S. Kumar, Biofiltration technique for removal of waterborne pathogens, in: *Waterborne Pathog.*, 2020. doi:10.1016/b978-0-12-818783-8.00007-4.
- [29] C.K. Pooi, H.Y. Ng, Review of low-cost point-of-use water treatment systems for developing communities, *Npj Clean Water*. (2018). doi:10.1038/s41545-018-0011-0.
- [30] A.K. Bayable, F.D. Adey, A. Fassil, Evaluating the efficacy of household filters used for the removal of bacterial contaminants from drinking water, *African J. Microbiol. Res.* (2020). doi:10.5897/ajmr2020.9344.
- [31] P.M.F. Maciel, L.P. Sabogal-Paz, Household slow sand filters with and without water level control: continuous and intermittent flow efficiencies, *Environ. Technol. (United Kingdom)*. (2020). doi:10.1080/09593330.2018.1515988.
- [32] A.R.M.N. Afrooz, A.B. Boehm, *Escherichia coli* removal in biochar-modified biofilters: Effects of biofilm, *PLoS One*. (2016). doi:10.1371/journal.pone.0167489.
- [33] M.S. Onyango, T.Y. Leswifi, A. Ochieng, D. Kuchar, F.O. Otieno, H. Matsuda, Breakthrough analysis for water defluoridation using surface-tailored zeolite in a fixed bed column, *Ind. Eng. Chem. Res.* 48 (2009) 931–937. doi:10.1021/ie0715963.

CHAPTER 5

REMOVAL OF 4-NITROPHENOL USING ACTIVATED CARBON SYNTHESIZED FROM RAVENNA GRASS¹

This chapter deals with the utilisation of activated carbon synthesized from Ravenna grass biomass for the removal of 4-Nitrophenol from an aqueous solution. The activated carbon was prepared using a two-step chemical activation process. The effect of varying molar concentrations of the activating agent on the textural properties of the activated carbon was also studied. The synthesized carbon was characterized using BET surface area analyser, SEM, FTIR, XRD and TGA. The removal efficiency of the activated carbon for 4-Nitrophenol was determined by batch adsorption test. Adsorption isotherms, adsorption kinetics and thermodynamics studies were investigated to understand the adsorption behaviour. Further, Density functional theory (DFT) calculations were performed at the B3LYP level to gain an insight into the adsorption mechanism. Cost analysis of the prepared carbon was also done to determine its economic viability.

¹The text of this chapter has been published as; **A. Supong, P.C. Bhomick, U.B. Sinha, D. Sinha. A combined experimental and theoretical investigation of the adsorption of 4-Nitrophenol on activated biocarbon using DFT method. Korean Journal of Chemical Engineering. 36, 2023–2034 (2019).** <https://doi.org/10.1007/s11814-019-0382-z>

5.1 Introduction¹

The contamination of water resources with various undesirable compounds and its remediation is one of the greatest challenges being faced in recent years. Phenolic compounds constitute a major group of hazardous pollutant, and among them, 4-Nitrophenol is considered as one of the priority pollutants since its presence in even minute concentrations can bring serious harm to human beings, animals and aquatic systems [1]. The main cause of pollution by 4-nitrophenol in waterbodies is the untreated effluent discharged from different types of industries such as oil refineries, pharmaceuticals, textiles, steel mills, petrochemicals, plywood industries, insecticides production units, coke processing units, resin plants, pulp and paper industries, among others[2]. Human contact with 4-Nitrophenol can leave acute as well as chronic impacts such as vomiting, sore throat, damage to kidney, liver and gastrointestinal tract, difficulty in swallowing, skin and eyes irritation, cardiovascular diseases, protein degeneration, central nervous system disorder, salivation, anorexia, fainting, tissue erosion, muscle weakening, vertigo etc [3–6]. Therefore, the development of simple, yet efficient wastewater treatment techniques is required to eliminate this recalcitrant chemical from wastewater and in this regard, several conventional and advanced technologies have been adopted over the years for the safe treatment of wastewater containing 4-Nitrophenol. These include adsorption and extraction[7,8] distillation[9,10], membrane processes[11,12], electrochemical oxidation[13,14], chemical oxidation[15,16], advanced oxidation process[17–20], biological treatment[21,22] and enzymatic treatment [23,24]. Among all the available methods, adsorption using activated carbon remains one of the best choices because of its efficiency and ability to remove not only one but all types of phenolic compounds from wastewater. The multifaceted characteristics of activated carbon such as high surface area, good thermal stability, large pore volume, abundant surface functional groups, lack of production of secondary by-products, simple design and easy operation make them one of the most prolific adsorbents.

In the present work, therefore, the removal of 4-nitrophenol from water was carried out using activated carbon prepared from Ravenna grass biomass. The utilization of biomass resources for synthesizing activated carbon provides a promising alternative to commercial activated carbon, with several advantages such as cost-effectiveness, availability, renewability and

¹ The text of this chapter has been published as; **A. Supong**, P.C. Bhomick, U.B. Sinha, D. Sinha. **A combined experimental and theoretical investigation of the adsorption of 4-Nitrophenol on activated biocarbon using DFT method.** *Korean Journal of Chemical Engineering*. 36, 2023–2034 (2019). <https://doi.org/10.1007/s11814-019-0382-z>

ecological suitability. For the preparation of activated carbon, a two-step activation process was followed, using potassium hydroxide as the activating agent. It is an established fact that the textural characteristics of activated carbon such as surface area and pore volume are known to have a large influence on the adsorption efficiency of activated carbon, and the present work thus aims at enhancing the surface area and pore volume of the activating carbon by varying the molar concentration of KOH. Several analytical techniques were used to examine the surface characteristics of the prepared activated carbon. Thereafter, application of the prepared activated carbon with the best textural characteristics was explored for the removal of 4-nitrophenol from an aqueous medium. Adsorption isotherm, kinetics and thermodynamic studies were also investigated. Also, theoretical calculations using DFT were employed to understand the possible interactions taking place between 4-Nitrophenol and the activated carbon surface during the adsorption process.

5.2. Materials and Method

5.2.1. Ravenna grass activated biocarbon preparation

The raw material Ravenna grass was collected locally (26°16'23"N| 94 ° 27' 55."E). The whole part of the plant was used for the production of activated biocarbon. The biomass was washed and placed in an oven at 110°C for 12 hours. The dried biomass was carbonized at a temperature of 400 °C for 1 hour, and the obtained char was further ground into a uniform fine powder. The powdered char was further subjected to chemical activation using KOH as the activating agent. For chemical activation, 20g of the powdered char was added to beakers containing 250ml of potassium hydroxide solution (KOH) of varying molar concentrations (1M to 3M) and the contents were magnetically stirred at 600rpm for 3 hours at room temperature. The contents were then allowed to dry in an oven at 110 °C, and subsequently, the KOH impregnated char was activated at 700 °C for 1 hour using a muffle furnace at 10 °C min⁻¹ heat flow rate. The sample was then rinsed with 0.1M HCl and deionized water to attain a neutral pH and dried at 105 °C to obtain the Ravenna grass activated carbon. The Ravenna grass activated carbon prepared using 1M, 2M and 3M KOH concentrations at 700°C were labelled as 1M RAC, 2M RAC and 3M RAC respectively and stored in air-tight containers for further use.

5.2.2 Characterization of Ravenna grass activated biocarbon

The physicochemical features of Ravenna grass activated carbon was characterized by using different analytical techniques. The surface area and pore volume were examined by Brunauer, Emmet and Teller (BET) analyser (Smart instrument, SS93/02). SEM analyses

were performed with SEM Model: JSM-6360 (JEOL) to investigate the surface morphology and texture of carbon samples. Thermogravimetric analysis (TGA-Perkin Elmer/STA-3000) was used to understand the thermal stability of the activated carbon while Fourier Transform Infrared Spectroscopy (Spectrum Two, Perkin Elmer) helps in determining the various functional group of activated carbon. XRD analysis was done using CuK α radiation at the scanned rate of 0.2 degrees/minute (Rigaky-Ultimaiv Japan). The zero-point charge was determined by batch equilibrium test for activated carbon[25].

5.2.3 Batch adsorption study of 4-Nitrophenol

The efficiency of the activated carbon to remove 4-Nitrophenol from an aqueous solution was studied by batch mode equilibrium method. The effect of contact time, pH, initial concentration of 4-Nitrophenol, and adsorbent dose on the removal efficiency of 4-Nitrophenol by activated carbon were studied. For the batch study, 50 ml of 4-Nitrophenol solutions of different concentrations (100-500mgL⁻¹) and pH ranging from 2 to 12 were contacted with different quantities of adsorbent dose (0.1g – 1g). The mixtures were taken in 250ml Erlenmeyer Flasks and agitated at 180rpm at a temperature of 25 \pm 2 °C for different contact time (0- 180 minutes). The samples were then filtered, and the residual filtrate concentration of 4-Nitrophenol was analysed using a UV-VIS spectrophotometer (Perkin-Elmer lambda-35) at 317 nm wavelength. All the experiments were done in triplicates, and the average value of the three readings was reported. The adsorption capacity of 4-Nitrophenol and its removal efficiency was determined by equation 1 and 2 respectively as given in chapter 2.

5.2.4 Theoretical study of 4-Nitrophenol adsorption onto activated carbon

All the necessary theoretical calculations pertaining to the understanding of adsorption of 4-Nitrophenol onto the activated carbon were carried out on the Gaussian 09[26] suite of programs. The geometry optimization, as well as frequency and energy calculations were performed at 6-31g basis set and B3LYP hybrid functional in a dielectric medium of $\epsilon = 80$ (corresponding to water). To study the possible interaction of 4-Nitrophenol with activated carbon, it is necessary to create a reasonable structure for the activated carbon surface. Since activated carbon is considered as macrostructures with an aromatic cluster of different sizes, a benzene ring cluster model with armchair edge shapes were used to simulate the activated biocarbon surface in the present study[27]. The upper edge atoms of the cluster model were unsaturated to create an active site whereas the carbon atoms on the remaining lower part of the cluster surface were terminated with hydrogen atoms. This unsaturated active site model

was taken as pristine activated carbon. Besides, the active site was functionalized with OH, CHO and COOH groups to study the effect of such functional groups on the 4-Nitrophenol adsorption process. Gauss view 05 was used to generate all the required models and the resulting structures were optimized in their electronic ground state. The optimized benzene ring cluster models are given in Figure 5.1. The cluster models were named pristine activated biocarbon (AC), OH functionalized carbon (AC)OH, CHO functionalized carbon (AC)CHO and COOH functionalized carbon (AC)COOH. The adsorption of 4-Nitrophenol at different sites of the carbon models were studied, and various possible ways of interaction were considered. The adsorption energy of 4-Nitrophenol on activated carbon surface was calculated using equation 21 given in chapter 2.

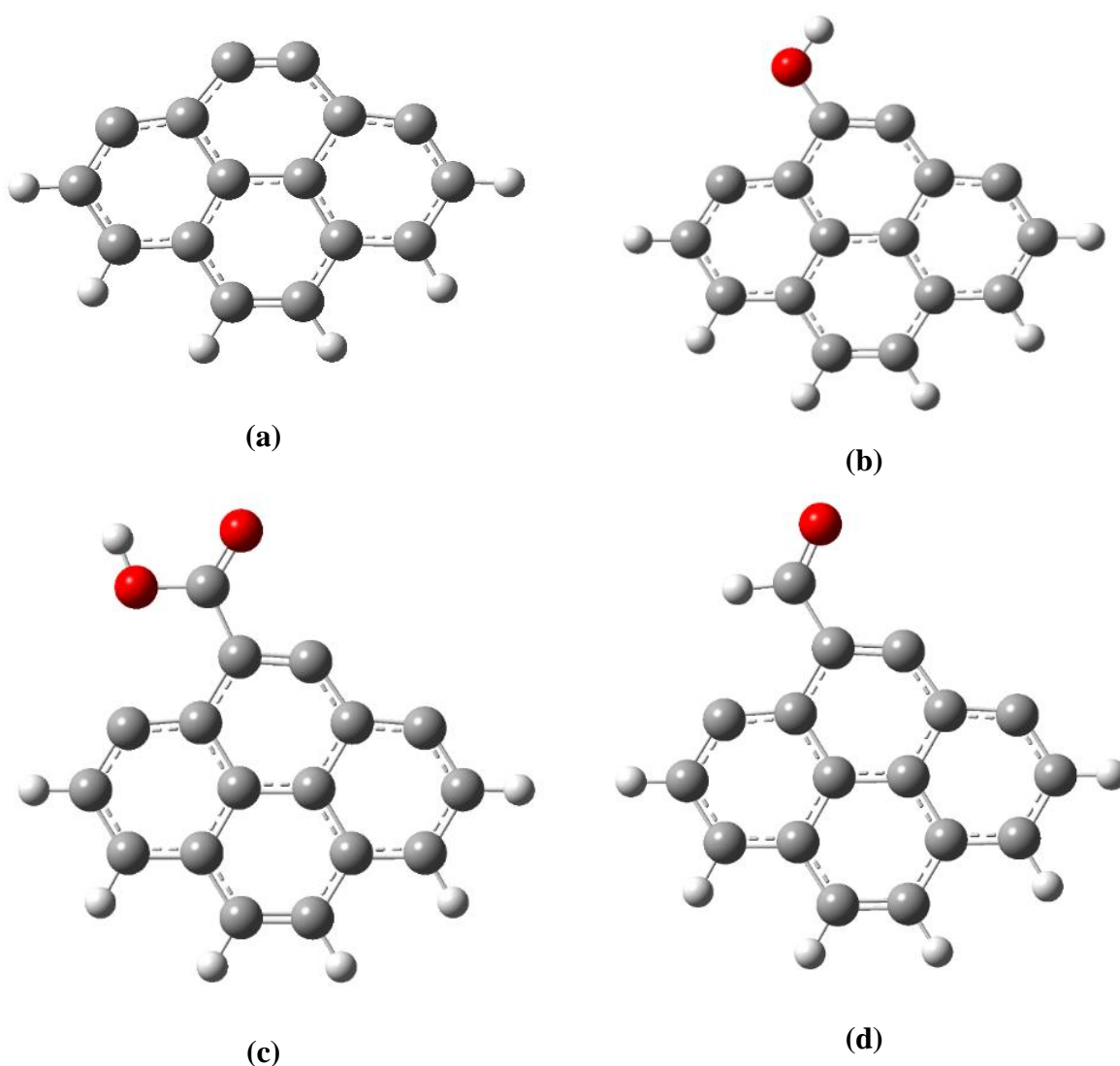


Figure 5.1 The optimized model of (a) AC (b) (AC)OH (c) (AC)COOH (d) (AC)CHO

5.3 Results and discussion

5.3.1 Characterisation of activated carbon

a) BET surface area and pore volume

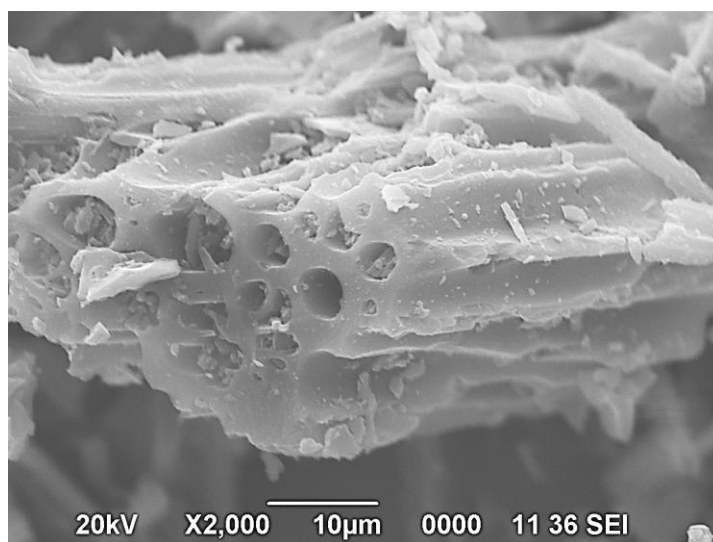
Experiments had been conducted to study the influence of different molar concentrations of KOH on the textural characteristics of the activated carbon. The results revealed that the varying KOH concentrations from 1M to 3M have a significant effect on the BET surface area and total pore volume. The highest surface area and pore volume were obtained for the activated carbon prepared at 700°C using 2M KOH concentration. The BET surface area of 1M RAC, 2M RAC and 3M RAC corresponded to 854.44 m²/g, 919 m²/g and 726.21 m²/g respectively and their respective pore volumes corresponded to 0.301 cm³/g, 0.324 cm³/g and 0.289 cm³/g.

b) Scanning Electron microscopy

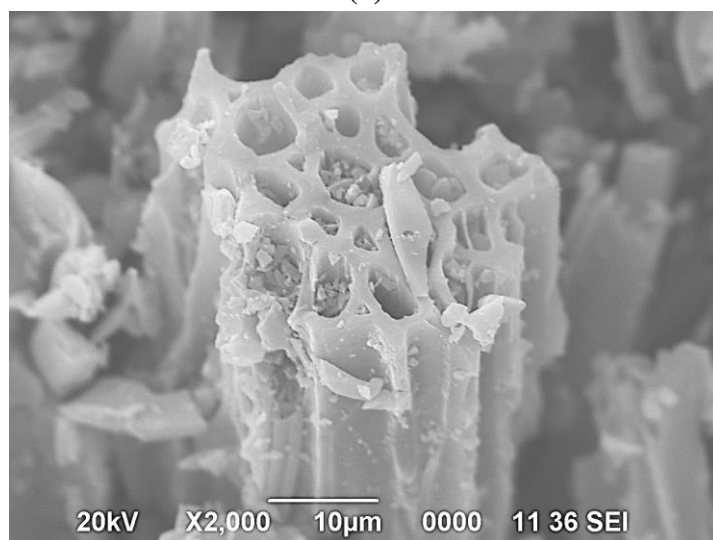
The SEM micrographs of the activated carbons synthesized at 700°C with different concentrations of KOH are shown in Figure 5.2. The images revealed a non-uniform surface structure with cracks, cavities and pores of different shapes and sizes. It is observed that the activated carbon obtained using 1M KOH concentration contain only some pores (Figure 5.2(a)), whereas, with an increase in molar concentration from 1M to 2M, the porous structure of activated carbon became more developed with numerous cavities, pits and pores distributed all over the activated carbon surface (Figure 5.2(b)). However, at higher KOH concentration (3M), the porous structure began to collapse and the pores became bigger, which may be due to the over-activation of the carbon with excess KOH(Figure 5.2(c))[28].

c) Fourier Transform Infrared Spectroscopy

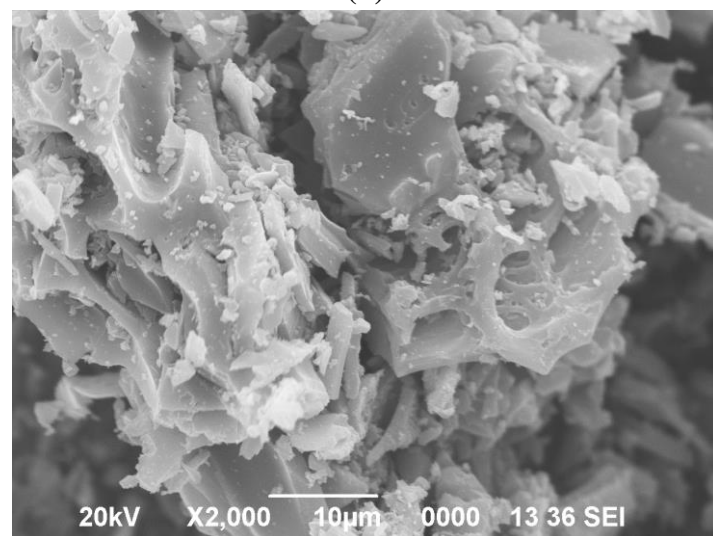
FTIR spectrum in Figure 5.3 shows the presence of the different surface functional groups. The strong and broad band between 3460-3440 cm⁻¹ represent OH stretching vibration [29]. The band between 2990 and 2810 cm⁻¹ may be due to C-H stretching vibration. The appearance of a peak at around 1741 cm⁻¹ is assigned to C=O stretching vibration of aldehydes, ketones, esters and acetyl derivatives[30]. The peak between 1640 and 1630 cm⁻¹ could be due to olefinic C=C stretching vibration, while the peak at between 1470 and 1420 cm⁻¹ represents the skeletal C=C vibrations in aromatic rings [31]. The transmittance at 1055 and 1035 cm⁻¹ is accounted to C-O stretching in alcohols, carboxylic acid or derivatives, phenols, ethers or esters group [32]. The bands between 800-500 cm⁻¹ correspond to the vibrations of C-H, O-H and C-O bonds.



(a)

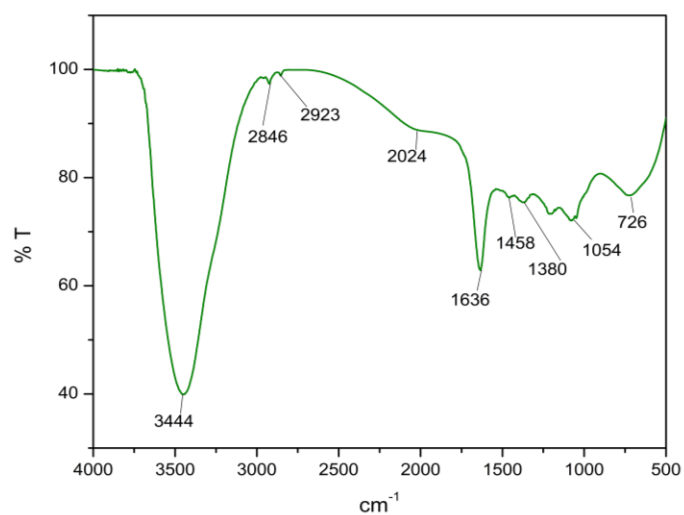


(b)

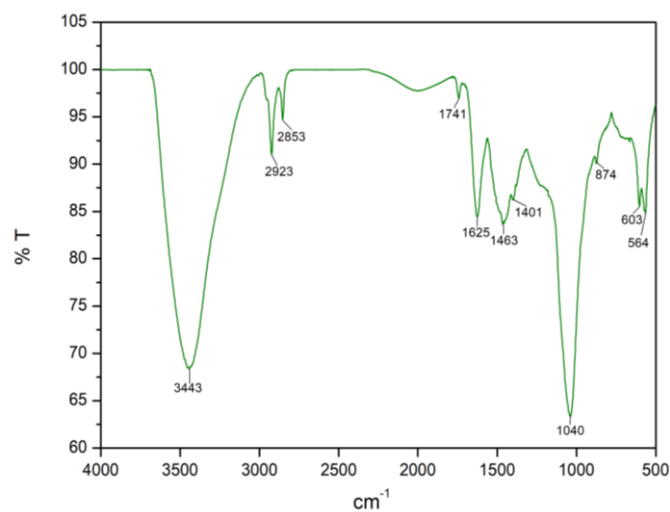


(c)

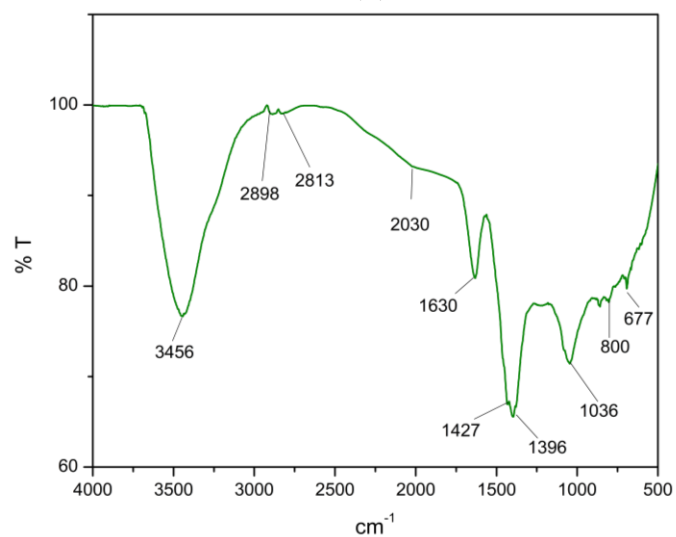
Figure 5.2 SEM micrograph of (a) 1M RAC (b) 2M RAC and (b) 3M RAC



(a)



(b)



(c)

Figure 5.3 FTIR spectra of (a) 1M RAC (b) 2M RAC and (c) 3M RAC

d) X-ray diffraction analysis (XRD)

The amorphous nature or crystalline nature of the prepared activated carbon was determined using XRD and Figure 5.4 represents the X-ray diffractogram of the synthesized carbons. In all the activated carbon samples, two broad bands appearing at $2\theta = \sim 23^\circ$ and $\sim 43^\circ$ were observed, which could be attributed to the reflection from the (002) plane and (100) plane, respectively. The existence of such bands suggests the graphite-like microcrystallite structure of the activated carbon [33].

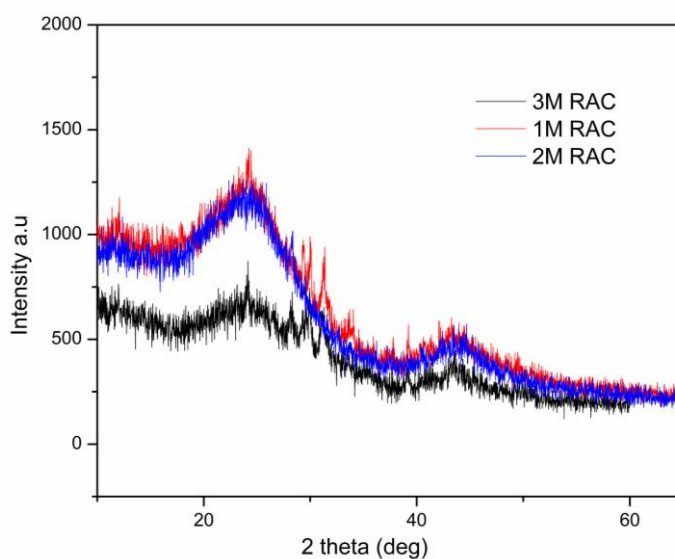


Figure 5.4 XRD patterns of 1M RAC, 2M RAC and 3M RAC

e) Thermogravimetric analysis

The thermogravimetric analysis helps in comprehending the thermal stability and decomposition pattern of the activated biocarbon. Figure 5.5 gives the thermogravimetric graph of the prepared activated carbons. Similar patterns of TGA curves were obtained for all the samples prepared using different concentrations of KOH.

The weight loss at temperatures below 200°C could be due to loss of moisture present on the carbon [34]. The release of volatiles such as CO_2 and CO may account for the gradual weight loss above 550°C [35]. The retention of about 60% unburned weight at around 1000°C indicates the resistance of the activated carbons to a high heating condition reflecting its excellent thermal-stable nature.

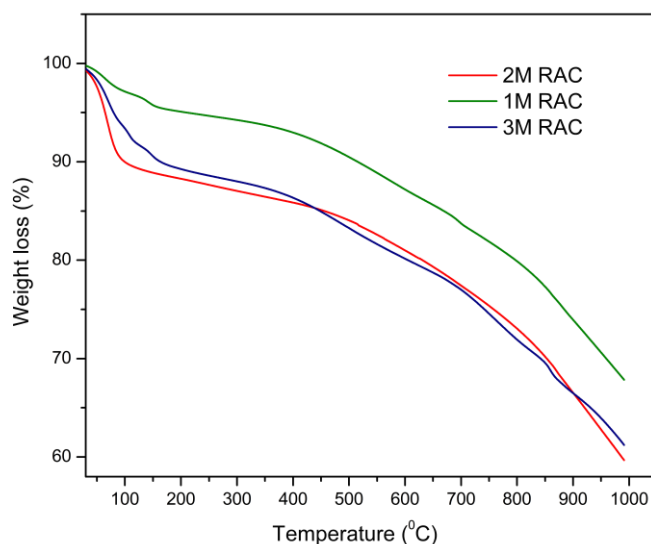


Figure 5.5 TGA profile of 1M RAC, 2M RAC and 3M RAC

5.3.2 Batch adsorption studies

The effect of adsorbent dose, contact time, initial concentration of 4-Nitrophenol and pH on the removal efficiency of 4-Nitrophenol from aqueous solution was investigated by batch adsorption method. For this study, the activated carbon obtained using 2M KOH concentration (2M RAC), showing the highest surface area of $854.44 \text{ m}^2\text{g}^{-1}$ and pore volume $0.445 \text{ cm}^3\text{g}^{-1}$ was used.

5.3.2.1 Effect of adsorbent dose

The adsorbent dose is one of the important factors in adsorption studies as it determines the capacity of activated biocarbon for the adsorption of an adsorbate. The optimum adsorbent dose was obtained by varying the dosage of RAC from 0.1 to 1 g at pH-7, 25°C temperature, initial 4-Nitrophenol concentration of 400 mg L^{-1} and 40 minutes contact time. As can be seen from Figure 5.6(a), the removal percentage of 4-Nitrophenol increased from 89.11% to 99.6% with the increase in adsorbent dose from 0.1g to 0.5g. This increase in removal percentage could be due to the availability of more adsorption active sites and greater surface area at increased adsorbent dose [36]. However, the removal percentage remained almost constant above 0.5g adsorbent dose and this may be attributed to the aggregation or overlapping of available adsorption sites at higher adsorbent dose[37]. The adsorbent quantity of 0.5g was chosen as the optimum dose for further studies.

5.3.2.2 Effect of contact time

The contact time helps determine the duration of equilibrium attainment between the adsorbate and adsorbent. The effect of contact time on removal efficiency was evaluated by

variation of contact time (5 to 180 minutes) at constant adsorbent dosage (0.5g), 400 mg L⁻¹ initial 4-Nitrophenol concentration, pH-7 and 25°C temperature. A plot of removal efficiency (%) of the activated carbon versus contact time is shown in Figure 5.6(b). The uptake of 4-Nitrophenol increased rapidly at the initial period and gradually proceeded at a slower rate as the equilibrium was attained. The higher adsorption rate during the initial stages is associated with the availability of a large number of readily accessible sites on the adsorbent surface[38,39]. However, with the progression of contact time, the removal rate became slow, and finally, the system reached equilibrium after around 40 minutes. As time precedes, the remaining vacant surface sites become less accessible as a result of the repulsive interaction between the 4-Nitrophenol molecules present on the adsorbent surface and in the solution, thereby decreasing the adsorption rate [40,41]. From the results, contact time of 40 minutes was fixed as the optimum time for subsequent adsorption studies.

5.3.2.3 Effect of initial concentration

The effect of initial concentration on the adsorption of 4-Nitrophenol onto activated carbon was investigated at different 4-Nitrophenol concentrations ranging from 100mg/L to 500 mg/L while other parameters i.e., adsorbent dose, contact time, temperature and pH were fixed at 0.5g, 40 minutes, 25°C and 7, respectively. A plot of removal efficiency (%) versus the initial 4-Nitrophenol concentration is given in Figure 5.6(c). The removal efficiency was inversely related to the initial concentration of 4-Nitrophenol. The higher removal percentage at lower 4-Nitrophenol concentrations may be due to the availability of more adsorption sites on the surface of the adsorbent than the number of adsorbate molecules present in the solution. However, at higher concentrations, the number of 4-Nitrophenol molecules competing for the same number of adsorption sites were higher, thus decreasing the removal efficiency [42].

5.3.2.4 Effect of pH

The pH of the solution plays a pivotal role in the process of adsorption. The effect of pH on the adsorption efficiency of 4-nitrophenol was determined by keeping all the other parameters at optimum conditions (adsorbent dose-0.5g, 25°C temperature, contact time - 40 minutes, initial concentration 400mg/L) and varying the pH from 2 to 12. There was a slight increase in removal percentage of 4-Nitrophenol (98.8 % to 99.9%) on increasing the pH from 2 to 7 whereas the removal efficiency decreased sharply when the pH of the solution was increased to values higher than 7 (Figure 5.6d). pKa value of 4-nitrophenol is 7.15 while the pH_{zpc} value of the activated carbon was found to be 8.1. Therefore, when the pH of the working

solution was at pH less than 7, 4-Nitrophenol molecule would remain in its molecular form (pK_a of 4-Nitrophenol =7.15) and the activated carbon surface would possess a positive charge($pH < pH_{ZPC}$); as a result, there was an increase in the adsorptive interaction between 4-Nitrophenol and RAC. However, at pH more than 7, the surface of activated carbon would be negatively charge($pH > pH_{ZPC}$), and the 4-Nitrophenol molecules will dissociate into their ionic form since the pH of the working solution is greater than the pK_a value of 4-Nitrophenol. As a result, there will be a repulsive interaction between the 4-Nitrophenolate anions and the negatively charged carbon surface, which would eventually decrease the removal efficiency.

5.3.2.5 Effect of temperature

The effect of temperature on the adsorption of 4-Nitrophenol was performed at four different temperatures; 298, 308, 318 and 328 K. The initial concentration of 4-Nitrophenol was set at 400 mg L^{-1} , contact time-40 minutes, pH-7 and 0.5 g adsorbent dose. Figure 5.6(e) represents the plot of removal efficiency versus temperature. It is observed that the removal percentage of 4-Nitrophenol increased with the increase in temperature attaining a maximum of 99.9% was at 328 K.

5.3.3 Adsorption isotherm studies

The adsorption isotherm studies were conducted by fitting the adsorption equilibrium data into three commonly used isotherms, namely Langmuir, Freundlich and Temkin isotherm models. Table 5.1 presents the isotherm parameters and the chi-squared value for 4-Nitrophenol adsorption. From the R^2 value and chi-squared test(χ^2), it is observed that Langmuir model best suited the experimental adsorption isotherm data which signifies the fact that 4-Nitrophenol adsorption onto the activated biocarbon proceeded through monolayer type of coverage. The value of maximum adsorption capacity(q_m) was 50.89 mg/g. The dimensionless separation value, $R_L = 0.001$, signifies that the adsorption of 4-Nitrophenol is favourable. From the Freundlich analysis, it can be seen that the reciprocal of Freundlich adsorption intensity value i.e $1/n$ was found to be less than 1, which indicates that the adsorption follows normal Langmuir isotherm.

Chi-squared test was conducted to validate the isotherm models. The lowest χ^2 value was observed for Langmuir adsorption model which suggests that Langmuir isotherm best elucidated the adsorption of 4-nitrophenol onto the present activated biocarbon.

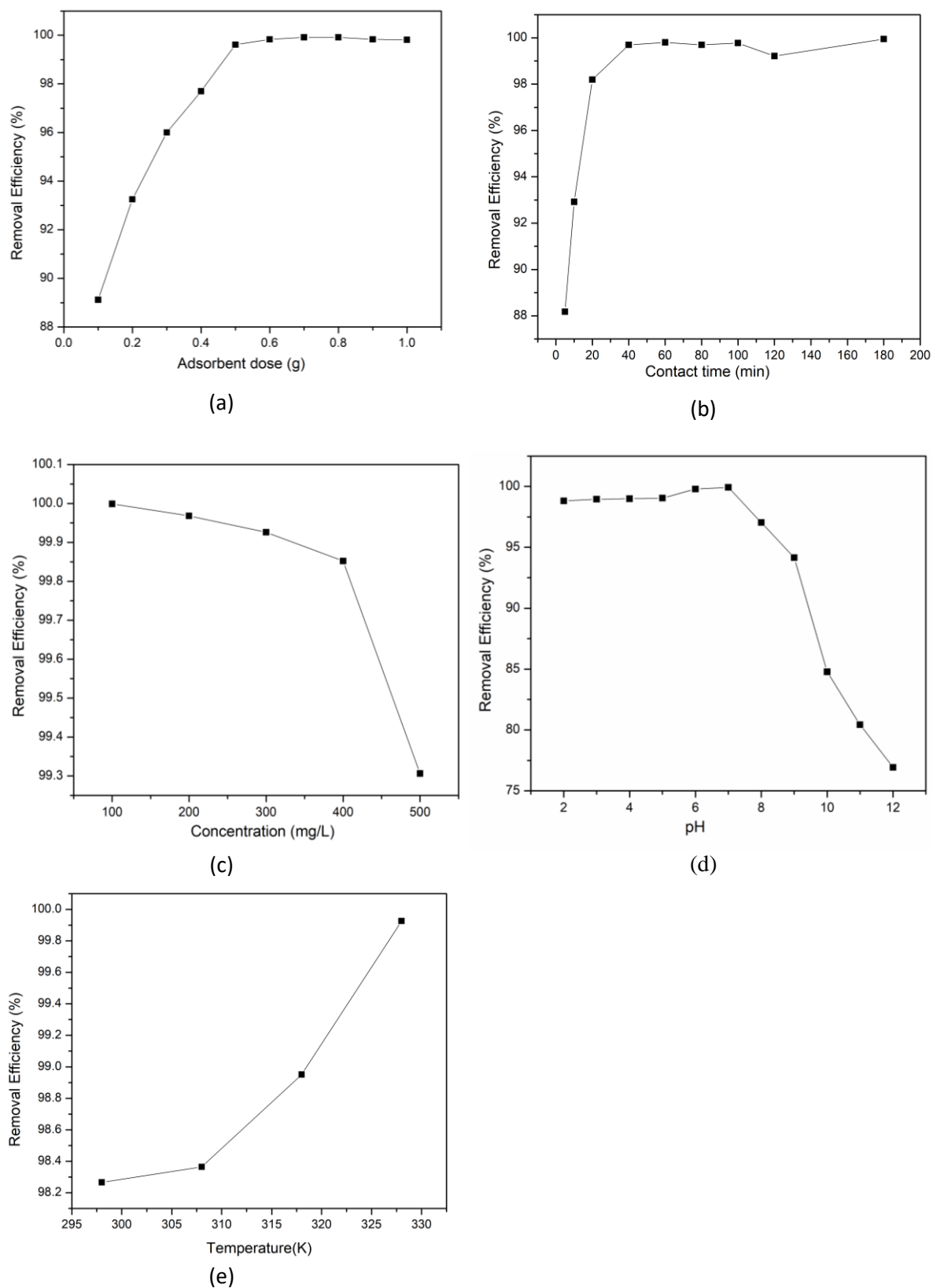


Figure 5.6 (a) Effect of adsorbent dose (b) Effect of contact time (c) Effect of initial 4-Nitrophenol concentration and (d) Effect of pH and (e) Effect of temperature on 4-Nitrophenol adsorption

Table 5.1. Adsorption isotherm parameters for 4-Nitrophenol adsorption onto activated carbon		
Isotherm	Parameters	
Langmuir	q_m	50.890
	K_L	9.013
	R_L	0.001
	R^2	0.996
	χ^2	3.04×10^{-6}
Freundlich	$1/n$	0.208
	n	4.807
	K_F	39.417
	R^2	0.983
	χ^2	1.23×10^{-3}
Temkin	b_T	0.496
	A_T	29.591
	R^2	0.902
	χ^2	24.094

5.3.4 Adsorption kinetic studies

The kinetics of the adsorption process was studied by considering two kinetic models, pseudo-first-order and pseudo-second-order. The obtained kinetic graphs and their plot parameters are shown in Figure 5.7 and Table 5.2, respectively.

The experimental adsorption capacity value, $q_{e,(exp)}$ of pseudo-first-order model showed a vast difference from the calculated adsorption capacity value $q_{e,(cal)}$, which indicates the poor applicability of pseudo-first-order model. However, for pseudo-second-order model, the $q_{e,(exp)}$ was found to be in close agreement with the $q_{e,(cal)}$. Moreover, the highest R^2 value (0.999) and lowest chi-square value ($\chi^2=1.06 \times 10^{-5}$) were obtained for the pseudo-second-order model. All these results indicate that pseudo-second-order kinetic model best elucidated the rate and mechanism of the 4-Nitrophenol adsorption and thus, it can be concluded that chemisorption plays a vital role in the adsorption of 4-Nitrophenol.

5.3.5 Thermodynamic study

The thermodynamics of the adsorption of 4-Nitrophenol onto activated carbon was studied in the temperature range of 298 K to 318 K. The obtained thermodynamic parameters are given in Table 5.3. The value of change in enthalpy (ΔH) is positive, indicating that the adsorption of 4-Nitrophenol onto activated carbon is endothermic. The positive values of ΔS indicated increased randomness at the liquid and solid interface during the process of 4-Nitrophenol adsorption. The negative ΔG value implied the spontaneity of the adsorption process. Moreover, the ΔG value became more negative with increasing temperature, indicating that the adsorption of 4-Nitrophenol is more favourable at higher temperatures.

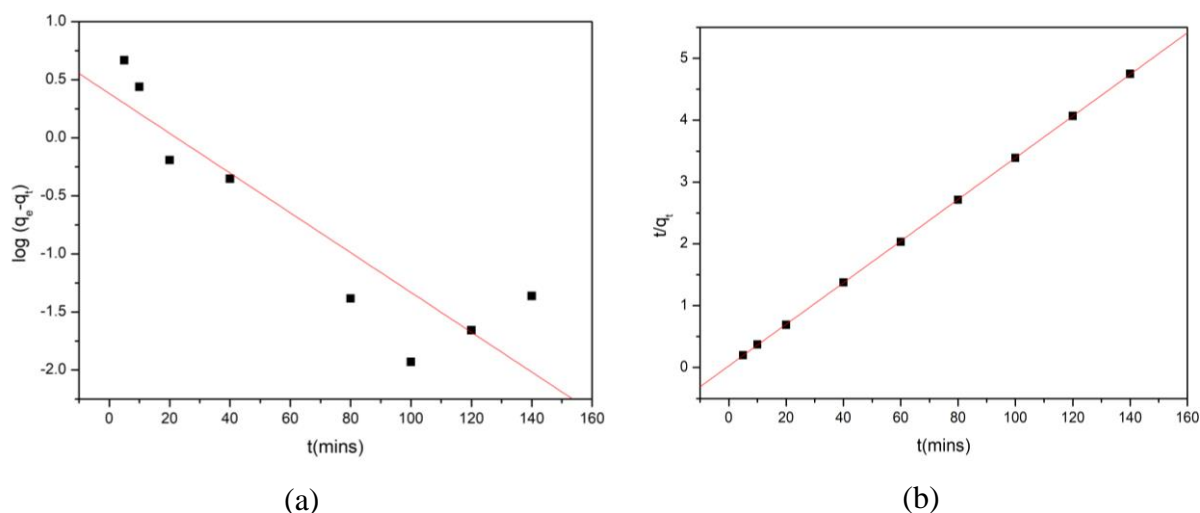


Figure 5.7 Linear plot of (a) Pseudo-first-order and (b) Pseudo-second-order model for the adsorption of 4-Nitrophenol.

Table 5.2 Plot parameters of pseudo-first-order and second-order-model									
Pseudo-first order					Pseudo-second order				
$q_{e,(exp)}$	$e_{e,(cal)}$	k_1	R^2	χ^2	$q_{e,(exp)}$	$q_{e,(cal)}$	k_2	R^2	χ^2
49.897	1.787	0.037	0.804	1.63×10^{-1}	49.897	49.900	0.113	0.999	1.06×10^{-5}

Table 5.3 Thermodynamic parameters for 4-Nitrophenol adsorption onto activated carbon					
ΔH (KJ mol ⁻¹)	ΔS (KJ mol ⁻¹)	ΔG (KJ mol ⁻¹)			
		298K	308K	318K	328K
50.80	0.17	0.06	-1.63	-3.34	-5.04

5.3.6 Theoretical calculations

Density Functional calculations were used to understand the interactions taking place during the adsorption of 4-Nitrophenol onto activated carbon. Phenolic compounds may bind to the activated biocarbon surface in several ways and most of the interactions proceed either through the aromatic ring of phenol or the hydroxyl group[43]. In this study, an attempt has been made to understand the probable mechanism taking place during the adsorption of 4-Nitrophenol onto activated carbon *via* its hydroxyl group. Arm chair model was used to simulate pristine and functionalized activated biocarbon surface and five different ways of interaction of 4-Nitrophenol with these activated biocarbon surface have been studied. Such studies would broaden our understanding of the bonding and reactivity involved in the adsorption process. Besides, the interaction studies of 4-Nitrophenol with the different functional groups on the activated biocarbon surface would help in identifying the functional group that would have the most significant impact on 4-Nitrophenol adsorption, and this

would provide an idea for surface modification of activated biocarbon during its preparation process. The optimized structures for the 4-Nitrophenol adsorption on different activated biocarbon surfaces are given in Figure 5.8, while the adsorption energies and bond distance between the adsorbate and adsorbent are given in Table 5.4.

4-Nitrophenol adsorption on pristine activated biocarbon (AC).

The interaction of the hydroxyl group of 4-Nitrophenol (NP)OH with the pristine activated biocarbon was studied by considering a bond formation between the oxygen atom belonging to the hydroxyl group of 4-Nitrophenol and the carbon atom of activated biocarbon surface (AC)C. The bond formation is represented as (NP)HO----C(AC) and the optimized structure is given in Figure 5.8a. It is clear from Figure 5.8a that the OH group of 4-Nitrophenol molecule adsorbed dissociatively onto the arm chair model of activated biocarbon surface. The (NP)OH dissociates into (NP)O and H atom resulting in the formation of two types of interactions: (NP)O----C(AC) and H_{NP}---C(AC). Moreover, the adjoining C-C bond length of the activated biocarbon surface where (NP)O and H atom were attached increased upon adsorption. This indicates that the electron cloud shifts towards the adsorption sites-(NP)HO--C(AC) resulting in weakening of the adjoining C-C bonds of the activated biocarbon surface. The adsorption energy corresponds to -313.54 KJ mol⁻¹ indicating that the 4-Nitrophenol adsorption on the pristine activated biocarbon is favourable and chemisorptive in nature.

4-Nitrophenol adsorption on (AC)OH

The 4-Nitrophenol (NP)OH adsorption on the OH-functionalized activated biocarbon was studied by considering two types of interactions: (NP)HO----HO(AC) and (NP)OH----OH(AC). The optimised interaction structures of (NP)HO----HO(AC) and (NP)OH----OH(AC) are given in Figure 5.8(b) and 5.8(c) respectively and their corresponding bond lengths are given in Table 5.4. The adsorption energies of (NP)HO----HO(AC) and (NP)OH--OH(AC) interactions correspond to -31.56 KJ/mol and -37.97 KJ/mol respectively. The O_{NP}-H_{AC} bond length of (NP)HO----HO(AC) mode of interaction corresponded to 1.72 Å while H_{NP}-O_{AC} bond length of (NP)OH----OH(AC) corresponded to 1.70 Å. The higher negative value of adsorption energy and shorter bond length of (NP)OH----OH(AC) system indicates that (NP)OH----OH(AC) mode of interaction is more favourable than (NP)HO----HO(AC) type. Moreover, it can be deduced from the adsorption energy values of -31.56KJ/mol and -37.97 KJ/mol that the interaction of hydroxyl group of 4-Nitrophenol with the OH-functionalized carbon is physisorptive in nature.

4-Nitrophenol adsorption on (AC)CHO

The interaction of CHO-functionalized activated biocarbon with the hydroxyl group of 4-Nitrophenol (NP)OH resulted in the formation of (NP)OH---OHC(AC) complex. The interaction occurred between the hydroxyl hydrogen atom of 4-Nitrophenol and the oxygen atom of CHO-functionalized carbon surface (Figure 5.8d). Such type of interaction increased the O-H bond length of 4-Nitrophenol from 0.97 Å to 1.02 Å and C=O bond length of CHO-functionalized carbon from 1.24 Å to 1.26 Å. Thus, it could be observed that the O-H bond of 4-Nitrophenol and C=O bond of functionalized carbon became weaker upon adsorption and this may be due to the shifting of electron cloud more towards the adsorption site i.e. O_{AC}-H_{NP} bond of (NP)OH---OHC(AC) system. The distance between the hydroxyl hydrogen atom of 4-Nitrophenol and oxygen atom of functionalized carbon were found to be 1.65 Å while the adsorption energy corresponded to -43.08 KJ/mol. All these results indicate that the 4-Nitrophenol adsorption on CHO-functionalized carbon is favourable.

4-Nitrophenol adsorption on (AC)COOH

Adsorption of 4-Nitrophenol on COOH-functionalized activated biocarbon (AC)COOH proceeded through the formation of (NP)OH---HOOC(AC) complex. The optimized interaction structures are given in Figure 5.8 (e). The interaction occurred by forming two types of hydrogen bonds between 4-Nitrophenol and COOH-functionalized carbon: one of the hydrogen bonds exist between the Hydroxyl hydrogen atom of 4-nitrophenol (NP)OH and the oxygen atom of COOH group of functionalized carbon surface (H_{NP}-O_{AC}) while the other bond exists between the hydroxyl oxygen atom of 4-Nitrophenol and the hydrogen atom of COOH group of functionalized activated biocarbon surface (O_{NP}-H_{AC}). The bond distances of H_{NP}-O_{AC} and O_{NP}-H_{AC} were found to be 1.74 Å and 1.77 Å respectively while the adsorption energy corresponds to -45.18KJ/mol. Upon adsorption, the O-H bond length of both 4-Nitrophenol and (AC)COOH increased from 1.00 Å to 1.37 Å and from 0.98 Å to 1.00 Å, respectively. This indicates that the O-H bond becomes weaker as a result of the formation of H_{NP}-O_{AC} and O_{NP}-H_{AC} bond between 4-Nitrophenol and (AC)COOH. The interaction of 4-Nitrophenol with (AC)COOH was found to possess the highest adsorption energy as compared to (AC)CHO and (AC)OH system. Thus, the high negative energy and decrease in bond length upon adsorption indicates that the interaction of 4-Nitrophenol with COOH-functionalized activated biocarbon is favourable.

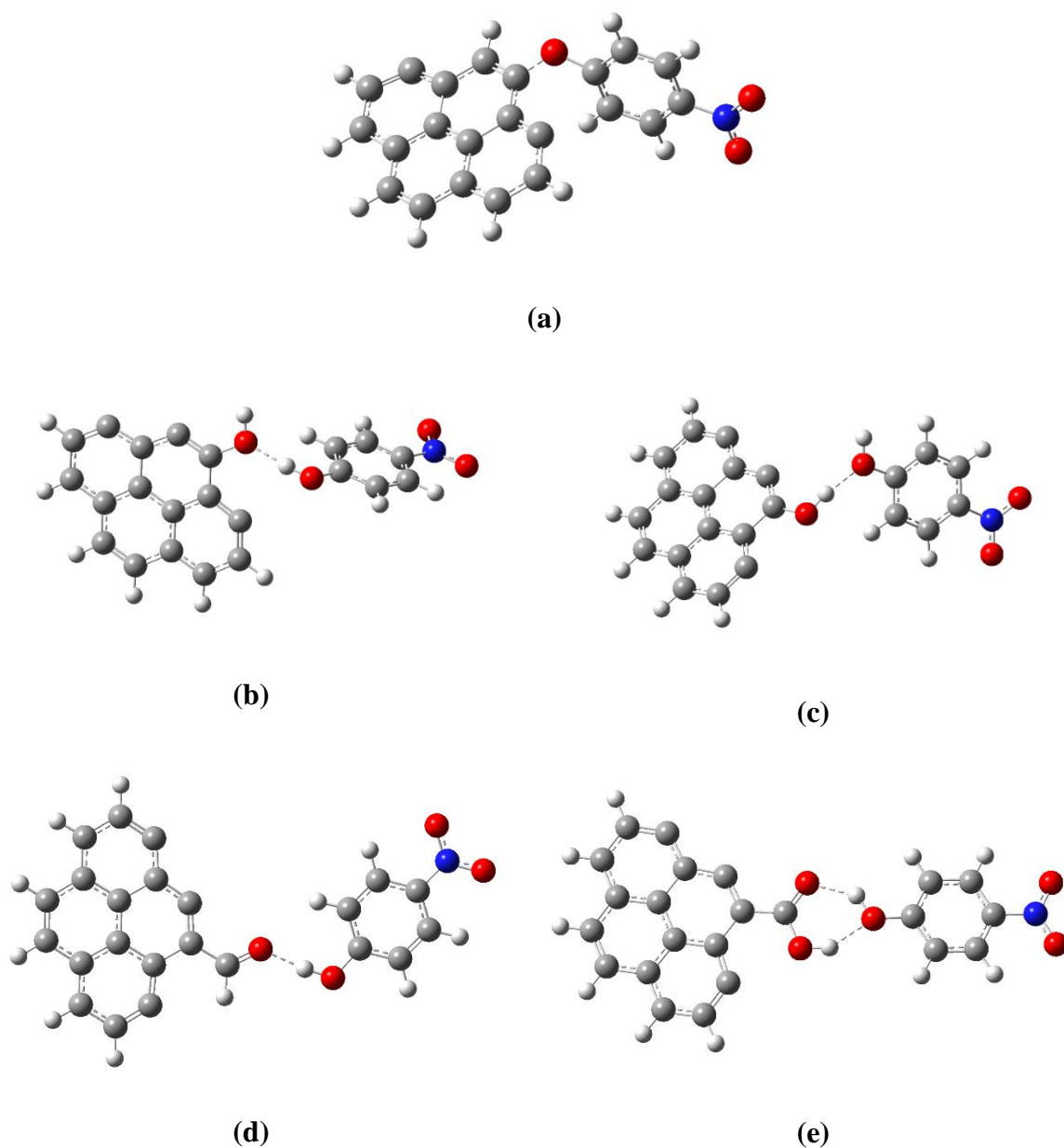


Figure 5.8 Optimized structures of 4-Nitrophenol adsorption onto activated biocarbon (a) (AC)C---OH(NP) (b) (AC)HO---HO(NP) (c) (AC)OH---OH(NP) (d) (AC)CHO---HO(NP) (e) (AC)COOH---OH(NP)

Table 5.4 Adsorption energies and bond distance between 4-Nitrophenol and activated biocarbon systems.			
System	Mode of interaction	Adsorption energy (KJ/mol)	Bond length(Å)
NP+ AC	(NP)HO----C(AC)	-313.54	1.40 (O _{NP} -C _{AC})
NP+ (AC)OH	(NP)HO----HO(AC)	-31.56	1.72 (O _{NP} -H _{AC})
	(NP)OH----OH(AC)	-37.97	1.70 (H _{NP} -O _{AC})
NP+ (AC)CHO	(NP)OH----OHC (AC)	-43.08	1.65 (H _{NP} -O _{AC})
NP+ (AC)COOH	(NP)OH----HOOC(AC)	-45.18	1.74 (H _{NP} -O _{AC})
			1.77 (O _{NP} -H _{AC})

A comparative study of the effect of functional groups on 4-Nitrophenol adsorption was analysed by considering their relative adsorption energies. The relative energy diagram of the optimized configurations of 4-Nitrophenol adsorption onto functionalized activated biocarbon system is presented as Figure 5.9. Among the various functional groups considered for this study, the interaction of 4-Nitrophenol with (AC)COOH was found to possess the highest adsorption energy as compared to (AC)CHO and (AC)OH systems. Hence, it can be assumed that the introduction of the carboxylic functional group into the activated biocarbon system would enhance the interaction of 4-Nitrophenol with the carbon surface more as compared to carbonyl and hydroxyl functional groups. The relative stability and energy of various configurations follow the order:

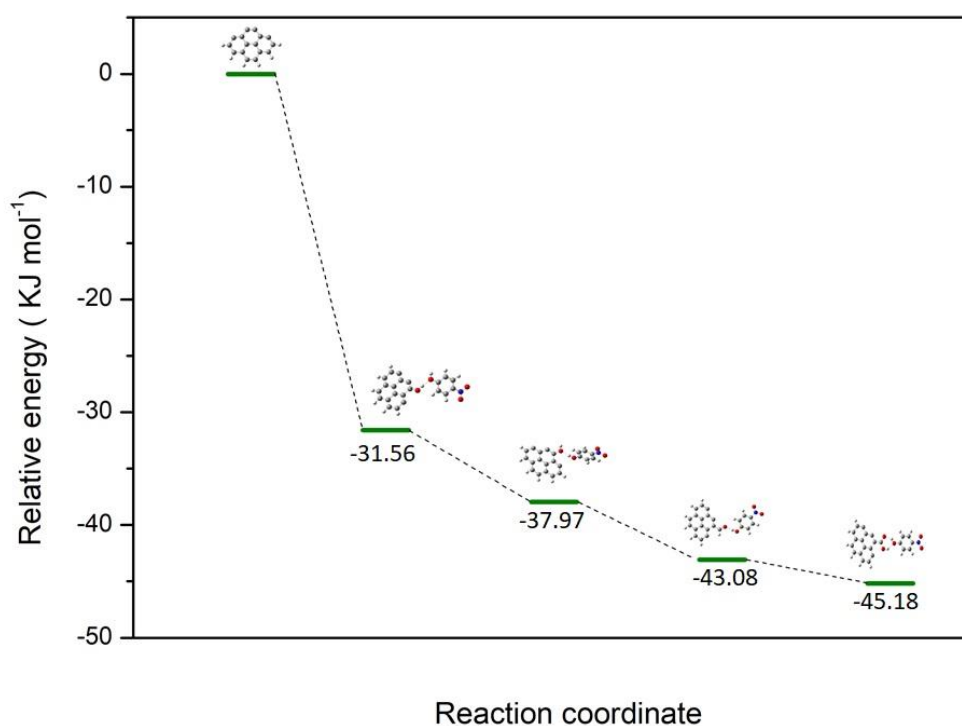


Fig.5.9 Relative energy diagram of 4-Nitrophenol adsorption onto functionalized activated biocarbon

5.3.7 Comparative study of Ravenna grass activated carbon with other adsorbents

A comparative study of activated carbon with other adsorbent materials reported in literature was done to understand the relative efficiency of the obtained biocarbon for 4-Nitrophenol removal and is shown in Table 5.5. The surface area and maximum adsorption capacity of adsorbent materials were considered for comparison. From Table 5.5 it can be seen that the

activated carbon has a comparatively high surface area of $919 \text{ m}^2 \text{ g}^{-1}$ and an adsorption capacity of 50.85 mg g^{-1} respectively as compared to other adsorbents. This shows that the activated biocarbon obtained through his study could be used as an efficient adsorbent for 4-Nitrophenol removal from water.

Table 5.5 Comparison of RAC with some other adsorbent materials for 4-Nitrophenol removal

Adsorbent	Adsorbent characteristics		Adsorption capacity for 4-Nitrophenol removal q_{\max} (mg g^{-1})	Source
	Surface Area ($\text{m}^2 \text{ g}^{-1}$)	Pore Volume ($\text{m}^3 \text{ g}^{-1}$)		
RAC	919	0.324	50.89	Present Study
Acacia glauca sawdust activated carbon	311.20	-	25.93	[33]
Mauritanian clay/alginate composite beads (Na-ZS26/SA)	-	-	27.1	[59]
Olive cake based activated carbon	672	-	1.550	[60]
Nano zirconium silicate coated manganese dioxide nanoparticles	-	-	2.619	[61]
Microporous activated carbon	780.06	0.468 (micro) 0.105 (meso)	184.86	[62]
Zeolite	-	-	1.02	[63]
Nanographite oxide	421.7	0.99	268.5	[64]
Eucalyptus seed derived carbon	150	0.595	0.126	[65]
15% acid treated activated carbon	80	0.020	0.194	
30% acid treated activated carbon	780	1.159	1.331	
15% base treated activated carbon	670	0.449	2.568	
30% base treated activated carbon				
Pyrolyzed oil shale	-	-	4.895	[66]
CO ₂ -oil shale	-	-	8.889	[66]
ZnCl ₂ -oil shale	-	-	0.026	[66]
KOH- oil shale	-	-	0.895	[66]
Metal-organic framework/reduced graphene oxide composite	0.66	-	327	[67]

5.3.8 Cost analysis

The total approximate cost involved in the production of 250 gram of the activated carbon was calculated, which included the price of KOH, electricity, water, HCl and raw precursor. The resulting production cost was subsequently compared with that of commercially available carbon to draw a comparison concerning economic feasibility. Table 5.6 presents the cost of the activated carbon, while Figure 5.10 represents the relative cost of different carbons in terms of Rupees (₹). In the present study, around 1.4 kg of raw material was used for the production of 0.250 Kg of activated biocarbon. The cost involved in the production of 250 g activated carbon was found to be ₹ 538 without considering the cost involved in initial investment, labour income, working capital, manufacturer's profits, recovery and reuse of KOH etc. This production cost is expected to reduce in scaling up from laboratory experiments to industrial scale. A comparative study of the production cost indicates that Ravenna grass activated biocarbon could be one of the most economical ones among all other commercially available carbons considered for this study.

Table 5.6 Cost estimates for production of 250g activated carbon		
Materials	Consumption (approx.)	Cost (approx.)
KOH	500g	₹480
HCL	200 ml of 0.1M HCL	₹1 (₹265/500ml)
Raw precursor	1.4 kg	₹ 0
Electricity	14 kWh	₹ 42
Water	50 L	₹ 15
Total Cost/250g (in Rupees)	-	₹ 538

*1 dollar (\$) = Approx.72.00 Rupees (₹)

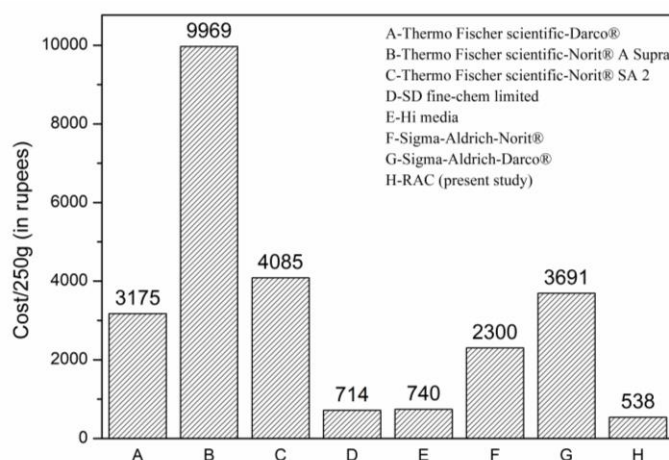


Figure 5.10 Comparative cost of Ravenna grass activated biocarbon with some commercially available activated carbon

5.4 Conclusion

Ravenna grass biomass served as a potent precursor for the preparation of activated biocarbon. The textural properties of activated carbon were found to vary with increasing KOH concentration. The highest surface area ($919 \text{ m}^2/\text{g}$) and pore volume ($0.324 \text{ cm}^3/\text{g}$) was obtained for the activated carbon prepared at 700°C using 2M KOH concentration. XRD analysis revealed the micro crystallite structure of the activated carbon while SEM image indicated the presence of numerous pores, cracks and cavities on the activated carbon surface. The Ravenna grass activated biocarbon could serve as a good adsorbent for the removal of 4-Nitrophenol from an aqueous solution. At best conditions *viz.*, adsorbent dose-0.5g, pH-7, contact time- 40minutes and initial 4-Nitrophenol concentration – 400 mg L^{-1} , the activated biocarbon exhibited a maximum removal percentage of 99.9%. The adsorption capacity was greatly influenced by the pH_{zpc} of the activated biocarbon and the pH of the working solution. The removal percentage decreased sharply when the pH value was raised from 7 to 12. Langmuir model best explained the equilibrium isotherm with q_m of 50.89 mg g^{-1} while pseudo-second-order model well described the kinetics data. The thermodynamics study indicated the temperature dependence, spontaneity and endothermic nature of the adsorption process. Density Functional Theory calculations also revealed the favourable adsorption of 4-Nitrophenol onto pristine and functionalized activated biocarbon. Among the different functional groups used to functionalize the activated biocarbon (-OH, -CHO, -COOH), the -COOH group interacted most strongly with 4-Nitrophenol. These results indicated that functionalization of activated biocarbon with COOH group would increase its interaction with 4-Nitrophenol, which would help enhance its the adsorption properties.

References

- [1] N.G. Rincón-Silva, J.C. Moreno-Piraján, L. Giraldo, Equilibrium, kinetics and thermodynamics study of phenols adsorption onto activated carbon obtained from lignocellulosic material (*Eucalyptus Globulus* labill seed), *Adsorption*. 22 (2016) 33–48. doi:10.1007/s10450-015-9724-2.
- [2] I. Ipek, N. Kabay, M. Yüksel, Journal of Water Process Engineering Separation of bisphenol A and phenol from water by polymer adsorbents : Equilibrium and kinetics studies, *J. Water Process Eng.* 16 (2017) 206–211. doi:10.1016/j.jwpe.2017.01.006.
- [3] R.R. Karri, J.N. Sahu, N.S. Jayakumar, Optimal isotherm parameters for phenol adsorption from aqueous solutions onto coconut shell based activated carbon: Error analysis of linear and non-linear methods, *J. Taiwan Inst. Chem. Eng.* 80 (2017) 472–487. doi:10.1016/j.jtice.2017.08.004.
- [4] E. Z-Flores, M. Abatal, A. Bassam, L. Trujillo, P. Juárez-Smith, Y. El Hamzaoui, Modeling the adsorption of phenols and nitrophenols by activated carbon using genetic programming, *J. Clean. Prod.* 161 (2017) 860–870. doi:10.1016/j.jclepro.2017.05.192.
- [5] A. Sukan, S. Sargin, Enzymatic Removal of Phenol from Industrial Wastewaters, *J. Biomater. Nanobiotechnol.* 04 (2013) 300–307. doi:10.4236/jbnb.2013.43038.
- [6] L.G.C. Villegas, N. Mashhadi, M. Chen, D. Mukherjee, K.E. Taylor, N. Biswas, A Short Review of Techniques for Phenol Removal from Wastewater, *Curr. Pollut. Reports*. 2 (2016) 157–167. doi:10.1007/s40726-016-0035-3.
- [7] E. Yagmur, S. Turkoglu, A. Banford, Z. Aktas, The relative performance of microwave regenerated activated carbons on the removal of phenolic pollutants, *J. Clean. Prod.* 149 (2017) 1109–1117. doi:10.1016/j.jclepro.2017.02.188.
- [8] S.K. Nadavala, H. Che Man, H. Woo, Biosorption of Phenolic Compounds from Aqueous Solutions using Pine (*Pinus densiflora* Sieb) Bark Powder, *BioResources*. 9 (2014) 5155–5174. doi:10.15376/biores.9.3.5155-5174.
- [9] A.Q. Jaradat, S. Gharaibeh, M. Abu Irjei, The application of solar distillation technique as a mean for olive mill wastewater management, *Water Environ. J.* 32 (2018) 134–140. doi:10.1111/wej.12308.
- [10] Y. Jiang, G. Ni, G. Zhao, Y. Meng, J. Li, X. Wang, Steam Plasma Jet Treatment of Phenol in Aqueous Solution at Atmospheric Pressure, *Plasma Process. Polym.* 10 (2013) 353–363. doi:10.1002/ppap.201200155.
- [11] F. Khazaali, A. Kargari, M. Rokhsaran, Application of low-pressure reverse osmosis for effective recovery of bisphenol A from aqueous wastes, *Desalin. Water Treat.* 52 (2013) 7543–7551. doi:10.1080/19443994.2013.831795.
- [12] Y. Wu, G. Tian, H. Tan, X. Fu, Desalination and Water Treatment Pervaporation of phenol wastewater with PVDF – PU blend membrane, *Desalin. Water Treat.* 51 (2013) 37–41. doi:10.1080/19443994.2013.768789.
- [13] N. Rabaaoui, M.E.K. Saad, Y. Moussaoui, M.S. Allagui, A. Bedoui, E. Elaloui, Anodic oxidation of o-nitrophenol on BDD electrode: Variable effects and mechanisms of degradation, *J. Hazard. Mater.* 250–251 (2013) 447–453. doi:10.1016/j.jhazmat.2013.02.027.
- [14] M. Tian, S.S. Thind, J.S. Dondapati, X. Li, A. Chen, Electrochemical oxidation of 4-chlorophenol for wastewater treatment using highly active UV treated TiO₂nanotubes,

- Chemosphere. 209 (2018) 182–190. doi:10.1016/j.chemosphere.2018.06.042.
- [15] V. Peings, J. Frayret, T. Pigot, Mechanism for the oxidation of phenol by sulfatoferrate (VI): Comparison with various oxidants, *J. Environ. Manage.* 157 (2015) 287–296. doi:10.1016/j.jenvman.2015.04.004.
- [16] Y. Song, J. Jiang, J. Ma, S.Y. Pang, Y.Z. Liu, Y. Yang, C.W. Luo, J.Q. Zhang, J. Gu, W. Qin, ABTS as an Electron Shuttle to Enhance the Oxidation Kinetics of Substituted Phenols by Aqueous Permanganate, *Environ. Sci. Technol.* 49 (2015) 11764–11771. doi:10.1021/acs.est.5b03358.
- [17] Y. Tu, Y. Xiong, S. Tian, L. Kong, C. Descorme, Catalytic wet air oxidation of 2-chlorophenol over sewage sludge-derived carbon-based catalysts, *J. Hazard. Mater.* 276 (2014) 88–96. doi:10.1016/j.jhazmat.2014.05.024.
- [18] M. Kuosa, J. Kallas, A. Häkkinen, Ozonation of p-nitrophenol at different pH values of water and the influence of radicals at acidic conditions, *J. Environ. Chem. Eng.* 3 (2015) 325–332. doi:10.1016/j.jece.2014.10.015.
- [19] M. Madani, M. Aliabadi, B. Nasernejad, R.K. Abdulrahman, M.Y. Kilic, K. Kestioglu, Treatment of olive mill wastewater using physico-chemical and Fenton processes, *Desalin. Water Treat.* 54 (2015) iv. doi:10.1080/19443994.2013.877225.
- [20] K. Akin, I. Arslan-Alaton, O.H. Tugba, M. Bekbolet, Degradation and detoxification of industrially important phenol derivatives in water by direct UV-C photolysis and H₂O₂/UV-C process: A comparative study, *Chem. Eng. J.* 224 (2013) 4–9. doi:10.1016/j.cej.2012.11.049.
- [21] G. Moussavi, S. Ghodrati, A. Mohseni-Bandpei, The biodegradation and COD removal of 2-chlorophenol in a granular anoxic baffled reactor, *J. Biotechnol.* 184 (2014) 111–117. doi:10.1016/j.jbiotec.2014.05.010.
- [22] H. Jalayeri, F. Doulati Ardejani, R. Marandi, S. Rafiee pur, Biodegradation of phenol from a synthetic aqueous system using acclimatized activated sludge, *Arab. J. Geosci.* 6 (2013) 3847–3852. doi:10.1007/s12517-012-0643-1.
- [23] D.Y. Xu, Z. Yang, Cross-linked tyrosinase aggregates for elimination of phenolic compounds from wastewater, *Chemosphere.* 92 (2013) 391–398. doi:10.1016/j.chemosphere.2012.12.076.
- [24] J.A. Torres, P.M.B. Chagas, M.C. Silva, C.D. Dos Santos, A.D. Corrêa, Evaluation of the protective effect of chemical additives in the oxidation of phenolic compounds catalysed by peroxidase, *Environ. Technol. (United Kingdom).* 37 (2016) 1288–1295. doi:10.1080/09593330.2015.1112433.
- [25] B.M. Babic, S.K. Milonjic, M.J. Polovina, B. V. Kaludierovic, Point of zero charge and intrinsic equilibrium constants of activated carbon cloth, *Carbon N. Y.* 37 (1999) 477–481. doi:10.1016/S0008-6223(98)00216-4.
- [26] M.J. Frisch, G.W. Trucks, H.B. Schlegel, G.E. Scuseria, M.A. Robb, J.R. Cheeseman, G. Scalmani, V. Barone, B. Mennucci, G.A. Petersson, H. Nakatsuji, M. Caricato, X. Li, H.P. Hratchian, A.F. Izmaylov, J. Bloino, G. Zheng, J.L. Sonnenberg, M. Hada, M. Ehara, K. Toyota, R. Fukuda, J. Hasegawa, M. Ishida, T. Nakajima, Y. Honda, O. Kitao, H. Nakai, T. Vreven, J.A. Montgomery Jr., J.E. Peralta, F. Ogliaro, M. Bearpark, J.J. Heyd, E. Brothers, K.N. Kudin, V.N. Staroverov, R. Kobayashi, J. Normand, K. Raghavachari, A. Rendell, J.C. Burant, S.S. Iyengar, J. Tomasi, M. Cossi, N. Rega, J.M. Millam, M. Klene, J.E. Knox, J.B. Cross, V. Bakken, C. Adamo, J.

- Jaramillo, R. Gomperts, R.E. Stratmann, O. Yazyev, A.J. Austin, R. Cammi, C. Pomelli, J.W. Ochterski, R.L. Martin, K. Morokuma, V.G. Zakrzewski, G.A. Voth, P. Salvador, J.J. Dannenberg, S. Dapprich, A.D. Daniels, Ö. Farkas, J.B. Foresman, J. V. Ortiz, J. Cioslowski, D.J. Fox, Gaussian 09, Rev. A.02, Gaussian Inc., Wallingford CT. (2009) Wallingford CT. doi:10.1159/000348293.
- [27] F. Shen, J. Liu, Z. Zhang, Y. Dong, C. Gu, Density functional study of hydrogen sulfide adsorption mechanism on activated carbon, *Fuel Process. Technol.* 171 (2018) 258–264. doi:10.1016/j.fuproc.2017.11.026.
- [28] X. Li, Q. Xu, Y. Fu, Q. Guo, Preparation and Characterization of Activated Carbon from Kraft Lignin via KOH Activation, 00 (2013) 1–8. doi:10.1002/ep.
- [29] M.L. Martínez, M.M. Torres, C.A. Guzmán, D.M. Maestri, Preparation and characteristics of activated carbon from olive stones and walnut shells, *Ind. Crops Prod.* 23 (2006) 23–28. doi:10.1016/j.indcrop.2005.03.001.
- [30] I.I. Gurten, M. Ozmak, E. Yagmur, Z. Aktas, Preparation and characterisation of activated carbon from waste tea using K₂CO₃, *Biomass and Bioenergy.* 37 (2012) 73–81. doi:10.1016/j.biombioe.2011.12.030.
- [31] J. Matos, C. Nahas, L. Rojas, M. Rosales, Synthesis and characterization of activated carbon from sawdust of Algarroba wood. 1. Physical activation and pyrolysis, *J. Hazard. Mater.* 196 (2011) 360–369. doi:10.1016/j.jhazmat.2011.09.046.
- [32] D. Angin, Production and characterization of activated carbon from sour cherry stones by zinc chloride, *Fuel.* 115 (2014) 804–811. doi:10.1016/j.fuel.2013.04.060.
- [33] S. Li, K. Han, J. Li, M. Li, C. Lu, Preparation and characterization of super activated carbon produced from gulfweed by KOH activation, *Microporous Mesoporous Mater.* 243 (2017) 291–300. doi:10.1016/j.micromeso.2017.02.052.
- [34] B.H. Diya'uddeen, I.A. Mohammed, A. Ahmed, B.Y. Jibril, Production of Activated Carbon from Corncobs and its Utilization in Crude Oil Spillage Clean Up, *Agric. Eng. Int.* 10 (2008) 1–9.
- [35] J. Bartram, R. Ballance, *Water quality monitoring: a practical guide to the design and implementation of freshwater quality studies and monitoring programmes*, 1st editio, E & FN Spon, 1996. doi:10.5711/morj.2.4.toc.
- [36] H. Soni, P. Padmaja, Palm shell based activated carbon for removal of bisphenol A: An equilibrium, kinetic and thermodynamic study, *J. Porous Mater.* 21 (2014) 275–284. doi:10.1007/s10934-013-9772-5.
- [37] H. Moazed, S.B. Nasab, Effect of reed and hydraulic retention time on the lead removal in horizontal subsurface flow of constructed wetland, *J. Mol. Liq.* 211 (2015) 448–456. doi:10.1016/j.molliq.2015.07.044.
- [38] D. Balarak, Kinetics, isotherm and thermodynamics studies on bisphenol a adsorption using barley husk, *Int. J. ChemTech Res.* 9 (2016) 681–690.
- [39] S.N. Muluh, J.N. Ghogomu, A.A.B. Alongamo, D.L. Ajifack, Adsorption of Phenol from Aqueous Solution by Avocado Seed Activated Carbon: Equilibrium, Kinetic, and Full Factorial Design Analysis, *Int. J. Adv. Eng. Res. Technol.* 5 (2017) 610–620.
- [40] M. Shirzad-Siboni, S.-J. Jafari, M. Farrokhi, J.K. Yang, Removal of Phenol from Aqueous Solutions by Activated Red Mud: Equilibrium and Kinetics Studies, *Environ. Eng. Res.* 18 (2013) 247–252. doi:10.4491/eer.2013.18.4.247.

- [41] D. Kavitha, Adsorptive removal of phenol by thermally modified activated carbon: Equilibrium, kinetics and thermodynamics, *J. Environ. Biotechnol. Res.* 3 (2016) 24–34.
- [42] P. Sudhakar, I.D. Mall, V.C. Srivastava, Adsorptive removal of bisphenol-A by rice husk ash and granular activated carbon—A comparative study, *Desalin. Water Treat.* 57 (2016) 12375–12384. doi:10.1080/19443994.2015.1050700.
- [43] L.M. Cam, L. Van Khu, N.N. Ha, Theoretical study on the adsorption of phenol on activated carbon using density functional theory, *J. Mol. Model.* 19 (2013) 4395–4402. doi:10.1007/s00894-013-1950-5.
- [44] P.T. Dhorabe, D.H. Lataye, R.S. Ingole, Removal of 4-nitrophenol from aqueous solution by adsorption onto activated carbon prepared from *Acacia glauca* sawdust, *Water Sci. Technol.* 73 (2016) 955–966. doi:10.2166/wst.2015.575.
- [45] A. Ely, M. Baudu, M. Ould, S. Ahmed, O. Kankou, J. Basly, Copper and nitrophenol removal by low cost alginate / Mauritanian clay composite beads, *Chem. Eng. J.* 178 (2011) 168–174. doi:10.1016/j.cej.2011.10.040.
- [46] E.S.A. Rawash, Equilibrium and kinetic study for the adsorption of p-nitrophenol from wastewater using olive cake based activated carbon, *Glob. J. Environ. Sci. Manag.* 2 (2016) 11–18. doi:10.7508/gjesm.2016.01.002.
- [47] M.E. Mahmoud, G.M. Nabil, Nano zirconium silicate coated manganese dioxide nanoparticles: Microwave-assisted synthesis, process optimization, adsorption isotherm, kinetic study and thermodynamic parameters for removal of 4-nitrophenol, *J. Mol. Liq.* 240 (2017) 280–290. doi:10.1016/j.molliq.2017.05.075.
- [48] M.J. Ahmed, S.K. Theydan, Adsorptive removal of p-nitrophenol on microporous activated carbon by FeCl_3 activation: equilibrium and kinetics studies, *Desalin. Water Treat.* 55 (2015) 522–531. doi:10.1080/19443994.2014.920731.
- [49] T. Sismanoglu, S. Pura, Adsorption of aqueous nitrophenols on clinoptilolite, *Colloids Surfaces A Physicochem. Eng. Asp.* 180 (2001) 1–6.
- [50] B. Zhang, F. Li, T. Wu, D. Sun, Y. Li, Colloids and Surfaces A : Physicochemical and Engineering Aspects Adsorption of p-nitrophenol from aqueous solutions using nanographite oxide, *Colloids Surfaces A Physicochem. Eng. Asp.* 464 (2015) 78–88. doi:10.1016/j.colsurfa.2014.10.020.
- [51] N.G. Rincón-Silva, J.C. Moreno-Piraján, L.G. Giraldo, Thermodynamic study of adsorption of phenol, 4-chlorophenol, and 4-nitrophenol on activated carbon obtained from eucalyptus seed, *J. Chem.* 2015 (2014) 1–12. doi:10.1155/2015/569403.
- [52] S. Al-Asheh, B. Fawzi, M. Asmahan, Kinetics and Equilibrium Sorption Studies of 4-Nitrophenol on pyrolyzed and activated oil shale residue, *Environ. Geol.* 45 (2004) 1109–1117. doi:10.1007/s00254-004-0969-4.
- [53] Z. Wu, X. Yuan, H. Zhong, H. Wang, G. Zeng, Enhanced adsorptive removal of p-nitrophenol from water by aluminum metal – organic framework / reduced graphene oxide composite, *Nat. Publ. Gr.* 6 (2016) 25638. doi:10.1038/srep25638.

CHAPTER 6

REMOVAL OF *Escherichia coli* USING RAVENNA GRASS ACTIVATED CARBON MODIFIED BY CTMATB

This chapter discusses the preparation of brominated activated carbon using cetyltrimethylammonium tribromide (CTMATB) through a simple and efficient route. The prepared brominated carbon was characterized using various analytical techniques and further tested for its efficiency as antibacterial agent. The antibacterial activity of the brominated activated carbon was evaluated against Gram-negative bacteria- Escherichia coli with the view of water purification. The efficiency of the brominated activated carbon in the removal of Escherichia coli from aqueous solution was investigated. Density functional theory studies were performed to understand the bromination mechanism. Further, molecular docking studies were also conducted to study the possible antibacterial mechanism of the brominated activated carbon.

6.1 Introduction

Carbon materials, known for their complex structures and multiple functionalities are classified into different types such as activated carbon, carbon fibres, carbon nano fibres and nanotubes, graphene, graphene oxide, fullerenes and biochar[1]. These materials have generated great interest due to their applications in diverse fields and one of the most promising carbon materials is activated carbon with wide-scale utility ranging from water treatment, catalysis, gas storage, biomedical, cosmetics and energy storage[2–10]. The versatility of activated carbon stems from its porous nature, large surface area and abundant chemical functionalities. Over the years, modification of activated carbon surface for enhancing its surface characteristics has become an important area of study and synthesis of activated carbons with surface properties specific to a particular pollutant has been specially interesting[11–14]. In fact, the number of reports available attest the application of surface-modified activated carbon as an adsorbent in various wastewater treatment methods with improved efficiency[15–18]. Therefore, modification of activated carbon surface has become a prospective technique for improving performance and rendering desired properties according to the target pollutant.

Activated carbon shows high adsorption capacity for microbial pathogens such as *E.coli* and coliform bacteria[19–22], wherein the bacteria preferably get adsorbed on the activated carbon. Though this method has become a popular water purification technique, however a major disadvantage is that, with continuous use, the activated carbon tends to become a breeding ground for the adhered bacteria, thereby rendering the activated carbon into a pollutant source instead[23]. Therefore, in order to fully exploit the high efficiency of activated carbon towards microbes removal from water, it becomes necessary to design activated carbons with synergistic properties of adsorption and antibacterial activity. Literature reports indicate that efforts have been made towards modification of the activated carbon surface, for example through the impregnation of silver and metal oxides on activated carbon for imparting antibacterial activity[23–25]. Although silver and metal oxides impregnated activated carbon are known to show attractive antibacterial activity, their limitations lie in the shorter durability of these materials on continuous usage as the metals tend to leach out since they are just weakly deposited on the activated carbon surface. Therefore, a better alternative for providing long-term effectiveness is required.

Brominated compounds are known to have good antibacterial activity and numerous studies have been reported on their efficiency against a wide range of bacteria[26–30]. On the other hand, though brominated activated carbon has been used for a wide range of applications

including mercury capture[31] and electrochemical energy storage[32], however, no works have been reported on the potency of brominated activated carbon against microbial pathogens. Nevertheless, it would be advantageous if antibacterial activity could be conferred on activated carbon surface through bromination of the activated carbon surface.

Review of the literature on brominated carbon materials reveals that in most cases the synthesis involved the utilization of bromine (Br_2) as the brominating agent[32–37]. While bromine is an effective reagent, however, the limitations of using Br_2 lies in the safety risk involved in the handling of bromine due to its toxicity. Therefore, a greener, mild and versatile brominating agent would provide a better alternative over the molecular bromine[38].

Therefore, in this present work, an attempt was made to synthesize brominated activated carbon using cetyltrimethylammonium tribromide (CTMATB) as a green and cost-effective brominating agent. The surface morphology and characteristics were analysed using FESEM-EDX, FTIR and XRD. The surface chemical composition and the bonding nature of the brominated carbon were studied using XPS. Since almost no work has been reported on the bromination mechanism of activated carbon by tribromides, it was considered pertinent to understand the possible mechanism involved and therefore density functional theory calculations were incorporated to explain the probable mechanism for bromination of activated carbon by CTMATB. Thereafter, the antibacterial activity of the brominated activated carbon against gram-negative bacteria *E.coli* was assessed and the possible antibacterial mechanism of the brominated activated carbon was also proposed based on theoretical molecular docking studies. The removal studies of *E.coli* from aqueous using the brominated activated carbon was also conducted.

6.2 Materials and method

6.2.1 Preparation of activated Carbon

Ravenna grass biomass was used as the starting material for the preparation of the activated carbon. The raw material was collected, washed, dried and carbonized at 500°C for 30 minutes. The obtained carbonized char was ground using a planetary ball mill and thereafter activated using potassium hydroxide at 800°C for 1 hour in a muffle furnace. The obtained sample was washed with hot double distilled water and then with cold double distilled water until the pH of the residual solution tested neutral. The obtained activated carbon was then dried in an oven at 110°C , labelled as AC and stored in a desiccator for further use.

6.2.2 Preparation of brominated activated carbon

The bromination of activated carbon was done using a quaternary ammonium salt, *viz.*, cetyltrimethylammonium tribromide (CTMATB) using one of our earlier reported methods[38]. For the bromination of AC surface, 1g of CTMATB was dissolved in 50 mL acetonitrile solution and was slowly added to 1g of the prepared activated carbon dispersed in aqueous solution. The mixture was stirred for 3 hours under reflux and the solid formed thereafter was separated using glass Buchner funnel and washed with deionised water multiple times. The full removal of free bromide ions from the activating carbon surface was confirmed by adding few drops AgNO_3 to the filtrate. The formation of a very pale cream precipitate suggested the presence of bromide ion. The obtained solid was dried under vacuum and stored in an airtight container for further use. The resulting solid product was labelled as brominated activated carbon (Br-AC).

6.2.3. Characterisation of Br-AC

The surface morphology and elemental composition of the newly synthesized adsorbents (AC and Br-AC) were recorded using a Field Emission Scanning Electron Microscopy (FESEM, Model: ZEISS SIGMA MAKE: Carl ZEISS Microscopy, Germany). Pore volume and surface area were determined using Brunauer-Emmett-Teller (BET) surface area analyser (Smart instrument, SS93/02). Powder XRD patterns were obtained from a Powder X-Ray Diffractometer (Make: Rigaku, Japan Model: ULTIMA IV) using $\text{Cu K}\alpha$ radiation ($\lambda = 1.5406 \text{ \AA}$). The functional groups of AC and Br-AC were identified using Fourier Transform Infrared (FT-IR) spectrometer (Spectrum Two, Made: Perkin Elmer) in the range of $4000\text{--}400 \text{ cm}^{-1}$ using KBr pellet. X-ray photoelectron spectroscopy (XPS) (Make: Thermo Fisher Scientific Pvt. Ltd., UK Model: ESCALAB Xi+) was used to confirm the binding of bromine onto carbon surface.

6.2.4 Density functional theory calculations

Density functional theory (DFT) was used to gain insight into the possible bromination of activated carbon surface by CTMATB[39]. Gaussian 09W program package was used for the structure optimization and energy calculations at the B3LYP hybrid functional/6-31g level of theory in a dielectric medium of $\epsilon = 80$ (corresponding to water). Gauss View 05 was used to construct the structures and were optimized in their electronic ground state. The interaction energy (E_I) of the CTMATB/ dissociated bromine and activated carbon was calculated using the following equation

$$E_I = E_A - (E_A + E_B)$$

where, E_I is the total energy of CTMATB/dissociated Bromine and activated carbon in an equilibrium state; E_A is the total energy of the CTMATB/dissociated bromine; E_B is the total energy of the activated carbon. Generally, the higher negative value of interaction energy indicates more stability and stronger interaction. Generally, the interaction energy of less than -30kJ/mol suggests physisorption whereas interaction energy of greater than -50kJ/mol indicate chemisorption [40].

The theoretical understanding of the interaction of activated carbon with any compound requires the development of a correct model for the activated carbon. Solid-state ^{13}C nuclear magnetic resonance experiments revealed that the activated carbon surface consists of three to seven fused benzene rings[41]. Therefore, armchair model consisting of four fused benzene ring cluster (C_{16}H_6) was used to simulate the activated carbon surface. The armchair models were unsaturated on the upper edge side to generate an active site while the lower side of the model was terminated with H atoms. The active site was also embedded with oxygen-containing functional groups such as OH, COOH and CHO groups to study their effect on the extent of bromination. The optimized arm-chair models of activated carbon used for this study are given in Figure 6.1. The models were named unsaturated armchair (AC-U), -OH armchair (AC-OH), -COOH armchair (AC-COOH) and -CHO armchair (AC-CHO).

6.2.5. Determination of antibacterial activity

The antibacterial activity of the Br-AC was determined using *E.coli* as the test bacteria. Since *E.coli* is used as the indicator organism for faecal contamination of water, the efficiency of Br-AC to kill *E.coli* would also indicate its ability to kill other water-borne pathogens. Initially, the qualitative determination of antibacterial activity was done by well-diffusion method. Further, the effect of pH, time and concentration on the antibacterial activity was studied. The detailed experimental procedures are discussed below:

Bacterial cell cultures

The antibacterial activity of Br-AC was tested against gram-negative bacteria *Escherichia coli* (MTCC 40). The cultures were maintained on nutrient agar slants at 4°C and sub-cultured after every 30 days.

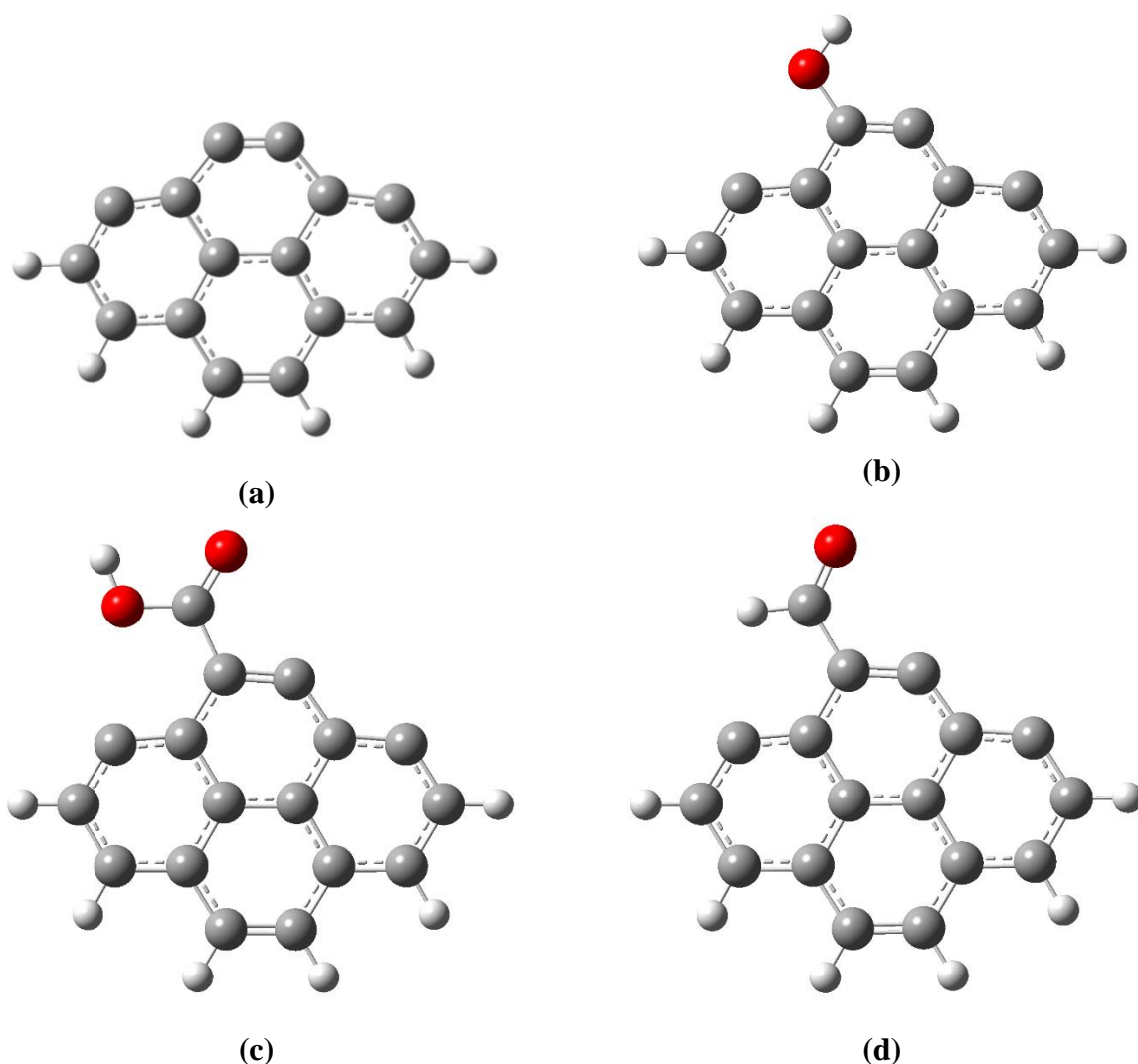


Figure 6.1 Optimized structures of (a) AC-U (b) AC-OH (c) AC-COOH (d) AC-CHO

Well diffusion method

The qualitative determination of the antibacterial activity of Br-AC was done by well diffusion method. A single pure colony of *E.coli* was inoculated in nutrient broth and grown overnight at 37°C. An aliquot of 200 μ l of freshly grown broth culture of the bacterium (10^7 – 10^8 cells as per McFarland standard) was seeded on nutrient agar plate and spread over the medium uniformly using a sterile glass spreader. Wells were made in the seeded agar with the help of a sterilized cork borer and Br-AC was added into the marked wells. The test was carried out at 10 mg/mL Br-AC concentration using Dimethyl sulfoxide (DMSO) as the solvent. The plates were incubated at 37°C for 24 hours and the antibacterial action of Br-AC was determined by measuring the diameter of the inhibition zone. The experiment was performed in triplicate to confirm reproducibility.

Concentration-dependent antibacterial activity

Minimum inhibitory concentration (MIC) and Minimum bactericidal concentration (MBC) test were conducted to study the concentration-dependent antibacterial activity of Br-AC. MIC is the lowest concentration of the test sample which prevents the growth of bacteria, and MBC is the lowest concentration at which the antimicrobial agent can kill the bacteria[23]. *E.coli* was grown in 250 ml of nutrient broth overnight at 37°C. The freshly grown culture broth was further centrifuged at 3000 rpm for 15 minutes, the bacterial cells obtained were washed with sterile phosphate-buffered solution (PBS) and resuspended in PBS to produce a cell count of approximately 10^8 CFU/mL. MIC was determined by taking 0.3g/mL initial Br-AC concentration in 2mL of sterile nutrient broth, the solution was serially diluted two-fold and ended at a concentration of 0.002g/mL. Each tube was inoculated with 200 μ L of $\sim 10^8$ CFU/mL of *E.coli* cells and incubated at 37°C for 24 hours. The lowest concentration at which no visible growth was observed was considered to be MIC. Furthermore, MBC was determined by sub-culturing the test dilutions that showed no visible growth/turbidity onto nutrient agar plates. The plates were incubated at 37°C for 24 hours and the lowest concentration that yielded no single *E.coli* colony on the agar plates was taken as MBC.

pH-dependent antibacterial activity

The effect of pH on the antibacterial activity of Br-AC was determined by growing the *E.coli* cultures in nutrient media with different pH. The pH of the media ranges from 5.5 to 9.0 and was adjusted using 0.1N HCl or 0.1 N NaOH. The *E.Coli* cells grown in different pH media were spread over nutrient agar plates, and the antibacterial activity of Br-AC was determined by the well diffusion method.

Removal of *Escherichia coli*

The removal of *Escherichia coli* was conducted by taking Br-AC (MIC concentration) in 100 ml of Erlenmeyer flask, and 50 mL of aqueous solution containing approximately 10^8 CFU/mL of *Escherichia coli* was added into it. The contents were placed in a shaking incubator at 37°C and the viable *E.coli* cells were counted at a different time intervals (0-120mins). After each time interval, an aliquot of 0.1 mL was pipetted from the culture flask and spread onto nutrient agar plates. After the plates were incubated overnight at 37°C, the viable *E.coli* cells or colonies were counted using a digital colony counter and the results were expressed in colony-forming units per millilitre (CFU/mL).

SEM analysis of ruptured bacterial cells

The morphological changes in the *E.coli* cells upon contact with Br-AC was visualised through scanning electron microscopy (JEOL/JSM-6360). Bacterial cells grown overnight in the nutrient broth were centrifuged at 5000 rpm for 5 minutes and washed twice with sterile PBS solution. The cells were further treated with Br-AC at MIC concentrations for 80 minutes followed by fixing with 4% glutaraldehyde solution for 24 h. The samples (both treated and control) were dehydrated by sequential treatment with 30%, 50%, 70%, 90% acetone for 5 minutes each and 100% acetone for 1 minute, then dried by critical point drying, gold sputter-coated, and imaged using SEM.

6.2.6 Molecular docking studies

Molecular docking studies were conducted to provide clear evidence and possible mechanism of the antibacterial activity of the brominated activated carbon. Molegro Virtual Docker (MVD) was used for the molecular docking simulations. Three brominated activated carbon models given in Figure 6.2 were used for the docking studies. The structures were drawn on Chem Draw and were optimized using the MM2 force field method. The brominated activated carbons were docked into the active sites of MurA (3ISS). MurA (UDP-*N*-acetylglucosamine enolpyruvyl transferase) is a key enzyme which plays a crucial role in the biosynthesis of *E.coli* cell wall peptidoglycan[42] and therefore, making it an attractive target for any antimicrobial agent. MurA inactivation destroys cell integrity and leads to osmotic lysis, which is lethal to the bacterial cell. The structure of MurA was retrieved from the Research Collaboratory for Structural Bioinformatics (RCSB) Protein Data Bank (<http://www.rcsb.org/>) as given in Figure 6.2(a). For docking simulations, charges were assigned and the water molecules were removed. By using MVD, cavities were predicted and the binding cavity was set at the site X: -4.82, Y: -6.84, Z: -0.85 within a constraint of radius 14 Å having a volume of 512 Å³ and a surface area of 1102.08 Å². The ligands were then docked against the target proteins and 30 independent runs were performed for each ligand. The top pose for the ligand from the docking score was selected to study molecular interactions[43–46].

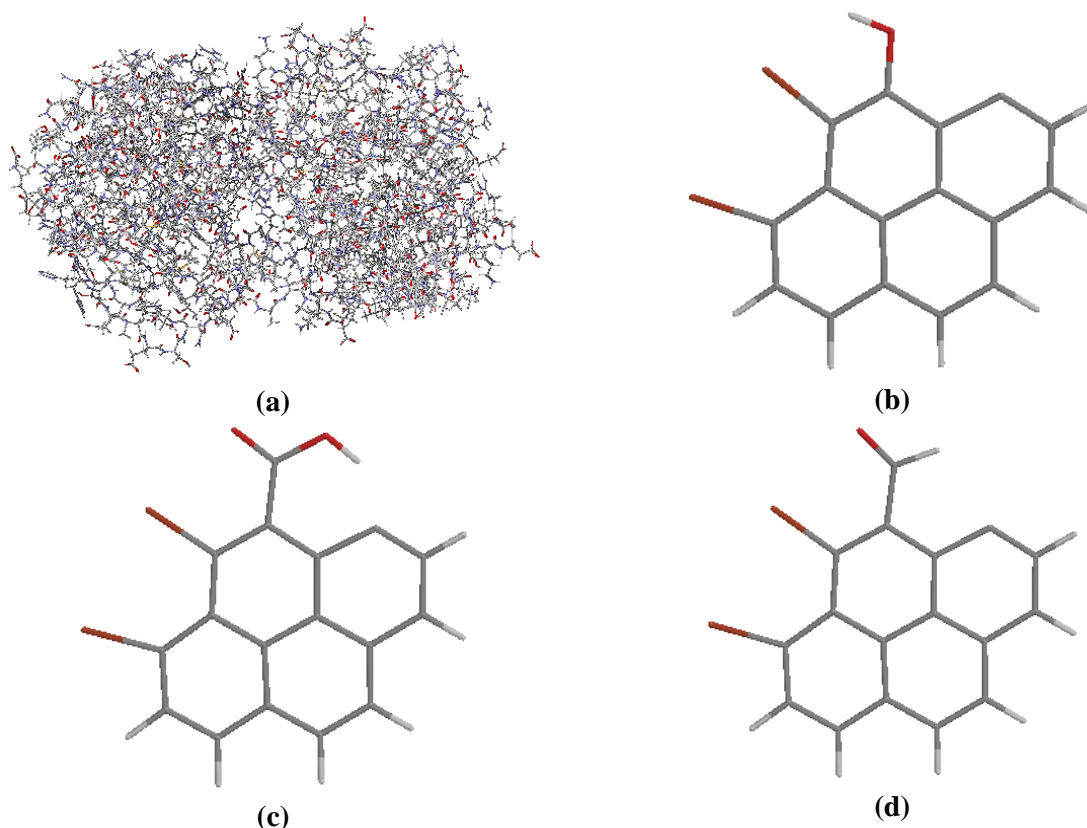


Figure 6.2 (a) MurA enzyme (b) Brominated AC-OH (c) Brominated AC-COOH and (d) Brominated AC-CHO

6.3. Results and Discussion

6.3.1. Characterisation of Br-AC

Field emission scanning electron microscopy

The field emission scanning electron microscopy (FESEM) micrographs of AC and Br-AC are presented as Figure 6.3. From the figures it can be observed that the surface of AC was quite smooth and exhibited a well-developed porous network. However, in case of Br-AC, the surface appeared rougher and the pores became relatively larger. The damaged surface of Br-AC might be due to the bromination of the AC surface. The presence of bonded bromine is further corroborated through the results of Energy-dispersive X-ray spectroscopy (EDX). Elemental composition obtained by EDX of AC showed only the presence of carbon and oxygen but EDX of Br-AC displayed a bromine peak in addition to carbon and oxygen, wherein the bromine concentration was 6.34 wt%. The presence of Br peak indicated the successful bromination of the AC surface.

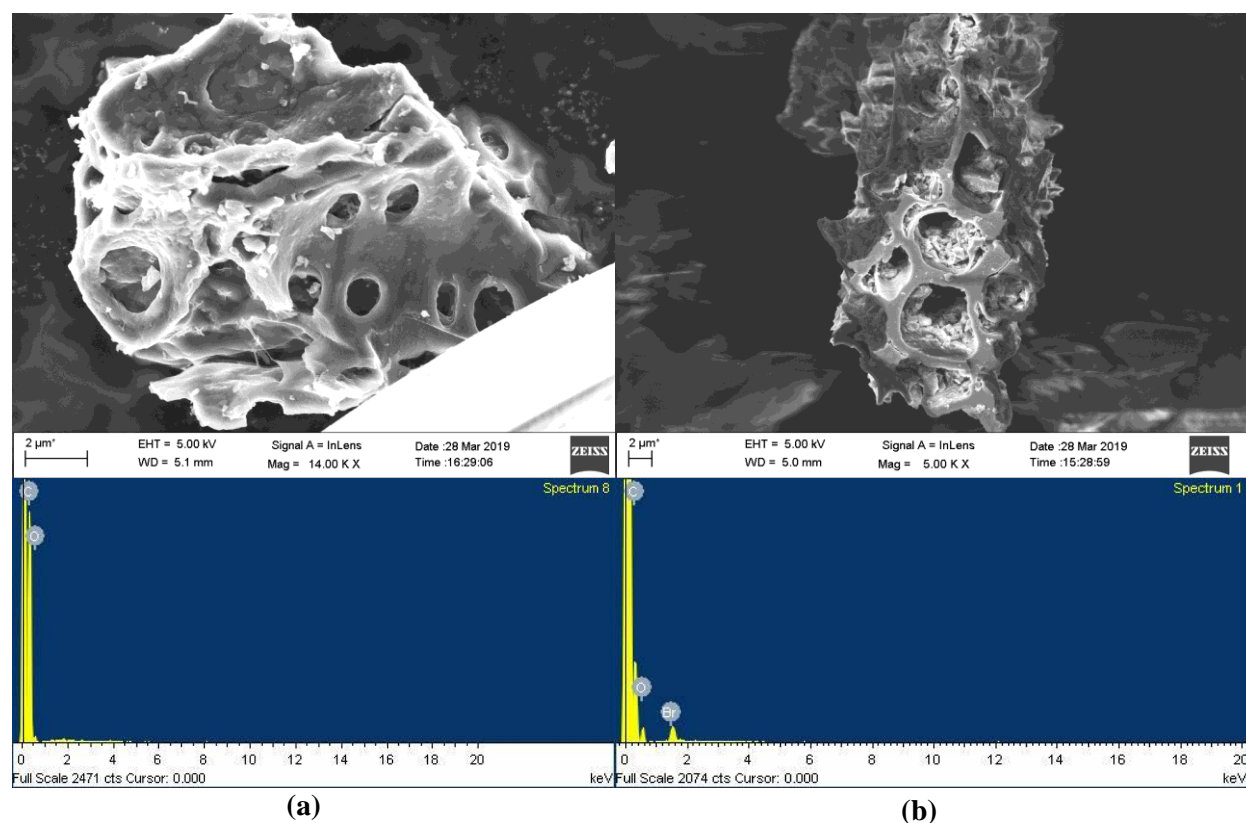


Figure 6.3 SEM and EDX images of (a) AC and (b) CTMATB-AC

BET surface area and pore volume

The BET surface area and pore volume of AC were found to be $687.66 \text{ m}^2/\text{g}$ and $0.301 \text{ cm}^3/\text{g}$ respectively. However, the surface area and pore volume decreased to $556.77 \text{ m}^2/\text{g}$ and $0.217 \text{ cm}^3/\text{g}$ respectively after the bromination of AC by CTMATB.

Fourier-transform infrared spectroscopy

The FTIR spectra of AC and Br-AC are given in Figure 6.4. The characteristic peaks observed for AC are: 3431.41 cm^{-1} (stretching vibrations of hydrogen-bonded hydroxyl groups), 2920.41 cm^{-1} ($-\text{CH}_2$ asymmetric stretching), 2852.16 cm^{-1} ($-\text{CH}_3$ symmetric stretching), 1736.40 cm^{-1} ($\text{C}=\text{O}$ stretching vibration of carbonyl, carboxyl and ester groups), 1480 cm^{-1} ($\text{C}=\text{C}$ stretching of aromatic rings), 1177 cm^{-1} and 1017 cm^{-1} ($\text{C}-\text{O}$ stretching in alcohols, phenols, carboxylic acid or derivatives, ethers or esters group) and 735.30 cm^{-1} ($\text{C}-\text{H}$, $\text{O}-\text{H}$ and $\text{C}-\text{O}$ bending vibrations) [47–49]. Thus, it could be observed that functional groups like carbonyl, hydroxyl and carboxyl were present in the activated carbon.

The peaks obtained for Br-AC are 3343.24 cm^{-1} (hydrogen-bonded -OH stretching vibrations), two shoulder peaks at 2922.91 cm^{-1} (-CH₂ asymmetric stretching) and 2848.54 cm^{-1} (-CH₃ symmetric stretching), 1704.15 cm^{-1} (C=O stretching vibration of carbonyl, carboxyl and ester groups), 1588 cm^{-1} (C=C stretching of aromatic rings), 1022.92 cm^{-1} (C-O stretching in alcohols, carboxylic acid or derivatives, ethers or esters group). In the case of Br-AC, additional peaks are observed at 1434.67 cm^{-1} and 1371.15 cm^{-1} corresponding to -CH₂ and CH₃ deformations. A strong peak at 1211.29 cm^{-1} corresponded to C-O vibration and a new peak was also observed at 527.21 cm^{-1} for Br-AC which indicated the presence of alkyl halide bond (C-Br)[50]. The occurrence of these new aforementioned peaks indicated the successful interaction of CTMATB with AC during the bromination process.

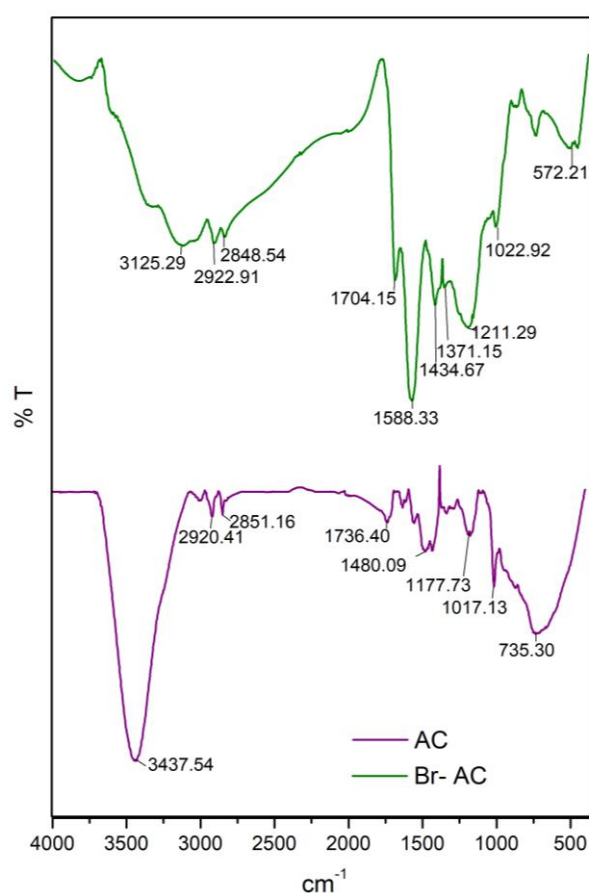


Figure 6.4 FTIR spectra of AC and Br-AC

X-ray diffraction analysis

X-ray diffraction analysis was done to determine the crystalline or amorphous nature of AC and Br-AC. Figure 6.5 presents the XRD profile of AC and Br-AC. AC showed two distinct peaks at $2\theta = \sim 23^\circ$ and $\sim 43^\circ$, ascribing to the reflection from the (002) and (100) planes respectively, and suggest the graphite-like micro crystallite nature of AC. Upon bromination,

the peak at $2\theta \sim 43^\circ$ was destroyed while the $2\theta = \sim 23^\circ$ peaks remained almost unaltered. Thus, it may be assumed that the bromination of AC destroyed the graphite-like micro crystallite structure and resulted in the amorphous nature of Br-AC. This type of structural disordering may have resulted from the destruction of the well-developed porous network of AC during the bromination process, resulting in a decrease of crystallinity. Similar structural changes have also been reported by various researchers, for example, Barbanta *et.al.* reported the sharp destruction of (100) peak upon successful bromination of activated carbon[32], while Liu *et.al.* reported the decrease in crystallinity of activated carbon upon modification by CTAB[51].

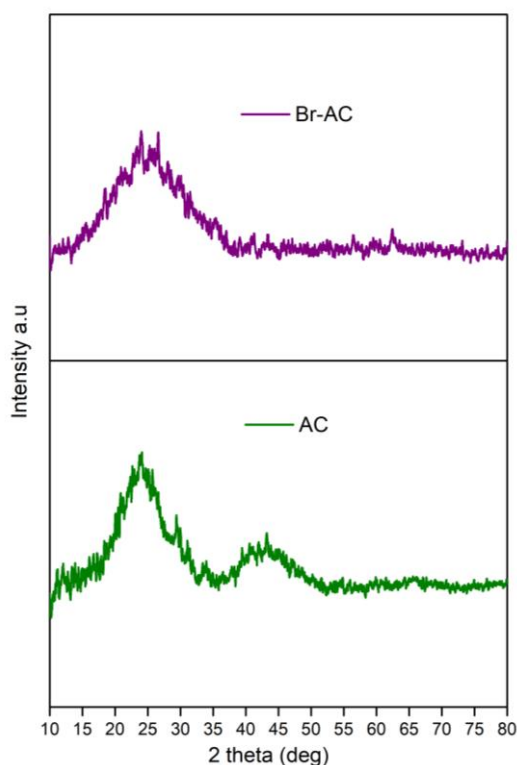


Figure 6.5 XRD image of AC and Br-AC

X-ray photoelectron spectroscopy

The surface elemental composition and chemical bonding nature of the Br-AC were further determined using XPS. The wide survey XPS spectrum of Br-AC are presented in Figure 6.6(a), where oxygen, carbon and bromine peaks are visible. The Br 3d peak was found at a binding energy of 70.2 eV and Br 3p peak at 183.0 eV, while the C 1s peak was observed at 284.8 eV and the O 1s peak at 532.8 eV.

Further, a detailed peak-fitting analysis of the high-resolution C 1s and Br 3d core level spectrum of Br-AC was done to analyse the bonding environment of these elements and are presented in Figure 6.6 (b) and 6(c) respectively.

The high-resolution C 1s spectrum was fitted into several peaks representing C-C at 284.1 eV [52,53], C=C aromatics at 284.6 eV [54], C-Br/C-H at 285.3 eV [33,55], C-O/C→Br at 286.2 eV [33,56–58], C=O at 286.9 eV [55,57] and 287.8 eV[36], O-C=O at 289.0 eV [59], pi-pi interactions at 290.1- 291.5 eV [37,60]. The C-Br and C-H groups are generally detected around the same binding energies; and accordingly, an unresolved single peak was observed for both the components. Likewise, the similar binding energies of C-O and C→Br groups also resulted in the overlapping of the peaks. The presence of covalently bonded C-Br and charge transfer C→Br complex suggests that CTMATB could have possibly brominated on the activated carbon surface.

Further, the high-resolution Br 3d were fitted into four peaks corresponding to binding energies of 70.0 eV, 71.1 eV, 68.4 eV and 67.4 eV. The peak observed at 68.4 eV are attributed to the physically bonded Br⁻, while the peaks at 70.0 eV, 71.1 eV and 67.4 eV are characteristics of chemically bonded bromine[33,36]. Depending on the binding energies, the chemically bonded bromine were further differentiated in two types; stronger peaks at 70.1 eV and 71.1 eV corresponding to bromine covalently bonded to sp² and sp³ carbon atoms (C-Br), and a weaker peak at 67.4 eV which could be attributed to carbon-bromine charge transfer complex(C→Br) [37].

From the peak area ratio, it could be deduced that around 85% of bromine was covalently bonded to carbon, ~10% was attributed to charge transfer complexes, and a very small fraction was physically bound bromine molecule (~5%). Strikingly, these results indicated that the major amount of bromine atoms were covalently bound to the carbon surface, and the amounts of bromine participating as charge transfer complexes or physically adsorbed bromine were very low.

The XPS data, therefore, presents significant evidence of the bromination of AC, mainly through the formation of strong covalent bonds.

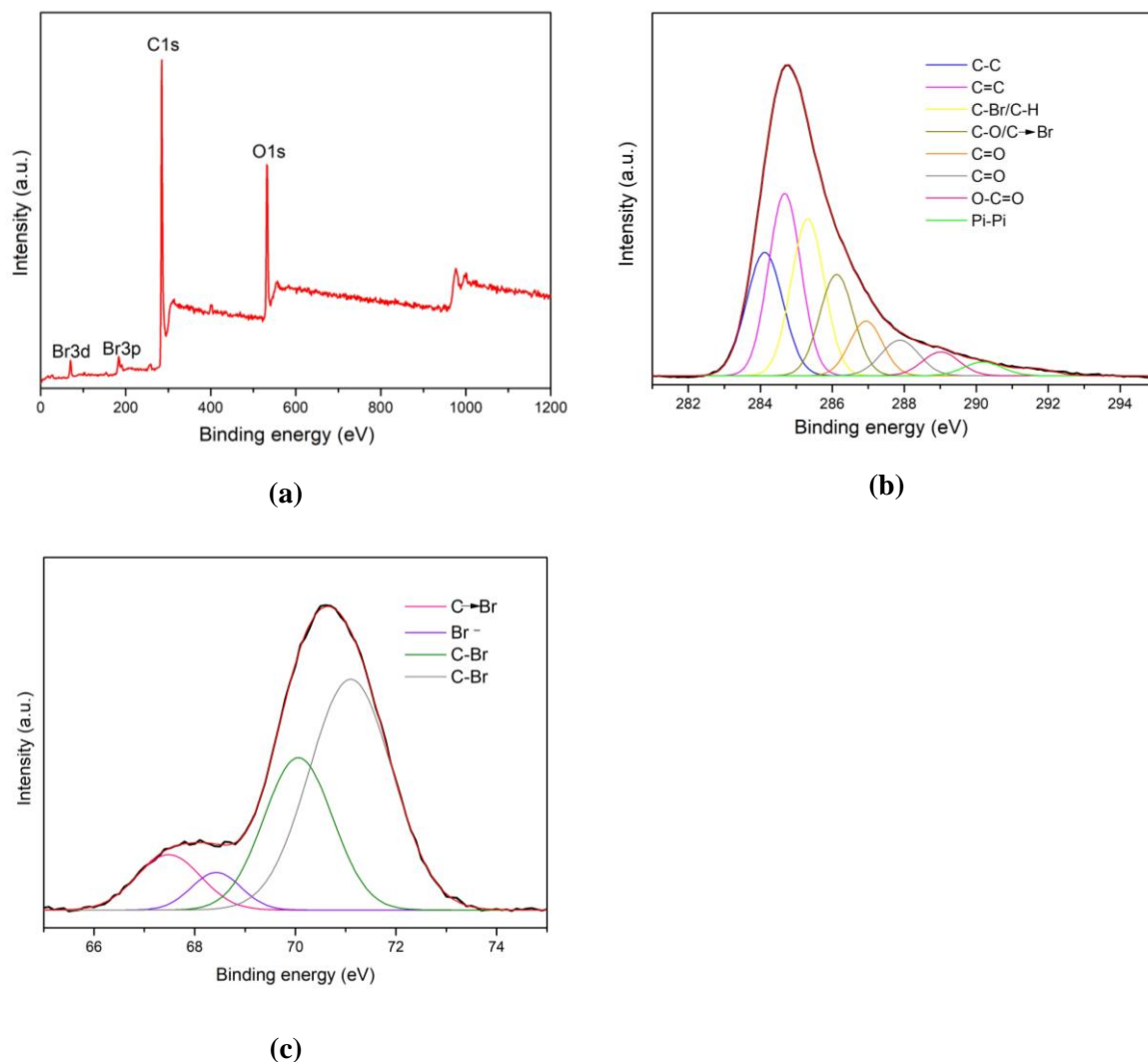


Figure 6.6 (a) XPS wide scan spectrum of Br-AC (b) High-resolution C 1s spectrum and (c) High-resolution Br 3d spectrum

6.3.2 Possible bromination mechanism

CTMATB is known to be an efficient brominating agent[61], therefore, its interaction with AC may mainly proceed through the bromination of the AC surface. Bromination of a solid surface using Br₂ has been widely studied and its mechanisms are well known. However, the bromination of activated carbon surfaces by tribromide compounds (-Br_3^-) is not very clear as almost no studies have been reported on the bromination of solid surfaces by tribromides moieties. Therefore, the present study attempted to study the possible mechanisms of the bromination of activated carbon surface by CTMATB at the molecular level using DFT calculations.

For the DFT study, five-carbon models depicting unsaturated AC (AC-U), hydroxyl AC (AC-OH), carboxyl AC (AC-COOH) and carbonyl AC (AC-CHO) were considered and their interactions with the CTMATB was studied. The consideration of activated carbon models

with different functional groups would aid in understanding the effect of such functionals on the extent of activated carbon bromination. The various interactions representing the bromination process are given in Figure 6.7, while the bond length and the interaction energies obtained for the various type of bromination interactions are given in Table 6.1.

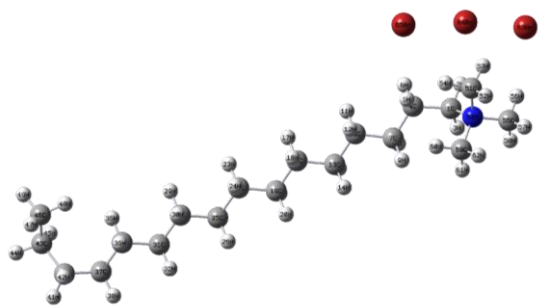
The bromination of AC's by CTMATB was studied by considering various possible ways of interaction mechanisms, and the most stable interactions were selected based on their interaction energy. For all the AC models, it was observed that the strongest and most stable interaction occurred when CTMATB bound with the AC's surfaces via bromination of the carbon atom of the AC's surface (Figure 6.7(b)-(e)). The interaction energies corresponded to -366.99 kJ/mol, -436.92 kJ/mol, -361.66 kJ/mol and -360.94 kJ/mol for CTMATB---AC-U, CTMATB---AC-OH, CTMATB---AC-COOH and CTMATB---AC-CHO respectively. It can be inferred that the bromination process possibly proceeded by dissociation of Br_3^- of CTMATB and further interaction of the dissociated species *viz.*, Br_2 with the carbon atom of the aromatic double bond of the AC's surface. The dissociation of Br_3^- can be explained from the lengthening of their bond length upon its interaction with AC. The Br_3^- is represented by 63Br-64Br-65Br in the optimized CTMATB structure as given in Figure 6.7(a). Initially, the 63Br-64Br and 64Br-65Br bond distance in 63Br-64Br-65Br of optimized CTMATB molecule corresponded to 2.70 Å and 2.68 Å respectively, and also the closest distance between CTAB⁺ moiety and 63Br was 2.74 Å. However, as given in Table 6.2, the distance of 63Br-64Br and 64Br-65Br increased to ≥ 3.10 Å after its interaction with AC's. This lengthening of distance between the bromine atoms upon their introduction to AC's indicated that the interatomic interaction within the tribromide species became weaker which may have led to dissociation. Although the dissociation mechanism of tribromides during the bromination process is not clear, some studies in organic bromination have hypothesized that the Br_3^- of tribromides dissociated into Br^- and Br_2 and the dissociated Br_2 further interacted with the double bond of the organic substrates, resulting in a brominated compound[62]. Therefore, it is envisaged that a similar dissociation mechanism may have occurred during the bromination of the AC's surfaces. This is also supported by the formation of a strong covalent bond between two bromine atoms and the carbon atoms in the aromatic double bond of AC. The two types of covalent bonds formed were 64Br-C and 65Br-C, the bond distances were between 1.94 Å and 2.00 Å; the shorter bond distance suggested that the two bromine species 64Br and 65Br were held firmly on the AC's surfaces. It was observed that the third bromine species *i.e.*, 63Br did not involve in strong interaction with the AC's surface, however, it tended to interact more strongly with the CTMA⁺ moiety which is explained by the shorter

bond distance between 63Br and the CTMA⁺, and the longer distance between 63 Br and AC's surfaces as given in Table 6.2. Therefore, from the above observations, it is likely that the 63Br-64Br-65Br dissociated into 63Br⁻ and Br₂ (64Br, 65Br) species. The 63Br⁻ favourably interacted with the CTMA⁺ species while the Br₂ interacted with the AC's surface via covalent bond formation. These theoretical findings also supported the experimental findings of the predominant presence of C-Br covalent bond.

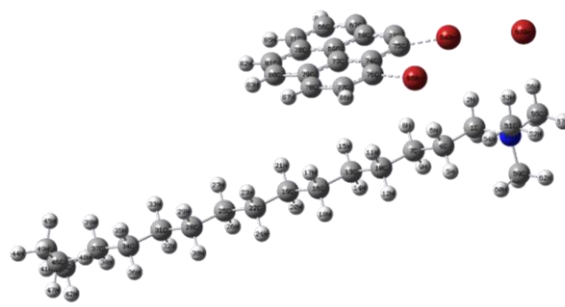
Since it was observed that CTMATB interacted more favourably via bromination of AC's surface by the Br₂ species, it is also important to understand the interaction mechanism of the dissociated Br₂ species with the AC surface and their structural stability. Therefore, we considered the above mentioned four carbon models (AC-U, AC-OH, AC-CHO, AC-COOH) and their interaction mechanisms with the active Br₂ species were studied. The Br₂ species is represented by 1Br and 2Br in the optimized structure given in Figure 6.7(f). The calculations showed that the distance between the two bromine species in its molecular Br₂ (1Br---2Br) form was 2.46Å, however, it increased to 3.28Å, 3.23Å, 3.23Å and 3.21Å upon its interaction with AC-U, AC-OH, AC-COOH and AC-CHO respectively. This lengthening of bond distance suggested the weakening of the molecular 1Br---2Br interaction which may have resulted in dissociation of the molecular Br₂ into individual 1Br and 2Br species. The dissociated species may have further interacted with the carbon in the aromatic double bond of AC surfaces forming C-Br covalent bond. The shorter C---1Br and C---2Br bond distances and the high negative interaction energies obtained for all the dissociated Br₂ and AC's interactions indicated the strong bonding of dissociated Br species with the AC surfaces. Moreover, the energy stability of all the Br₂ and AC's interactions (Figure 6.7(g)-(j)) was more as compared to the CTMATB and AC's interactions (Figure 6.7 (b)-(e)), indicating that Br₂ and AC type of complex is more likely to exist as compared to CTMATB and AC complex.

Among the various types of Br₂ and AC interaction, the Br₂---AC-OH complex showed the highest energy stability (-483.61 kJ/mol), indicating that the presence of -OH group may probably enhance the bromination process. Also, AC-COOH and AC-CHO carbon favoured the bromination process with interaction energy of -451.92 kJ/mol and -450.74 kJ/mol respectively. The unsaturated ACs also favoured the bromination process with high interaction energy but was lower as compared to the ACs containing oxygenated functional groups. The overall favourability of the bromination process by various carbon models decreased in the following order;

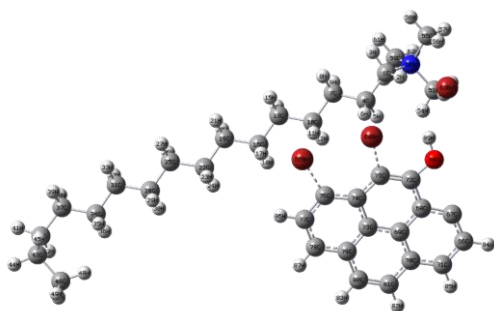




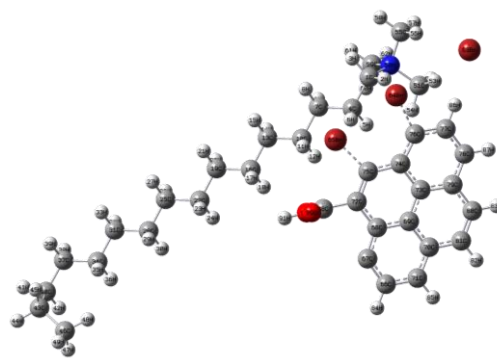
(a)



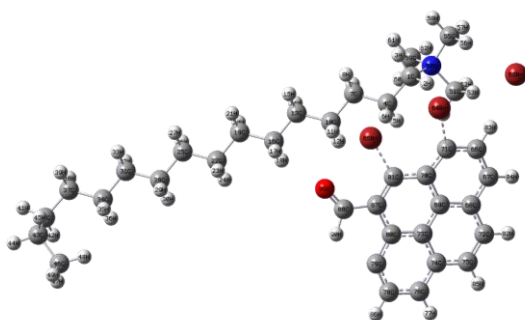
(b)



(c)



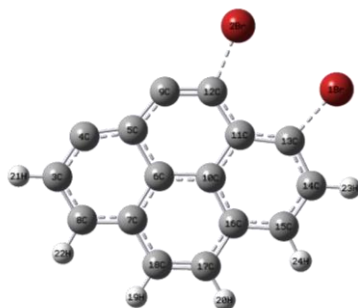
(d)



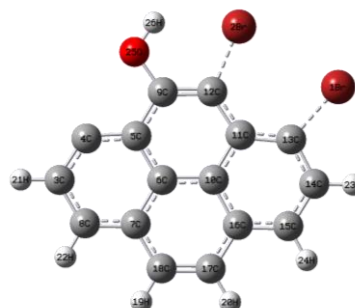
(e)



(f)



(g)



(h)

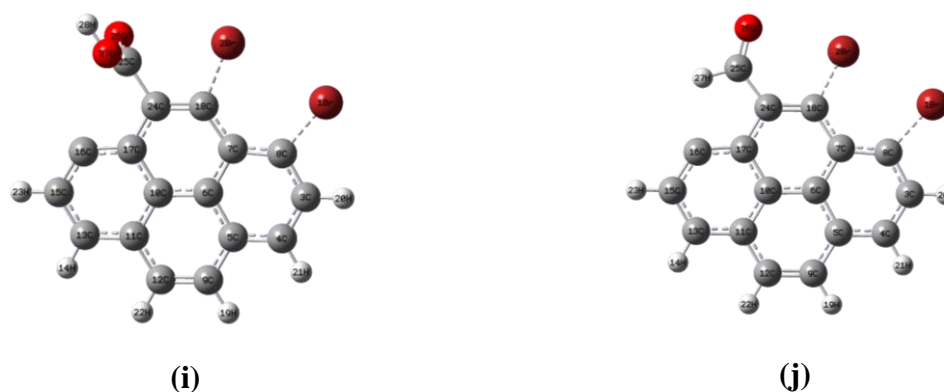


Figure 6.7 Optimized structure of (a) CTMATB (b) CTMATB---AC-U (c) CTMATB---AC-OH (d) CTMATB---AC-COOH (e) CTMATB---AC-CHO (f) dissociated Br₂ (g) Br₂---AC-U (h) Br₂---AC-OH (i) Br₂---AC-COOH and (j) Br₂---AC-CHO

Table 6.1 Bond distance and Interaction energy obtained for various type of bromination interactions.						
Models	Bond distance (Å)					Interaction energy (kJ/mol)
	63Br-64Br	64Br-65Br	C-64Br	C-65Br	63Br-CTMA ⁺	
CTMATB	2.70	2.68	-	-	2.74	
CTMATB---AC-U	3.10	3.27	2.00	1.95	2.59	-366.99
CTMATB---AC-OH	3.96	3.21	1.95	1.96	2.55	-436.92
CTMATB---AC-COOH	4.20	3.22	1.96	1.95	2.65	-361.66
CTMATB---AC-CHO	4.19	3.19	1.96	1.94	2.63	-360.94
	1Br-2Br	C-1Br	C-1Br			
Br ₂	2.46	-	-			
Br ₂ ---AC-U	3.28	1.98	1.95			-442.07
Br ₂ ---AC-OH	3.23	1.96	1.96			-493.61
Br ₂ ---AC-COOH	3.23	1.95	1.96			-451.92
Br ₂ ---AC-CHO	3.21	1.96	1.94			-450.74

In addition to the above-discussed bromination mechanisms, it is also possible that the CTMATB may interact with the AC through other modes of interaction. Therefore, the possibility of the interaction of CTMATB with AC via alkyl chain and ammonium moiety of CTMATB was also explored by considering (a) hydrophobic interaction of alkyl group of CTMATB with the hydrophobic planar part of AC surface and (b) Interaction via the ammonia moiety of CTMATB with the AC.

Two different carbon models, AC-U and AC-OH corresponding to unsaturated activated carbon and oxidized activated carbon respectively were considered. Figure 6.8(a) and (b) represent the hydrophobic interaction of CTMATB with AC and CTMATB with AC-OH respectively. The interaction of CTMATB *via* hydrophobic interactions resulted in low interaction energies of -3.81 kJ/mol for CTMATB---AC and -6.53 kJ/mol for CTMATB---

AC-OH. Also, Figure 6.8 (c) represents the interaction of CTMATB with AC via ammonium moiety and the interaction energy corresponded to -11.35 kJ/mol suggesting a weak physical interaction.

These results suggested that although the existence of such weak physical interactions cannot be ruled out, there is a high possibility for the weakly held CTMATB molecules to be leached out during the experimental washing process. Thus, physical interactions via alkyl chain and ammonium moiety cannot be the predominant mode of interaction in the binding of CTMATB with the activated carbon surface.

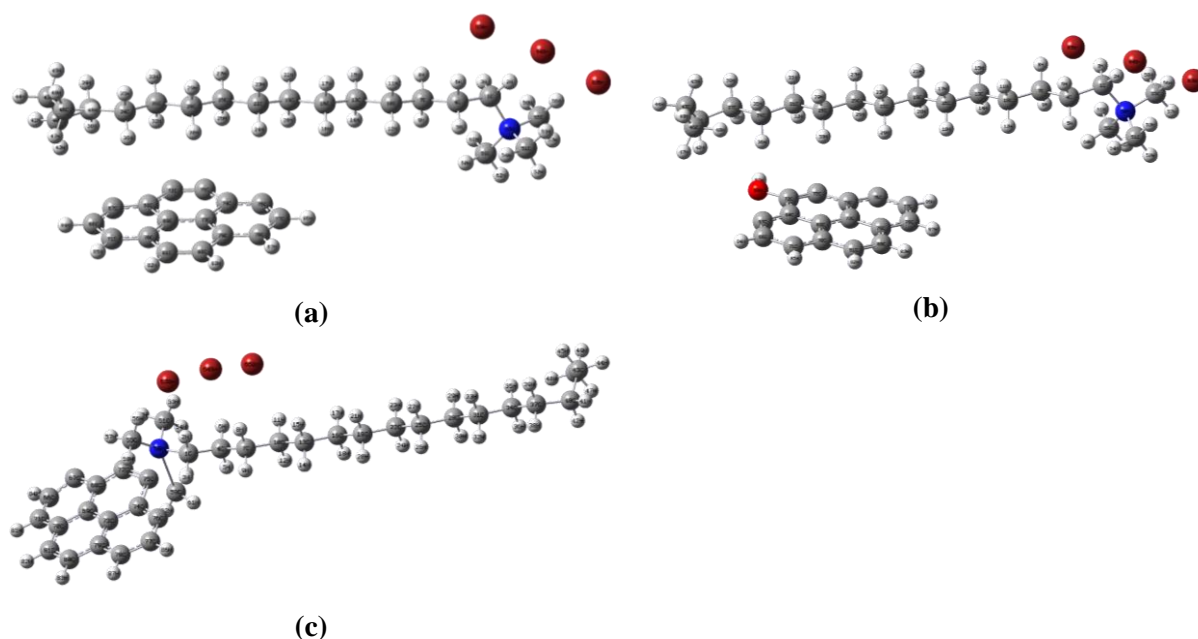


Figure 6.8 (a) Hydrophobic interaction between CTMATB and AC-OH (b) Hydrophobic interaction between CTMATB and AC-OH and (C) Physical interaction between CTMATB and AC-U via ammonium moiety

6.3.3 Antibacterial activity of Br-AC

6.3.3.1 Well-diffusion assay

The well-diffusion method gives a qualitative assessment of the antibacterial activity of Br-AC. The zone of inhibition obtained after 24 hours of incubation is shown in Figure 6.9. A clear inhibition zone of 16 mm (in diameter) was observed around the Br-AC sample after 24 hours of incubation, while there was no inhibition zone observed for the AC sample. The results demonstrated that the AC alone was not capable of inhibiting the *E.coli* growth. However, the brominated AC could inhibit the *E.coli* growth, suggesting the efficiency of Br-AC as an antibacterial material.

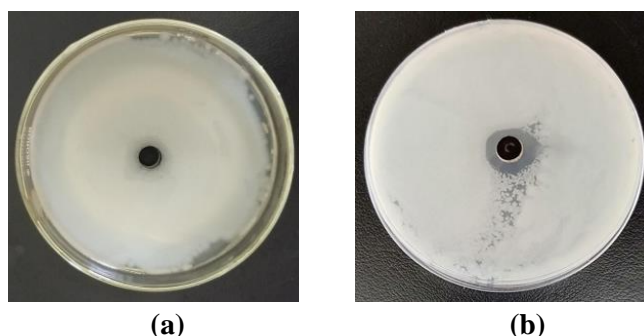


Figure 6.9 Inhibitory effect of (a)AC and (b) Br-AC against *E.coli*

6.3.3.2 Concentration and pH-dependent antibacterial activity

The antibacterial activity was found to vary in different Br-AC concentrations. Initially, 0.30 g/mL Br-AC concentration was taken in 2mL broth and the solutions was serially diluted two-fold to 0.15g/mL, 0.07g/mL, 0.03g/mL, 0.01 g/mL till 0.002g/mL. The broth media with different Br-AC concentrations were inoculated with *E.coli* and the bacterial growth was observed. There was no visible *E.coli* growth in Br-AC concentrations ranging from 0.3 to 0.01g/mL, however, *E.coli* growth was observed at concentrations below 0.01 g/mL. The results suggested that the Br-AC concentrations between 0.3 to 0.01 g/mL were capable of preventing the bacterial growth, and the lowest Br-AC concentration i.e 0.01g/mL was taken as the MIC. Further, the test-dilutions without any visible growth were sub-cultured on agar plates to determine the MBC i.e., the lowest concentration at which the *E.coli* cells are killed. The test dilutions containing 0.3 to 0.03 g/mL did not allow any bacterial colony formation on the agar plates and the lowest concentration i.e., 0.03 g/mL was taken as the MBC.

Taking the MIC concentration of Br-AC, the effect of pH on the antibacterial activity was calculated. As observed from Figure 6.10, the antibacterial activity of Br-AC varied with an increase in pH of the medium. The zone of inhibitions were found to be 15mm, 14mm, 16mm, 16mm and 17 mm at pH 5,6,7,8 and 9 respectively. Br-AC showed higher antibacterial activity in alkaline condition. The results indicated the efficiency of Br-AC at different pH and thus suggest its applicability in the treatment of wastewater with varying pH

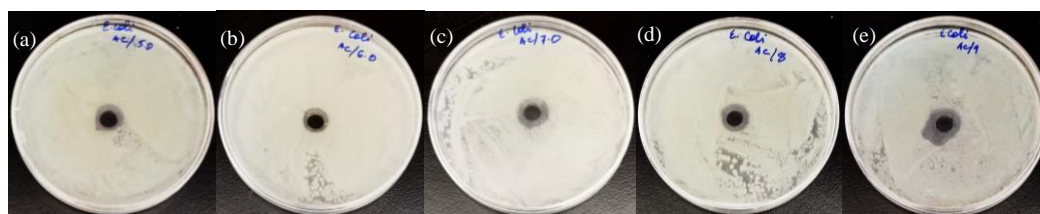


Figure 6.10 Antibacterial activity against *E.coli* at (a) pH 5 (b) pH 6 (c) pH 7 (d) pH 8 (e) pH 9

6.3.3.3 Removal of *Escherichia coli*

The removal of *Escherichia coli* from aqueous solution containing approximately 10^8 CFU/mL of *Escherichia coli* indicated that almost 100% bacteria removal was achieved after 80 minutes. No bacterial colony was observed after 80 minutes of incubation, indicating that the Br-AC was capable of killing the *Escherichia coli* present in the sample and thus achieving a 100% removal efficiency. The effect of contact time on the bacterial removal/killing by Br-AC was analysed by the time-kill curves shown in Figure 6.11. The curve represents the decrease in viable *E.coli* cell count (expressed in \log_{10} CFU/ml) with variation in contact time. The test results showed that the viable *E.coli* cell count decreased by 3 orders of magnitude in the first 10 minutes and this decrease in cell count was enhanced with time. After 1 hour, the viable cell count decreased by around 5 orders of magnitude and no viable *E.coli* cells were observed after 80 minutes contact time with the Br-AC.

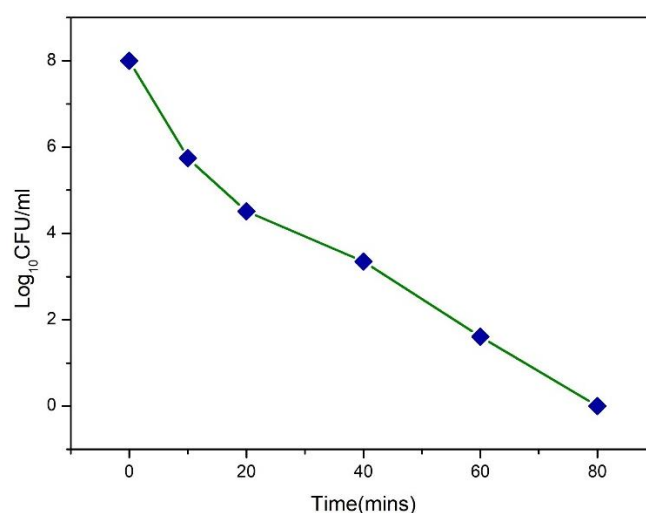


Figure 6.11 Time kill curve for *E.coli* with Br-AC at MIC concentration.

6.3.3.4 SEM image of ruptured bacterial cell

Scanning electron microscopy was employed to observe the damage on the *E.coli* cells after their exposure to Br-AC. The SEM micrographs of untreated and treated *E.coli* cells are given in Figure 6.12. The untreated *E.coli* cells were typically rod-shaped and displayed relatively smooth surfaces with a distinct outline. In contrast, the *E.coli* cells exposed to Br-AC were significantly damaged, distorted and wrinkled. The results showed that the Br-AC acted as an effective membrane destructive agent which may have caused the leakage of intracellular components and led to cell death.

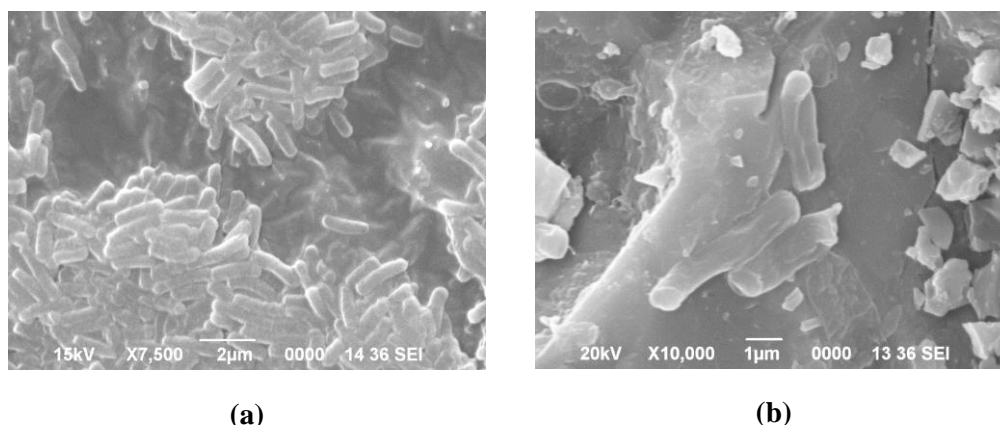


Figure 6.12 SEM image of (a) Untreated *E.coli* cells and (b) Cells exposed to Br-AC

6.3.4 Possible antibacterial mechanism

The Br-AC synthesized in the present study showed good antibacterial activity against the Gram-negative bacteria-*E.coli*. The possible antibacterial activity of the Br-AC may be explained as follows: firstly, the large surface area and porous nature of the Br-AC increased the chances of bacteria to come in contact with the Br-AC. Secondly, the Br-AC may have interacted with the lipid-protein membrane of *E.coli* cells leading to disorganisation of the bacterial membrane. The damage in the cellular membrane may have resulted in leakage of cellular components such as inorganic ions (K^+ , Na^+ , Ca^+ , PO_4^{-2} , SO_4^{-2} etc.), intracellular proteins, DNA and RNA, disrupting the normal functioning of the *E. coli* cells and eventually leading to cell death[63,64].

To further provide a comprehensible explanation of the antibacterial mechanism, molecular docking studies were conducted using the MVD. The activated carbon models, Br_2 ---AC-OH, Br_2 ---AC-COOH, Br_2 ---AC-CHO were considered as the ligands and were docked with the target enzyme MurA. The interactions and bonding between each ligand and the target enzyme MurA would convey the possible antibacterial effects. The molecular docking simulation results showed favourable binding of the brominated carbons with the target enzyme MurA with interaction energies ranging from -0.022 kJ/mol to 2.511 kJ/mol. Figure 6.13 shows the binding mode of the brominated activated carbons with MurA at the active site of the target depicting the possible mode of interaction, revealing strong hydrogen bonds formation at the active site of the target protein. Additionally, Table 6.2 shows the results of ligand-protein interaction energy and the docking scores (The interacting atoms, their interaction distance and the interaction energy). The docking hits predicted common interaction with Arg371 through sp^2 hybridization and Asp369 through sp^3 hybridization of the target enzyme.

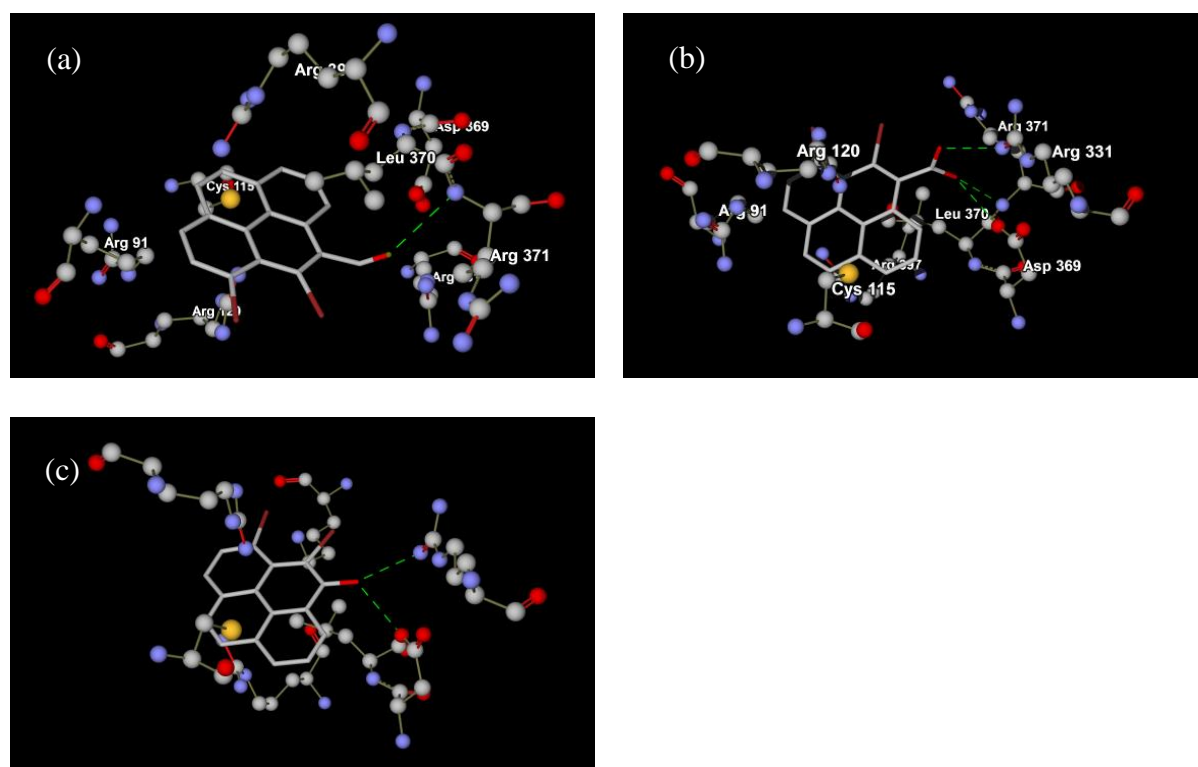


Figure 6.13 (a) Br₂---AC-OH (b) Br₂---AC-OH and (c) Br₂---AC-OH at the active site of MurA showing the mode of interactions

Ligand	Protein active sites	Docking score (kJ/mol)	Interaction energy (kJ/mol)	Hybridization (Protein)	Hybridization (Ligand)
Br ₂ -AC-OH	Arg371	-94.78	-0.794	Sp ² (Donor)	Sp ² (Acceptor)
Br ₂ -AC-COOH	Arg331	-102.48	-0.022	Sp ² (Donor)	Sp ² (Acceptor)
	Asp369		-2.5	Sp ³ (Acceptor)	Sp ³ (Both)
	Arg371		-1.266	Sp ² (Donor)	Sp ³ (Both)
Br ₂ -AC-CHO	Arg331	-87.40	-0.667	Sp ² (Donor)	Sp ³ (Both)
	Asp369		-2.5	Sp ³ (Acceptor)	Sp ³ (Both)

6.4. Conclusion

Brominated activated carbon was prepared successfully using greener brominating agent CTMATB by a simple preparation route. The characterisation of the prepared sample by confirmed the bromination of the activated surface. The destruction in the porous network of the activated carbon after the bromination process was visualized by FESEM-EDX. FTIR indicated the change in the chemical functional groups and the presence of C-Br bond. XPS results presented the chemical nature and the binding mode of bromine to carbon surface mainly by C-Br bond, while XRD analysis revealed the amorphous nature of the prepared

bromo carbon. The brominated activated carbon imparted antibacterial properties with MIC and MBC concentration of 0.01g/mL and 0.03g/mL respectively. SEM image of the *E.coli* cells showed the destruction in the cell integrity after their exposure to brominated activated carbon. The brominated carbon exhibited good killing kinetics with approximately 100% *E.coli* being killed within 80 minutes. The probable antibacterial mechanism of the brominated activated carbon was explained theoretically using MVD, which indicated the efficiency of the brominated carbon to bind with *E.coli* cell wall protein. Further, DFT calculations explained the possible bromination of the activated carbon surface by CTMATB. Finally, the present study shows the good antibacterial activities of brominated activated carbon and thus, provides an alternative to silver and metal oxides coating for imparting antibacterial activities to activated carbon for application in water treatment.

References

- [1] D.D.L. Chung, Carbon Materials, 2019. doi:10.1142/10487.
- [2] S.F. Lütke, A. V. Igansi, L. Pegoraro, G.L. Dotto, L.A.A. Pinto, T.R.S. Cadaval, Preparation of activated carbon from black wattle bark waste and its application for phenol adsorption, *J. Environ. Chem. Eng.* 7 (2019). doi:10.1016/j.jece.2019.103396.
- [3] U.S. Im, J. Kim, S.H. Lee, S. mi Lee, B.R. Lee, D.H. Peck, D.H. Jung, Preparation of activated carbon from needle coke via two-stage steam activation process, *Mater. Lett.* 237 (2019) 22–25. doi:10.1016/j.matlet.2018.09.171.
- [4] R.T. Ayinla, J.O. Dennis, H.M. Zaid, Y.K. Sanusi, F. Usman, L.L. Adebayo, A review of technical advances of recent palm bio-waste conversion to activated carbon for energy storage, *J. Clean. Prod.* 229 (2019) 1427–1442. doi:10.1016/j.jclepro.2019.04.116.
- [5] G.P. Awasthi, D.P. Bhattarai, B. Maharjan, K.S. Kim, C.H. Park, C.S. Kim, Synthesis and characterizations of activated carbon from *Wisteria sinensis* seeds biomass for energy storage applications, *J. Ind. Eng. Chem.* 72 (2019) 265–272. doi:10.1016/j.jiec.2018.12.027.
- [6] E. Elaiyappillai, R. Srinivasan, Y. Johnbosco, P. Devakumar, K. Murugesan, K. Kesavan, P.M. Johnson, Low cost activated carbon derived from *Cucumis melo* fruit peel for electrochemical supercapacitor application, *Appl. Surf. Sci.* 486 (2019) 527–538. doi:10.1016/j.apsusc.2019.05.004.
- [7] O.E. Eleri, K.U. Azuatalam, M.W. Minde, A.M. Trindade, N. Muthuswamy, F. Lou, Z. Yu, Towards high-energy-density supercapacitors via less-defects activated carbon from sawdust, *Electrochim. Acta.* 362 (2020). doi:10.1016/j.electacta.2020.137152.
- [8] S.A. Palsan, J.Y. Lim, A. Nor Asfaliza, Synthesis and characterization of active biocarbon material for use in cosmetics and personal care products, in: *Key Eng. Mater.*, 2020: pp. 266–272. doi:10.4028/www.scientific.net/KEM.841.266.
- [9] H. Hammani, F. Laghrib, A. Farahi, S. Lahrich, T. El Ouafy, A. Aboulkas, K. El Harfi, M.A. El Mhammedi, Preparation of activated carbon from date stones as a catalyst to the reactivity of hydroquinone: Application in skin whitening cosmetics samples, *J. Sci. Adv. Mater. Devices.* 4 (2019) 451–458. doi:10.1016/j.jsamd.2019.07.003.
- [10] R. V. Ramanujan, S. Purushotham, M.H. Chia, Processing and characterization of activated carbon coated magnetic particles for biomedical applications, *Mater. Sci. Eng. C.* 27 (2007) 659–664. doi:10.1016/j.msec.2006.06.007.
- [11] L. Gu, D. Wang, R. Deng, H. Liu, H. Ai, Effect of surface modification of activated carbon on its adsorption capacity for bromate, *Desalin. Water Treat.* 51 (2013) 2592–2601. doi:10.1080/19443994.2012.749052.
- [12] J.P. Chen, S. Wu, K.H. Chong, Surface modification of a granular activated carbon by citric acid for enhancement of copper adsorption, *Carbon N. Y.* (2003). doi:10.1016/S0008-6223(03)00197-0.
- [13] L. Li, S. Liu, J. Liu, Surface modification of coconut shell based activated carbon for the improvement of hydrophobic VOC removal, *J. Hazard. Mater.* 192 (2011) 683–690. doi:10.1016/j.jhazmat.2011.05.069.

- [14] S. He, G. Chen, H. Xiao, G. Shi, C. Ruan, Y. Ma, H. Dai, B. Yuan, X. Chen, X. Yang, Facile preparation of N-doped activated carbon produced from rice husk for CO₂ capture, *J. Colloid Interface Sci.* 582 (2021) 90–101. doi:10.1016/j.jcis.2020.08.021.
- [15] M. Goswami, P. Phukan, Enhanced adsorption of cationic dyes using sulfonic acid modified activated carbon, *J. Environ. Chem. Eng.* (2017). doi:10.1016/j.jece.2017.07.016.
- [16] M. Mazarji, B. Aminzadeh, M. Baghdadi, A. Bhatnagar, Removal of nitrate from aqueous solution using modified granular activated carbon, *J. Mol. Liq.* (2017). doi:10.1016/j.molliq.2017.03.004.
- [17] M. Naushad, A.A. Alqadami, Z.A. AlOthman, I.H. Alsohaimi, M.S. Algamdi, A.M. Aldawsari, Adsorption kinetics, isotherm and reusability studies for the removal of cationic dye from aqueous medium using arginine modified activated carbon, *J. Mol. Liq.* (2019). doi:10.1016/j.molliq.2019.111442.
- [18] Y. Zhi, J. Liu, Surface modification of activated carbon for enhanced adsorption of perfluoroalkyl acids from aqueous solutions, *Chemosphere.* (2016). doi:10.1016/j.chemosphere.2015.09.097.
- [19] H.J. Busscher, R.J.B. Dijkstra, E. Engels, D.E. Langworthy, D.I. Collias, D.W. Bjorkquist, M.D. Mitchell, H.C. Van Der Mei, Removal of two waterborne pathogenic bacterial strains by activated carbon particles prior to and after charge modification, *Environ. Sci. Technol.* 40 (2006) 6799–6804. doi:10.1021/es061282r.
- [20] C. Pongener, P. Bhomick, S. Upasana Bora, R.L. Goswamee, A. Supong, D. Sinha, Sand-supported bio-adsorbent column of activated carbon for removal of coliform bacteria and *Escherichia coli* from water, *Int. J. Environ. Sci. Technol.* 14 (2017) 1897–1904. doi:10.1007/s13762-017-1274-6.
- [21] M.A. Hussain, M. Al-Ani, S. Al-Khalidi, Adsorption of Coliform Bacteria from water by Activated Carbon, *Eng. Tech. J.* 34 (2016) 1782–1788.
- [22] S. Siwila, I.C. Brink, Drinking water treatment using indigenous wood filters combined with granular activated carbon, *J. Water Sanit. Hyg. Dev.* 9 (2019) 477–491. doi:10.2166/washdev.2019.187.
- [23] T.K.M. Prashantha Kumar, T.R. Mandlimath, P. Sangeetha, P. Sakthivel, S.K. Revathi, S.K. Ashok Kumar, S.K. Sahoo, Highly efficient performance of activated carbon impregnated with Ag, ZnO and Ag/ZnO nanoparticles as antimicrobial materials, *RSC Adv.* 5 (2015) 108034–108043. doi:10.1039/c5ra19945j.
- [24] R. Bandyopadhyaya, M.V. Sivaiah, P.A. Shankar, Silver-embedded granular activated carbon as an antibacterial medium for water purification, *J. Chem. Technol. Biotechnol.* 83 (2008) 1177–1180. doi:10.1002/jctb.1985.
- [25] R. Selvakumar, S.P. Suriyaraj, V. Jayavignesh, K. Swaminathan, Silver nanoparticle impregnated bio-based activated carbon with enhanced antimicrobial activity, *Int. J. Nanosci.* 12 (2013). doi:10.1142/S0219581X13500245.
- [26] M.V. Raimondi, S. Cascioferro, D. Schillaci, S. Petruso, Synthesis and antimicrobial activity of new bromine-rich pyrrole derivatives related to monodeoxypyroluteorin, *Eur. J. Med. Chem.* 41 (2006) 1439–1445. doi:10.1016/j.ejmech.2006.07.009.
- [27] F. Jia, Y. Zhang, J. Wang, J. Peng, P. Zhao, L. Zhang, H. Yao, J. Ni, K. Wang, The

- effect of halogenation on the antimicrobial activity, antibiofilm activity, cytotoxicity and proteolytic stability of the antimicrobial peptide Jelleine-I, *Peptides*. 112 (2019) 56–66. doi:10.1016/j.peptides.2018.11.006.
- [28] N. Molchanova, J.E. Nielsen, K.B. Sørensen, B.K. Prabhala, P.R. Hansen, R. Lund, A.E. Barron, H. Jenssen, Halogenation as a tool to tune antimicrobial activity of peptoids, *Sci. Rep.* 10 (2020). doi:10.1038/s41598-020-71771-8.
- [29] N. Bayrak, M. Yıldız, H. Yıldırım, E. Mataracı Kara, B. Ozbek Celik, A.F. Tuyun, Brominated plastoquinone analogs: Synthesis, structural characterization, and biological evaluation, *J. Mol. Struct.* (2020). doi:10.1016/j.molstruc.2020.128560.
- [30] J.S. Ibrahim, H.. Adamu, O.. Shakede, Antibacterial Activity of Marula [*Sclerocarya Birrea*] and Brominated Marula Seed Oil, *Int. J. Innov. Sci. Res. Technol.* 5 (2020) 1120–1124. doi:10.38124/ijisrt20aug668.
- [31] N.D. Hutson, B.C. Attwood, K.G. Scheckel, XAS and XPS characterization of mercury binding on brominated activated carbon, *Environ. Sci. Technol.* 41 (2007) 1747–1752. doi:10.1021/es062121q.
- [32] P. Barpanda, G. Fanchini, G.G. Amatucci, Structure, surface morphology and electrochemical properties of brominated activated carbons, *Carbon N. Y.* 49 (2011) 2538–2548. doi:10.1016/j.carbon.2011.02.028.
- [33] E. Papirer, R. Lacroix, J.B. Donnet, G. Nanse, P. Fioux, XPS Study of the halogenation of carbon black-part 1. Bromination, *Carbon N. Y.* 32 (1994) 1341–1358. doi:10.1016/0008-6223(94)90121-X.
- [34] Z. xia Jin, G.Q. Xu, S.H. Goh, A preferentially ordered accumulation of bromine on multi-wall carbon nanotubes, *Carbon N. Y.* (2000). doi:10.1016/S0008-6223(99)00237-7.
- [35] J.F. Friedrich, G. Hidde, A. Lippitz, W.E.S. Unger, Plasma bromination of graphene for covalent bonding of organic molecules, in: *Plasma Chem. Plasma Process.*, 2014. doi:10.1007/s11090-013-9509-x.
- [36] O. Jankovský, P. Šimek, K. Klimová, D. Sedmidubský, S. Matějková, M. Pumera, Z. Sofer, Towards graphene bromide: Bromination of graphite oxide, *Nanoscale*. 6 (2014) 6065–6074. doi:10.1039/c4nr01154f.
- [37] L.G. Bulusheva, A. V. Okotrub, E. Flahaut, I.P. Asanov, P.N. Gevko, V.O. Koroteev, Y. V. Fedoseeva, A. Yaya, C.P. Ewels, Bromination of double-walled carbon nanotubes, *Chem. Mater.* 24 (2012) 2708–2715. doi:10.1021/cm3006309.
- [38] N. Longkumer, K. Richa, R. Karmaker, V. Kuotsu, A. Supong, L. Jamir, P. Bharali, U.B. Sinha, Green synthesis of bromo organic molecules and investigations on their antibacterial properties: An experimental and computational approach, *Acta Chim. Slov.* 66 (2019) 276–283. doi:10.17344/acsi.2018.4580.
- [39] M.J. Frisch, G.W. Trucks, H.B. Schlegel, G.E. Scuseria, M.A. Robb, J.R. Cheeseman, G. Scalmani, V. Barone, B. Mennucci, G.A. Petersson, H. Nakatsuji, M. Caricato, X. Li, H.P. Hratchian, A.F. Izmaylov, J. Bloino, G. Zheng, J.L. Sonnenberg, M. Hada, M. Ehara, K. Toyota, R. Fukuda, J. Hasegawa, M. Ishida, T. Nakajima, Y. Honda, O. Kitao, H. Nakai, T. Vreven, J.A. Montgomery Jr., J.E. Peralta, F. Ogliaro, M. Bearpark, J.J. Heyd, E. Brothers, K.N. Kudin, V.N. Staroverov, R. Kobayashi, J.

- Normand, K. Raghavachari, A. Rendell, J.C. Burant, S.S. Iyengar, J. Tomasi, M. Cossi, N. Rega, J.M. Millam, M. Klene, J.E. Knox, J.B. Cross, V. Bakken, C. Adamo, J. Jaramillo, R. Gomperts, R.E. Stratmann, O. Yazyev, A.J. Austin, R. Cammi, C. Pomelli, J.W. Ochterski, R.L. Martin, K. Morokuma, V.G. Zakrzewski, G.A. Voth, P. Salvador, J.J. Dannenberg, S. Dapprich, A.D. Daniels, Ö. Farkas, J.B. Foresman, J. V. Ortiz, J. Cioslowski, D.J. Fox, Gaussian 09, Rev. A.02, Gaussian Inc., Wallingford CT. (2009) Wallingford CT. doi:10.1159/000348293.
- [40] F. Shen, J. Liu, Z. Zhang, Y. Dong, C. Gu, Density functional study of hydrogen sulfide adsorption mechanism on activated carbon, *Fuel Process. Technol.* 171 (2018) 258–264. doi:10.1016/j.fuproc.2017.11.026.
- [41] S.T. Perry, E.M. Hambly, T.H. Fletcher, M.S. Solum, R.J. Pugmire, Solid-state ¹³C NMR characterization of matched tars and chars from rapid coal devolatilization, *Proc. Combust. Inst.* 28 (2000) 2313–2319.
- [42] S. Eschenburg, W. Kabsch, M.L. Healy, E. Schonbrunn, A new view of the mechanisms of UDP-N-acetylglucosamine enolpyruvyl transferase (MurA) and 5-enolpyruvylshikimate-3-phosphate synthase (AroA) derived from X-ray structures of their tetrahedral reaction intermediate states., *J. Biol. Chem.* 278 (2003) 49215–49222. doi:10.1074/jbc.M309741200.
- [43] C.S. Mizuno, A.G. Chittiboyina, F.H. Shah, A. Patny, T.W. Kurtz, H.A. Pershadsingh, R.C. Speth, V.T. Karamyan, P.B. Carvalho, M.A. Avery, Design, synthesis, and docking studies of novel benzimidazoles for the treatment of metabolic syndrome, *J. Med. Chem.* 53 (2010) 1076–1085. doi:10.1021/jm901272d.
- [44] D. Pathak, N. Chadha, O. Silakari, Identification of non-resistant ROS-1 inhibitors using structure based pharmacophore analysis, *J. Mol. Graph. Model.* 70 (2016) 85–93. doi:10.1016/j.jmgm.2016.09.013.
- [45] V. BM, B. YD, One Pot Synthesis, Antimicrobial and In Silico Molecular Docking Study of 1,3-Benzoxazole-5-Sulfonamide Derivatives, *Org. Chem. Curr. Res.* 5 (2016). doi:10.4172/2161-0401.1000163.
- [46] M. Madhuri, C. Prasad, V. Rao Avupati, In Silico Protein-Ligand Docking Studies on Thiazolidinediones as Potential Anticancer Agents, *Int. J. Comput. Appl.* 95 (2014) 13–16. doi:10.5120/16597-6403.
- [47] F.M. Kasperiski, E.C. Lima, G.S. do. Reis, J.B. da Costa, G.L. Dotto, S.L.P. Dias, M.R. Cunha, F.A. Pavan, C.S. Correa, Preparation of CTAB-functionalized acai stalk and its efficient application as adsorbent for the removal of Direct Blue 15 and Direct Red 23 dyes from aqueous media, *Chem. Eng. Commun.* 205 (2018) 1520–1536. doi:10.1080/00986445.2018.1458028.
- [48] D. Angin, Production and characterization of activated carbon from sour cherry stones by zinc chloride, *Fuel*. 115 (2014) 804–811. doi:10.1016/j.fuel.2013.04.060.
- [49] Y. Liu, X. Liu, G. Zhang, T. Ma, T. Du, Y. Yang, S. Lu, W. Wang, Adsorptive removal of sulfamethazine and sulfamethoxazole from aqueous solution by hexadecyl trimethyl ammonium bromide modified activated carbon, *Colloids Surfaces A Physicochem. Eng. Asp.* 564 (2019) 131–141. doi:10.1016/j.colsurfa.2018.12.041.
- [50] N. Sankararamakrishnan, N. Singh, A. Gupta, One pot green synthetic route for the preparation of cetyl trimethyl ammonium bromide grafted multiwalled carbon

- nanotubes and their application towards defluoridation, *RSC Adv.* 3 (2013) 22421–22429. doi:10.1039/c3ra43467b.
- [51] W. Liu, D. Ren, J. Wu, Z. Wang, S. Zhang, X. Zhang, X. Gong, Adsorption behavior of 2,4-DCP by rice straw biochar modified with CTAB, *Environ. Technol.* (United Kingdom). (2020). doi:10.1080/09593330.2020.1743367.
- [52] B.X. Zou, Y. Wang, X. Huang, Y. Lu, Hierarchical N- and O-Doped porous carbon composites for high-performance supercapacitors, *J. Nanomater.* 2018 (2018). doi:10.1155/2018/8945042.
- [53] A.F. Azevedo, M.R. Baldan, N.G. Ferreira, Nanodiamond Films for Applications in Electrochemical Systems, *Int. J. Electrochem.* 2012 (2012) 1–16. doi:10.1155/2012/508453.
- [54] I. Bouabibsa, S. Lamri, F. Sanchette, Structure, mechanical and tribological properties of Me-doped diamond-like carbon (DLC) (Me = Al, Ti, or Nb) hydrogenated amorphous carbon coatings, *Coatings*. 8 (2018). doi:10.3390/COATINGS8100370.
- [55] H. Au, N. Rubio, M.S.P. Shaffer, Brominated graphene as a versatile precursor for multifunctional grafting, *Chem. Sci.* 9 (2017) 209–217. doi:10.1039/c7sc03455e.
- [56] W. Wang, J. Peng, F. Li, B. Su, X. Chen, X. Chen, Phosphorus and chlorine co-doped carbon dots with strong photoluminescence as a fluorescent probe for ferric ions, *Microchim. Acta.* 186 (2019). doi:10.1007/s00604-018-3140-8.
- [57] N. Karikalan, M. Velmurugan, S.M. Chen, C. Karuppiah, K.M. Al-Anazi, M.A. Ali, B.S. Lou, Flame synthesis of nitrogen doped carbon for the oxygen reduction reaction and non-enzymatic methyl parathion sensor, *RSC Adv.* 6 (2016) 71507–71516. doi:10.1039/c6ra10130e.
- [58] S.A. Al-Bataineh, L.G. Britcher, H.J. Griesser, XPS characterization of the surface immobilization of antibacterial furanones, *Surf. Sci.* 600 (2006) 952–962. doi:10.1016/j.susc.2005.12.028.
- [59] S.F. Tan, S. Raj, G. Bisht, H. V. Annadata, C.A. Nijhuis, P. Král, U. Mirsaidov, Nanoparticle Interactions Guided by Shape-Dependent Hydrophobic Forces, *Adv. Mater.* 30 (2018). doi:10.1002/adma.201707077.
- [60] R. Sadri, M. Hosseini, S.N. Kazi, S. Bagheri, N. Zubir, K.H. Solangi, T. Zaharinie, A. Badarudin, A bio-based, facile approach for the preparation of covalently functionalized carbon nanotubes aqueous suspensions and their potential as heat transfer fluids, *J. Colloid Interface Sci.* 504 (2017) 115–123. doi:10.1016/j.jcis.2017.03.051.
- [61] U. Bora, M.K. Chaudhuri, D. Dey, S.S. Dhar, Peroxometal-mediated environmentally favorable route to brominating agents and protocols for bromination of organics, in: *Pure Appl. Chem.*, 2001. doi:10.1351/pac200173010093.
- [62] J. Berthelot, Y. Benammar, B. Desmazières, Action of tetrabutylammonium tribromide with para -substituted chalcones in protic and aprotic media, *Can. J. Chem.* 73 (1995) 1526–1530. doi:10.1139/v95-189.
- [63] Z. Shi, K.G. Neoh, E.T. Kang, Antibacterial and adsorption characteristics of activated carbon functionalized with quaternary ammonium moieties, *Ind. Eng. Chem. Res.* 46 (2007) 439–445. doi:10.1021/ie0608096.

- [64] Y. Xue, H. Xiao, Y. Zhang, Antimicrobial polymeric materials with quaternary ammonium and phosphonium salts, *Int. J. Mol. Sci.* 16 (2015) 3626–3655. doi:10.3390/ijms16023626.

CHAPTER 7

SUMMARY AND CONCLUSIONS

This chapter presents the overall summary and conclusions of the thesis. The future scope of the work is also highlighted in this chapter.

.

Biomass materials of *Tithonia diversifolia* and Ravenna grass served as a potential precursor for the preparation of activated carbon. The surface characteristics of the prepared activated carbon was successfully tailored to enhance the performance of the activated carbon towards a wide variety of pollutants such as phenols and bacterial pathogens. A summary of the overall thesis work is presented below:

1. A low-cost activated carbon was successfully synthesized from *Tithonia diversifolia* biomass using potassium hydroxide as the chemical activating reagent. Taguchi's experimental design approach was applied to determine the best preparation conditions. An optimum 2:1 impregnation ratio and 700°C activation temperature produced the best carbon with a high 854.44 m²g⁻¹ surface area, 0.445 cm³g⁻¹ total pore volume and 18.3 % yield. From ANOVA, the impregnation ratio was found to be the most influential factor in preparing activated carbon with the maximum surface area. SEM and XRD studies revealed the porous microcrystallite structure of the obtained activated carbon. The prepared carbon showed a maximum 98.2% removal percentage of bisphenol A. The Langmuir isotherm model described the equilibrium adsorption of bisphenol A well with a maximum adsorption capacity(q_m) of 15.69 mg g⁻¹ while the kinetic adsorption study indicated a pseudo second order model. A theoretical investigation suggested that the adsorption of bisphenol A onto the activated carbon mainly proceeds via chemisorption and the presence of a carboxyl functional group on the activated carbon surface yielded a greater adsorptive impact on bisphenol A. This study indicates that *Tithonia diversifolia* could be used as a potential raw material for preparing activated carbon for removing of bisphenol A from water.
2. The *Tithonia diversifolia* activated carbon (0.445 cm³g⁻¹ pore volume and 854.44 m²/g BET surface area) also served as an effective adsorbent for the removal of phenol and 2,4-dinitrophenol from water. A maximum of 99.98% and 97.81% removal efficiency was attained for phenol and 2,4-dinitrophenol respectively at optimised conditions. The pseudo-second-order model described the adsorption kinetics well, while the Langmuir model best-elucidated the adsorption isotherm with a maximum adsorption capacity of 50.552 mg g⁻¹ for phenol and 42.607 mg g⁻¹ for 2,4-dinitrophenol. According to the calculated thermodynamic parameters, the adsorption process was spontaneous and endothermic. The process performance was further validated using real wastewater, and the removal efficiency of 84-90% was attained for both analytes. Theoretical investigations through density functional theory calculations suggested that the presence

- of oxygenated functional group on activated carbon surface decreased the adsorbate-adsorbent interaction. Meanwhile, a comparative study of the adsorption energies of various interactions indicated that phenol interacted more strongly with the activated carbon as compared to 2,4-dinitrophenol. Regeneration studies indicated the reusability of the exhausted carbon up to the fifth cycle with significant removal efficiency.
3. A simple and efficient activated carbon biofilter column was developed for the treatment of bacteria-contaminated water. The biofilter columns were amended with *Tithonia diversifolia* activated carbon along with supporting media such as brick, sand or pebbles. The activated carbon biofilter columns achieved a high removal efficiency of up to 99.99 % of *Escherichia coli* from aqueous solution. Among the different supporting media used, the biofilter column with brick attained the highest removal efficiency of *Escherichia coli* from aqueous solution. This proves the higher effectiveness of brick powder as a supporting media compared to sand and pebbles. Further, the brick supported activated carbon biofilter column could perform efficiently in real wastewater environment achieving high removal efficiency of 98% total heterotrophic bacteria, 99.4% total coliform and 99.8 % *Escherichia coli*, indicating the applicability of the column in the real world scenario.
 4. Porous activated carbon was prepared using Ravenna grass and was successfully utilized as an adsorbent for the removal of 4-Nitrophenol from aqueous solution. The surface features of the activated carbon were enhanced using different molar concentrations of KOH. The activated carbon prepared using 2M KOH concentration at 700°C, resulted in the best features of the prepared adsorbent represented by BET surface area, pore volume and pH_{ZPC} of $919 \text{ m}^2\text{g}^{-1}$, $0.324 \text{ cm}^3\text{g}^{-1}$ and 8.1 respectively. SEM, FTIR, XRD and TGA analysis revealed the micro-crystallite and porous structure of the synthesised biocarbon with abundant functional groups and high thermal stability. The prepared carbon showed a high removal efficiency for 4-nitrophenol removal. The equilibrium isotherm study revealed the suitability of the Langmuir isotherm with a maximum adsorption capacity of 50.89 mg/g. The pseudo-second-order kinetic model well represented the adsorption kinetics data while thermodynamics study indicated the spontaneity ($\Delta G < 0$) and endothermic nature ($\Delta H > 0$) of the adsorption of 4-Nitrophenol. Density functional theory (DFT) calculations performed at the B3LYP level indicated that the interaction of 4-Nitrophenol with pristine and functionalized activated biocarbon is favourable.

5. Ravenna grass activated carbon was successfully modified using cetyltrimethyl ammonium tribromide (CTMATB) to render antibacterial activity in addition to the adsorption characteristics of the activated carbon. The modification of activated carbon was done using a simple and efficient route which resulted in brominated activated carbon. SEM and XRD analysis revealed the change in porous and crystalline structure after the modification process. Characterisation of the brominated activated carbon using XPS demonstrated that majority of the bromine form C-Br covalent bond with the carbon of the activated carbon. The prepared brominated activated carbon displayed antibacterial activity against Gram-negative bacteria- *Escherichia coli*. The kill-kinetic studies indicated that the *Escherichia coli* colonies reduced to 5 orders of magnitude within 80 minutes of their contact with the brominated activated carbon, while the minimum inhibitory concentration and minimum bactericidal concentration against *Escherichia coli* cells were found to be 0.01 g/mL and 0.03 g/mL respectively. The smooth rod-shaped *Escherichia coli* cells visualized using scanning electron microscopy became distorted and wrinkled after their exposure to brominated activated carbon. Molecular docking studies demonstrated the binding of the brominated carbon with *Escherichia coli* cell wall protein-MurA. Furthermore, DFT calculations suggested a strong favourability of the bromination of carbon surfaces via C-Br bond formation with interaction energies ranging between -442.07 kJ/mol to -493.61 kJ/mol.

Thus, it can be concluded from the current thesis work that activated carbon has been successfully produced using cost-effective and readily available biomass materials. The surface characteristics of the prepared activated carbon were efficiently tailored and used for the enhanced removal of a wide variety of pollutants such as phenol, 4-nitrophenol, 2,4-dinitrophenol, bisphenol A, coliform and *Escherichia coli* bacteria from water. Also, the activated carbon could be endowed with antibacterial properties for its usage in the removal/killing of bacterial pathogens from water.

Future scope of the work













- The modifications of the activated carbon surface can be further explored using different techniques to enhance its adsorption efficiency or to increase its affinity towards a specific pollutant.
- The activated carbon can be endowed with antibacterial properties by exploring other green antibacterial reagents or chemicals.

- The prepared carbons can be tested for their efficiency in the removal of inorganic pollutants such as heavy and trace metals from water samples.
- Composite material can be prepared by doping the prepared activated carbon with other materials for its use in catalytic process, energy storage and other environmental applications.
- The regeneration of the spent carbon can be studied using biological, chemical and physical methods to develop an economical regeneration process.

Document Information

Analyzed document	Studies on surface modifications of activated carbon for removal of organic and biological pollutants from water by Aola Supong.docx (D100387335)
Submitted	4/1/2021 9:59:00 AM
Submitted by	Dipak Sinha
Submitter email	dipaksinha@gmail.com
Similarity	3%
Analysis address	dipaksinha.naga@analysis.orkund.com

Sources included in the report

W	URL: https://iopscience.iop.org/article/10.1088/1755-1315/237/2/022049/pdf Fetched: 4/1/2021 10:12:00 AM		1
W	URL: https://core.ac.uk/download/pdf/36154339.pdf Fetched: 4/1/2021 10:12:00 AM		6
W	URL: https://www.desotec.com/en/carbonology/carbonology-academy/raw-materials-activated ... Fetched: 4/1/2021 10:12:00 AM		1
W	URL: https://link.springer.com/article/10.1007/s40789-019-0262-5 Fetched: 4/1/2021 10:12:00 AM		1
J	Adsorption of Cr(VI) from aqueous solutions by HNO₃-purified and chemically activated pyrolytic tire char URL: aa6eb1dd-c505-47fe-8e13-1aaa34e7464a Fetched: 3/13/2019 12:37:50 AM		2
W	URL: https://www.hindawi.com/journals/isrn/2014/201626/ Fetched: 10/25/2019 6:59:47 AM		2
W	URL: https://core.ac.uk/download/pdf/53189039.pdf Fetched: 5/18/2020 8:11:06 AM		4
W	URL: https://iopscience.iop.org/article/10.1088/1757-899X/309/1/012072/pdf Fetched: 4/1/2021 10:12:00 AM		1
W	URL: https://link.springer.com/article/10.1007/s13201-019-0942-8 Fetched: 10/7/2019 6:54:04 AM		5
W	URL: https://www.nature.com/articles/s41598-017-12805-6 Fetched: 4/1/2021 10:12:00 AM		2
W	URL: https://link.springer.com/article/10.1007/s11164-015-2397-3 Fetched: 12/7/2020 9:22:55 PM		2
W	URL: https://www.ijee.ieefoundation.org/vol3/issue2/IJEE_05_v3n2.pdf Fetched: 4/1/2021 10:12:00 AM		1

CURRICULUM VITAE

Personal Details

Name in Full **AOLA SUPONG**
Date of Birth 29th June 1990
Address of Correspondence Department of Chemistry
Nagaland University
Lumami Campus-798627
Zunheboto, Nagaland
Email ID aolas@rediffmail.com

Academic qualifications

Exam Passed	Board/ University	Year of Passing	Division	Percentage of marks	Subjects	Rank/ Distinction
Matriculation(10 th)	Nagaland Board of School Education	2007	1 st Div	73.4 %	Mathematics, Science, Social Science, English, Alternative English	Science (Distinction)
Higher Secondary (10+2)	Nagaland Board of School Education	2009	2 nd Div	57.4 %	Chemistry, Physics, Biology, English, Alternative English	
B.Sc.	St. Pious X, Degree & P.G College for women (Osmania University)	2013	1 st Div	80.5 %	Chemistry, Botany, Bio- Technology, English, Env.Sc., Indian heritage and culture, Computer skills, Sanskrit	
M.Sc.	Nagaland University	2015	1 st Div	76.06 %	Chemistry	1st Rank (Gold medal)
Ph.D thesis submitted						

Additional Courses completed

Online certification course under SWAYAM

- Plastic waste management, NPTEL (8 weeks course), Score-88%.
- Organic farming for Sustainable agricultural production, NPTEL (8 weeks course), Score-74%.
- Sustainable and affordable sanitation solutions for small towns: policy, planning and practice, NPTEL (4 weeks course), Score-73%.

Academic Achievements/Awards

- Qualified Joint CSIR-NET (Lectureship) in Chemical Sciences, Date of award: 09/08/2019.
- Awarded Gold medal at Post Graduation (Chemistry) by Nagaland University-2015.

- DST-INSPIRE fellowship (JRF-17th August 2017 to 15th August 2019, SRF-16th August 2019 to current).
- National Fellowship for Higher Education (NFHE) (17th September 2015- 16th August 2017).
- Awarded the “STE Young Researcher” by Save the Environment organisation, Kolkata, West Bengal- December 2020.

Areas of Research Interest

- Development of biomass-based materials for removal of organic, inorganic and biological pollutants from water.
- Synthesis of antimicrobial materials for use in water treatment.
- Nanomaterials and composites for wastewater treatment.
- Activated carbon and its composite for various environmental applications.

Research Publications

A. Research papers published

1. Experimental and theoretical insight into the adsorption of phenol and 2,4-dinitrophenol onto *Tithonia diversifolia* activated carbon, *Applied surface Science*, 529, 1-15, 2020.

Aola Supong, Parimal Chandra Bhomick, Soremo L Ezung, Latonglila Jamir, Upasana Bora Sinha, Dipak Sinha

2. Batch sorption–photodegradation of Alizarin Red S using synthesized TiO₂/activated carbon nanocomposite: an experimental study and computer modelling. *Nanotechnology for Environmental Engineering*, 5, 8, 2020.

Mridushmita Baruah, **Aola Supong**, Parimal Chandra Bhomick, Rituparna Karmaker, Chubaakum Pongener, Dipak Sinha

3. Adsorptive removal of Bisphenol A by biomass activated carbon and insights into the adsorption mechanism through Density Functional theory calculations, *Sustainable chemistry and pharmacy*, 13, 1-13, 2019.

Aola Supong, Parimal Chandra Bhomick, Mridushmita Baruah, Chubaakum Pongener, Upasana Bora Sinha, Dipak Sinha

4. Pine Cone biomass as an efficient precursor for the synthesis of activated biocarbon for adsorption of anionic dye from aqueous solution: Isotherm, kinetic, thermodynamic and regeneration studies, *Sustainable Chemistry and Pharmacy*, 10, 41-49, 2019.

Parimal Chandra Bhomick, **Aola Supong**, Mridushmita Baruah, Chubaakum Pongener, Dipak Sinha

5. Activated carbon synthesized from biomass material using single-step KOH activation for adsorption of fluoride: Experimental and theoretical investigation, *Korean Journal of Chemical Engineering*, 31, 551-562, 2019.

Parimal Chandra Bhomick, **Aola Supong**, Mridushmita Baruah, Chubaakum Pongener, Dipak Sinha

6. A combined experimental and theoretical investigation of the adsorption of 4-Nitrophenol towards activated biocarbon using DFT method, *Korean Journal of chemical engineering*, 36, 2023-2034, 2019.

Aola Supong, Parimal Chandra Bhomick, Upasana Bora Sinha, Dipak Sinha

7. Green Synthesis of Bromo Organic Molecules and Investigations on Their Antibacterial Properties: An Experimental and Computational Approach, *Acta Chimica Slovenica*, 66, 276-283, 2019.

Naruti Longkumer, Kikoleho Richa, Rituparna Karmaker, Visekhono Kuotsu, **Aola Supong**, Latonglila Jamir, Pranjal Bharali, Upasana Bora Sinha

8. Alizarin Red S adsorption onto biomass-based activated carbon: optimization of adsorption process parameters using Taguchi experimental design, *International Journal of Environmental Science and Technology*, 17, 1137-1148, 2018.

Parimal Chandra Bhomick, **Aola Supong**, Mridushmita Baruah, Chubaakum Pongener, Champa Gogoi, Dipak Sinha

9. *Manihot esculenta* Biomass as an Efficient Precursor for Synthesis of Activated Carbon for defluoridation- Equilibrium, Kinetics and Thermodynamic Studies, *Journal of Environmental Chemical Engineering*, 6, 2382-2389, 2018.

Chubaakum Pongener Parimal Chandra Bhomick, **Aola Supong**, Mridushmita Baruah, Upasana Bora Sinha and Dipak Sinha

10. Sand-Supported bio-adsorbent column of activated carbon for removal of coliform bacteria and *Escherichia coli* from water, *International Journal of Environmental Science and Technology*, 14 1897-1904, 2017.

Chubaakum Pongener Parimal Chandra Bhomick, Upasana Bora Sinha, R. L. Goswamee, **Aola Supong**, and Dipak Sinha

B. Book Chapters published

11. Waste biomass for synthesis of porous activated carbon and its application in waste treatment in the book titled “Climate Change and Sustainable Development (Perspective from North East India)”, First Edition, Purbayon Publication, Guwahati, 2019, 170-190.

M.Baruah, **A.Supong**, P.C. Bhomick, C.Pongener, S.Jamir, D.Sinha.

C. Opinions Published

12. Waterborne Pathogens in Drinking Water- Existing Removal Techniques and Method, *MOJ. Toxicology*, 3, 00072, 2017.

A.Supong, P.C. Bhomick, D.Sinha.

13. Organic Pollutants in Water and its Remediation Using Biowaste Activated Carbon as Greener Adsorbent, *International Journal of Hydrology*, 1, 00017, 2017.

P.C. Bhomick, **A.Supong**, D.Sinha.

Papers Presented

- **Oral presentation** on “Synthesis of Low-Cost Activated Biocarbon for the Effective Removal of 4-Nitrophenol from aqueous solution”, at International seminar on Chemistry and

environmental sustainability, organised by Department of Chemistry, Mizoram university, February 19th to 22nd 2019

- **Poster Presentation** on “*Tithonia diversifolia* as a potent precursor for preparation of biochar and activated carbon”, at Research conclave, Organized by IIT Guwahati, 8th -11th March, 2018.
- **Oral presentation** on “Efficient removal of Bisphenol A by *Tithonia diversifolia* activated carbon: Adsorption equilibrium, kinetics and thermodynamics study”, at National seminar on Chemistry in Interdisciplinary research, organised by Department of Chemistry, Nagaland university, November 09th-10th November, 2018.
- **Oral presentation** on “Taguchis design of experiment for sustainable production of low-cost adsorbent from *Tithonia diversifolia* Biomass”, at National seminar on Bio-resource exploration and utilization: Application in modern biology organised by BIF, Nagaland university, October 09th-10th, October, 2018.
- **Oral presentation** on “Sustainable production of activated carbon from Elephant grass for enhanced removal of phenolic compounds from water”, at National seminar on Climate change and sustainable development, with special focus on North-East India Nagaland university, Organised by Nagaland University Teachers association, Nagaland University, May 17th -18th 2017.
- **Oral presentation** on “A new bio-adsorbent synthesized from *Tithonia diversifolia* for the removal of organic pollutant from aqueous solution” at National Seminar on advances in Biological sciences research, Organised by Department of Botany, Nagaland University, 28th to 1st March, 2017.

Conferences/Seminars/Webinars/Workshops Attended

- Attended webinar on JCR- South Asia training and certification programme 2020 by Web of Science group, 3rd June, 2020.
- Attended Webinar on Introduction to the realms of research organised by Department of Chemistry Immanuel college Nagaland, 28th September, 2020.
- Attended Webinar on Biowaste as a resource for water purification organised by Department of Chemistry St. John College, Dimapur Nagaland, 7th August 2020.
- Attended Short term course on analytical techniques for physical, chemical and bio-inspired materials organised by NIT, Dimapur, July 23rd-27th 2018.
- Participated in a workshop on advanced excel, advanced origin, image J, patent writing and copyright organised by IIT, Guwahati, March 8th -11th 2018.
- Participated in sensitization workshop on DST women scientist scheme, 4th-5th March, 2019
- Attended one day workshop on importance of IPR in academic Institutions, IPR cell, Nagaland University 29th may 2019.
- Attended National Workshop on Computational Drug Designing-I, organised by BIF centre, Nagaland University, 5th -6th, 2015.

Members of Professional bodies/ Organisations.

Life member of Indian Science Congress Association (Membership No. L29785)

Life member of Save the Environment society (Membership No. 34)